DISCLAIMER

This research was funded through the Wisconsin Highway Research Program by the Wisconsin Department of Transportation and the Federal Highway Administration under Project # 0092-04-07. The contents of this report reflect the views of the authors who are responsible for the facts and the accuracy of the data presented herein. The contents do not necessarily reflect the official views of the Wisconsin Department of Transportation or the Federal Highway Administration at the time of publication.

Technical Report Documentation Page

1. Report No. WHRP 07-06	2. Government Accession No	3. Recipient's Catalog No
4. Title and Subtitle Testing Wisconsin Asphalt Mixtures for the AASHTO 2002 Mechanistic Design Procedure		5. Report Date July 2007 6. Performing Organization Code Univ. of Wisconsin - Madison
7. Authors R. Christopher Williams		8. Performing Organization Report No.
9. Performing Organization Name and Address Department of Civil, Construction and Environmental Engineering, Iowa State University		10. Work Unit No. (TRAIS) 11. Contract or Grant No. WisDOT SPR# 0092-04-07
12. Sponsoring Agency Name and Address Wisconsin Department of Transportation Division of Business Services Research Coordination Section 4802 Sheboygan Avenue, Room 104 Madison, WI 53707		13. Type of Report and Period Covered Final Report, 2004-2007 14. Sponsoring Agency Code
15. Supplementary Notes		

16. Abstract

The intent of this project was to examine typical hot mix asphalt (HMA) pavements that are constructed in the state of Wisconsin. The analysis compares the suggested pavement structures based on the 1972 pavement design guide currently used in Wisconsin and the same ones based on the new Mechanistic-Empirical Pavement Design Guide. In order to develop the pavement structure as outlined by the new Design Guide, the mechanical properties of the HMA layers were measured from 21 field sampled mixtures. These properties include dynamic modulus and flow number, which have been found to be significant predictors of rutting and fatigue by Witczak et al. (2002). Properties of the other layers in the system have been obtained from the Wisconsin Department of Transportation pavement design inputs. The objective was to account for typical construction variability that occurs and to determine its impact upon both mechanical tests. Further, the authors examined these mechanical test results on pavement design to determine if the performance tests and new Design Guide, as they currently exist, are ready for implementation by owners/agencies.

17. Key Words	18. Distribution Statement
asphalt mixtures—mechanistic-empirical—pavement design guide—state of Wisconsin	No restriction. This document is available to the public through the National Technical Information Service, 5285 Port Royal Road Springfield, VA 22161

19. Security Classif.(of this report)	19. Security Classif. (of this page)	20. No. of Pages	21. Price
Unclassified	Unclassified	267	

Form DOT F 1700.7 (8-72) Reproduction of completed page authorized

WISCONSIN HIGHWAY RESEARCH PROGRAM #0092-04-07

TESTING OF WISCONSIN ASPHALT MIXTURES FOR THE FORTHCOMING AASHTO MECHANISTIC-EMPIRICAL PAVEMENT DESIGN PROCEDURE

FINAL REPORT

By
R. Christopher Williams, Ph.D.
Christopher J. Robinette
Jason Bausano, Ph.D.
Tamer Breakah

SUBMITTED TO THE WISCONSIN DEPARTMENT OF TRANSPORTATION

SEPTEMBER 2007

ACKNOWLEDGMENTS

The authors would like to acknowledge the support of this project by the Wisconsin Department of Transportation (DOT) and the technical coordination of the Wisconsin Highway Research Program. Specifically, the Wisconsin DOT, the Wisconsin Asphalt Pavement Association (WAPA), and their members are greatly appreciated for assisting in the identification of field projects, sampling assistance, and technical guidance for this project. Lenny Makowski, Laura Fenley, Judie Ryan, and Tom Brokaw at the Wisconsin DOT provided significant assistance in moving this project forward and their efforts are appreciated. The authors would also like to thank Scot Schwandt of WAPA and participating members Erv Dukatz and Signe Erickson from WAPA for work associated with this project. The authors also appreciated the comments and project coordination with the technical oversight committee that Dr. Hani Titi at the University of Wisconsin – Milwaukee provided. The authors would also like to thank the numerous support staff at Michigan Technological University for sample preparation, basic testing and general laboratory operation support, including Ed Tulppo, Jim Vivian, Danielle Ladwig, Michelle Colling, and others. A special thanks to Sabrina Shields-Cook at the Center for Transportation Research and Education at Iowa State University for the substantial editorial review and production of a quality report.

EXECUTIVE SUMMARY

The Wisconsin Department of Transportation (WisDOT) currently uses the AASHTO 1972 Interim Guide for the Design of Pavement Structures for hot mix asphalt. This pavement design procedure is a strictly empirical pavement design approach; however, with the latest research and available computer capabilities, mechanistic pavement design procedures have become more feasible. The new Mechanistic-Empirical Pavement Design Guide and its associated software have been built on the mechanical properties of the pavement layers while still using functions to predict pavement life, thus making its approach a mechanistic-empirical pavement design approach. This pavement design procedure also allows for default values of the mechanical properties to be used, which are based on previous measurements of these properties.

The intent of this project was to examine typical hot mix asphalt (HMA) pavements that are constructed in the state of Wisconsin. Projects were sampled throughout the state of Wisconsin during the 2004 and 2005 construction seasons. Sampling materials from across the state represented a better cross-section of the materials that were used during the season. However, most high traffic volume projects were found in the southern regions of Wisconsin, whereas lower traffic volumes could be found all around the state. This was mainly due to the population distributions and the location of major trunk lines throughout the state. Sampling was conducted at the plant site, just after trucks had been loaded out.

The analysis compares the suggested pavement structures based on the 1972 pavement design guide currently used in Wisconsin and based on the new Design Guide. In order to develop the pavement structure as outlined by the Design Guide, the mechanical properties of the HMA layers were measured. These properties include dynamic modulus and flow number, which have been found to be significant predictors of rutting and fatigue by Witczak et al. (2002). Properties of the other layers in the system have been obtained from the WisDOT pavement design inputs. The objective was to account for typical construction variability that occurs and to determine its impact upon both mechanical tests. Further, the authors examined these mechanical test results on pavement design to determine if the performance tests and Design Guide as they currently exist are ready for implementation by owners/agencies.

Chapter 1 of this document provides an introduction to pavement design and the AASHTO Pavement Design Guide. Chapter 2 discusses past research and studies that have been

conducted that pertain directly to the Superpave™ Simple Performance Test (SPT). Included is a brief description of the research conducted, along with the major findings of the studies that directly apply to this project. Chapter 3 explains the procedures that were undertaken to sample, prepare, and test the specimens for this project. Chapter 4 discusses the mixes that were sampled and some of the difficulties with the original experimental plan. Chapter 5 reviews the specimen preparation, in terms of the volumetric properties. Chapter 6 presents the results of the SPT testing of the 21 mixtures from the state of Wisconsin, and Chapter 7 shows the results of the simulations using the forthcoming AASHTO M-E PDG version 0.800 and compares them to the 1972 AASHTO pavement design guide. Chapter 8 summarizes the conclusions that were reached. Chapter 9 outlines the recommendations for future work based on the findings of this project.

LIST OF CONTENTS

LIST OF FIGURES

LIST OF TABLES

ACRONYMS AND SYMBOLS

2D	A heavy single unit truck with two axles and 6 tires
3SU	A heavy single unit truck with three axles
2S-1	A heavy tractor-semitrailer truck with three axles
2S-2	A heavy tractor-semitrailer with four axles
3S-2	A heavy tractor-semitrailer with five or more axles
2-S1-2	A heavy tractor-semitrailer-trailer combination with five or more axles
A	Witczak Predictive Equation Regression Intercept
AADT	Average Annual Daily Traffic
AADTT	Average Annual Daily Truck Traffic
AASHO	American Association of State Highway Officials
AASHTO	American Association of State and Highway Transportation Officials
ALF	Accelerated Loading Facility
AMS	Accumulated Microstrain at Flow Number
ASTM	American Society for Testing and Materials
BSG (G_{mb})	Bulk Specific Gravity
COV	Coefficient of Variation
D60	Grain size that corresponds to 60 percent passing
E* and $\lvert E^* \rvert$	Complex Modulus and Dynamic Modulus, respectively
E' and E"	Elastic and Viscous Modulus, respectively
ESAL	Equivalent Single Axle Load
FHWA	Federal Highway Administration
F_N	Flow Number
F/P_b	Fines to Asphalt Binder Ratio
G_b	Asphalt Specific Gravity
G_{sb}	Aggregate Bulk Specific Gravity
G_{se}	Aggregate Effective Specific Gravity
HMA	Hot Mix Asphalt
IDT	Indirect Tension Test
IRI	International Ride Index
JMF	Job Mix Formula
JTFP	Joint Task Force for Pavements
LTPP	Long Term Pavement Performance
LVDT	Linear Variable Differential Transducer
M-E	Mechanistic-Empirical
MTSG (G_{mm})	Maximum Theoretical Specific Gravity
MTU	Michigan Technological University
NCAT	National Center for Asphalt Technology
NCHRP	National Cooperative Highway Research Program
N_{design}	Design number of gyrations for a Superpave™ Mix Design
NMAS	Nominal Maximum Aggregate Size
P_b	Asphalt Binder Content

P_{eff}	Effective Asphalt Binder Content
PI	Plasticity Index
PTF	Pavement Testing Facility
QC/QA	Quality Control/Quality Assurance
R^2	Coefficient of Determination
RAP	Recycled Asphalt Pavement
RTFO	Rolling Thin Film Oven
SGC	Superpave™ Gyratory Compactor
SHRP	Strategic Highway Research Program
SMA	Stone Matrix Asphalt
SSD	Saturate Surface Dry
SPS	Special Pavement Study
SPT	Simple Performance Test
SST	Superpave™ Shear Tester
TAI	The Asphalt Institute
TOC	Technical Oversight Committee
UTM	Universal Testing Machine
V	Witczak Predictive Equation Regression Slope
VFA	Voids Filled with Asphalt
VMA	Voids in the Mineral Aggregate
WHRP	Wisconsin Highway Research Program
WisDOT	Wisconsin Department of Transportation
WSDOT	Washington Department of Transportation
ε_o	Strain
ϕ	Phase Angle
σ_o	Stress

CHAPTER 1. INTRODUCTION

1.1 Pavement Design Development

The American Association of State Highway Officials (AASHO) Road Test in the late 1950s formed the basic principles for flexible pavement design in the United States. The AASHO Road Test was meant to identify relationships between the loading magnitude and arrangement as well as between pavement thickness and performance. Based on the results of the Road Test, empirical relationships were developed that made the pavement design process relatively simplistic. Some of the basic inputs include a soil support value, pavement loading, and a regional factor, used to develop a structural number for a layer and ultimately a layer thickness (Washington DOT Manual 1995). This procedure is outlined in the 1972 American Association of State Highway and Transportation Officials (AASHTO) Interim Guide for Design of Pavement Structures. There have been continual revisions to the initial design guide, leading to the development of the AASHTO Guide for Design of New and Rehabilitated Pavement Structures (Design Guide), which is the culmination of research and field experience. The newest Design Guide is based on a mechanistic-empirical (M-E) design approach and has been put together under the auspices of the National Cooperative Highway Research Program (NCHRP) as projects 1-37, 1-37A, 1-40A & B, 9-19, and 9-29 (Guide for Mechanistic-Empirical Design of New and Rehabilitated Pavement Structures 2004).

1.2 Project Objectives

The Wisconsin Department of Transportation (WisDOT) currently uses the AASHTO 1972 Interim Guide for the Design of Pavement Structures for hot mix asphalt. This pavement design procedure is a strictly empirical pavement design approach; however, with the latest research and available computer capabilities, mechanistic pavement design procedures have become more feasible. The Design Guide and its associated software have been built on the mechanical properties of the pavement layers while still using functions to predict pavement life, thus making its approach a mechanistic-empirical pavement design approach. This pavement design procedure also allows for default values of the mechanical properties to be used, which are based on previous measurements of these properties.

The intent of this project was to examine typical hot mix asphalt (HMA) pavements that are constructed in the state of Wisconsin. The analysis compares the suggested pavement structures based on the 1972 pavement design guide currently used in Wisconsin and based on the new Design Guide. In order to develop the pavement structure as outlined by the Design Guide the mechanical properties of the HMA layers were measured. These properties include dynamic modulus and flow number, which have been found to be significant predictors of rutting and fatigue by Witczak et al. (2002). Properties of the other layers in the system have been obtained from the WisDOT pavement design inputs. The objective was to account for typical construction variability that occurs and to determine its impact upon both mechanical tests. Further, the authors examined these mechanical test results on pavement design to determine if the performance tests and Design Guide as they currently exist are ready for implementation by owners/agencies.

1.3 Overall Project Experimental Plan

The first step in developing the experimental plan was to identify HMA designs that have realistic construction parameters. The pavements should be representative of HMA designs used in practice by owners/agencies. Predominate factors that have been identified in the mix design process are (1) the level of anticipated traffic, (2) the nominal maximum aggregate size (NMAS), and (3) mix type (dense- or open-graded).

In this research plan, the level of traffic had been initially segmented into three categories by equivalent single axle loads (ESAL), which corresponds to an 18,000-lb axle load. Low volume traffic levels were considered to have less than or equal to $1x10^6$ ESALs. Medium volume traffic levels were greater than $1x10^6$ ESALs up to $3x10^6$ ESALs. Finally, high volume traffic levels were greater than $3x10^6$ ESALs. The reason for this segmentation is that the level of anticipated traffic is a critical variable in the pavement design process that ultimately results in aggregate angularity and thickness recommendations. Changes in pavement thickness can significantly affect the amount of rutting that occurs in the pavement structure and, consequently, has been noted as one of the variables important in the experimental matrix.

The second factor that was considered was the nominal maximum aggregate size (NMAS). The sizes that were considered are as follows: 25.0-mm, 19.0-mm, and 12.5-mm. As

noted by Akhter and Witczak (1985), the size of the aggregate plays a significant role in permanent deformation.

The type of mix was also analyzed in terms of dense- and open-graded and is a function of the gradation. A Stone Matrix Asphalt (SMA) will be considered an open-graded mix for this project. A SMA promotes stone-on-stone contact by having highly crushed material, with a higher fines content and added fibers. SMAs have been utilized in Europe for many years and were introduced to the United States in 1991 (Brown 1997). As part of Brown's study, it was observed that 31 SMA projects had been paved in the U.S. between 1991 and 1993. This is not to say that SMA projects have not been paved after this time frame—they have—but it points to the increased utilization of this type of mix design. As a result of this higher utilization, the SMA mix type has been included in this study for the high traffic level pavements, where it is intended to mitigate permanent deformation. It should be noted that owners/agencies predominately pave dense-graded mixes, with open-graded mixes used only on high volume roads; this has been factored into the experimental matrix found in Table 1.1.

Table 1.1. Preliminary experimental matrix for field sampling

Nominal maximum aggregate size	Mix type	Traffic level		
		Low	Medium	High
25.0mm	Dense		X[1]	XXX
	Open			
19.0mm	Dense	X	XXX	X
	Open			X
12.5mm	Dense	XXX	XXX	XXX
	Open			X

[1]An X denotes a single mix.

This plan directly emphasizes low and medium volume roads because these represent the majority of the roadway miles an owner/agency maintains and, hence, the greatest number of mix designs performed annually. However, the high volume roadways have the greatest vehicle-miles traveled in the state, making them more prone to failure by permanent deformation; thus, these mixes have been included as well.

1.4 Individual Job Experimental Plan

For each job, a replicate experimental plan that examines the effects of changes in air voids and asphalt binder content has been developed. The reason for this portion of the research project was to understand variations that typically occur during field production. Depending on the ease of compaction and the temperature of the mat, the in-situ air voids after initial construction can vary significantly. This variability can significantly affect pavement performance. Contractors will typically seek 92.0% G_{mm}, or 8.0% air voids, so that they can receive full pay for a job in Wisconsin. However, this may not always be achievable and thus higher air void contents were examined (Wisconsin Construction Specification 2004).

In terms of the asphalt content, the contractors are allowed to deviate ±0.3% from that of the asphalt content stipulated in the accepted job mix formula (JMF), which was stated in Section 460.2.8.2.1.5 of the Wisconsin Constructions Specifications (2004) and is typical of most owners/agencies. It should be noted that since mixes were being sampled from field produced mixes being placed on roadways, testing at a lower asphalt binder content than that produced was not possible. This portion of the experimental plan can be found in Table 1.2.

Table 1.2. Experimental plan for volumetric changes

		Asphalt binder content	
		Sampled (assumed optimum)	**Sampled + 0.3%**
Air voids (compaction effort)	Low	X[1]	N/T[2]
	Target	X	X
	High	X	N/T

[1] An X denotes six specimens for each project.

[2] N/T denotes not tested.

Changes in air voids were obtained through changing the weight of mix in the specimen and compacting to a given height of 170.0-mm. Low, target, and high refer to 4.0, 7.0, and 10.0% air voids, respectively. Testing was also carried out with specimens in which the asphalt binder content was increased 0.3% by weight of the mix. This material necessitated further mixing. The extra asphalt binder was sampled from the plant where the mixture was produced. The procedures for sample procurement and preparation for testing are outlined in Chapter 3.

1.5 Hypotheses for Testing Results

Based on past testing and research from the literature review, hypotheses were developed regarding the factors considered in the experimental plan. The statistical analyses of these hypotheses are presented in Chapter 6. These hypotheses are outlined in the following sections for dynamic modulus, flow number, and pavement design.

1.5.1 Dynamic Modulus

Following are the relationships that are expected to be observed from dynamic modulus testing and developed prior to the use of Superpave™ Simple Performance Test (SPT).

- As temperature increases, dynamic modulus will decrease and phase angle will increase.
- As air voids increase and likewise compaction effort decreases, dynamic modulus will decrease.
- As the asphalt cement content increases, dynamic modulus will decrease.
- As the aggregate angularity (corresponding with traffic volume) increases, dynamic modulus will increase.

1.5.2 Flow Number

The following relationships that are expected to be observed from flow number testing and developed prior to the use of Superpave™ SPT.

- As air voids increases, the flow number will decrease.
- As the asphalt cement content increases, the flow number will decrease.
- As the aggregate angularity (corresponding with traffic volume) increases, the flow number will increase.

1.5.3 Pavement Structure

It is expected that the mechanistic-empirical pavement design would yield a slightly thinner HMA layer than compared to that of the solely empirical pavement design procedure. The reason being is that the empirical pavement design has a greater factor of safety built into the model than mechanistic-empirical pavement design. Minimal distresses would be indicative of thinner layer thicknesses. The current Design Guide software is more of a design check as opposed to a design guide. The analysis approach was to input varying thicknesses for the layer in question with the pavement structure remaining constant and the level of distress through simulations conducted with the Design Guide software.

1.6 Contents of this Document

Chapter 2 of this document discusses past research and studies that have been conducted that pertain directly to the Superpave™ SPT. Included is a brief description of the research conducted, along with the major findings of the studies that directly apply to this project. Chapter 3 explains the procedures that were undertaken to sample, prepare, and test the specimens for this project. Chapter 4 discusses the mixes that were sampled and some of the difficulties with the original experimental plan. Chapter 5 reviews the specimen preparation, in terms of the volumetric properties. Chapter 6 presents the results of the SPT testing of the 21 mixtures from the state of Wisconsin, and Chapter 7 shows the results of the simulations using the forthcoming AASHTO M-E PDG version 0.800 and compares them to the 1972 AASHTO pavement design guide. Chapter 8 summarizes the conclusions that were reached. Chapter 9 outlines the recommendations for future work based on the findings of this project.

CHAPTER 2. LITERATURE REVIEW

2.1 Mechanistic and Mechanistic Empirical Design Approach

In 1885, Joseph Boussinesq developed a method for determining induced stresses and strains in an infinite elastic half-space based on a point load (Coduto 1999). These equations were based on a linear elastic material and have been applied to asphalt pavements. Asphalt pavement mixtures have been around since 1874 (Roberts 2002), with informal pavement design procedures starting to be developed in 1920 (Vesic 1964). These early pavement design procedures were based primarily on "rules of thumb," as well as past experience. Burmister (1943) appears to be the first researcher to apply a mechanistic analysis to a multi-layer system for the purposes of pavement design. A considerable amount of work has been conducted since Burmister, which has ultimately led to the development of the current AASHTO Design Guide for New and Rehabilitated Pavements, henceforth referred to as the Design Guide.

A mechanistic pavement design utilizes mechanical modeling to determine the stress, strain, and displacement under a load (Timm 1998) and, more importantly, a wheel load. With knowledge of the various layer properties (which depends on the method of analysis) of the pavement structure, these reactions can be determined and incorporated into empirical transfer functions to determine the number of load applications to failure. Numerous transfer functions have been developed that center on the distresses of rutting and fatigue. Current pavement design procedures are based on empirical relationships that were derived from testing conducted at the AASHO Road Test in the late 1950s. However, these procedures have become outdated due to changes in load configurations and the general magnitude of the loads. The AASHO Road Test was conducted over a relatively short period of time and did not capture the effects of aging. In addition, being a test track, the applicability of the results to other regions is limited due to the lack of variability in climate and materials with which the structure was built. Other issues are addressed in section 2.3. With a mechanistic pavement design procedure, these issues can be addressed, where the mechanical properties of the HMA can be determined under varied climatic conditions and materials specific to the pavement. Mechanistic models can easily adapt to changes in the vehicle configuration and load spectra. It should be noted that the mechanistic pavement design procedure does not drastically change the pavement cross-section from that of

empirically based designs; however, it provides the ability to analyze changes in traffic and materials and employ them in the design (Newcomb 2001).

In order to conduct an analysis of a flexible pavement system (Figure 2.1) using a multi-layered theory, several assumptions must be made (Huang 2003):

- Each layer is homogeneous, isotropic, and linearly elastic and has an elastic modulus, E, and Poisson's ratio, *v*, which is representative of that particular layer.
- The layer itself does not induce a load on the supporting layers due to its presence and the layer is infinite in the horizontal directions.
- Each layer has a specific layer thickness and the lowest layer is considered to be infinite in thickness.
- The load that is applied to the surface layer is uniform over a circular area with radius *a* and is applied as a pressure *q*.
- The interfaces of the layers are in constant contact with one another and act together; thus, the normal and shearing stresses and the horizontal and vertical displacements present at the interface are equal for each layer.

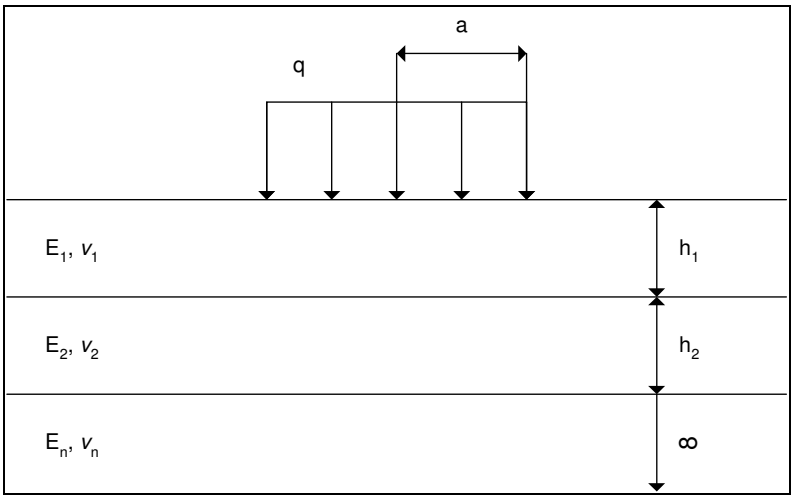

Figure 2.1. n-Layered system (Huang 2003)

2.2 Mechanistic and Mechanistic-Empirical Pavement Design Development

Donald Burmister was the first researcher to apply the elastic layer theories developed by Love and Timeshenko to determine stress and displacement of a pavement structure (1943). Burmister realized that most pavements were multi-layer systems and that the theories that were developed by Boussinesq (infinite elastic half-space) and Boit, and later Pickett (infinitely elastic second layer), were not applicable to such systems. Burmister deemed that settlement was the most important aspect to consider in pavement design. Burmister used the basic Boussinesq equations to develop his own set of equations for a two-layered system. A correction coefficient was employed and compared to that of the Boussinesq results to verify the solutions. The correction coefficient was a function of the radius of the load to the thickness of the first layer and the ratio of the elastic modulus of the second layer to that of the first layer. Burmister demonstrated through example pavements how the graphical representation of the correction coefficient could be used in various material and loading conditions for the determination of layer thicknesses. In addition, an approach for a three-layer system was presented. In the discussion of the paper by Burmister (1943), T.A. Middlebrook, U.S. Engineer Department, War Department, cited that there was no field knowledge of the true stress-strain characteristics to warrant the use of the developed method by Burmister. It was also noted that pavement failures are not caused by deflections but rather by the stresses and strains that are developed under loading (Huang 2003).

In an effort to better understand the mechanisms of pavement failure, the critical location where the failure originates needed to be identified. There are two major modes of failure for flexible pavement: permanent deformation and fatigue cracking. Kerkhoven and Dormon determined that the critical location where rutting was believed to occur could be readily attributed to compressive strains at the surface of the subgrade (1953). The interface of the other pavement layers should also be examined to ensure that higher compressive strains do not persist. The mode of fatigue cracking was found to be the horizontal strains at the bottom of the asphalt layer (Saal and Pell 1960).

Foster and Ahlvin developed charts to determine the vertical, radial, tangential, and shear stresses, as well as deflections, due to a circular load (1954). A designer could use these charts for specific depths and distances from the load in the pavement structure. The charts were based

on a single layer with a specific modulus and a Poisson's ratio of 0.50. From the charts of the stresses, the strains could be determined.

Jones (1962) conducted a study to measure the vertical and horizontal stresses and strains in a three-layer system at the bottom of the asphalt layer and at the surface of the subgrade. Jones considered the ratio of the modulus of adjacent layers, the ratio of the thickness of adjacent layers, and the radius of the load to that of the thickness of the second layer to determine the stress. Utilizing these inputs, stress and strain factors were calculated and applied for a given load. It should be noted that a Poisson's ratio of 0.50 was also used in the study and that, in practice, not all materials adhere to this value. Huang cites that the Poisson's ratio has only a small impact on pavement response and, thus, differences with the actual ratio are negligible (2003). In working with Jones, Peattie developed graphical representations of the stresses and strains within the various layers of the system (1962). The drawback to this system is that interpolation between the values is both arbitrary and difficult.

In an effort to validate the mechanistic functions of Boussinesq and Burmister, an analysis of the AASHO Road Tests was conducted by Vesic and Domaschuk (1964). The true stress-strain characteristics of a pavement under a variety of loading and environmental conditions were readily available from this field study. It was determined that the stress distribution and the deflection basins closely approximated the Boussinesq results. This does not discount Burmister's findings, but demonstrates that there is a need to better understand the mechanics of flexible pavement because field results inherently have greater variability and uncontrollable environmental conditions. Areas where additional research was recommended included the effects of pavement temperature, the presence of moisture, and the rate of load application.

Molenaar and Van Gurp (1982) presented a mechanistic-empirical model for the design of flexible pavements. This study examined 93 in-service pavement structures and used the program BISAR to relate layer equivalent thicknesses to that of maximum radial strain in the asphalt layer and vertical strain in the surface of subgrade. BISAR is a computer program that was developed by Shell; it considers both vertical and horizontal stresses and is based on Burmister's layered theory (Huang 2003). By using the elastic modulus values of the pavement at a reference temperature that was representative of Dutch conditions, an equivalent layer thickness could be determined. Equation 2.1 shows the definition of equivalent layer thickness.

$$h_e = \sum_{i=1}^{2} 0.9 h_i \sqrt[3]{\frac{E_i}{E_3}} \qquad (2.1)$$

where:

h_e = equivalent layer thickness (m),
h_i = thickness of layer i (m),
E_i = elastic modulus of layer i (N/m^2), and
E_3 = elastic modulus of the subgrade (N/m^2).

The equivalent layer thickness could also be used to determine the number of loads until failure occurred due to a 100-kN axle load. In addition, probability-of-survival curves were developed which showed that as the equivalent layer thickness increased, the number of loads until failure likewise increased.

To better understand the response of flexible pavements to loading, an explanation of the models used to describe the interaction of loading and the response of flexible pavements was identified by Lytton et al. (1993). Lytton et al. present, in detail, the different models that are used to describe the elastic, plastic, viscoelastic, and viscoelastoplastic models as they apply to the different distresses and temperatures that a pavement endures throughout its life. At low temperatures, a linear elastic, or viscoelastic, model is appropriate, with Maxwell, Kelvin-Voigt, and Burger components in series or in parallel as illustrated in Figure 2.2. The Burger model with Kelvin model elements in series can capture the viscoelastoplastic behavior of a flexible pavement at the higher temperatures. The reason that a series of Kelvin models are required is that a single Kelvin model is not adequate to capture the retarded strain that takes place over time.

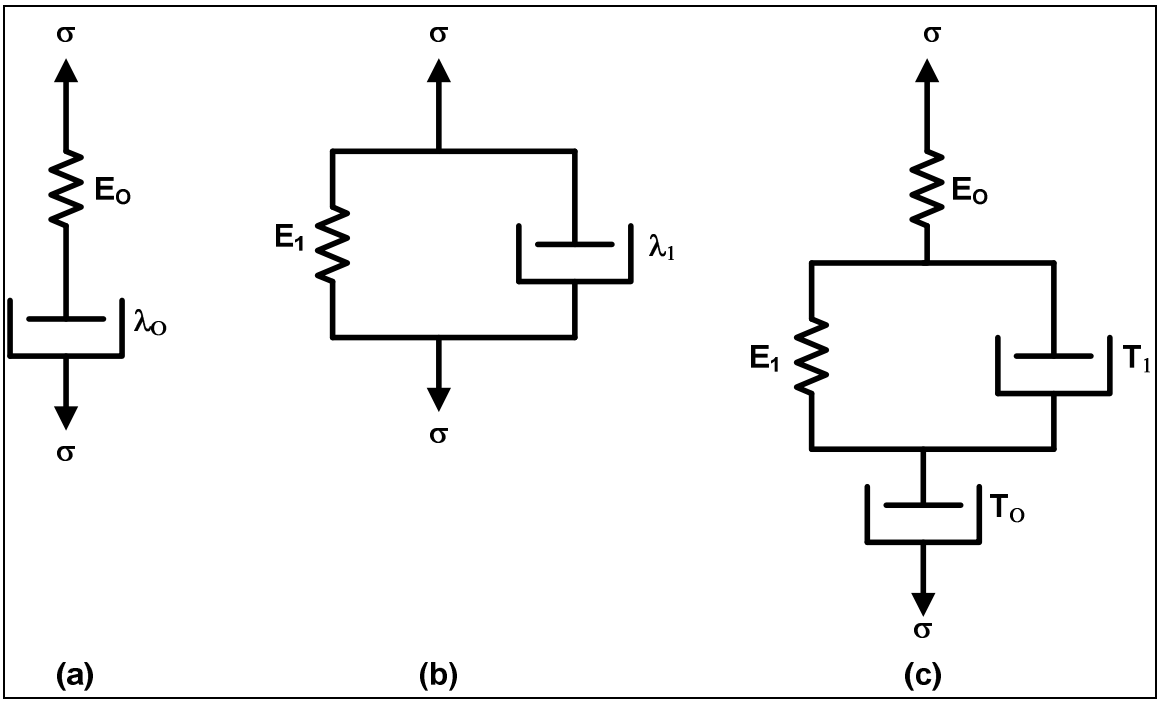

Figure 2.2. Mechanical models: (a) Maxwell, (b) Kelvin-Voigt, and (c) Burger

The equations for these particular models can be found in Huang (2003, pp. 78-80). For higher temperatures, the response of flexible pavements is said to best be described by a viscoelastoplastic model. A viscoelastoplastic model (Figure 2.3) is representative of a repeated load, where a load is placed on a pavement and there is instantaneous deformation followed by some creep, and with the unloading of the pavement, there is an instantaneous elastic rebound followed by creep recovery. Figure 2.3 displays a single loading cycle and the materials' response due to the loading.

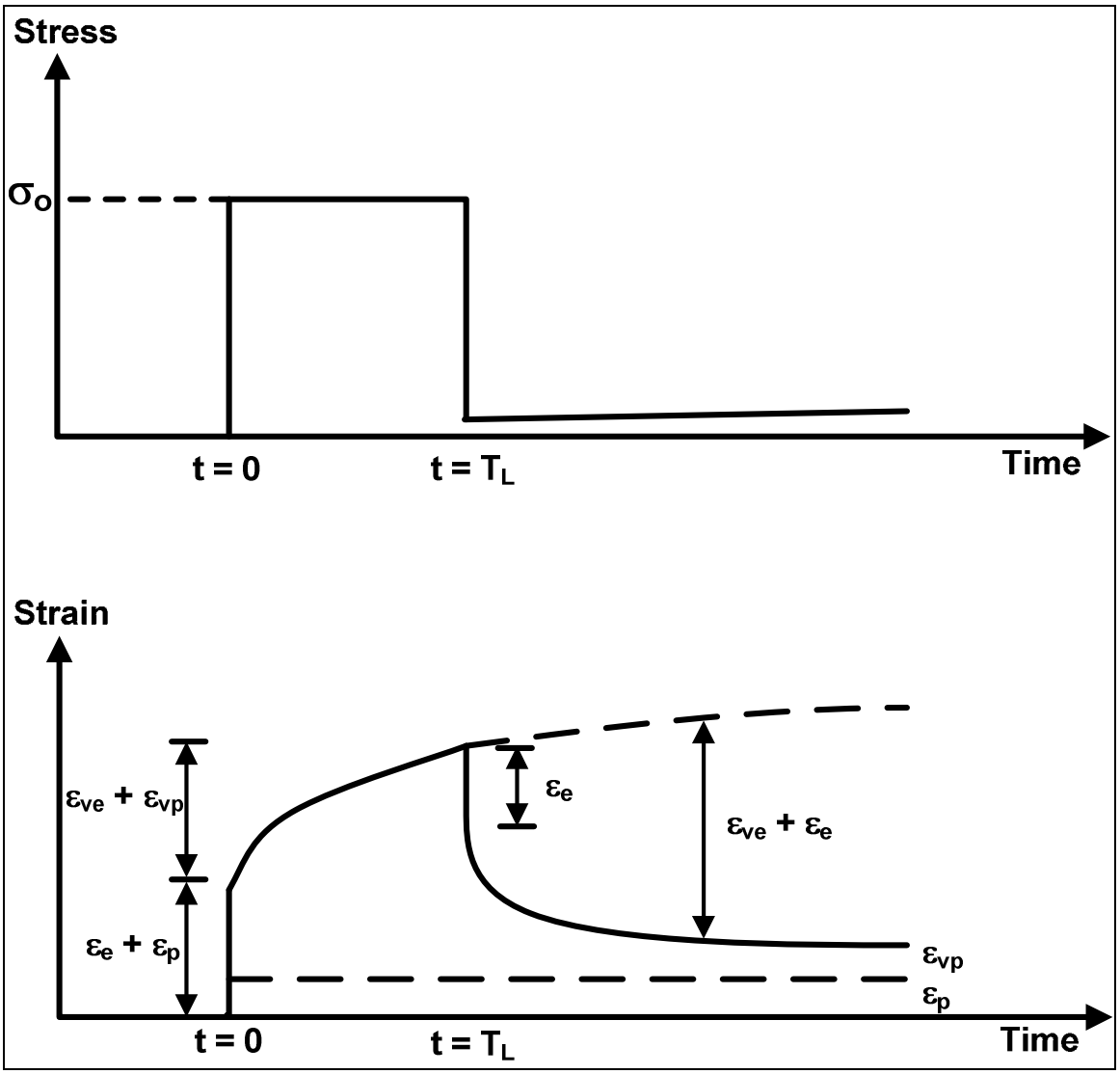

Figure 2.3. Viscoelastoplastic component model (Lytton et al, 1993)

In Figure 2.3, ε_e is the elastic strain—recoverable and time independent, ε_p is the plastic strain—irrecoverable and time independent, ε_{ve} is the viscoelastic strain—recoverable and time dependent, and ε_{vp} is the viscoplastic strain—irrecoverable and time dependent (Uzan et al. 1985).

Lytton et al. (1993) went on to develop a 2D finite element analysis program similar to that developed by Owen and Hinton (1980), with only minor modifications based on a viscoelastoplastic model. The model that Owen and Hinton use is a four-parameter model with a spring and dashpot in series and a second spring and dashpot in parallel to the first series. Additionally, one of the dashpots is modeled with a friction slider to account for the initial

viscoelastic response prior to initial yielding followed by viscoplastic response. The model for fatigue used by Lytton et al. was similar to that used by VESYS. The VESYS cracking model follows equation 2.2.

$$N_q = k_1 \varepsilon^{-k_2} \quad (2.2)$$

N_q represents the number of loads until failure, k_1 and k_2 are model constants, and ε is maximum tensile strain. Miner's law was also incorporated to determine the fatigue ratio. The models used by Lytton et al. were then calibrated to field observations for both distresses.

Van Cauwelaert et al. (1988) developed a linear-elastic program that could be utilized on a standard personal computer; the name of the program was WESLEA. This program was in contrast to other programs, such as BISAR, which required a mainframe. WESLEA can analyze up to five layers with a semi-infinite base layer and 20 loads. The deflection of the pavement was based on a Newton-Coates integration formula and required a minimum of six steps. The steps of the integration are based on the modulus ratio (the ratio of the elastic modulus of upper layer to that of the lower layer). By optimizing the number of steps required to perform the deflection calculation, the analysis period could be minimized. In addition, WESLEA has a component that accounts for friction at the interface of the layers. The interface friction component was developed based upon composite beams. Van Cauwalaert et al. showed that there was no significant difference between the deflections determined by BISAR and that the time of computation was significantly lower. The comparison included varying wheel loads, distance from the loaded area, pavement structures, and wheel configurations, all showing similar solutions. Additionally, a subroutine of BISDEF was added to WESLEA to create WESDEF to back calculate pavement modulus through nondestructive testing (NDT). WESDEF utilized WESLEA's optimization routine to determine the individual pavement layer modulus values. BISDEF and WESDEF showed a good correlation between the modulus values of the individual layers.

Collop et al. (2003) have developed a finite element program named CAPA-3D which uses the viscoelastoplastic model to determine the stresses throughout an element due to loading. This program uses the Burger model for material characterization, as it was mainly concerned with permanent deformation. The program allows for the development of the pavement structure

where each layer is characterized by its Young's Modulus, Poisson's ratio, and thickness. Collop et al. ran a simulation with a load of 700kPa at 20°C to show the stress, accumulated strain and damage, and equivalent viscosities throughout the element, due to a single load application. The simulations illustrated that the location of the maximum strain was reliant on the stress-dependence of the flexible pavement. Stress-dependent pavements showed the greatest stress at approximately one-half the thickness of the asphalt layer, whereas non-stress-dependent pavements showed more of an even distribution of vertical strain.

Uzan (2004) presented a mechanistic-empirical pavement design method that considered the ratio of the resilient to plastic strain as a function of traffic composition, temperature changes throughout the day, environmental conditions, and changes in material response with depth. This method allows the surface and the underlying layers to be broken down into sublayers so that permanent strains can be more effectively determined as opposed to the overall deformation of the entire layer. Uzan used the program JULEA to conduct the pavement analysis, examining numerous points within the pavement structure in response to the loading (not just directly under the load). This research yielded two important findings: 1) a design load can be used to reduce the number of axle configurations, and 2) the stiffness of the pavement can be improved by increasing the thickness of the asphalt pavement layer, which reduces permanent deformation.

2.3 Development and Design of the Current Mechanistic-Empirical Design Approach

The foundation for the 1972 AASHO Design Guide and later revisions of the Design Guide are based on conditions existing at the AASHO Road Test and are thus solely empirical in nature. Many of the conditions used during the test have changed considerably and are not readily applicable to the later iterations of the Design Guide. Some of the major conditions that have spurred the need for changes contained in the new Design Guide are as follows (McGhee 1999):

1. Pavement rehabilitation design procedures were not originally considered.
2. The AASHO Road Test was carried out in a single geographic location, making it difficult to readily address differences in climatic conditions.

3. There was only one type of underlying material used for the subgrade and an unstabilized dense-graded subbase, which once again makes it difficult to address differences in materials.
4. Vehicles have drastically changed and, as a result, the vehicles used during the AASHO Road Test are not representative of today's vehicles.
5. Drainage of the underlying layers was not addressed.
6. The level of loading was considerably lower than the levels experienced by some of the arterials of the U.S. Highway system today.
7. The length of the test was only 2 years and most pavements are expected to perform for 20 to 50 years.

Considerable steps have been taken to resolve many of the aforementioned issues through research and field performance testing. One of the methods employed is the use of test tracks like WesTrack and the National Center for Asphalt Technology's (NCAT) test track. These testing facilities focused mainly on flexible pavement performance, but utilized a better cross-section of materials that are used in practice through repeated load applications with typical vehicle configurations. These testing facilities produced recommendations for better selection of pavement structures and material characteristics sought in flexible pavement designs. Both test tracks also considered the rehabilitation of a pavement structure. These rehabilitations included crack repair, mill and fill, as well as full-depth reconstruction, depending on the level of distress and goals of the test track (Epps et al. 1999).

While test tracks are one solution to determining pavement performance, an examination of actual road performance (e.g., highways, freeways, etc.) is just as beneficial. In 1987, the Long Term Pavement Performance (LTPP) program was implemented under the Strategic Highway Research Program (SHRP), and the LTPP continues today. The main goal of the LTPP is to collect meaningful data pertinent to field pavement performance. Numerous test sections have been studied all over the continental U.S. and in parts of Canada. Data collected from these test sections include climatic conditions, traffic (load spectra and configuration), material properties, and pavement structure, with numerous pavement performance measures being employed. An extensive data analysis is being performed and tailored so that the information can be used in the calibration and development of later AASHTO Design Guides.

With this abundance of information from both field data and test tracks, different testing procedures have been applied in order to find a "golden test," which predicts pavement performance based on the measured mechanical properties of test specimens. M.W. Witczak of Arizona State University has done considerable work in this area by developing a testing procedure that correlates the mechanical properties of asphalt pavement to test track performance under NCHRP 9-19 (Witczak et al. 2002). Several tests have shown promising results, including dynamic modulus, flow time, and flow number. Considerable work has been done to incorporate these tests into a pavement design procedure as part of the current AASHTO Design Guide under an M-E design approach.

2.3.1 Previous Barriers to Mechanistic-Empirical Design Implementation

The 1986 Design Guide recognized that future designs would have to be based upon M-E principles. However, the process is calculation-intensive, and the computers of the time were not capable of analyzing these advanced pavement design procedures. The main reason for the lack of computational capability is that differential equations and finite element analysis were utilized in the different analysis methods (McGhee 1999). Today's computers now make these design processes possible and a move has been made to put them into practice. The intent of the current Design Guide and its associated software was to fully characterize the fundamental engineering properties of the materials used in pavement structure for an M-E design.

The 1986 Design Guide identified additional benefits of an M-E design procedure with particular emphasis to flexible pavements. These benefits are as follows:

1. Design traffic loading is simply an estimate in the design phase; however, pavement loading conditions are dynamic throughout the pavement's life. These changes can be easily factored into the rehabilitation and maintenance schedule as necessary under an M-E pavement design.
2. Procedures can easily be developed to analyze in-situ pavement performance. These procedures can be used to determine factors that contribute to pavement performance that exceeds or does not meet expectations.

3. A hot mix asphalt (HMA) pavement oxidizes with time. With the oxidation process, the binder stiffens. This phenomenon can be factored into the design through the use of mechanistic procedures.
4. Mountainous regions and northern portions of the U.S. experience seasonal fluctuations, particularly freeze-thaw cycles, which leads to the weakening of the pavement and can be considered.

However, the most prominent reason not identified by the 1986 Design Guide is the ability to more accurately determine when failure would occur in a pavement through performance-based testing of the materials that make up the structure. Having a better understanding of a pavement's structural performance can lead to economic benefits. The rehabilitation schedule can be more efficiently developed because the variability in pavement performance can be reduced and the life of the pavement extended through a better assessment of the climate, materials, vehicle loadings, and the variation of performance in the design life. As a result of being able to better identify when rehabilitations need to be scheduled, McGhee cited that an annual savings of $1.14 billion per year over the next 50 years could be realized (1999).

A purely mechanistic pavement design can not currently be used as a stand-alone procedure independent from necessary empirical relationships. Simply knowing the locations of the greatest stress and strain within the pavement does not reflect its ability to withstand loading. Hence, empirical relationships are then used to predict the life of the pavement in terms of the number of load cycles to failure. This is why the procedure is referred to as an M-E design. The 1993 AASHTO Design Guide cites that the primary benefits from the proper use of a mechanistic design are: (1) an improved reliability of design in terms of the longevity of the pavement; (2) the ability to predict specific types of distress in terms of rutting and fatigue, thus making it possible to develop rehabilitation and maintenance schedules accordingly; and (3) a mechanistic design procedure will have the ability to extrapolate from limited field and laboratory results.

2.3.2 The Current Design Guide

The AASHTO Joint Task Force for Pavements (JTFP) is in charge of the development and implementation of pavement design processes. This responsibility has led to the

development of past Design Guides (1972, 1986, and 1993). The newest Design Guide was the 2002 edition, released in 2004. The recognition of the necessity for re-evaluation of the pavement design process came from the JTFP. In an effort to better understand what experts from federal and state highway agencies, contractors, and academics sought in an improved Design Guide, a workshop was conducted by the JTFP on March 24-26, 1996. The areas that were determined of particular interest were as follows (McGhee 1999):

- traffic loading
- foundations
- material characterization
- pavement performance
- environment

The ultimate goal of the Design Guide was to utilize a primarily mechanistic design approach. This would involve establishing an ideal test that could be used to determine the fundamental engineering properties of the individual layers of the pavement structure.

The current Design Guide uses two different software packages to determine the stresses, strains, and deflections in the pavement structure due to loading. The first is JULEA, which is a multi-layer elastic theory program (AASHTO Design Guide 2004). The Design Guide states that "JULEA provides an excellent combination of analysis features, theoretical rigor, and computational speed for linear pavement analysis" (AASHTO Design Guide 2004). However, some unbound materials (predominately subbase and subgrade materials) exhibit non-linear response to loading in that they exhibit stress-dependent stiffness, which can vary with thickness. To account for non-linear responses, the program DSC2D has been incorporated into the analysis package (AASHTO Design Guide, 2004). Both JULEA and DSC2D use specific coordinates to perform their analyses of four axle types (single, dual, tandem, and tridem). Both programs calculate the location of the maximum damage based upon the given conditions and this calculation is used to determine the pavement's performance. One reservation for using the program DSC2D is that, unlike JULEA, it has not been calibrated based on field experience for use in the current Design Guide.

The design procedure outlined in the current Design Guide is mechanistic-empirical in nature due to the fact that calibration factors must be used to relate the properties that predict permanent deformation, fatigue cracking, and the International Roughness Index (IRI). IRI measures the longitudinal profile of a pavement by means of a profilometer and is relevant to the comfort of the motorists utilizing the facility. Models to relate field performance to the laboratory-measured parameters have been developed. These models are as follows (AASHTO Design Guide 2004):

Permanent deformation in the AC layer: $\frac{\varepsilon_p}{\varepsilon_r} = 10^{-3.1552} \beta_{r1} T^{1.734 \beta_{r2}} N^{0.39937 \beta_{r3}}$ (2.3)

where:

β_{r1}, β_{r2}, β_{r3} = calibration factors,
ε_p = permanent strain,
ε_r = resilient strain,
T = AC temperature, and
N = number of load repetitions.

Fatigue Cracking: $N_f = C k_1 (\frac{1}{\varepsilon_t})^{k_2} (\frac{1}{E})^{k_3}$ (2.4)

where:

C = lab to field adjustment factor,
k_1, k_2, k_3 = laboratory developed constants,
ε_t = tensile strain at the bottom of the asphalt layer, and
E = elastic modulus of the asphalt layer.

The permanent deformation model has been derived from the work of Leahy, Ayers, and Kaloush as part of NCHRP 9-19 (AASHTO Design Guide 2004, Appendix GG-1). The fatigue model is the general form of the model and the models most commonly used were developed by Shell and the Asphalt Institute (AASHTO Design Guide 2004, Appendix II-1). Calibration factors for these models have been developed for national, state, and local levels. These calibration factors come from the Long Term Pavement Performance Program, MnRoad, and the AASHO Road Test for new construction, rehabilitation, and overlays.

2.4 Superpave™ Simple Performance Test (SPT)

The initial development of the Superpave™ mixture design procedure included steps for aggregate and binder characterization, aggregate blending, and volumetric testing of Superpave™ Gyratory Compactor (SGC) prepared specimens. Two performance tests were also developed: 1) the Superpave™ Shear Tester (SST), and 2) the Indirect Tensile Tester (IDT) (The Asphalt Institute 1996). However, these tests are typically not conducted as part of the mix design process.

Various projects, such as WesTrack, NCAT, and MnRoad, have been conducted to measure the field performance of the newer Superpave™ mixture design method. As a result of these projects and NCHRP Project 9-7, volumetric testing as a stand-alone procedure has been put into question. As part of the current Design Guide, mixture performance characteristics are used as inputs into the design.

In 1996, the Federal Highway Administration (FHWA) developed a request for bids on a research project to develop a simple performance test to be used in conjunction with a new Design Guide. This test would measure the performance of HMA to be used in a particular pavement layer based upon fundamental engineering properties in conjunction with the established volumetric testing procedures. Various tests were employed, analyzed, and correlated with performance data from test track facilities that could be used as the Superpave™ Simple Performance Test (SPT). As previously mentioned, Witczak et al. (2002a) found that dynamic modulus, flow time, and flow number have been shown to have promising correlations with field performance.

The fundamental engineering properties for the hot mix asphalt (HMA) layer are obtained from what has been termed the Superpave™ SPT. Witczak et al. (2002b) defined the SPT as "[a] test method(s) that accurately and reliably measures a mixture response characteristic or parameter that is highly correlated to the occurrence of pavement distress (e.g., cracking and rutting) over a diverse range of traffic and climatic conditions" (Witczak et al. 2002a). These tests include dynamic modulus $|E^*|$, flow time (F_T), and flow number (F_N), which are conducted at elevated temperatures to determine the mixtures' stiffness analogous to permanent deformation. Dynamic modulus $|E^*|$ alone is run at other stipulated temperatures so that it can be applied to field conditions and to correlate stiffness to crack development at the intermediate

end of the temperature spectrum. Correlations to field performance, along with the advantages and disadvantages of these tests from both Brown et al. (2001) and Witczak et al. (2002b), can be found in Table 2.1.

Table 2.1. SPT advantages and disadvantages (NCHRP Report 465 2002 and NCAT Report 01-05)

	Parameter	Test condition	Model	R^2	Se/Sy	Advantages	Disadvantages
Dynamic modulus	$E^*/\sin\phi$	Sinusoidal Linear 130°F 5 Hz	Power	0.91	0.310	• Direct input for 2002 Pavement Design Guide • Not forced to use master curves • Easily linked to established regression equations • Non destructive tests	• Coring and sawing • Arrangement of LVDTs • Confined testing gave poor results • Need further study of reliability of confined open graded specimens • Equipment is more complex • Difficult to obtain 1.5:1height-to-diameter ratio specimens in lab
Repeated loading (flow number)	F_N	Unconfined 130°F various frequencies	Power	0.88	0.401	• Better simulates traffic conditions	• Equipment is more complex • Restricted test temperature and load levels does not simulate field conditions • Difficult to obtain 1.5:1height-to-diameter ratio specimens in lab

Past research on the performance tests that have been incorporated into the current Design Guide are discussed herein.

2.4.1 Dynamic Modulus Test Setup

Dynamic modulus is one of the oldest tests used to measure the fundamental properties of hot mix asphalt (HMA). Dynamic modulus testing has been studied since the early 1960s by Papazian and became a standard test in 1979 by the American Society for Testing and Materials (ASTM) under D3497 "Standard Test Method for Dynamic Modulus of Asphalt Concrete Mixtures." Under the testing procedure for dynamic modulus, a haversine compressive stress is applied to the axial ends of a test specimen. The testing procedure includes various frequencies

and temperatures to capture the viscoelastic properties of the HMA. This testing scheme is intended to account for various loading and temperature conditions observed in the field. Figure 2.4 shows the typical load application along with a specimen's response to the loading.

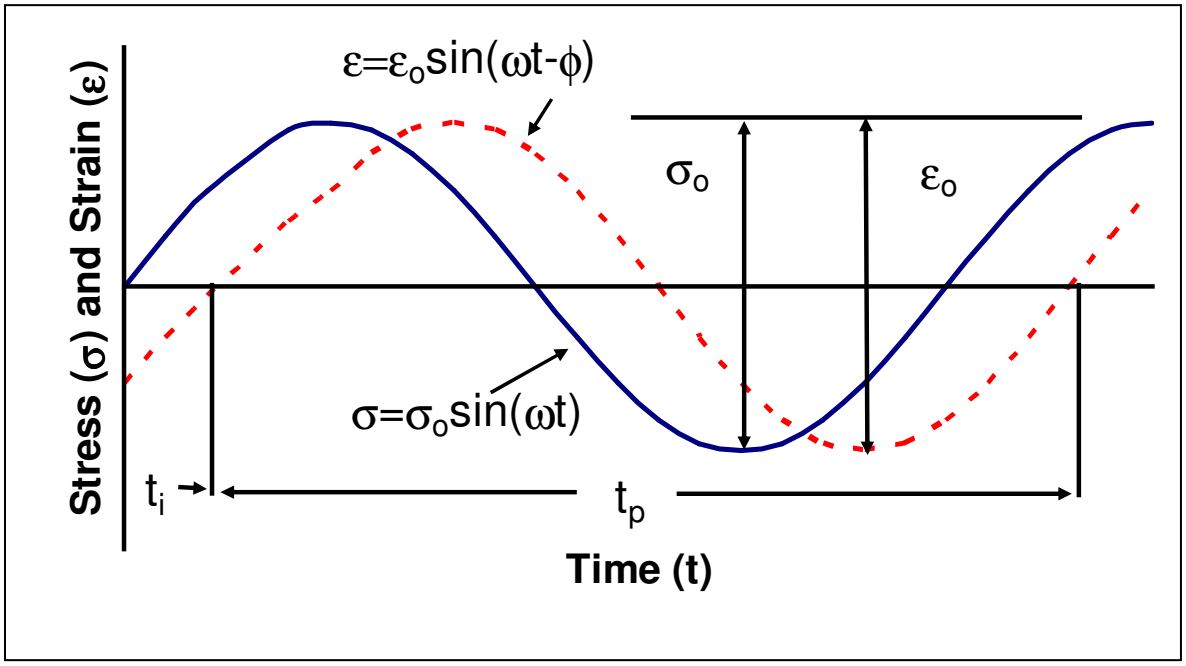

Figure 2.4. Dynamic modulus loading

Under the established testing protocol ASTM D3497-79, the stress is applied to the specimen (solid line) and the axial strain (dashed line) that results from the stress is measured during the course of the test. The complex modulus (E*) is mathematically defined as the maximum (e.g., peak) dynamic stress (σ_o) divided by the peak recoverable axial strain (ε_o) (Witczak et al. 2002b). The complex modulus is sometimes referred to as the dynamic modulus $|E^*|$ and is just the absolute value of the complex modulus. Equation 2.5 shows the mathematical equation for dynamic modulus.

$$|E| = \frac{\sigma_o}{\varepsilon_o} \qquad (2.5)$$

In order to determine the materials' susceptibility to changes in environmental conditions with particular interest to temperatures, the phase angle (ϕ) is measured. This is mathematically defined as the time lag between a cycle of stress and strain divided by the duration of the stress cycle. Mixtures that have a phase angle of 0° (ϕ = 0°) during the test exhibit purely elastic behavior, whereas those that have a phase angle of 90° (ϕ = 90°) exhibit purely viscous behavior. In practice, the phase angle ranges from roughly 10° to 45°, but this is mainly temperature-dependent and this will be discussed later in the literature review. Equation 2.6 shows the mathematical definition of phase angle.

$$\phi = \frac{t_i}{t_p} \times 360 \tag{2.6}$$

where:

t_i = time lag between a cycle of stress and strain (s),
t_p = time for a stress cycle (s), and
i = imaginary number.

The complex modulus can be related to the phase angle through the elastic and viscous moduli (E' and E", respectively). The elastic (eq. 2.7) and viscous moduli (eq. 2.8) are determined by the following:

$$E' = \frac{\sigma \cos(\phi)}{\varepsilon_o} \tag{2.7}$$

$$E'' = \frac{\sigma \sin(\phi)}{\varepsilon_o} \tag{2.8}$$

Dynamic modulus is a measure of the relative stiffness of a mix. Mixes that tend to have good rut resistance at high temperatures likewise have high stiffness. Although the tradeoff is at intermediate temperatures, stiffer mixes tend to be more prone to cracking for thicker pavements (Shenoy and Romero 2002). For this reason, dynamic modulus testing is conducted at both intermediate and high temperatures to measure HMA's resistance to these two distresses for the current Design Guide.

2.4.2 Dynamic Modulus Literature Review

Dynamic modulus has been one of the most studied tests in terms of determining the mechanical properties of asphalt pavement. As previously mentioned, Papazian (1962) was the first to develop the test procedure for dynamic modulus. Papazian took into account that HMA is a viscoelastic material and that, by applying a sinusoidal stress at a given frequency, the measured strain would follow the same frequency although lagged by the stress by an angle ϕ. The stress is therefore related to the strain by a complex number which is a function of the frequency.

Coffman et al. (1964) conducted dynamic modulus tests with a simulated mix from the AASHO Road Test; the only aggregate characterization that was performed was that of a gradation. Some of the basic relationships that are inherent in dynamic modulus testing were realized from this research study. These relationships include the following: 1) as temperature increases, dynamic modulus decreases, and 2) phase angle increases with an increase in temperature.

Shook and Kallas (1969) conducted a study which identified factors that directly influence the measurement of dynamic modulus. A matrix of specimen variables was developed, which included varying asphalt content, air voids, asphalt viscosity, and compaction effort. Four-inch diameter by eight-inch high cylindrical specimens were prepared for testing. A sinusoidal uniaxial stress was applied to the specimen and the axial strain was measured by strain gauges affixed to the sides of the test specimens. The specimens were tested under varying temperatures and frequencies to accurately measure the effects the variables had on the measured value of the dynamic modulus. With everything else being held constant, several relationships were recognized, including the following:

1. With an increase in air voids, dynamic modulus decreases.
2. As asphalt viscosity decreases, so does dynamic modulus.
3. As asphalt content decreases, dynamic modulus increases.
4. Decreasing the compaction effort decreases dynamic modulus.

Numerous models have been developed to predict dynamic modulus values of HMA by using measurable variables, such as aggregate and asphalt characteristics, as well as the loading

regimen. An extensive study was undertaken by Akhter and Witczak (1985) in an effort to identify variables that were relevant to a dynamic modulus predictive equation. These variables apply to the mix design process because they have a direct influence on the stiffness of the pavement layer. Over 130 mix designs were evaluated under this study, with data contributions being made by The Asphalt Institute (TAI). From an analysis of the mix designs, it was determined that mixture temperature was the most significant variable in a dynamic modulus predictive equation. This was in addition to the already identified variables that were controllable in terms of material properties, which include the amount and type of asphalt (asphalt content and viscosity), the gradation of the aggregate (percent retained on the 3/4 in, 3/8 in, and #4 sieves and percent passing the #200), and air voids in the mix. The frequency of loading also played a significant role in a dynamic modulus predictive equation. Equation 2.9 shows the latest dynamic modulus equation developed by Witczak (2002b).

$$\log|E^*| = -1.249937 + 0.029232(\rho_{200}) - 0.001767(\rho_{200})^2 - 0.002841(\rho_4) - 0.058097(V_a) - \frac{0.802208(V_{beff})}{V_{beff} + V_a} + \frac{3.871977 - 0.0021(\rho_4) + 0.003958(\rho_{3/8}) - 0.000017(\rho_{3/8})^2 + 0.005470(\rho_{3/4})}{1 + e^{(-0.603313 - 0.313351 \times \log(f) - 0.393532 \times \log(\eta))}} \quad (2.9)$$

where:

E* = dynamic modulus (10^5 psi),
η = bitumen viscosity (10^6 psi),
f = loading frequency (Hz),
V_a = air void content (%),
V_{beff} = effective bitumen content (% by volume),
$\rho_{3/4}$ = cumulative percent retained on 19 mm sieve,
$\rho_{3/8}$ = cumulative percent retained on 9.5 mm sieve,
ρ_4 = cumulative percent retained on 4.75 mm sieve, and
ρ_{200} = percent passing 0.075 mm sieve.

The main result of the study concluded that coarse aggregate mixes (mixes containing 3/4 in. material and greater) provided a higher modulus value and would result in a longer performance life. In addition, mixes that were gap-graded, or had very little material retained on the No. 4 sieve, tended to yield higher modulus values.

Witczak et al. (2002b) found that dynamic modulus testing has a strong relationship with field performance data from WesTrack, the FHWA's Accelerated Loading Facility (ALF), and MnRoad for permanent deformation. Four-inch diameter by six-inch high cylindrical specimens were procured from materials from the individual test sites and tested under confined and

unconfined loads. Various frequencies and temperatures were tested and the strains induced by a dynamic load were recorded. Different models for measuring dynamic modulus values were employed and statistically analyzed for goodness-of-fit. The strongest relationship that was shown was with $E^*/\sin\phi$, where the specimen is tested unconfined and modeled linearly. Tests that were conducted with a confining stress exhibited a poor relationship when compared to field measured rutting. Table 2.1, shown previously, lists some of the major advantages and disadvantages of dynamic modulus for permanent deformation as found by this study.

In addition to testing dynamic modulus to correlate rut performance, dynamic modulus was run at low and intermediate temperatures by Witczak et al. (2002b) to determine its relationship with that of thermal and fatigue cracking from materials procured from the ALF, MnROAD, and WesTrack test sites. The testing was once again conducted on confined and unconfined specimens using various parameters relating to dynamic modulus related to field performance. None of the testing showed strong correlation with field performance, but because of the compatibility with dynamic modulus testing for use in a fatigue model for the current Design Guide, the dynamic modulus test was recommended for further development. Witczak et al. found that results from testing were highly correlated with field distresses when the test results were analyzed by $E^*\max(\sin\phi)$ and run unconfined.

Further field validation of dynamic modulus as a predictor of pavement performance was conducted by Zhou and Scullion (2003). Zhou and Scullion were able to use field performance as a benchmark for determining the rutting susceptibility of a mix, using the SHRP Special Pavement Studies (SPS-1) sections on US-281. There were a total of 20 test sections, all of which underwent varying degrees of permanent deformation but had the same traffic levels. Rut depths were measured via a trenching operation and information available from DATAPAVE (2004) was used in the analysis. DATAPAVE is a software program provided by LTPP and consists of an online database of all the test sections for the SHRP program. DATAPAVE also uses models to estimate temperature in flexible pavement at varying depths with varying levels of reliability. Samples were taken from between the wheelpaths and specimens remolded to yield the necessary dimensions as stipulated by ASTM D-3497. The specimens were run unconfined at 40°C with an axial stress level of 138kPa. A frequency sweep was also conducted as part of the testing. Zhou and Scullion found that, as the frequency increased, there was an increase in the measured E^*. In addition, the poor-performing mixes could be discerned from the well-

performing mixes, regardless of frequency. The general relationship that was recognized was that as the E* increased, the amount of measured rutting decreased. It was also found that E* and E*/sinϕ were highly correlated and both could be used for comparison purposes as to whether a mix was more or less rut susceptible.

Clyne et al. (2003) performed an analysis of materials from four sections of the MnROAD test site. The testing that was performed focused on the dynamic modulus test setup as stipulated by NCHRP 9-29. Testing was conducted over five frequencies (0.01, 0.1, 1, 10, and 25 Hz) and six test temperatures (-20°C, -10°C, 4°C, 20°C, 40°C, 54°C). For sawed/cored specimens, it was found that coefficients of variation (COV) of 30%–50% were not uncommon. The following four relationships were realized from this testing:

- First, that holding frequency constant, the dynamic modulus decreases with an increase in temperature.
- Second, that as temperature increases from -20°C to 20°C the phase angle increases, but from 40°C to 50°C it decreases as aggregate interlock becomes the controlling factor.
- Third, under constant temperature, as the frequency increases, so does the measured dynamic modulus.
- Finally, the dynamic modulus data provides a smooth data set when plotted over the testing temperature and frequencies, but the phase angle is more significantly scattered, meaning that it is difficult to obtain consistent data.

Mohammad et al. (2005) performed extensive dynamic modulus testing on both field- and laboratory-prepared specimens from a 25.0 mm dense-graded mixture paved in Louisiana. The study examined the effects of changes in asphalt content, sampled materials over several days of production, and multi-laboratory variability. Mohammad et al. showed that decreasing the asphalt binder content of laboratory prepared mixtures increases dynamic modulus and decreases the phase angle. The study also showed that the phase angle changes with a change in frequency and with temperature. At 25°C, the phase angle decreases with an increase in frequency and at 45°C and 54°C, the phase angle increases with frequency up to about 10 Hz and then begins to decrease. In terms of the multi-laboratory variability, at 25°C, there was no

statistical difference between the results found by FHWA and the Louisiana Transportation Research Center (LTRC). At the high test temperature of 54°C, there was a statistical difference, in that the dynamic modulus results as found by the FHWA testing facility were lower the results found by the LTRC.

2.4.3 Tertiary Flow

Tertiary flow, defined in section 1.5.2, has been identified as a measure of the fundamental engineering properties of HMA. Tertiary flow was first identified by Hills (1973) in a study that pertained to the creep of asphalt mixtures. It was found that the rate of deformation decreased until a critical strain was reached and then the strain rate began to increase. During the course of the test, Hills also observed that the volume of the specimen increased, which meant that the individual aggregate particles were moving past each other in order for additional deformation to occur in the specimen. It was noted that no field-rutted pavement had been observed as undergoing this dilation (an increase in air voids and change in the specimen volume). Subsequent research has identified dilation of asphalt pavement (Mallick 1995).

Tertiary flow, along with dynamic modulus, can then be linked to distress prediction models (Witczak et al. 2002a). Extensive testing has been conducted in terms of correlating tertiary flow to pavement performance by Witczak et al. (2002b) as part of NCHRP Projects 9-19 and 9-29. This testing parameter is anticipated to be one of the inputs used in later revisions of the current Design Guide.

2.4.4 Repeated Load (Flow Number) Test Setup

The test for flow number is based on the repeated loading and unloading of a HMA specimen, where the permanent deformation of the specimen is recorded as a function of the number of load cycles. The loading is for 0.1 sec followed by a 0.9 sec dwell (or unloading) of the specimen. There are three phases of flow that occur during this type of test: primary, secondary, and tertiary. Under primary flow, there is a decrease in the strain rate with time. With continuous repeated load application, the next phase is secondary flow, which is characterized by a relatively constant strain rate. Finally, the material enters tertiary flow, where the strain rate begins to increase as the test progresses. Tertiary flow signifies that the specimen is beginning to

deform significantly and the individual aggregates that make up the skeleton of the mix are moving past each other. Flow number is based upon the initiation of tertiary flow (or the minimum strain rate recorded during the course of the test). The sample loading and strain measurements can be found in Figure 2.5.

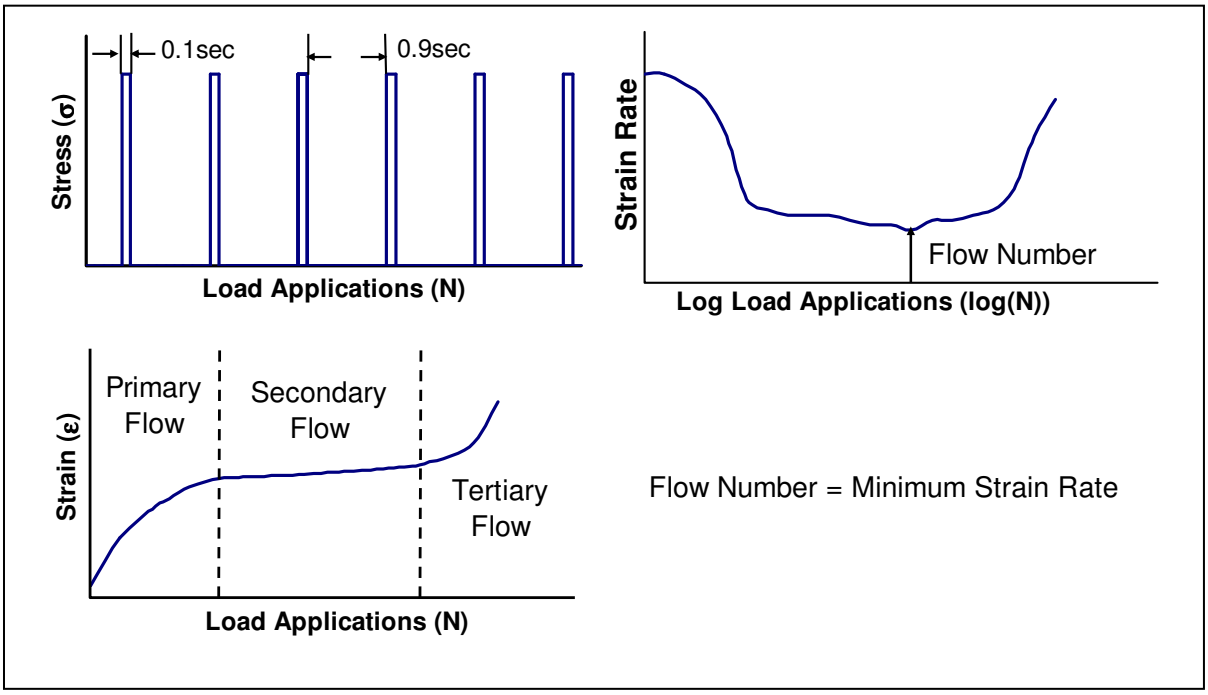

Figure 2.5. Flow number loading

Flow number is more analogous to field conditions because loading of the pavement is not continuous—there is a dwell period between loadings. This allows the pavement a period to recover some of the strain induced by the loading. According to Don Christensen, Ray Bonaquist, and Leslie Ann Myers, flow number has currently been selected as a test to be used to complement dynamic modulus in the current Design Guide, whereas flow time is not being used in practice (personal conversation, 2004).

2.4.5 Repeated Load Test (Flow Number) Literature Review

Brown and Snaith (1974) conducted an investigation of multiple variables and their effects on the number of load applications to failure. With all other variables remaining constant, only one variable was tested at a time. Failure was defined by a marked increase in the

deformation rate and the number of cycles that had occurred to what was considered the failure point (similar to that of tertiary flow). The most noteworthy results of the testing were as follows:

1. As temperature increased, strain increased substantially.
2. As the applied stress was increased, the strain increased.
3. As confining stress was increased, the strain decreased.
4. The rate of strain was time-dependent upon frequencies above 1Hz.
5. A binder content of 4% by mass of the mix yielded the highest stiffness at lower temperatures (10°C to 30°C or 50°F to 86°F) and 3% by mass of the mix at higher temperatures (40°C or 104°F).

One of the variables that showed an insignificant effect on strain was the rest period between load applications. It should be noted that some of the specimens that were tested under unconfined conditions developed cracks within the specimen; these cracks led to dilation of specimens.

Brown and Cooper (1984) tested cored specimens from a roller compacted slab. These specimens were tested under a repeated triaxial load with different levels of aggregate gradation, confining stress, and binder based upon penetration grading (AASHTO T 49 and ASTM D). One of the conclusions found in the study was that, for the formulated mixtures, there was little influence of the penetration grade on the development of permanent shear strain in the specimen, with all other variables held constant. Further testing showed that major changes in gradation, particularly with gap-graded mixes, developed higher shear strain under fewer load cycles. Additional testing discounted the Marshall flow and stability testing, which showed a negative correlation with the results of repeated triaxial loading tests.

A study was conducted by Mallick et al. (1995) in three phases to determine the effects of air voids on: (1) dynamic creep testing (repeated loading), (2) correlating field rutting with the measured strain from dynamic creep testing of field samples, and (3) crushed aggregate performance. Testing was conducted in accordance with ASTM D4123-82. All of the dynamic creep tests were conducted at 60°C (140°F), which is representative of average high pavement temperatures throughout the U.S. Varying deviator and confining stresses were applied to the

specimens depending on the phases of the study, but were typical of field conditions. During the first and second phases of the study, an 826.8 kPa (120 psi) normal pressure and 137.8 kPa (20 psi) confining pressure was used. For the third phase, a normal pressure of 1653.6 kPa (240 psi) and a confining pressure of 275.6 kPa (40 psi) were used, which were analogous to common applied airfield stresses. From the first phase of the study, a rather clear logarithmic relationship was found between air voids and permanent strain. It was noted that a level at or below 3.0% air voids was a defining point at which permanent strain began to increase rapidly. The change in air voids of the specimens after testing was also analyzed during this phase of the study. It was found that specimens with 3.0% or lower initial air voids underwent dilation, while specimens with greater than 3.0% initial air voids underwent consolidation. This was consistent with observed field behavior, where pavements with low initial air voids tended to shove, creating more air voids, and under-compacted pavements experience densification through traffic loading. The second phase used field procured samples with known loading levels to analyze the permanent deformation that occurred in the field in relation to the permanent strain from repeated loading. This phase showed a very strong correlation with permanent strain and rutting rate (defined as millimeters of rutting/square root of million of ESALs). This means that dynamic confined creep testing could potentially be used to identify rutting potential of a mix. The last phase of testing was with varying angular materials; with the dynamic creep testing, inferior mixes were identified by the higher measured permanent strain. These inferior mixes contained little or no angular material.

Brown and Gibb (1996) studied the effects of varied gradation and asphalt type, as well as asphalt content, on permanent deformation and uniaxially loaded specimens. A small-scale Pavement Testing Facility (PTF) was setup and four pavement sections were cored for repeated load testing. Pavements that showed high levels of rutting in the wheel track testing also showed a good correlation with the specimen going to failure when tested at the same temperature in uniaxial compression. Testing performed at different temperatures from that of the PTF tended to misrepresent the performance of the pavement. With this realization, an effort was placed on understanding the roles of the binder and the aggregate. Through estimates of the binder stiffness, the strain rate decreases on a log-log scale; in other words, as binder stiffness decreases, the aggregate structure must carry the load to resist permanent deformation. One of the major conclusions of the study was that repeated loading in terms of uniaxial compression

was better at measuring permanent deformation because permanent strains were analogous to field loading conditions. In the field, there is an accumulation of strain in the pavement with each additional loading, but there is a dwell period before the next load application. A repeated loading configuration best simulates this condition.

Flow number is defined as the number of load applications when shear deformation begins (Witczak et al. 2002b). Flow number attempts to identify a mixture's resistance to permanent deformation by measuring the shear deformation that occurs due to a haversine loading. The testing regimen calls for repeated cyclical loads to be applied for 0.1 sec followed by 0.9 sec dwell (or rest). The point at which shear deformation (tertiary flow) begins is where the flow number is recorded. A power model was used in the data analysis. Unconfined testing showed a higher correlation with permanent deformation data from MnRoad, ALF, and WesTrack. The volumetric data from some of the test sections at WesTrack may have been inaccurately reported; as a result, the correlation could actually be higher in testing conducted from these test sections. Table 2.1, shown previously, lists some of the major advantages and disadvantages of flow number as found by Brown et al. (2001) and Witczak et al. (2002b).

Kaloush and Witczak (2002) found that repeated loading simulated field loading and that test parameters could be used for several applications. However, the disadvantages to such a test are the complexity with developing design guidelines and the fact that the specimens may need to be confined. In this particular study, it was found that confined testing correlated best with field results and that either axial or radial strains could be used for flow time measurement.

In addition to evaluating dynamic modulus as a means of comparing poor- and well-performing mixes, Zhou and Scullion (2003) also ran their specimens through a repeated loading test. In the analysis, models that were developed (and later presented in Zhou et al. 2004) were employed to so that each of the stages of permanent deformation (primary, secondary, and tertiary creep) could be characterized. Once again, Zhou and Scullion found that there was positive correlation between field performance and the flow number. They concluded that the flow number test could be used as a means of comparing mixes for rut susceptibility.

Mohammad et al. also examined the effects of binder content flow number. The asphalt binder content changes were ±0.5% from optimum. Through a statistical analysis, flow number was found not to be as sensitive to changes in asphalt content as dynamic modulus. The analysis did show that the specimens with the low asphalt binder content had the highest flow number.

2.5 Specimen Geometry

Witczak et al. (2000) examined the effects of specimen geometry on dynamic modulus, flow time, and flow number test results. Three different Superpave™ mixes were developed with a single PG 64-22 binder. Over 200 specimens were prepared using a Superpave™ Gyratory Compactor (SGC); these specimens were then cut down to fill a matrix of heights and diameters to be tested for the uniaxial compression tests. It was generally recognized that smaller specimens, in terms of the diameter, were observed to have lower air void contents. One of the major findings was that the lower the height-to-diameter ratio (H/D), the higher the recorded dynamic modulus. This finding is likely due to the proximity of the Linear Variable Differential Transformers (LVDTs) to the load platens. For the determination of phase angle, the effects of H/D are exceptionally notable, in that stiffness decreases with an increasing diameter. This is especially important because at 40°C (140°F), there was a difference greater than 10 degrees in the phase angle between 70 and 150 mm diameter specimens. It was believed that the relationship between the specimen diameter and the measured phase angle was attributable to the radial changes in the structure of the gyratory specimen. The flow number was also observed to decrease as the H/D ratio increased. It was stated that this result was rational because with "short specimens, end friction restricts large lateral expansion that accompanies tertiary flow in uniaxial specimens" (Witczak 2000). An effort was made to standardize an exact specimen for dynamic modulus testing, flow time, and flow number, based on the information in Table 2.2. It was recommended that a height-to-diameter ratio of 1.5 would be sufficient; the diameter of the test specimens was selected to be 100 mm (4.0 in) with a height of 150 mm (6.0 in).

Table 2.2. Uniaxial data analysis (Witczak et al. 2000)

Parameter	H/D ratio			
	Graphical[1]	Analysis of variance		
	Effect for increasing H/D	Significant	Multiple comparisons	Limit
$\|E^*\|$ 4C	Decreases	No	1=1.5=2=3	1.5
Diameter 4C	None	No	1=1.5=2=3	1.0
$\|E^*\|$ 40C	None	No	1=1.5=2=3	1.0
Diameter 40C	None	No	1=1.5=2=3	1.0
$\varepsilon_{\pi 2000}$	None	No	1=1.5=2=3	1.0
Flow	Decreases	Yes	1>1.5=2=3	1.5
Parameter	**Diameter**			
	Graphical	**Analysis of variance**		
	Effect for increasing D	**Significant**	**Multiple comparisons**	**Limit**
$\|E^*\|$ 4C	None	No	70=100=150	70
Diameter 4C	Decreases	Yes	70>100>150	None
$\|E^*\|$ 40C	None	No	70=100=150	70
Diameter 40C	Decreases	Yes	70>100>150	None
$\varepsilon_{\pi 2000}$	Decreases	Yes	70>100=150	100
Flow	Increases	Yes	70<100=150	100

[1]References the graphical change in the test parameter with a change in the H/D ratio.

In addition to performing an analysis on Mn/ROAD material for dynamic modulus, Clyne et al. (2003) also performed a comparison on specimen preparation. Testing included specimens that were sawed/cored to a diameter of 100 mm and a height of 150 mm and specimens that were compacted to the same diameter and height. Clyne et al. found that the specimens compacted to the test specimen geometries had lower coefficients of variation (COVs), but higher E* values, as compared to the cored specimens, by 40%–50%. It was also noted that the sawed/cored group had higher phase angle values by 10%–20%.

Birgisson et al. (2005) found that there was as little as 0.6%–1.9% difference between the two specimen preparation procedures used by Clyne et al. (2003) for the measured dynamic modulus values at 40°C. It was further noted by Birgisson et al. that there was only a difference of 0.2%–0.3% air voids between the center and the outer edges of the specimen, further

validating the legitimacy of using a 100 mm diameter by 150 mm high gyratory compacted specimen as opposed to a specimen sawed and cored to those dimensions.

2.6 Specimen Variability

Hills (1973) experimented with various compaction methods and their effects on creep. A gyratory compactor, impact hammer (Marshall Method), static, and rolling loads were used to compact the specimens, with the varying levels of compactive effort employed for the gyratory and Marshall methods. It was observed that the rolling compaction method yielded the lowest mix stiffness of all the compaction methods, with the gyratory compactor showing the highest mix stiffness for both compactive efforts. The compactive effort significantly affected the voids in the mix, but there seemed to be no direct correlation between voids and mix stiffness.

As previously mentioned (Mallick, Akter and Witczak, and Shook and Kallas), the volumetric properties can significantly affect the parameter that is being tested. In a round robin study by the University of Connecticut (Mahoney and Stephens 2003), trends were noticed in the type of SGC that was employed. Differences that are a result of the selection of the compactor can significantly affect the volumetric properties. This study found that a Pine AFG1A consistently yielded the lowest air void contents, and that a Troxler 4140 SGC generated the highest air void contents of the SGCs included in the round robin study. The sample size for this study was relatively limited, but showed that there is variation among the SGCs in use. Although this article did not directly pertain to Superpave^{TM} SPT, it does illustrate that the type of SGC used can have an influence on air voids, which plays a significant role in mix stiffness.

Azari et al. (2004) analyzed the effects of specimen homogeneity on the measurement of dynamic modulus and flow number. Eight specimens were procured that were homogeneous in composition and verified through x-ray computed tomography. Another eight specimens were procured that were inhomogeneous, where the bottom of the specimen was coarse graded and the top was fine graded. The specimens were tested at 21°C and 45°C with 10Hz frequency for the dynamic modulus test. It was found that there were no statistical differences between the means of the two groups at both temperatures. The listed rejection probabilities for the t-values were 17% and 90% for 21°C and 45°C, respectively, thus showing that there was not a significant statistical difference between the two groups. The inhomogeneous specimens were noted as having a higher degree of variability at both temperatures, but were not analyzed statistically.

Azari et al. found that there was no difference between the flow number results of the two groups and that the t-value corresponded to a 55% rejection probability.

Birgisson et al. (2005) examined the effects of specimen preparation on dynamic modulus results. Specimens were compacted in a 102 mm diameter mold and compacted to the test height. Another set of specimens included a 102 mm diameter specimen which was cored out from a 150 mm gyratory compacted specimen (it could not be determined whether the specimen was cut down to the testing height). Testing was conducted at 0.1, 1, 10, and 25 Hz at 40°C. Birgisson et al. found that differences in the two sample preparation methods ranged from 0.6%–1.9%. It was also noted when the data was plotted that the lines between the frequencies crossed, which implied that there was not a bias in the sample preparation method.

2.7 Test Variability

In addition to studying specimen geometry, Witczak et al. (2000), studied the repeatability of the testing through LVDT configuration and the number of specimens needed for testing. Based on dynamic modulus, phase angle, permanent deformation regression constants, and flow number testing, the recommendation was that three replicate specimens with four LVDTs be used per test. However, the configuration of the LVDTs was not given. It was found with this testing system that the standard error associated with the tests could be reduced to 10.0% for mixes with nominal maximum aggregate sizes (NMAS) of 25.0 mm or less.

2.8 Volumetric Sensitivity

A quarter fractional factorial experimental design was carried out by Anderson et al. (1998) to explore the effects of key mixture components on both volumetric and mechanical properties of mixes. The key mix components that were varied during testing included the following: asphalt content, fine gradation, coarse gradation, intermediate gradation, and the natural to crushed stone ratio. A baseline mixture was developed and the aforementioned mix components were varied based on typical production tolerances. In terms of the volumetric testing, asphalt content and fine gradation were identified as the prominent factors, along with several lower order interactions. As a result of the experimental design being a quarter fractional factorial, the lower order interactions could not be eliminated from the analysis and a single

variable could not be identified as a major contributor to the changes in volumetric properties of the mix. This was found to hold true for the mechanical testing that was performed. The mechanical tests that were employed included both the Repeated Shear Test (at constant specimen height) and Simple Shear, at various frequencies. The mechanical testing resulted in assorted interactions, but the asphalt content was the most prominent factor in the mix performance.

In a study of the data from WesTrack (Epps and Hand 2001), it was determined that changes in asphalt content and the percent passing the #200 sieve significantly affected the volumetric properties and the rut performance of the mix. Coarse-graded mixes indicated a higher sensitivity to decreases in asphalt content as measured by rutting at WesTrack than compared to that of fine-graded mixes. As expected, mixes that had higher than optimum asphalt content experienced significantly greater rutting. Finer mixes were found to be more sensitive to changes in the material passing the #200 sieve. With the typical standard deviations for asphalt content and percent passing the #200 stated as being 0.3% and 0.9%, respectively, there is considerable variation that can occur in material that is plant-produced. Having identified these sensitivities and taking into account the aforementioned variations, it was recommended that performance-based tests supplement the existing Superpave™ volumetric mix design system. It was suggested that these tests could be used to measure the potential variability of field-produced mixes.

CHAPTER 3. PROCEDURES

3.1 Materials Collection

As part of the current Design Guide, three replicate specimens are required for two tests that are conducted as part of the Superpave™ SPT. Three specimens should reduce the amount of error that is inherent in each test. Since flow number tests are destructive, a minimum of 12 specimens need to be procured per mix. However, 24 specimens were initially compacted for each mix design under the assumption that flow time would be stipulated as a Superpave™ SPT. As a result, the determination of the amount of material needed was as follows: each specimen weighs roughly 7000g; therefore, 24 specimens, multiplied by a factor of safety of roughly two, yields 327kg (720lb) of mix from each project sampled. This extra material could then be used for additional and supplemental testing as needed. K.L. Hoffman (2002) found that there were considerable differences between sampling from the truck and sampling from behind the paver. This study only showed that there were differences, which were highly correlated to the NMAS of the mix, but it does not point to one as being a better choice over the other. Truck sampling was noted as being more convenient, while materials sampled from behind the paver would be more representative of the in-situ pavement. For ease and time, materials were sampled directly from the back of the truck, in accordance with ASTM Standard D979 and D3665. In addition to the mix, the asphalt binder was also sampled so that the sensitivity of the binder in the Superpave™ SPT could be evaluated by adding asphalt binder to the sampled field mix. Five gallons of the liquid binder was found to be more than sufficient in procuring samples with additional asphalt binder for the testing required.

In addition to the collection of materials pertinent to each job, the job mix formula (JMF), a load ticket, and the pavement design for each job were obtained. This information was required for the analysis in later portions of this research project and aided in the identification of key variables in the designs that resist the two prominent distresses of permanent deformation and fatigue.

3.2 Specimen Preparation and Testing

Outlined below are the specimen preparation methods that were used to procure gyratory compacted specimens for testing. Methods used included the following:

- Sample splitting
- Maximum theoretical gravity determination
- Specimen compaction
- Specimen sawing/coring
- Bulk specific gravity determination
- Performance testing

3.2.1 Splitting

Loose mix that was sampled from each of the 20 jobs was heated to 143°C or 160°C for approximately 2 hours, depending on the level of traffic (>10million ESALs or ≤10million ESALs, respectively). Buckets contained roughly 27 kg (60 lbs) of mix and required splitting. Splitting was conducted in accordance with ASTM C702. Sample sizes included two 1250 g samples for maximum theoretical specific gravity (Gmm) testing for optimum and bumped binder contents, as well as 24 samples of approximately 7000 g for the two Superpave™ SPTs with different air voids and binder contents. The two Gmm samples were taken from separate buckets in order to obtain a representative sample of the mix being tested.

Special care was taken to ensure that a representative sample was prepared for each specimen. Krutz and Sebaaly (1993) noted that particularly coarse mixes tended to yield higher coefficients of variation when repeated and static triaxial tests were performed. The high coefficient of variation was attributed mainly to the segregation in the mix; therefore, great care was taken to minimize segregation when splitting coarser mixes.

3.2.2 Maximum Theoretical Specific Gravity (G_{mm})

Maximum theoretical specific gravity (Gmm) was conducted in accordance with AASHTO T209/ASTM D2041 for two 1250 g split samples for each job. The Gmm was used to determine the volumetric properties of the original gyratory compacted sample and the volumetric properties of the sample after it had been sawed/cored for performance testing.

3.2.3 Specimen Compaction

Specimens were compacted in a Pine AFGC125X SGC that can procure specimens in the dimensions of roughly 150 mm in diameter by 170 mm in height. Specimens were compacted to 4.0%, 7.0%, 10.0% air voids to fulfill the matrix previously presented. To obtain specimens at 4.0%, 7.0%, and 10.0% air voids, a correction factor was used to determine the weight needed to produce a specimen that had a height of 170 mm and was at the target air void percentage. WisDOT stipulates that specimens be compacted to Ndes; thus, a correction factor was not readily available for each mix. As a result, a typical value of 1.020 was used for each mix. Section 6.3 provides additional comments on correction factors.

3.2.4 Bulk Specific Gravity (G_{mb})

The bulk specific gravity was determined before and after the sawing/coring of the specimen. The testing was conducted in accordance with AASHTO T166/ASTM D2726. During the sawing/coring procedure, the specimen was exposed to a wet environment, as the saw blades and coring bit are water-cooled. The procedure for determining bulk specific gravity for a wet specimen calls for it to be dried at 52°C for a 24 hour period to ensure a constant dry weight. Unfortunately, at this temperature, the specimen could potentially undergo creep, thus changing the volumetrics and dimensions of the specimen—this was to be avoided. Lytton et al. (1993) found that the weight of a specimen in which the bulk specific gravity had been determined could change up to 25 g over a 15 day period. It appeared that, after two days of drying, the rate of weight change went asymptotical towards its true dry weight; the same trend was also found during this research project, as shown in Figure 3.1.

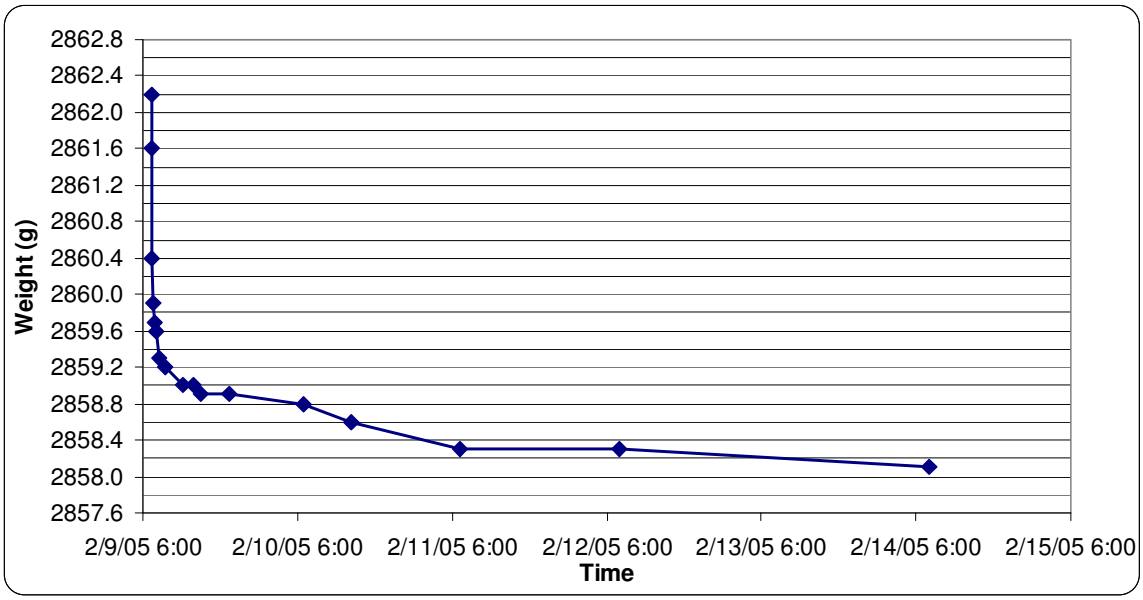

Figure 3.1. Changes in weight of specimen after G_{mb} determination

Figure 3.1 shows the change in weight of a specimen that was sawed/cored where the bulk specific gravity was immediately determined and the change in weight monitored over the proceeding days. As a result, the dry weights of the sawed/cored specimens were not determined until at least two days of drying had occurred. This precaution also mitigated the effects of water on test results, particularly at the intermediate temperature for the dynamic modulus testing. The submerged and saturated surface dry (SSD) weight was determined immediately after sawing/coring. The Draft Test Protocol in NCHRP 9-29 calls for the specimens to only deviate by ±0.5% from the target air void contents of 4.0%, 7.0% and 10.0%; however, this standard was relaxed to ±1.0% for this study (2001). The reason for this change was that there was variability in the HMA due to the fact that it was a field sample as opposed to a laboratory-batched specimen. The change was also intended to account for the lack of availability of a correction factor for each mix.

3.2.5 Specimen Cutting and Coring

The two diametrical ends of the specimen were sawed off using dual parallel diamond bladed saws that are water cooled, to yield a specimen with a cut height of 150 mm, with less than two degrees from absolute parallelism for the ends. There was a twofold reason for sawing off both ends: first, to remove high air void content areas from the specimen ends; second, to

provide a smooth and parallel surface, which mitigates the necessity of caps where caps add restraint to the specimen during testing (Bonaquist 2001). The Draft Test Protocol from NCHRP 9-19 calls for a 100 mm diameter specimen after coring. A coring machine with a diamond tip was used to obtain the 100 mm diameter specimen from the 150 mm gyratory specimen. The sawing and coring were done all-inclusive of a single piece of equipment.

3.3 Specimen Measurement

The specimen's diameters were measured at 0° and 90° of the third points and the mid-height, to constitute a total of six diameter measurements. The diameter measurements were averaged and the standard deviation determined. Per the NCHRP 9-29 Interim report, if the standard deviation of the diameter was greater than 2.5 mm, it was discarded. Measurements are reported to the nearest 0.1 mm. The height of the specimen was determined at 0°, 90°, 180°, and 270° and averaged. The only requirement on specimen height was that it should be between 148 and 152 mm.

3.4 Testing and Calculations

Outlined below are the testing procedures and calculations associated with the three Superpave™ SPTs. The three Superpave™ SPTs are dynamic modulus at intermediate temperature, dynamic modulus at high temperature, and flow number.

3.4.1 Dynamic Modulus

The testing procedure described herein is derived from NCHRP 9-29 Interim Report under the First Article Equipment Specification for the Flow Number Test Version 2.0 (September 26, 2001). This testing protocol has been referred to as Project 9-19 Draft Protocol A1: Dynamic Modulus of Asphalt Concrete Mixtures and Master Curves.

A 100-mm diameter by 150-mm high cylindrical specimen was tested under a repeated haversine compressive stress at two effective test temperatures unconfined. A Universal Testing Machine (UTM) 100 was used to conduct the testing with a temperature controlled testing chamber. The testing configurations for dynamic modulus are given in Table 3.1.

Table 3.1. Dynamic modulus testing configurations

	SPT for fatigue	SPT for rutting
Temperature	$T_{eff\ fatigue}$	$T_{eff\ rutting}$
Dynamic load	Induce 75-150 μ strain	Induce 75-150 μ strain
Loading rates	0.1 to 25 Hz	0.1 to 25 Hz

The effective fatigue and rutting temperatures are discussed in section 6.1.1. The dynamic load was determined based on the conditioning cycle which produced a corresponding pavement strain of 75-150 μ strain (Leslie Ann Myers, personal conversation, 2004).

There were a total of four different frequencies run at each temperature. These frequencies are stated in Table 3.2, along with the number of load cycles for each frequency.

Table 3.2. Cycles for test sequence

Frequency, Hz	Number of cycles
25	200
10	100
1	25
0.1	6

Testing was conducted from the higher to lower frequencies to mitigate the amount of deformation that is induced upon specimens during testing. The same specimen was tested throughout the duration of the testing procedure.

Three axial Linear Variable Differential Transducers (LVDTs) were affixed around the perimeter of the specimen to record the strain in the specimen over the length of the test. Witczak et al. (2002b) found that as the number of LVDTs and replicate specimens was increased, the standard error of the mean decreased. It should be noted that Witczak et al. found that the amount of error, however, was far more dependent upon the NMAS of the mix. The testing that was conducted as part of this study used only three LVDTs (because of the testing setup available from Shedworks) and three replicate specimens. The LVDTs were adjusted to the end of their linear range so as to keep the entire range available during the course of the application of the compressive stress.

The specimen was placed in the testing chamber until the effective test temperature was attained in the test specimen. The effective test temperature was found with the aid of a dummy

specimen with a temperature sensor embedded in the center. After the effective test temperature was reached, the specimen was then centered under the loading platens so as to not place an eccentric load on the specimen. The test was conducted in accordance with the aforementioned parameters in Tables 3.1 and 3.2.

There are four main calculations that are performed by the associated software. The first is the loading stress, σ_o, that is applied to the specimen during the test (Equation 3.1).

$$\sigma_o = \frac{\overline{P}}{A} \tag{3.1}$$

where:

σ_o = stress,
$\overline{P}$ = average load amplitude, and
A = area of specimen.

The recoverable axial strain from the individual strain gauges, ε_o, is determined as follows:

$$\varepsilon_o = \frac{\overline{\Delta}}{GL} \tag{3.2}$$

where:

ε_o = strain,
$\overline{\Delta}$ = average deformation amplitude, and
GL = gauge length.

Dynamic modulus, $|E^*|$ for each LVDT:

$$|E^*| = \frac{\sigma_o}{\varepsilon_o} \tag{3.3}$$

The final equation is to determine the phase angle, for each LVDT:

$$\phi = \frac{t_i}{t_p}(360) \tag{3.4}$$

where:

ϕ = phase angle,
t_i = average time lag between a cycle of stress and strain (sec), and
t_p = average time for a stress cycle (sec).

The software that was available for this project performed the above calculations. It reported the $|E^*|$ and the phase angle for all three LVDTs, as well as the permanent and resilient micro-strain and the applied stress for each load cycle.

3.4.2 Flow Number

The testing procedure described herein was derived from NCHRP 9-29 Interim Report under the First Article Equipment Specification for the Flow Number Test Version 2.0 (September 26, 2001). This testing protocol has been referred to as Project 9-19 Draft Protocol W1: Simple Performance Test for Permanent Deformation Based upon Repeated Load Test of Asphalt Concrete Mixtures.

A 100 mm diameter by 150 mm high cylindrical specimen was tested under a repeated haversine compressive stress at a single effective temperature, unconfined. UTM 100 and UTM 5 machines were used to conduct the tests, with a temperature-controlled testing chamber. The two machines were used due to the fact that the flow number test was the most time-intensive test. The load was applied for a duration of 0.1 sec and a dwell period of 0.9 sec. No design axial stress levels have been stipulated in the NCHRP 9-19 or 9-29 Protocols, but in discussions with Leslie Ann Myers a deviator stress of 600 kPa (87 psi) was found to be reasonable, which is analogous to the load used in the Superpave™ gyratory compactor (2004). Since no confining pressure was used, the axial stress is the deviator stress stated (600 kPa). The effective test temperature was considered the temperature at which permanent deformation would occur, which is equivalent to a seasonal correction throughout the year. The methodology for determining the effective temperature is found in section 6.1.1.

The strains for these tests were measured directly through the machine's actuator as opposed to affixing axial LVDTs to the sides of the specimen. Additionally, the LVDTs that were available for the dynamic modulus tests would not work for this test because they only had a range of 1 mm, whereas most specimens did not fail until at least 3–7 mm of permanent deformation occurred—well beyond the 1 mm range.

Specimens were placed in the testing chambers until the effective test temperature was obtained in the test specimens. This was found with the aid of dummy specimens with a temperature sensor embedded in the center. After the effective test temperature had been

reached, the specimen was then centered under the loading platens so as to not place an eccentric load on the specimen. The test was conducted in accordance with the aforementioned parameters.

The loading regime was applied to the specimens for a total of 15,000 continuous cycles or until the specimen failed and resulted in excessive tertiary deformation, whichever occurred first. Excessive deformation was considered 30,000μ strain. The exact length of the test was variable as it was contingent on the test temperature and the properties of the material tested.

There was a three step process for flow time calculation. The procedure consisted of (1) numerical calculation of the strain rate, (2) smoothing of the creep data, and (3) identification of the minimum smoothed creep rate, as this is where the flow number occurs. The following equation was used to determine the creep rate:

$$\frac{d(\varepsilon_p)_i}{dN} = \frac{(\varepsilon_p)_{i+\Delta N} - (\varepsilon_p)_{i-\Delta N}}{2\Delta N} \qquad (3.5)$$

where:

$\frac{d(\varepsilon_p)_i}{dN}$ = rate of change of strain with respect to cycles or creep rate at i cycle (1/cycle),

$(\varepsilon_p)_{i+\Delta N}$ = strain at i+ΔN cycles,

$(\varepsilon_p)_{i-\Delta N}$ = strain at i-ΔN cycles, and

ΔN = number of cycles sampling points.

The next step required that the data be smoothed through a running average of five points. Creep rates before and after as well as the creep rate at that instant were used. Equation 3.6 was used to determine the smoothed creep rate.

$$\frac{d\varepsilon_i'}{dN} = \frac{1}{5}\left(\frac{d\varepsilon_{i-2\Delta N}}{dN} + \frac{d\varepsilon_{i-\Delta N}}{dN} + \frac{d\varepsilon_i}{dN} + \frac{d\varepsilon_{i+\Delta N}}{dN} + \frac{d\varepsilon_{i+2\Delta N}}{dN}\right) \qquad (3.6)$$

where:

$\frac{d\varepsilon_i'}{dN}$ = smoothed creep rate at i sec (1/cycles),

$\frac{d\varepsilon_{i-2\Delta N}}{dN}$ = creep rate at i-2ΔN cycles (1/cycles),

$\frac{d\varepsilon_{i-\Delta N}}{dN}$ = creep rate at i-ΔN cycles (1/cycles),

$\frac{d\varepsilon_i}{dN}$ = creep rate at i cycles (1/cycles),

$\frac{d\varepsilon_{i+\Delta N}}{dN}$ = creep rate at i+ΔN cycles (1/cycles), and

$\frac{d\varepsilon_{i+2\Delta N}}{dN}$ = creep rate at i+2ΔN cycles (1/cycles).

The final step was to determine the cycle where the minimum creep rate occurred in the data set. If no minimum occurred during the test, then the flow number was reported as being greater than or equal to the number of loads applied during the course of the test. When several minimum creep rates occurred in a data set, then the first minimum value was reported as the flow number.

3.4.3 Testing Durations

Table 3.3 shows the durations of each of the activities associated with the Superpave™ SPT Protocol. This table shows time requirements, not only for the individual specimen testing, but also for one job and for the entire Superpave™ SPT conducted for this research project. Several of these activities can be done in parallel, with multiple samples.

Table 3.3. Durations for SSPT preparation and testing (NCHRP 465, 2002b)

Laboratory activity		**Estimated time for one prepared specimen**	**Estimated time for one job[1]**	**Estimated time for all testing**
Sample preparation	Heating up	2 hrs	2 hrs	40 hrs
	Splitting	2 min	2 hrs	40 hrs
	G_{mm} testing	4 hrs	4 hrs	80 hrs
	Aging	2 hrs	2 hrs	40 hrs
	Compaction	5 min	2 hrs	40 hrs
	Extraction	2.5 min	1 hr	20 hrs
	Run G_{mb}	6 min	2.4 hrs	48 hrs
	Sawing and coring	30 min	12 hrs	240 hrs
	Run G_{mb}	6 min	2.4 hrs	48 hrs
	Measure specimen	2 min	40 min	13.3 hrs
	Total setup time	**1.3 hrs**	**30.5 hrs**	**609.3 hrs**
Specimen preparation	Glue studs	2 min	2 hrs	40 hrs
	Mount LVDT brackets	2 min	2 hrs	40 hrs
	Condition specimens	6-8 hrs	6-8 hrs	120-160 hrs
	Affix LVDTs	2 min	2 hr	40 hrs
	Total preparation time	**6-8 hrs**	**12-13 hrs**	**240-280 hrs**
SPT	Dynamic modulus / one temperature	20 min	2 hrs	40 hrs
	Dynamic modulus / all temperatures	6 hrs	10 hrs	20 days[2]
	Flow number	30-180 min	3-12 hrs[3]	60-240 hrs
	Total testing time	**1-4.3 hrs**	**13-22 hrs**	**260-440 hrs**

[1]Based on a total of 24 specimens procured per job with only 3 test specimens per SSPT.
[2]Time is based on two different test temperatures being conducted.
[3]Assumes two testing machines.

CHAPTER 4. PROJECTS SAMPLED

4.1 Experimental Plan Changes

It was realized that some experimental cells could not easily be filled upon contacting and setting up jobs to sample that were applicable to the first iteration of the experimental plan for this project. The WisDOT does specify a 25.0 mm mix, but this mix is reserved mainly for new construction as a base material. In working with both state agencies and contractors in Wisconsin, it was found that 25.0 mm mixes are rare regardless of the traffic volume; in fact, to our knowledge, only two were paved during the 2004 construction season. One 25.0 mm mix was completed before the research team was aware of the mix being placed and the other was an open-graded mix that was substituted for a dense-graded mix in the experimental matrix. The other problem identified was finding open-graded mixes that fit the proposed experimental matrix. Only one open-graded mix (12.5 mm SMA) was found and sampled. Another open-graded HMA mixture (19.0 mm) was sampled in the summer of 2005. It should also be noted that WisDOT only specifies gradation requirements for 9.5 and 12.5 mm SMA mixes. As a result, some modifications had to be made to the experimental matrix. Instead of deleting jobs that could not be found, the jobs were reallocated to other portions of the matrix, thus maintaining the overall number of jobs for the research project as well as making the subsequent analysis more robust. The updated matrix can be found in Table 4.1.

Table 4.1. Revised project matrix

Nominal maximum aggregate size	Mix type	Traffic level			
		E-0.3	E-1	E-3	>E-3
25.0mm	Dense				
	Open			X	
19.0mm	Dense	X	XX	XXX	XXX
	Open				X
12.5mm	Dense	XX	XX	XXX	XXX
	Open				X

The “E” presented in Table 4.1 is for equivalent single axle loads (ESALs) and is the standard by which the load spectrum is normalized for highway design.

4.2 Sampled Projects

Projects were sampled throughout the state of Wisconsin during the summer 2004 and 2005 construction seasons. Sampling materials from across the state represented a better cross-section of the materials that were used during the season. However, most high traffic volume projects were found in the southern regions of Wisconsin, whereas lower traffic volumes could be found all around the state. This was mainly due to the population distributions and the location of major trunk lines throughout the state. Figure 4.1 illustrates the locations of mixes that were sampled for this particular project, whereas Appendix A: Project JMFs contains all of the material properties related to these jobs.

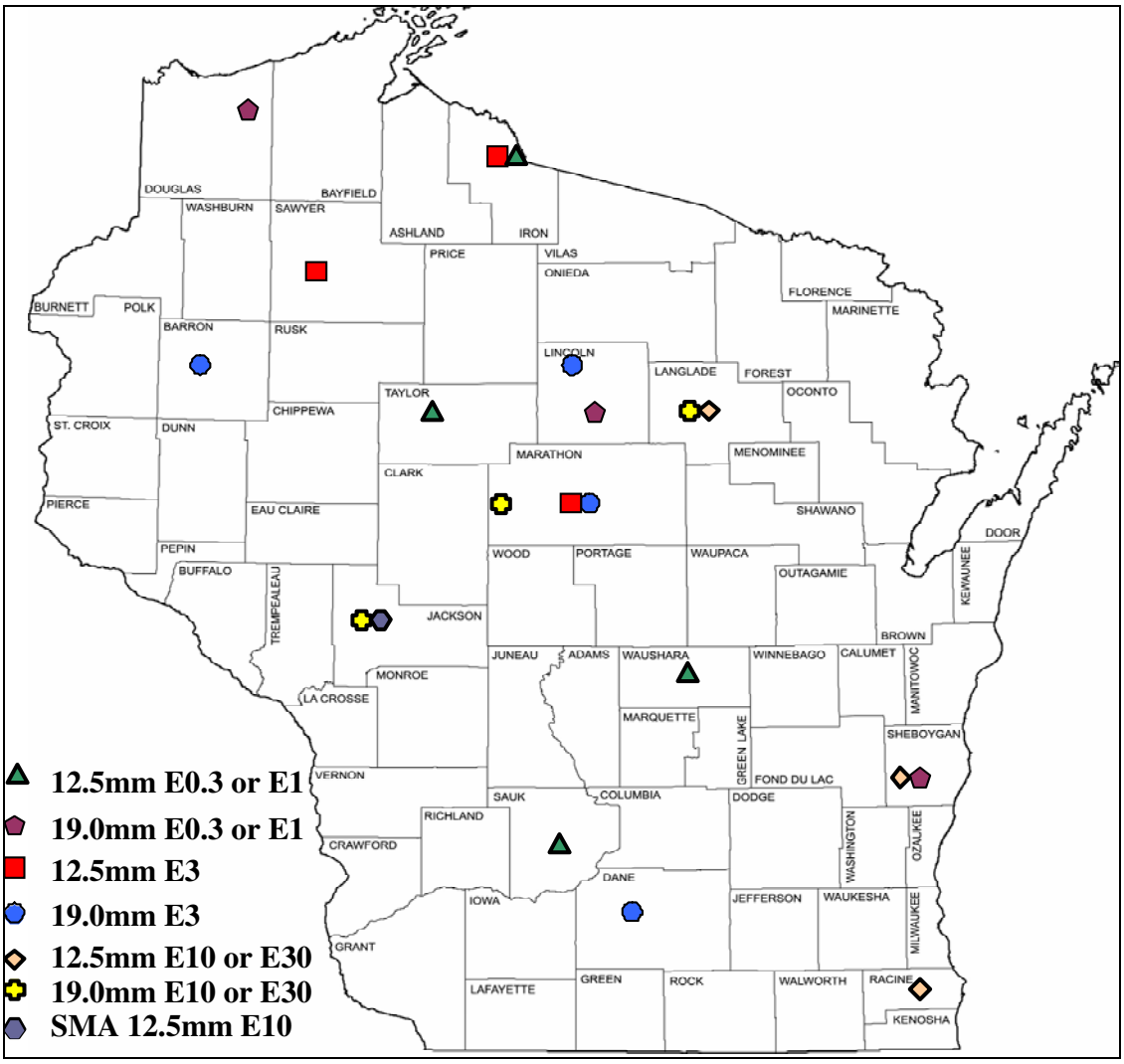

Figure 4.1. Project locations (prepared by Demographic Services Center, Wisconsin Department of Administration and the Wisconsin State Cartographer's Office)

It is worth observing that the sampling that was conducted as part of this project went smoothly for every job. The contractors, consultants, and the WisDOT officials were all extremely helpful during this sampling process. These people are recognized in the acknowledgements section at the beginning of this document.

4.3 Sampling

As previously mentioned, sampling was conducted at the plant site, just after trucks had been loaded out. Figure 4.2 shows a truck being loaded out.

Figure 4.2. Truck being loaded out

The truck then pulls up to the sampling rack where it receives its load ticket and the materials can be sampled from the back of the truck. Figures 4.3 and 4.4 show examples of a sampling rack and the methodology used when sampling materials from the back of a truck, respectively.

Figure 4.3. Sampling rack

Figure 4.4. HMA sampling

All except one job was sampled from the back of the truck. The one exception was a job that was sampled by a method of creating a mini-stockpile from material run through the reject chute of the hot mix plant.

A total of twelve 5-gallon pails of the HMA were obtained from each job. Samples procured from the back of the truck were taken from 12 different locations so as to obtain a representative sample of the mix being produced. The surface layer was scraped off in an effort

to minimize the amount of segregated material being sampled, since the coarser fraction of the HMA will tend to roll down the sides of the pile, leaving the finer fraction at the top of the pile (Dukatz 1996). However, underneath the surface layer is an ideal representation of the material. For the HMA sampled from the mini-stockpile, locations were selected from the base to the top of the pile and around its perimeter, while keeping in mind the different strata of the stockpile. The bottom of pile comprises the greatest percentage of the material; hence, the greatest percentage of the material was sampled from this location.

Figure 4.5 illustrates the composition of a cone stockpile in terms of its percentages with height.

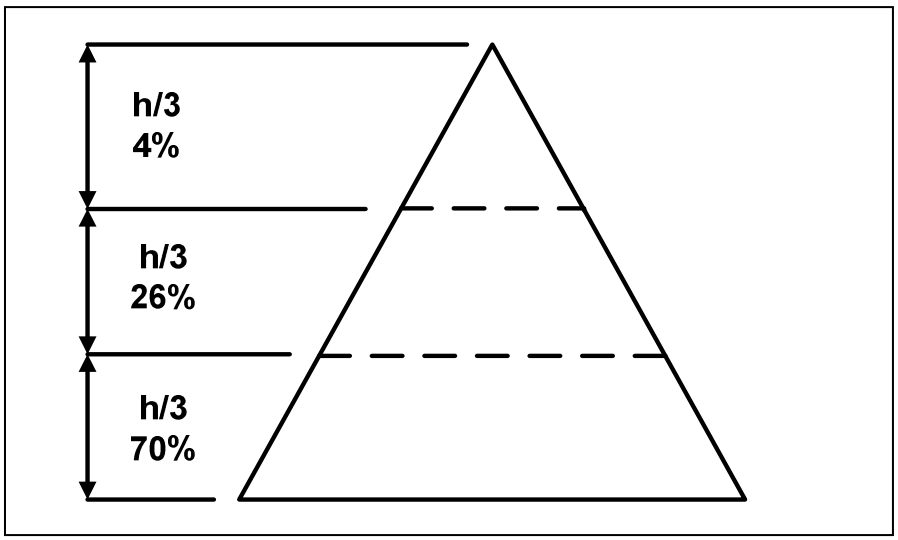

Figure 4.5. Stockpile cone proportions

Materials were brought back from the various plant sites and stored either in the Water Resources Building or in the basement of Dillman Hall at Michigan Technological University prior to sample preparation.

CHAPTER 5. SAMPLE PREPARATION

5.1 Sample Preparation Flowchart

Figure 5.1 depicts the sample preparation activities. The following sections discuss the procurement of quality samples that are representative of the mix that was sampled and paved during the 2004 construction season.

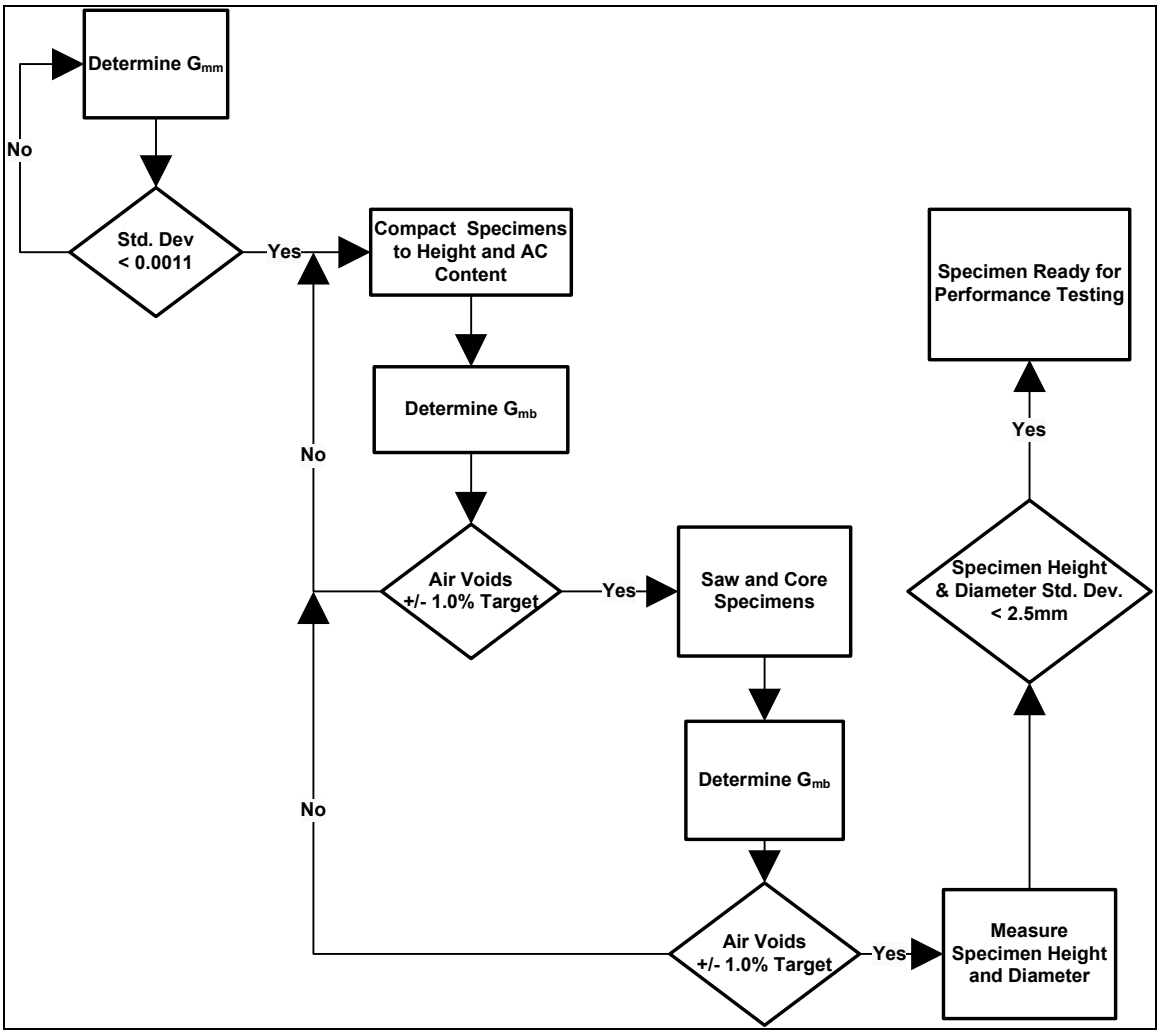

Figure 5.1. Sample preparation flow chart

5.2 Maximum Theoretical Specific Gravity

The maximum theoretical specific gravity (G_{mm}) was determined by AASHTO T209/ASTM D2041. The precision outlined in the specification states that the single-operator is 0.0011 for two standard deviations, which represents "the difference between the results of two properly conducted tests" (ASTM, 2003). These guidelines are based upon laboratory-prepared specimens, where the aggregate gradations are closely monitored. For this study, there was significantly less control over what was in the sample as there would have been for a field mix. Every attempt was made to obtain a representative sample by means of quartering, thus mitigating the differences between samples. In reviewing the standard deviations of the two G_{mm} samples for each project, it was found that all except one mix fell within the single-operator precision. The standard deviation for this particular mix was 0.0158, but this was for the SMA, which had a tendency to segregate. It was determined that the difference was not significant enough to warrant further testing. Considering the nature of the samples (field mix), the results are acceptable for the work conducted in this study. Table 5.1 shows the mean and standard deviations for each of the projects.

Table 5.1. G_{mm} Mean and standard deviation for each project

Project	Optimum AC			Optimum +0.3% AC		
	Mean G_{mm}	Std. Dev.	COV(%)	Mean G_{mm}	Std. Dev.	COV (%)
Baraboo E-0.3 12.5mm	2.486	0.0052	0.21	2.474	0.0005	0.02
Medford E-1 12.5mm*	2.502	0.0032	0.13	2.489	0.0119	0.48
Wautoma E-1 12.5mm*	2.532	0.0086	0.34	2.521	0.0036	0.14
Hurley E-0.3 12.5mm*	2.498	0.0058	0.23	2.476	0.0100	0.40
Hayward E-3 12.5mm	2.543	0.0069	0.27	2.483	0.0082	0.33
Wausau E-3 12.5mm*	2.450	0.0009	0.04	2.436	0.0073	0.30
Hurley E-3 12.5mm*	2.484	0.0048	0.19	2.472	0.0050	0.20
Antigo E-10 12.5mm	2.551	0.0051	0.20	2.492	0.0038	0.15
Plymouth E-10 12.5mm	2.588	0.0005	0.02	2.581	0.0013	0.05
Racine E-10 12.5mm*	2.510	0.0086	0.34	2.486	0.0039	0.16
Northfield E-10 12.5mm SMA	2.517	0.0158	0.63	2.504	0.0035	0.14
Cascade E-1 19.0mm	2.578	0.0083	0.32	2.554	0.0056	0.22
Bloomville E-1 19.0mm	2.521	0.0015	0.06	2.505	0.0006	0.02
Brule E-0.3 19.0mm*	2.569	0.0086	0.34	2.553	0.0012	0.05
Waunakee E-3 19.0mm*	2.511	0.0025	0.10	2.495	0.0035	0.14
Mosinee E-3 19.0mm*	2.445	0.0043	0.18	2.438	0.0001	0.004
Cumberland E-3 19.0mm*	2.586	0.0069	0.27	2.572	0.0136	0.53
Antigo E-10 19.0mm	2.535	0.0031	0.12	2.521	0.0075	0.30
Northfield E-10 19.0mm	2.505	0.0015	0.06	2.493	0.0006	0.02
Tomahawk E-3 25.0mm*	2.560	0.0118	0.46	2.529	0.0111	0.44
Wisconsin Rapids E-10 19.0mm	2.581	0.0055	0.21	2.576	0.0086	0.33

*Utilized RAP in the mix

Of the 21 mixes presented in Table 5.1, recycled asphalt pavement (RAP) constituted a portion of the aggregate mixture in 11 mixes. RAP is inherently variable in nature, due to the fact that one stockpile can constitute several sources and that each source has a unique gradation, depth of milling, binder content, and age. These factors all contribute to the variability in field samples and can additionally explain some of the inconsistency in the G_{mm} samples and the comparisons that are made later in this section with that of the contractor's G_{mm} determination.

As expected, the G_{mm} decreased with an increase in asphalt content due to the fact that asphalt binder has a lower specific gravity (~1.020–1.030) than aggregate (~2.600–2.700,

depending on the aggregate source). When additional asphalt binder was added to the mix, the percentage of the aggregate correspondingly decreased. The aggregate had a higher specific gravity and, since there was a slightly smaller proportion of aggregate once asphalt binder had been added to the mix, the specific gravity decreased.

The measured standard deviation appears to be insensitive to the NMAS with the testing that was conducted. This indicates that the variability in the test results was not contingent on the NMAS of the mix.

A comparison was made between the MTU and the contractor's G_{mm} supplied in the JMF for both the optimum and asphalt cement bump. Figures 5.2 and 5.3 reflect both of the G_{mm}s, respectively.

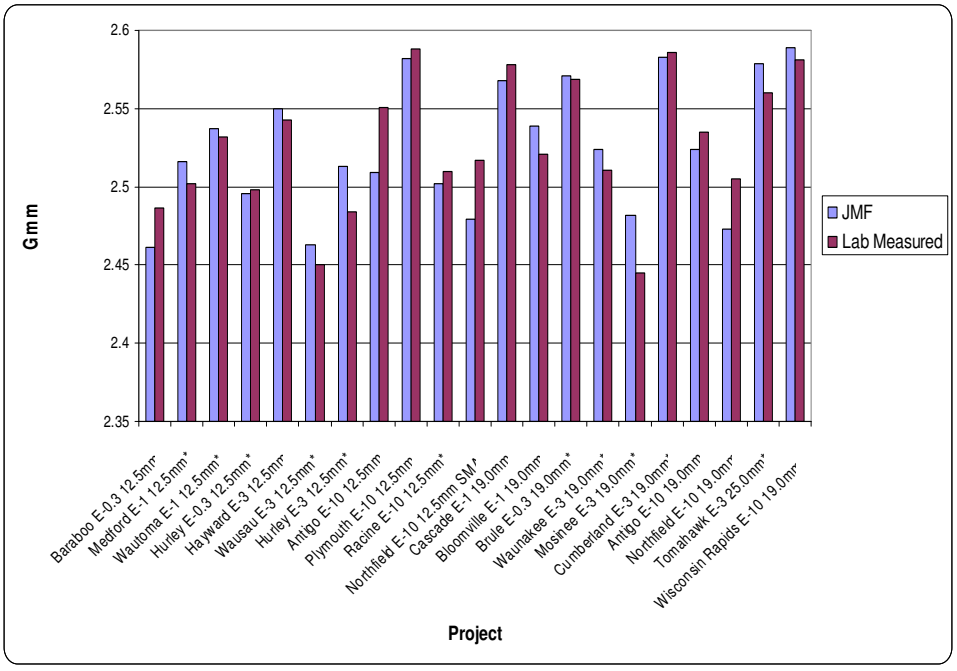

*Utilized RAP in the mix

Figure 5.2. MTU and contractor G_{mm} optimum asphalt binder content

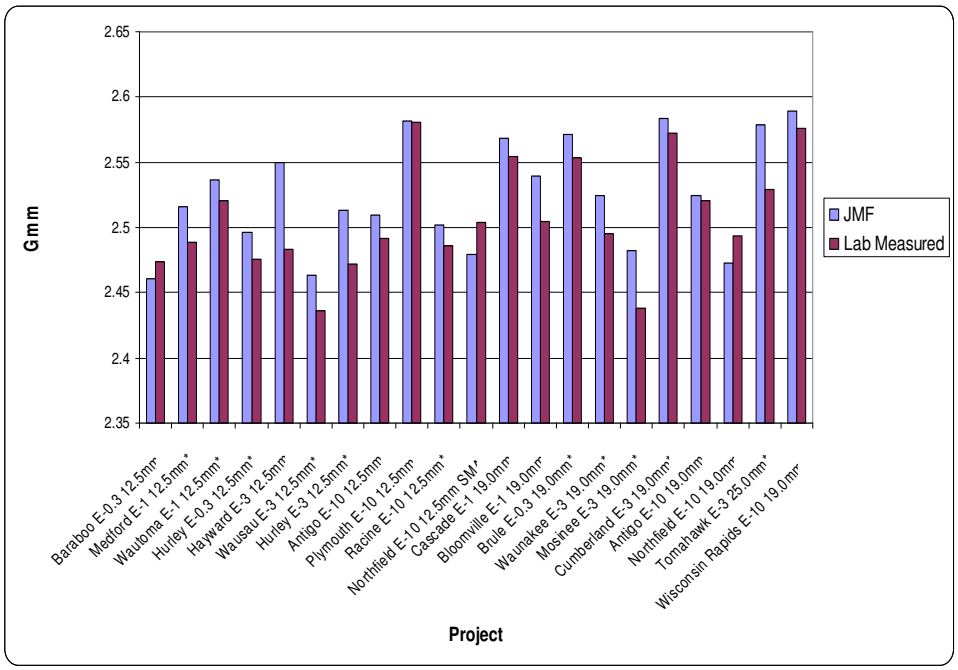

*Utilized RAP in the mix

Figure 5.3. MTU and contractor G_{mm} +0.3% optimum asphalt binder content

There were some differences between the MTU- and contractor-determined G_{mm}, as seen in Figures 5.2 and 5.3. Some, in fact, do not fall within the multilaboratory precision of 0.0190 as outlined in AASHTO T209. There are several possible explanations for these differences, in addition to the RAP component. One reason for the difference lies in the fact that the samples were from the field, which means there are numerous sources where both variability and segregation can occur. Every effort was made to obtain representative samples both from the back of the truck and during the sample reduction process, but the processes prior to these steps could not be controlled. A second possible reason is that there could have been changes in mix design that deviate from the JMF. These changes are made when issues arise during the lay down of the HMA. A third reason could be that the asphalt binder content in the sampled mix is higher than that of the binder content stated in the JMF; this will be commented on later in this section.

A regression analysis was conducted on the G_{mm} from MTU and the G_{mm} from the contractor for both optimum asphalt binder content and asphalt binder content with an increase of 0.3 percent. A simple linear regression was developed between the two datasets and the p-values for the slopes and intercepts were analyzed. If the two datasets were truly equal, the intercept would equal zero and the slope would equal one, indicating unity. For the optimum

asphalt binder content, the p-value for the intercept equal to zero was 0.25 and for the slope equal to one was 0.29 (coefficient of correlation = 0.87). For the asphalt binder content increase of 0.3%, the p-value for the intercept equal to zero was 0.11 and for the slope equal to one was 0.25 (coefficient of correlation = 0.86). Thus, it was reasonable to assume that the G_{mm} measurements were equal.

5.3 Compaction

In Wisconsin, HMA mix designs are based on compacting specimens to N_{des}; thus, the air voids of the specimen can be directly measured via the AASTHO T166/ASTM D2726 method. This presents a problem because in order to compact the specimens to height, a correction factor is needed. The ratio of the estimated G_{mb} to that of the measured G_{mb} constitutes the correction factor; thus, a specimen must either be compacted to N_{max} or a correction factor must be estimated for each mix. To save time on sample preparation, a correction factor was estimated. Drawing from previous knowledge with HMA, a typical range for correction factor is 1.01 to 1.03; thu,s an estimate of 1.02 was used for the correction factor of each mix. In examination of the actual correction factors, there was a range from 1.011 to 1.022, so in some instances the estimate was slightly conservative. However, this did not significantly affect the measured air voids of the compacted specimens, as will be shown in section 5.4.

All specimens for this project were compacted using a Superpave™ Gyratory Compactor (SGC) model AFGC125X; this machine was selected because of its familiarity and higher production. The gyratory compactor was fully calibrated to ensure that the specimens were compacted at an angle of 1.25° with a pressure of 600 kPa and that the height was being measured properly. The calibration was again verified halfway through specimen production to ensure that specimens were undergoing similar compaction processes.

The specimens were split according to the weights required to produce a specimen that was compacted to approximately 170.0 mm at the targeted air voids. These weights were determined from the G_{mm} test results and the guidance outlined in TAI's SP-2 (1996). The optimum +0.3% asphalt binder content specimens were split first so that they were up to the proper temperature for mixing. The other 18 samples were then split and placed back in the convection oven at the prescribed temperature. The six specimens were then mixed with the +0.3% asphalt binder content and placed in the convection oven. Specimens were compacted in

the order of 7.0%, 4.0%, and 10.0% air voids at the optimum binder content followed by the optimum +0.3% asphalt binder content specimens to 7.0% air voids.

Specimens were then left to cool until room temperature was reached; at that time they were labeled and prepared for G_{mb} testing. Figure 5.4 shows 360 of the 456 specimens that have been prepared for this study; the specimens are two deep.

Figure 5.4. Prepared gyratory specimens

The 12.5 mm SMA mix from Northfield was not compacted, as creep is a problem with this particular mix.

5.4 Bulk Specific Gravity of Gyratory

The G_{mb} of all the gyratory specimens was determined after they were allowed to cool to room temperature (25°C). There was a noticeable variability in the measured G_{mb} and the determined air voids for specimens from the same job compacted to the same target air void content. This was likely attributable to the variability in the constituent properties of the mix from either the mixing, sampling, or splitting processes. As stated in section 3.2.5, an initial criterion of specimen acceptance for air voids, as stipulated by NCHRP 9-29, was ±0.5% air

voids from the target for mix design purposes. This specification was relaxed for this study to account for the aforementioned sources of variability. The new specification was set at ±1.0% air voids from the target. This was based on the gyratory compacted specimen. It was anticipated that the air voids would not change significantly after sawing and coring, but these attributes are measured directly, without cutting the sample. Hence, this specification only applied to the gyratory compacted specimens. All volumetric data for the specimens used in this project can be found in Appendix B: Specimen Volumetrics.

The general trend that was realized during the bulk specific gravity testing of the gyratory specimen was as follows:

- At 10.0% target air voids, the specimens had a lower than desired air void content
- At 7.0% target air voids, the specimens tended to be on target
- At 4.0% target air voids, the measured air voids were higher than desired.

The number of gyrations for the 10.0% air voids tended to be in the range of 5–20 gyrations. After the gyratory compactor reached the predetermined height, based on sample weight and the G_{mm}, the gyratory compactor still applied a load to square the specimen. As a direct result, the specimen underwent further compaction and was typically found to be 1.5 mm. This further compaction decreased the air voids, whereas if the specimen had been compacted to the desired height, the desired air voids might have been obtained. The 4.0% air void specimens tended to be undercompacted. The reason for this trend was not readily apparent, but a vast majority of the specimens fell within the constraints of the target air voids. Any specimens that did not fall within the range of ±1.0% air voids of target were not included in the experimental plan.

As previously mentioned, it was anticipated that the air voids would not change significantly in the specimens after they had been sawed/cored, except for the mixtures that were coarse-graded and had large surface voids on the compacted specimens. The only jobs that were believed to have significantly different air voids were the Northfield E-30 19.0 mm and the Tomahawk E-3 25.0 mm mixtures, which showed air voids significantly lower than targeted. In addition, a large quantity of water drained out of this specimen when removed from the water tank during bulk specific gravity testing.

5.5 Volumetrics of Sawed/Cored Test Specimens

The volumetric properties of the sawed/cored test specimens can be found in Appendix C. Only three mixtures are reported, as these were the three that were tested for this project. To comment on the volumetrics of the Northfield mix, this mix was extremely coarse and had significant surface and interconnected voids. In addition, it was observed that water was draining out of the Northfield mix during the SSD method of air void determination. It was believed that these voids led to the low air void determination as found by the SSD method. To address this issue, it would have been beneficial to run the Corelok on the compacted gyratory specimen, but the specimen did not fit in the Corelok's chamber. The Corelok determines the bulk specific gravity of a specimen through the use of a vacuumed bag. The sawed/cored specimens were, however, run through the Corelok machine, as they did fit in the chamber. It was found that there was no difference in the air voids of the specimen when compared to that of the saturated surface dry (SSD) method. The most probable reason for this result was that the sawed/cored specimen did not have the same surface irregularities as its compacted counterpart. In the later plots and analysis, the air voids on the Northfield job were lower than the target values of 4.0%, 7.0%, and 10.0%, but it was felt that the differences were negligible, as the general trends in the data are present.

The air voids of the sawed/cored specimens were slightly lower than that of the gyratory measured air voids. The decrease was typically by about 0.5% to 1.0% air voids. These changes are not significant and if the test air voids are to be specified for performance testing phase instead of the gyratory air voids, this would increase the complexity of the mix design process. The correction factors for the three mixes are presented in the Appendix C: Specimen Volumetrics after Sawing/Coring.

CHAPTER 6. WISCONSIN MIX TESTING

6.1 Jobs Tested

The tests were conducted per the outlined parameters according to Robinette 2005 and NCHRP Report 465. This chapter discusses all of the mixtures that have been tested.

The test results for the intermediate and high temperature dynamic modulus and flow number can be found below in the following sections. Before proceeding, the phase angle variations in the test data warrant comment. The phase angle for the 0.02 and 25.0 Hz frequencies at the high test temperatures exhibited the highest coefficient of variation (COV) in the data sets; this was once again believed to be caused by the compliance issues with the testing machine and its inability to properly apply the desired stress level. During testing, the phase angle was not of the greatest interest since the dynamic modulus was the direct input into the Design Guide software. Contained herein are the results from the dynamic modulus and flow number testing as well as an analysis of the Design Guide software as it pertains to the tested mixtures.

6.2 Dynamic Modulus Loading Stress

All of the testing parameters have been discussed in Section 6.1, except for the axial stress that was applied to the specimen. The reason for this is that the axial stress that yielded 75-125 μm strain needed to be determined for both the intermediate and high test temperatures through iterative testing. The same stress was used for each of the frequencies, except at the high temperature for 25.0 Hz, for which an axial stress of 69 kPa was actually used. This was due to the capacity of the machine; at the high frequency, the testing machine was not able to apply the programmed load and it would frequently apply approximately a zero load, leading to obviously erroneous results. To overcome this obstacle, the axial load for only this frequency was increased. This frequency was carefully monitored to ensure that the excessive permanent axial micro-strain was not imparted during testing. This deficiency in the axial stress was probably another cause for inaccurate phase angle measurements at the high temperature.

6.3 Dynamic Modulus and Dynamic Creep Test Results

Contained in this chapter are the results of the dynamic modulus and dynamic creep testing as they pertain to the development of the library of values. Also, the validity of the hypotheses put forth in Section 1.5.1 will be verified. The effects of temperature, air voids, asphalt binder content, and traffic level will be discussed further in the ensuing subsections. Statistical Analysis Software (SAS) was used to determine the effects of temperature, air voids, asphalt binder content, NMAS, gradation, and traffic level. The general linear model (GLM) using a 95% level of confidence ($\alpha = 0.05$) was used to determine if the above factors affect flow number, accumulated microstrain at flow number, and dynamic complex modulus. The GLM provides a Type I and Type III sum of squares error using an F-statistic and p-value, which is analogous to performing a multiple analysis of variance (ANOVA). Multiple comparison using least squares difference (LSD) t-tests were performed on air voids, traffic level, binder content, and temperature to determine if there were statistical differences within a given factor. A 95% level of confidence was used for the multiple comparison procedure.

The following subsections, 6.3.1 through 6.3.21, summarize the test data for each project. Subsection 6.3.22 summarizes the pooled data by NMAS, including traffic level, air void level, and binder content level, in Tables 6.22 through 6.32.

6.3.1 Brule

Table 6.1. Dynamic modulus and creep testing for the Brule mixture

								E* (MPa)				Dynamic Creep Testing		
Project	NMAS	Gradation	Traffic	Air Voids	Binder Content	Test Temperature (°C)	Test Statistic	0.1 Hz	1.0 Hz	10.0 Hz	25.0 Hz	FN	Min. Slope	Accumulated Strain at FN
Brule	19	Dense	300000	4%	Optimum	16.6	Mean	1711.9	4513.5	11374.3	18456.8	N/A	N/A	N/A
							Std. Dev.	321.1	872.5	1470.0	2794.6	N/A	N/A	N/A
							COV, %	18.8%	19.3%	12.9%	15.1%	N/A	N/A	N/A
						35.5	Mean	474.8	800.0	2381.5	3849.8	140.7	45.3	10913.0
							Std. Dev.	10.2	54.4	174.9	492.4	18.9	4.1	947.6
							COV, %	2.1%	6.8%	7.3%	12.8%	13.5%	8.9%	8.7%
				7%	Bump	16.6	Mean	1330.3	3762.8	10394.8	18857.1	N/A	N/A	N/A
							Std. Dev.	71.6	474.5	461.9	2398.7	N/A	N/A	N/A
							COV, %	5.4%	12.6%	4.4%	12.7%	N/A	N/A	N/A
					Bump	35.5	Mean	426.4	697.3	1998.9	2991.9	74.0	165.4	16647.3
							Std. Dev.	64.7	87.1	161.9	347.4	10.0	17.1	1172.5
							COV, %	15.2%	12.5%	8.1%	11.6%	13.5%	10.3%	7.0%
				7%	Optimum	16.6	Mean	1438.1	3768.3	8756.4	15191.1	N/A	N/A	N/A
							Std. Dev.	83.8	639.3	1292.3	3973.6	N/A	N/A	N/A
							COV, %	5.8%	17.0%	14.8%	26.2%	N/A	N/A	N/A
					Optimum	35.5	Mean	383.4	617.7	1984.1	3090.8	75.7	135.8	14743.7
							Std. Dev.	68.0	86.7	185.2	682.0	10.4	12.9	592.0
							COV, %	17.7%	14.0%	9.3%	22.1%	13.8%	9.5%	4.0%
				10%	Optimum	16.6	Mean	1114.0	2878.4	7305.7	15268.7	N/A	N/A	N/A
							Std. Dev.	191.4	654.7	1454.2	1990.2	N/A	N/A	N/A
							COV, %	17.2%	22.7%	19.9%	13.0%	N/A	N/A	N/A
					Optimum	35.5	Mean	290.7	476.2	1370.2	2287.6	37.3	398.2	18501.0
							Std. Dev.	31.7	47.2	114.7	322.5	2.9	53.1	727.5
							COV, %	10.9%	9.9%	8.4%	14.1%	7.7%	13.3%	3.9%

6.3.2 Baraboo

Table 6.2. Dynamic modulus and creep testing for the Baraboo mixture

								E* (MPa)				Dynamic Creep Testing		
Project	NMAS	Gradation	Traffic	Air Voids	Binder Content	Test Temperature (°C)	Test Statistic	0.1 Hz	1.0 Hz	10.0 Hz	25.0 Hz	FN	Min. Slope	Accumulated Strain at FN
Baraboo	12.5	Dense	300000	4%	Optimum	19.0	Mean	1794.4	4243.8	9776.4	15882.7	N/A	N/A	N/A
							Std. Dev.	263.6	796.0	1859.4	1313.5	N/A	N/A	N/A
							COV, %	14.7%	18.8%	19.0%	8.3%	N/A	N/A	N/A
						36.6	Mean	464.1	820.8	2573.4	4471.9	154.0	70.6	15847.3
							Std. Dev.	41.4	58.9	290.6	755.4	8.7	6.8	1410.2
							COV, %	8.9%	7.2%	11.3%	16.9%	5.6%	9.6%	8.9%
				7%	Bump	19.0	Mean	939.9	2429.9	5796.6	8230.8	N/A	N/A	N/A
							Std. Dev.	69.4	67.6	253.4	478.2	N/A	N/A	N/A
							COV, %	7.4%	2.8%	4.4%	5.8%	N/A	N/A	N/A
					Bump	36.6	Mean	273.4	495.4	1599.3	2769.5	87.3	186.0	21532.3
							Std. Dev.	22.2	32.5	226.4	700.0	11.5	32.7	1268.4
							COV, %	8.1%	6.6%	14.2%	25.3%	13.2%	17.6%	5.9%
				7%	Optimum	19.0	Mean	1386.5	3491.6	8003.0	12959.8	N/A	N/A	N/A
							Std. Dev.	93.5	318.3	887.4	1503.8	N/A	N/A	N/A
							COV, %	6.7%	9.1%	11.1%	11.6%	N/A	N/A	N/A
					Optimum	36.6	Mean	380.6	687.5	2040.9	3244.3	79.0	159.5	16808.3
							Std. Dev.	3.4	54.2	160.5	492.3	13.2	36.5	1298.0
							COV, %	0.9%	7.9%	7.9%	15.2%	16.7%	22.9%	7.7%
				10%	Optimum	19.0	Mean	997.1	2435.7	5978.1	9570.8	N/A	N/A	N/A
							Std. Dev.	45.3	36.7	684.4	2475.9	N/A	N/A	N/A
							COV, %	4.5%	1.5%	11.4%	25.9%	N/A	N/A	N/A
					Optimum	36.6	Mean	256.4	441.0	1421.7	3103.9	45.7	336.6	19178.3
							Std. Dev.	42.4	55.4	130.3	453.4	2.9	47.8	1966.5
							COV, %	16.5%	12.6%	9.2%	14.6%	6.3%	14.2%	10.3%

6.3.3 Hurley

Table 6.3. Dynamic modulus and creep testing for the Hurley mixture

								E* (MPa)				Dynamic Creep Testing		
Project	NMAS	Gradation	Traffic	Air Voids	Binder Content	Test Temperature (°C)	Test Statistic	0.1 Hz	1.0 Hz	10.0 Hz	25.0 Hz	FN	Min. Slope	Accumulated Strain at FN
Hurley	12.5	Dense	300000	4%	Optimum	16.6	Mean	1504.1	3664.2	8014.3	10979.6	N/A	N/A	N/A
							Std. Dev.	276.6	535.3	950.8	1802.7	N/A	N/A	N/A
							COV, %	18.4%	14.6%	11.9%	16.4%	N/A	N/A	N/A
						35.7	Mean	367.4	650.7	2290.5	3857.3	205.7	37.7	13909.7
							Std. Dev.	38.1	51.0	182.3	217.7	37.5	2.9	1257.4
							COV, %	10.4%	7.8%	8.0%	5.6%	18.2%	7.6%	9.0%
				7%	Bump	16.6	Mean	1054.9	2522.0	6050.7	8784.4	N/A	N/A	N/A
							Std. Dev.	67.4	121.4	514.0	309.2	N/A	N/A	N/A
							COV, %	6.4%	4.8%	8.5%	3.5%	N/A	N/A	N/A
					Bump	35.7	Mean	256.5	459.0	1331.3	2115.1	109.0	149.5	22505.0
							Std. Dev.	34.6	84.9	81.2	111.6	31.2	34.5	1257.1
							COV, %	13.5%	18.5%	6.1%	5.3%	28.6%	23.1%	5.6%
				7%	Optimum	16.6	Mean	1316.1	3190.8	7529.8	10845.7	N/A	N/A	N/A
							Std. Dev.	168.9	365.2	1161.1	1313.5	N/A	N/A	N/A
							COV, %	12.8%	11.4%	15.4%	12.1%	N/A	N/A	N/A
					Optimum	35.7	Mean	295.4	547.4	2285.0	3502.7	102.3	122.1	18368.7
							Std. Dev.	33.9	46.8	375.9	929.5	15.3	13.5	1321.9
							COV, %	11.5%	8.5%	16.5%	26.5%	14.9%	11.0%	7.2%
				10%	Optimum	16.6	Mean	884.3	2188.8	5372.6	7890.7	N/A	N/A	N/A
							Std. Dev.	70.3	90.8	292.0	639.4	N/A	N/A	N/A
							COV, %	7.9%	4.1%	5.4%	8.1%	N/A	N/A	N/A
					Optimum	35.7	Mean	263.1	440.8	1289.3	2000.3	62.3	328.1	26749.3
							Std. Dev.	59.3	91.3	217.1	323.8	2.9	52.1	2642.6
							COV, %	22.5%	20.7%	16.8%	16.2%	4.6%	15.9%	9.9%

6.3.4 Cascade

Table 6.4. Dynamic modulus and creep testing for the Cascade mixture

								E* (MPa)				Dynamic Creep Testing		
Project	NMAS	Gradation	Traffic	Air Voids	Binder Content	Test Temperature (°C)	Test Statistic	0.1 Hz	1.0 Hz	10.0 Hz	25.0 Hz	FN	Min. Slope	Accumulated Strain at FN
Cascade	19	Dense	1000000	4%	Optimum	19.8	Mean	2314.3	6043.6	13794.5	19564.8	N/A	N/A	N/A
							Std. Dev.	274.9	1055.8	3082.1	3500.7	N/A	N/A	N/A
							COV, %	11.9%	17.5%	22.3%	17.9%	N/A	N/A	N/A
						37.7	Mean	587.3	1042.3	3029.8	4838.7	300.7	24.0	13218.3
							Std. Dev.	73.3	131.2	176.2	483.6	67.9	4.5	1907.8
							COV, %	12.5%	12.6%	5.8%	10.0%	22.6%	18.6%	14.4%
				7%	Bump	19.8	Mean	1441.5	3546.2	9021.0	13601.8	N/A	N/A	N/A
							Std. Dev.	290.8	794.1	3144.8	4438.0	N/A	N/A	N/A
							COV, %	20.2%	22.4%	34.9%	32.6%	N/A	N/A	N/A
					Bump	37.7	Mean	334.6	555.6	1619.6	2941.5	114.0	94.2	16213.3
							Std. Dev.	12.9	44.5	143.8	171.2	10.0	3.0	814.6
							COV, %	3.8%	8.0%	8.9%	5.8%	8.8%	3.2%	5.0%
				7%	Optimum	19.8	Mean	1550.0	3645.7	8418.4	12944.4	N/A	N/A	N/A
							Std. Dev.	313.8	822.3	2156.6	4750.9	N/A	N/A	N/A
							COV, %	20.2%	22.6%	25.6%	36.7%	N/A	N/A	N/A
					Optimum	37.7	Mean	594.7	998.7	2908.4	4633.0	122.3	82.8	15646.3
							Std. Dev.	99.2	133.8	508.7	615.3	7.6	6.2	615.4
							COV, %	16.7%	13.4%	17.5%	13.3%	6.2%	7.5%	3.9%
				10%	Optimum	19.8	Mean	958.3	2254.2	5516.6	8834.5	N/A	N/A	N/A
							Std. Dev.	32.2	179.4	39.8	1388.8	N/A	N/A	N/A
							COV, %	3.4%	8.0%	0.7%	15.7%	N/A	N/A	N/A
					Optimum	37.7	Mean	383.1	601.3	1733.8	2827.6	70.7	183.6	17572.0
							Std. Dev.	96.5	126.2	317.7	463.8	16.1	19.3	1711.7
							COV, %	25.2%	21.0%	18.3%	16.4%	22.7%	10.5%	9.7%

6.3.5 Bloomville

Table 6.5. Dynamic modulus and creep testing for the Bloomville mixture

								E* (MPa)				Dynamic Creep Testing		
Project	NMAS	Gradation	Traffic	Air Voids	Binder Content	Test Temperature (°C)	Test Statistic	0.1 Hz	1.0 Hz	10.0 Hz	25.0 Hz	FN	Min. Slope	Accumulated Strain at FN
Bloomville	19	Dense	1000000	4%	Optimum	17.5	Mean	1898.3	4034.1	8297.8	12492.9	N/A	N/A	N/A
							Std. Dev.	78.9	306.7	763.0	1847.6	N/A	N/A	N/A
							COV, %	4.2%	7.6%	9.2%	14.8%	N/A	N/A	N/A
						36.6	Mean	738.5	1275.8	2953.7	4870.2	914.0	5.3	13005.3
							Std. Dev.	116.2	170.7	189.6	329.2	132.9	1.0	366.2
							COV, %	15.7%	13.4%	6.4%	6.8%	14.5%	18.2%	2.8%
				7%	Bump	17.5	Mean	1288.9	2797.2	6224.5	8685.0	N/A	N/A	N/A
							Std. Dev.	108.8	173.9	782.7	943.0	N/A	N/A	N/A
							COV, %	8.4%	6.2%	12.6%	10.9%	N/A	N/A	N/A
					Bump	36.6	Mean	582.8	961.9	2220.6	3438.6	184.0	61.0	18781.0
							Std. Dev.	139.5	210.5	285.7	470.1	32.8	3.1	2153.2
							COV, %	23.9%	21.9%	12.9%	13.7%	17.8%	5.0%	11.5%
				7%	Optimum	17.5	Mean	1230.7	2841.5	6108.8	8404.9	N/A	N/A	N/A
							Std. Dev.	60.2	507.1	1383.1	2171.2	N/A	N/A	N/A
							COV, %	4.9%	17.8%	22.6%	25.8%	N/A	N/A	N/A
					Optimum	36.6	Mean	397.0	710.8	1918.8	2793.2	149.0	69.5	17117.0
							Std. Dev.	47.8	106.6	338.8	376.2	30.4	7.6	1492.2
							COV, %	12.1%	15.0%	17.7%	13.5%	20.4%	11.0%	8.7%
				10%	Optimum	17.5	Mean	870.1	1870.4	4463.7	6681.5	N/A	N/A	N/A
							Std. Dev.	96.3	35.3	237.6	406.9	N/A	N/A	N/A
							COV, %	11.1%	1.9%	5.3%	6.1%	N/A	N/A	N/A
					Optimum	36.6	Mean	687.1	1329.4	2008.2	2789.4	70.7	165.8	17850.0
							Std. Dev.	283.6	468.0	139.4	83.2	10.4	20.4	713.3
							COV, %	41.3%	35.2%	6.9%	3.0%	14.7%	12.3%	4.0%

6.3.6 Medford

Table 6.6. Dynamic modulus and creep testing for the Medford mixture

								E* (MPa)				Dynamic Creep Testing		
Project	NMAS	Gradation	Traffic	Air Voids	Binder Content	Test Temperature (°C)	Test Statistic	0.1 Hz	1.0 Hz	10.0 Hz	25.0 Hz	FN	Min. Slope	Accumulated Strain at FN
Medford	12.5	Dense	1000000	4%	Optimum	17.6	Mean	1600.9	4054.6	8847.4	11686.3	N/A	N/A	N/A
							Std. Dev.	101.8	227.2	586.9	985.3	N/A	N/A	N/A
							COV, %	6.4%	5.6%	6.6%	8.4%	N/A	N/A	N/A
						35.7	Mean	489.1	955.7	3029.1	4946.3	336.3	25.6	14855.3
							Std. Dev.	9.6	60.6	656.1	1460.5	71.3	8.3	5126.8
							COV, %	2.0%	6.3%	21.7%	29.5%	21.2%	32.4%	34.5%
				7%	Bump	17.6	Mean	1264.6	3525.7	7855.5	10438.2	N/A	N/A	N/A
							Std. Dev.	323.5	1173.7	2952.2	4185.2	N/A	N/A	N/A
							COV, %	25.6%	33.3%	37.6%	40.1%	N/A	N/A	N/A
					Bump	35.7	Mean	339.6	642.1	2295.5	3230.6	154.0	88.0	20208.7
							Std. Dev.	70.2	128.3	561.0	548.0	22.9	9.4	2481.7
							COV, %	20.7%	20.0%	24.4%	17.0%	14.9%	10.7%	12.3%
				7%	Optimum	17.6	Mean	1019.1	2603.7	6042.0	9531.9	N/A	N/A	N/A
							Std. Dev.	145.6	331.6	655.7	567.2	N/A	N/A	N/A
							COV, %	14.3%	12.7%	10.9%	6.0%	N/A	N/A	N/A
					Optimum	35.7	Mean	437.8	867.0	2416.3	3613.5	159.0	75.2	17912.7
							Std. Dev.	108.2	316.4	822.7	1046.5	18.0	19.6	2474.7
							COV, %	24.7%	36.5%	34.0%	29.0%	11.3%	26.0%	13.8%
				10%	Optimum	17.6	Mean	895.3	2003.3	4707.3	6949.9	N/A	N/A	N/A
							Std. Dev.	152.2	80.3	426.5	1330.2	N/A	N/A	N/A
							COV, %	17.0%	4.0%	9.1%	19.1%	N/A	N/A	N/A
					Optimum	35.7	Mean	292.7	539.0	1607.3	2539.3	89.0	237.9	27920.3
							Std. Dev.	60.5	115.9	293.2	490.2	0.0	5.6	928.7
							COV, %	20.7%	21.5%	18.2%	19.3%	0.0%	2.3%	3.3%

6.3.7 Wautoma

Table 6.7. Dynamic modulus and creep testing for the Wautoma mixture

								E* (MPa)				Dynamic Creep Testing		
Project	NMAS	Gradation	Traffic	Air Voids	Binder Content	Test Temperature (°C)	Test Statistic	0.1 Hz	1.0 Hz	10.0 Hz	25.0 Hz	FN	Min. Slope	Accumulated Strain at FN
Wautoma	12.5	Dense	1000000	4%	Optimum	18.8	Mean	2178.7	5306.2	12093.9	16667.0	N/A	N/A	N/A
							Std. Dev.	262.5	673.6	2346.3	1388.4	N/A	N/A	N/A
							COV, %	12.0%	12.7%	19.4%	8.3%	N/A	N/A	N/A
						37.7	Mean	542.2	1000.4	3878.3	5511.9	184.0	39.5	12550.3
							Std. Dev.	23.7	93.1	47.3	216.5	18.0	3.0	865.9
							COV, %	4.4%	9.3%	1.2%	3.9%	9.8%	7.5%	6.9%
				7%	Bump	18.8	Mean	1429.1	3485.2	8249.4	10871.1	N/A	N/A	N/A
							Std. Dev.	88.7	314.5	992.0	1315.6	N/A	N/A	N/A
							COV, %	6.2%	9.0%	12.0%	12.1%	N/A	N/A	N/A
					Bump	37.7	Mean	353.4	606.2	2291.2	3376.5	95.7	127.7	16955.3
							Std. Dev.	66.6	119.3	276.0	730.3	25.2	9.8	2657.9
							COV, %	18.8%	19.7%	12.0%	21.6%	26.3%	7.7%	15.7%
				7%	Optimum	18.8	Mean	1325.7	3252.4	7862.3	13621.2	N/A	N/A	N/A
							Std. Dev.	116.3	359.4	769.7	2367.2	N/A	N/A	N/A
							COV, %	8.8%	11.0%	9.8%	17.4%	N/A	N/A	N/A
					Optimum	37.7	Mean	336.5	588.7	2577.2	3824.8	84.0	123.7	15105.7
							Std. Dev.	39.0	47.3	202.5	110.5	5.0	5.9	667.2
							COV, %	11.6%	8.0%	7.9%	2.9%	6.0%	4.8%	4.4%
				10%	Optimum	18.8	Mean	1139.0	2940.2	7783.5	10720.1	N/A	N/A	N/A
							Std. Dev.	95.2	435.9	938.2	1290.2	N/A	N/A	N/A
							COV, %	8.4%	14.8%	12.1%	12.0%	N/A	N/A	N/A
					Optimum	37.7	Mean	245.1	395.8	1497.4	2133.7	45.7	345.8	19593.0
							Std. Dev.	4.6	11.5	89.7	216.6	2.9	30.7	480.0
							COV, %	1.9%	2.9%	6.0%	10.2%	6.3%	8.9%	2.4%

6.3.8 Tomahawk

Table 6.8. Dynamic modulus and creep testing for the Tomahawk mixture

								E* (MPa)				Dynamic Creep Testing		
Project	NMAS	Gradation	Traffic	Air Voids	Binder Content	Test Temperature (°C)	Test Statistic	0.1 Hz	1.0 Hz	10.0 Hz	25.0 Hz	FN	Min. Slope	Accumulated Strain at FN
Tomahawk	25	Open	3000000	4%	Optimum	17.3	Mean	3964.5	10368.2	27417.1	34924.2	N/A	N/A	N/A
							Std. Dev.	635.7	548.5	3327.4	4848.2	N/A	N/A	N/A
							COV, %	16.0%	5.3%	12.1%	13.9%	N/A	N/A	N/A
						35.6	Mean	938.4	1674.3	5297.5	9301.6	2880.0	2.5	16225.3
							Std. Dev.	72.5	266.3	829.9	730.0	524.4	0.5	1020.6
							COV, %	7.7%	15.9%	15.7%	7.8%	18.2%	22.1%	6.3%
				7%	Bump	17.3	Mean	2070.7	5258.3	12004.0	14751.1	N/A	N/A	N/A
							Std. Dev.	230.5	343.6	859.6	1238.2	N/A	N/A	N/A
							COV, %	11.1%	6.5%	7.2%	8.4%	N/A	N/A	N/A
					Bump	35.6	Mean	471.6	870.6	3320.1	5541.7	774.0	20.1	26157.0
							Std. Dev.	85.2	148.7	704.7	1011.3	101.1	2.6	4543.5
							COV, %	18.1%	17.1%	21.2%	18.2%	13.1%	13.1%	17.4%
				7%	Optimum	17.3	Mean	2913.2	6942.3	15695.8	20416.9	N/A	N/A	N/A
							Std. Dev.	622.6	875.5	744.0	1249.8	N/A	N/A	N/A
							COV, %	21.4%	12.6%	4.7%	6.1%	N/A	N/A	N/A
					Optimum	35.6	Mean	562.8	1032.4	4118.9	6826.6	1387.3	7.1	20829.3
							Std. Dev.	111.9	177.4	1259.2	1893.5	615.5	3.5	6672.6
							COV, %	19.9%	17.2%	30.6%	27.7%	44.4%	49.5%	32.0%
				10%	Optimum	17.3	Mean	2158.8	5286.9	13680.9	17857.8	N/A	N/A	N/A
							Std. Dev.	187.2	500.7	1920.7	2226.2	N/A	N/A	N/A
							COV, %	8.7%	9.5%	14.0%	12.5%	N/A	N/A	N/A
					Optimum	35.6	Mean	509.6	862.9	2999.7	4825.7	447.7	29.7	21742.7
							Std. Dev.	38.3	34.2	170.4	987.1	47.5	1.9	676.1
							COV, %	7.5%	4.0%	5.7%	20.5%	10.6%	6.3%	3.1%

6.3.9 Waunakee

Table 6.9. Dynamic modulus and creep testing for the Waunakee mixture

								E* (MPa)				Dynamic Creep Testing		
Project	NMAS	Gradation	Traffic	Air Voids	Binder Content	Test Temperature (°C)	Test Statistic	0.1 Hz	1.0 Hz	10.0 Hz	25.0 Hz	FN	Min. Slope	Accumulated Strain at FN
Waunakee	19	Dense	3000000	4%	Optimum	20.1	Mean	1806.6	4218.2	10321.8	17818.5	N/A	N/A	N/A
							Std. Dev.	115.7	599.8	2486.8	5773.0	N/A	N/A	N/A
							COV, %	6.4%	14.2%	24.1%	32.4%	N/A	N/A	N/A
						37.9	Mean	601.2	1123.9	3756.1	6877.7	904.0	6.8	12773.0
							Std. Dev.	81.6	172.9	842.0	1045.6	335.0	1.7	1547.5
							COV, %	13.6%	15.4%	22.4%	15.2%	37.1%	24.4%	12.1%
				7%	Bump	20.1	Mean	1336.5	3093.2	7729.3	12348.2	N/A	N/A	N/A
							Std. Dev.	98.8	55.8	583.7	1399.3	N/A	N/A	N/A
							COV, %	7.4%	1.8%	7.6%	11.3%	N/A	N/A	N/A
					Bump	37.9	Mean	505.8	828.6	2514.2	4160.2	357.3	28.6	17764.0
							Std. Dev.	51.1	34.1	412.7	1173.3	10.4	2.3	923.4
							COV, %	10.1%	4.1%	16.4%	28.2%	2.9%	8.0%	5.2%
				7%	Optimum	20.1	Mean	1750.9	4064.1	9793.9	14632.7	N/A	N/A	N/A
							Std. Dev.	338.3	599.7	703.4	1185.4	N/A	N/A	N/A
							COV, %	19.3%	14.8%	7.2%	8.1%	N/A	N/A	N/A
					Optimum	37.9	Mean	548.6	936.7	2811.2	4746.0	304.0	24.0	13965.0
							Std. Dev.	87.8	71.8	263.1	710.9	75.7	1.1	2063.9
							COV, %	16.0%	7.7%	9.4%	15.0%	24.9%	4.7%	14.8%
				10%	Optimum	20.1	Mean	1286.8	3023.1	6394.9	9231.7	N/A	N/A	N/A
							Std. Dev.	161.6	735.5	1636.3	1772.2	N/A	N/A	N/A
							COV, %	12.6%	24.3%	25.6%	19.2%	N/A	N/A	N/A
					Optimum	37.9	Mean	447.7	756.4	2168.8	3307.2	134.0	83.2	16601.7
							Std. Dev.	138.3	143.8	701.2	813.9	5.0	4.0	188.8
							COV, %	30.9%	19.0%	32.3%	24.6%	3.7%	4.8%	1.1%

6.3.10 Mosinee

Table 6.10. Dynamic modulus and creep testing for the Mosinee mixture

								E* (MPa)				Dynamic Creep Testing		
Project	NMAS	Gradation	Traffic	Air Voids	Binder Content	Test Temperature (°C)	Test Statistic	0.1 Hz	1.0 Hz	10.0 Hz	25.0 Hz	FN	Min. Slope	Accumulated Strain at FN
Mosinee	19	Dense	3000000	4%	Optimum	18.7	Mean	1179.2	3010.4	7048.7	9628.5	N/A	N/A	N/A
							Std. Dev.	46.0	205.4	671.2	713.7	N/A	N/A	N/A
							COV, %	3.9%	6.8%	9.5%	7.4%	N/A	N/A	N/A
						36.9	Mean	367.7	661.7	1892.1	3265.7	120.7	54.5	11236.0
							Std. Dev.	42.5	73.7	210.6	724.6	29.3	5.8	1175.7
							COV, %	11.6%	11.1%	11.1%	22.2%	24.3%	10.7%	10.5%
				7%	Bump	18.7	Mean	835.9	2111.1	4880.7	6867.0	N/A	N/A	N/A
							Std. Dev.	75.9	217.4	569.3	985.1	N/A	N/A	N/A
							COV, %	9.1%	10.3%	11.7%	14.3%	N/A	N/A	N/A
					Bump	36.9	Mean	320.3	563.9	1486.6	2356.2	72.3	160.8	16509.0
							Std. Dev.	49.1	90.8	140.5	233.5	5.8	18.1	810.5
							COV, %	15.3%	16.1%	9.5%	9.9%	8.0%	11.3%	4.9%
				7%	Optimum	18.7	Mean	784.5	1969.6	4790.3	6979.6	N/A	N/A	N/A
							Std. Dev.	43.0	197.4	740.6	1212.2	N/A	N/A	N/A
							COV, %	5.5%	10.0%	15.5%	17.4%	N/A	N/A	N/A
					Optimum	36.9	Mean	287.6	505.2	1478.4	2851.0	62.3	169.3	15047.0
							Std. Dev.	46.8	74.4	213.6	587.1	5.8	3.8	700.0
							COV, %	16.3%	14.7%	14.4%	20.6%	9.3%	2.2%	4.7%
				10%	Optimum	18.7	Mean	730.9	1882.0	4793.4	6869.5	N/A	N/A	N/A
							Std. Dev.	119.8	305.3	865.4	1129.7	N/A	N/A	N/A
							COV, %	16.4%	16.2%	18.1%	16.4%	N/A	N/A	N/A
					Optimum	36.9	Mean	278.3	438.7	1324.5	2193.9	44.0	400.6	22329.3
							Std. Dev.	45.1	79.3	349.3	642.4	5.0	35.5	2557.3
							COV, %	16.2%	18.1%	26.4%	29.3%	11.4%	8.9%	11.5%

6.3.11 Cumberland

Table 6.11. Dynamic modulus and creep testing for the Cumberland mixture

								E* (MPa)				Dynamic Creep Testing		
Project	NMAS	Gradation	Traffic	Air Voids	Binder Content	Test Temperature (°C)	Test Statistic	0.1 Hz	1.0 Hz	10.0 Hz	25.0 Hz	FN	Min. Slope	Accumulated Strain at FN
Antigo	12.5	Dense	>3,000,000	4%	Optimum	17.3	Mean	1213.4	2627.3	6493.7	10282.7	N/A	N/A	N/A
							Std. Dev.	108.0	155.2	953.7	2110.4	N/A	N/A	N/A
							COV, %	8.9%	5.9%	14.7%	20.5%	N/A	N/A	N/A
						35.2	Mean	494.2	734.6	1875.5	2746.3	4704.0	0.8	11820.0
							Std. Dev.	94.1	117.9	430.9	487.2	985.4	0.1	1981.8
							COV, %	19.0%	16.1%	23.0%	17.7%	20.9%	8.6%	16.8%
				7%	Bump	17.3	Mean	808.9	1663.6	4011.7	6427.9	N/A	N/A	N/A
							Std. Dev.	120.1	247.1	775.6	1370.7	N/A	N/A	N/A
							COV, %	14.8%	14.9%	19.3%	21.3%	N/A	N/A	N/A
					Bump	35.2	Mean	428.6	582.4	1874.2	3115.8	516.3	14.6	14873.7
							Std. Dev.	99.1	88.2	612.1	1062.6	230.6	2.6	6993.1
							COV, %	23.1%	15.1%	32.7%	34.1%	44.7%	17.7%	47.0%
				7%	Optimum	17.3	Mean	1047.1	2355.3	6589.8	9321.4	N/A	N/A	N/A
							Std. Dev.	183.6	433.1	1236.7	2022.2	N/A	N/A	N/A
							COV, %	17.5%	18.4%	18.8%	21.7%	N/A	N/A	N/A
					Optimum	35.2	Mean	445.5	669.3	1793.9	2893.1	858.0	8.5	16472.3
							Std. Dev.	55.3	81.5	301.4	473.2	103.0	1.7	664.6
							COV, %	12.4%	12.2%	16.8%	16.4%	12.0%	20.5%	4.0%
				10%	Optimum	17.3	Mean	602.5	1279.1	3109.1	4530.8	N/A	N/A	N/A
							Std. Dev.	24.0	89.0	142.1	145.2	N/A	N/A	N/A
							COV, %	4.0%	7.0%	4.6%	3.2%	N/A	N/A	N/A
					Optimum	35.2	Mean	307.2	412.0	1154.9	1877.6	560.3	17.5	19189.0
							Std. Dev.	54.0	132.1	161.5	162.2	184.3	1.0	2882.0
							COV, %	17.6%	32.1%	14.0%	8.6%	32.9%	5.6%	15.0%

6.3.12 Hayward

Table 6.12. Dynamic modulus and creep testing for the Hayward mixture

								E* (MPa)				Dynamic Creep Testing		
Project	NMAS	Gradation	Traffic	Air Voids	Binder Content	Test Temperature (°C)	Test Statistic	0.1 Hz	1.0 Hz	10.0 Hz	25.0 Hz	FN	Min. Slope	Accumulated Strain at FN
Hayward	12.5	Dense	3000000	4%	Optimum	17.2	Mean	1263.5	3397.4	8155.8	11716.9	N/A	N/A	N/A
							Std. Dev.	106.8	227.9	519.8	1173.9	N/A	N/A	N/A
							COV, %	8.5%	6.7%	6.4%	10.0%	N/A	N/A	N/A
						36.1	Mean	385.9	677.5	2162.6	3543.2	104.0	78.5	13208.3
							Std. Dev.	105.6	143.8	352.2	225.4	8.7	21.7	1660.3
							COV, %	27.4%	21.2%	16.3%	6.4%	8.3%	27.7%	12.6%
				7%	Bump	17.2	Mean	817.6	2051.7	4951.1	6742.5	N/A	N/A	N/A
							Std. Dev.	193.2	439.2	941.6	967.9	N/A	N/A	N/A
							COV, %	23.6%	21.4%	19.0%	14.4%	N/A	N/A	N/A
					Bump	36.1	Mean	278.1	431.4	1294.6	2193.5	55.7	375.9	24779.3
							Std. Dev.	20.5	54.9	222.3	115.3	16.1	186.4	5568.3
							COV, %	7.4%	12.7%	17.2%	5.3%	28.9%	49.6%	22.5%
				7%	Optimum	17.2	Mean	1221.7	2875.1	6114.4	8431.8	N/A	N/A	N/A
							Std. Dev.	303.9	619.2	722.9	1073.8	N/A	N/A	N/A
							COV, %	24.9%	21.5%	11.8%	12.7%	N/A	N/A	N/A
					Optimum	36.1	Mean	442.8	754.6	2133.3	3396.4	59.0	249.6	18765.3
							Std. Dev.	257.7	408.9	1065.4	1360.6	15.0	69.2	278.0
							COV, %	58.2%	54.2%	49.9%	40.1%	25.4%	27.7%	1.5%
				10%	Optimum	17.2	Mean	714.5	1898.7	4665.9	6657.1	N/A	N/A	N/A
							Std. Dev.	49.6	93.5	174.3	316.4	N/A	N/A	N/A
							COV, %	6.9%	4.9%	3.7%	4.8%	N/A	N/A	N/A
					Optimum	36.1	Mean	243.1	409.9	1105.0	1900.1	37.3	568.9	24918.3
							Std. Dev.	24.4	39.9	36.2	185.3	7.6	168.4	1129.4
							COV, %	10.0%	9.7%	3.3%	9.7%	20.5%	29.6%	4.5%

6.3.13 Wausau

Table 6.13. Dynamic modulus and creep testing for the Wausau mixture

								E* (MPa)				Dynamic Creep Testing		
Project	NMAS	Gradation	Traffic	Air Voids	Binder Content	Test Temperature (°C)	Test Statistic	0.1 Hz	1.0 Hz	10.0 Hz	25.0 Hz	FN	Min. Slope	Accumulated Strain at FN
Wausau	12.5	Dense	3000000	4%	Optimum	18.7	Mean	1569.9	4433.0	11850.4	14795.6	N/A	N/A	N/A
							Std. Dev.	210.8	159.7	1726.3	3064.9	N/A	N/A	N/A
							COV, %	13.4%	3.6%	14.6%	20.7%	N/A	N/A	N/A
						36.9	Mean	429.9	910.2	2962.7	4986.1	217.3	33.1	13490.0
							Std. Dev.	131.7	209.1	410.9	982.7	20.2	12.1	1937.0
							COV, %	30.6%	23.0%	13.9%	19.7%	9.3%	36.6%	14.4%
				7%	Bump	18.7	Mean	1195.5	3286.9	7622.6	10343.7	N/A	N/A	N/A
							Std. Dev.	110.1	330.4	92.3	1348.6	N/A	N/A	N/A
							COV, %	9.2%	10.1%	1.2%	13.0%	N/A	N/A	N/A
					Bump	36.9	Mean	293.3	610.0	1891.4	3436.2	185.7	59.7	18056.0
							Std. Dev.	67.9	145.9	543.5	1341.5	23.6	11.4	3096.0
							COV, %	23.2%	23.9%	28.7%	39.0%	12.7%	19.1%	17.1%
				7%	Optimum	18.7	Mean	1094.0	3280.4	9335.9	14888.1	N/A	N/A	N/A
							Std. Dev.	197.3	545.0	1831.3	4620.4	N/A	N/A	N/A
							COV, %	18.0%	16.6%	19.6%	31.0%	N/A	N/A	N/A
					Optimum	36.9	Mean	295.4	604.6	2015.3	3692.4	109.0	98.7	16188.3
							Std. Dev.	22.7	47.5	151.4	764.7	20.0	20.8	1272.4
							COV, %	7.7%	7.9%	7.5%	20.7%	18.3%	21.0%	7.9%
				10%	Optimum	18.7	Mean	982.5	2901.3	9344.2	12177.1	N/A	N/A	N/A
							Std. Dev.	96.3	322.1	1446.4	2309.7	N/A	N/A	N/A
							COV, %	9.8%	11.1%	15.5%	19.0%	N/A	N/A	N/A
					Optimum	36.9	Mean	318.4	626.4	2156.8	3463.2	185.7	109.6	24728.0
							Std. Dev.	82.4	165.1	715.8	901.6	132.9	43.8	5384.1
							COV, %	25.9%	26.4%	33.2%	26.0%	71.6%	39.9%	21.8%

6.3.14 Hurley

Table 6.14. Dynamic modulus and creep testing for the Hurley mixture

								E* (MPa)				Dynamic Creep Testing		
Project	NMAS	Gradation	Traffic	Air Voids	Binder Content	Test Temperature (°C)	Test Statistic	0.1 Hz	1.0 Hz	10.0 Hz	25.0 Hz	FN	Min. Slope	Accumulated Strain at FN
Hurley	12.5	Dense	3000000	4%	Optimum	16.6	Mean	4183.6	7709.2	13947.7	16681.9	N/A	N/A	N/A
							Std. Dev.	450.0	869.7	1658.1	2236.6	N/A	N/A	N/A
							COV, %	10.8%	11.3%	11.9%	13.4%	N/A	N/A	N/A
						35.7	Mean	1038.4	1977.4	6953.2	8850.1	7626.7	0.4	11025.7
							Std. Dev.	194.2	282.9	1721.8	1784.3	1556.4	0.1	795.6
							COV, %	18.7%	14.3%	24.8%	20.2%	20.4%	13.3%	7.2%
				7%	Bump	16.6	Mean	3207.1	6866.2	13407.9	16049.2	N/A	N/A	N/A
							Std. Dev.	478.3	877.0	862.1	316.2	N/A	N/A	N/A
							COV, %	14.9%	12.8%	6.4%	2.0%	N/A	N/A	N/A
					Bump	35.7	Mean	823.5	1582.9	4978.9	8063.0	1450.0	9.1	16330.7
							Std. Dev.	146.5	241.0	1343.5	2850.6	900.8	9.1	1393.2
							COV, %	17.8%	15.2%	27.0%	35.4%	62.1%	99.5%	8.5%
				7%	Optimum	16.6	Mean	2622.4	5570.8	10691.1	13528.3	N/A	N/A	N/A
							Std. Dev.	245.9	542.3	779.4	1560.9	N/A	N/A	N/A
							COV, %	9.4%	9.7%	7.3%	11.5%	N/A	N/A	N/A
					Optimum	35.7	Mean	634.9	1277.8	5055.5	6592.7	908.7	8.1	16488.0
							Std. Dev.	152.8	189.0	439.2	869.8	240.7	1.1	2929.2
							COV, %	24.1%	14.8%	8.7%	13.2%	26.5%	13.9%	17.8%
				10%	Optimum	16.6	Mean	1865.2	3971.6	8322.0	11496.0	N/A	N/A	N/A
							Std. Dev.	206.0	418.9	81.7	1284.8	N/A	N/A	N/A
							COV, %	11.0%	10.5%	1.0%	11.2%	N/A	N/A	N/A
					Optimum	35.7	Mean	421.5	756.6	2451.0	4102.6	378.0	25.3	27382.7
							Std. Dev.	85.7	159.1	175.2	486.2	27.8	8.4	20248.3
							COV, %	20.3%	21.0%	7.1%	11.9%	7.4%	33.1%	73.9%

6.3.15 Antigo

Table 6.15. Dynamic modulus and creep testing for the Antigo mixture

								E* (MPa)				Dynamic Creep Testing		
Project	NMAS	Gradation	Traffic	Air Voids	Binder Content	Test Temperature (°C)	Test Statistic	0.1 Hz	1.0 Hz	10.0 Hz	25.0 Hz	FN	Min. Slope	Accumulated Strain at FN
Antigo	19	Dense	>3,000,000	4%	Optimum	17.3	Mean	1551.0	3567.0	8777.5	12070.8	N/A	N/A	N/A
							Std. Dev.	256.9	523.8	434.5	467.5	N/A	N/A	N/A
							COV, %	16.6%	14.7%	4.9%	3.9%	N/A	N/A	N/A
						35.2	Mean	528.7	829.4	2085.0	3285.0	3016.0	1.5	12652.0
							Std. Dev.	97.2	163.8	398.5	517.0	302.4	0.5	1049.4
							COV, %	18.4%	19.7%	19.1%	15.7%	10.0%	32.8%	8.3%
				7%	Bump	17.3	Mean	1034.0	2205.8	5340.9	7412.0	N/A	N/A	N/A
							Std. Dev.	14.7	63.1	917.1	2051.4	N/A	N/A	N/A
							COV, %	1.4%	2.9%	17.2%	27.7%	N/A	N/A	N/A
					Bump	35.2	Mean	367.7	535.1	1515.8	2741.1	725.3	9.9	16276.7
							Std. Dev.	30.4	47.5	140.9	384.5	92.9	2.1	492.5
							COV, %	8.3%	8.9%	9.3%	14.0%	12.8%	21.6%	3.0%
				7%	Optimum	17.3	Mean	919.6	1988.2	4970.3	8257.0	N/A	N/A	N/A
							Std. Dev.	91.7	247.9	738.1	2461.8	N/A	N/A	N/A
							COV, %	10.0%	12.5%	14.9%	29.8%	N/A	N/A	N/A
					Optimum	35.2	Mean	396.1	591.8	1521.5	2511.0	1421.3	3.2	12623.7
							Std. Dev.	47.8	92.9	130.2	78.8	377.2	1.3	1988.4
							COV, %	12.1%	15.7%	8.6%	3.1%	26.5%	39.5%	15.8%
				10%	Optimum	17.3	Mean	739.4	1556.9	3959.5	5610.3	N/A	N/A	N/A
							Std. Dev.	167.0	329.8	924.4	1094.2	N/A	N/A	N/A
							COV, %	22.6%	21.2%	23.3%	19.5%	N/A	N/A	N/A
					Optimum	35.2	Mean	341.8	493.8	1319.1	2084.7	239.0	40.5	18053.3
							Std. Dev.	100.2	135.3	269.9	485.6	26.0	6.7	1894.5
							COV, %	29.3%	27.4%	20.5%	23.3%	10.9%	16.5%	10.5%

6.3.16 Northfield

Table 6.16. Dynamic modulus and creep testing for the Northfield mixture

								E* (MPa)				Dynamic Creep Testing		
Project	NMAS	Gradation	Traffic	Air Voids	Binder Content	Test Temperature (°C)	Test Statistic	0.1 Hz	1.0 Hz	10.0 Hz	25.0 Hz	FN	Min. Slope	Accumulated Strain at FN
Northfield	19	Dense	>3,000,000	4%	Optimum	18.4	Mean	4190.8	9778.3	19079.9	23125.0	N/A	N/A	N/A
							Std. Dev.	1055.5	2357.3	4090.0	3961.6	N/A	N/A	N/A
							COV, %	25.2%	24.1%	21.4%	17.1%	N/A	N/A	N/A
						36.5	Mean	943.3	2300.0	6221.8	9689.3	2985.0	1.7	11633.3
							Std. Dev.	74.8	144.2	137.9	574.7	837.6	0.5	309.0
							COV, %	7.9%	6.3%	2.2%	5.9%	28.1%	28.9%	2.7%
				7%	Bump	18.4	Mean	3127.8	7606.1	15474.9	18760.1	N/A	N/A	N/A
							Std. Dev.	65.7	506.3	2678.1	3619.9	N/A	N/A	N/A
							COV, %	2.1%	6.7%	17.3%	19.3%	N/A	N/A	N/A
					Bump	36.5	Mean	672.2	1434.6	4117.0	6252.9	4467.7	1.4	14946.3
							Std. Dev.	179.6	307.3	570.6	937.8	828.4	0.4	1016.5
							COV, %	26.7%	21.4%	13.9%	15.0%	18.5%	27.5%	6.8%
				7%	Optimum	18.4	Mean	2481.2	6006.7	11964.0	15104.5	N/A	N/A	N/A
							Std. Dev.	161.6	390.7	678.0	419.6	N/A	N/A	N/A
							COV, %	6.5%	6.5%	5.7%	2.8%	N/A	N/A	N/A
					Optimum	36.5	Mean	947.7	1772.7	4191.3	5826.4	2112.3	2.8	13961.3
							Std. Dev.	79.2	79.7	293.3	663.1	283.4	0.2	920.0
							COV, %	8.4%	4.5%	7.0%	11.4%	13.4%	6.4%	6.6%
				10%	Optimum	18.4	Mean	2624.8	5666.2	10937.9	13776.6	N/A	N/A	N/A
							Std. Dev.	808.9	1875.8	3568.2	4273.9	N/A	N/A	N/A
							COV, %	30.8%	33.1%	32.6%	31.0%	N/A	N/A	N/A
					Optimum	36.5	Mean	589.4	1178.0	3164.6	4975.6	2081.7	5.0	20425.7
							Std. Dev.	134.6	263.1	656.2	701.4	779.8	1.7	3785.2
							COV, %	22.8%	22.3%	20.7%	14.1%	37.5%	33.3%	18.5%

6.3.17 Wisconsin Rapids

Table 6.17. Dynamic modulus and creep testing for the Wisconsin Rapids mixture

								E* (MPa)				Dynamic Creep Testing		
Project	NMAS	Gradation	Traffic	Air Voids	Binder Content	Test Temperature (°C)	Test Statistic	0.1 Hz	1.0 Hz	10.0 Hz	25.0 Hz	FN	Min. Slope	Accumulated Strain at FN
Wisconsin Rapids	19	Open	>3,000,000	4%	Optimum	19.0	Mean	3857.6	9768.8	20501.9	26066.9	N/A	N/A	N/A
							Std. Dev.	516.2	982.4	2802.6	3735.4	N/A	N/A	N/A
							COV, %	13.4%	10.1%	13.7%	14.3%	N/A	N/A	N/A
						37.5	Mean	603.2	1240.6	5317.4	8942.5	2365.3	2.3	13094.3
							Std. Dev.	157.9	437.7	2328.7	3113.3	1176.3	1.2	1431.0
							COV, %	26.2%	35.3%	43.8%	34.8%	49.7%	52.5%	10.9%
				7%	Bump	19.0	Mean	3281.0	8090.4	16007.9	19866.1	N/A	N/A	N/A
							Std. Dev.	420.2	1192.5	3002.7	3504.3	N/A	N/A	N/A
							COV, %	12.8%	14.7%	18.8%	17.6%	N/A	N/A	N/A
					Bump	37.5	Mean	474.1	975.7	3378.0	5629.0	1076.0	10.2	21902.0
							Std. Dev.	66.4	188.4	803.5	2115.8	335.6	4.3	4264.1
							COV, %	14.0%	19.3%	23.8%	37.6%	31.2%	42.3%	19.5%
				7%	Optimum	19.0	Mean	2586.9	7055.6	16404.3	20837.2	N/A	N/A	N/A
							Std. Dev.	296.7	920.2	1980.5	2077.1	N/A	N/A	N/A
							COV, %	11.5%	13.0%	12.1%	10.0%	N/A	N/A	N/A
					Optimum	37.5	Mean	466.7	940.1	3267.4	4899.8	1024.7	9.0	17924.3
							Std. Dev.	56.1	122.7	581.6	937.7	364.5	4.0	1140.9
							COV, %	12.0%	13.1%	17.8%	19.1%	35.6%	44.5%	6.4%
				10%	Optimum	19.0	Mean	2706.0	7106.7	15883.6	20204.5	N/A	N/A	N/A
							Std. Dev.	963.4	2226.2	4442.1	5723.3	N/A	N/A	N/A
							COV, %	35.6%	31.3%	28.0%	28.3%	N/A	N/A	N/A
					Optimum	37.5	Mean	529.6	980.7	3504.2	6173.9	579.7	20.0	22173.3
							Std. Dev.	173.8	206.6	461.8	1545.7	76.0	3.4	1246.3
							COV, %	32.8%	21.1%	13.2%	25.0%	13.1%	17.0%	5.6%

6.3.18 Antigo

Table 6.18. Dynamic modulus and creep testing for the Antigo mixture

								E* (MPa)				Dynamic Creep Testing		
Project	NMAS	Gradation	Traffic	Air Voids	Binder Content	Test Temperature (°C)	Test Statistic	0.1 Hz	1.0 Hz	10.0 Hz	25.0 Hz	FN	Min. Slope	Accumulated Strain at FN
Antigo	12.5	Dense	>3,000,000	4%	Optimum	17.3	Mean	1213.4	2627.3	6493.7	10282.7	N/A	N/A	N/A
							Std. Dev.	108.0	155.2	953.7	2110.4	N/A	N/A	N/A
							COV, %	8.9%	5.9%	14.7%	20.5%	N/A	N/A	N/A
						35.2	Mean	494.2	734.6	1875.5	2746.3	4704.0	0.8	11820.0
							Std. Dev.	94.1	117.9	430.9	487.2	985.4	0.1	1981.8
							COV, %	19.0%	16.1%	23.0%	17.7%	20.9%	8.6%	16.8%
				7%	Bump	17.3	Mean	808.9	1663.6	4011.7	6427.9	N/A	N/A	N/A
							Std. Dev.	120.1	247.1	775.6	1370.7	N/A	N/A	N/A
							COV, %	14.8%	14.9%	19.3%	21.3%	N/A	N/A	N/A
					Bump	35.2	Mean	428.6	582.4	1874.2	3115.8	516.3	14.6	14873.7
							Std. Dev.	99.1	88.2	612.1	1062.6	230.6	2.6	6993.1
							COV, %	23.1%	15.1%	32.7%	34.1%	44.7%	17.7%	47.0%
				7%	Optimum	17.3	Mean	1047.1	2355.3	6589.8	9321.4	N/A	N/A	N/A
							Std. Dev.	183.6	433.1	1236.7	2022.2	N/A	N/A	N/A
							COV, %	17.5%	18.4%	18.8%	21.7%	N/A	N/A	N/A
					Optimum	35.2	Mean	445.5	669.3	1793.9	2893.1	858.0	8.5	16472.3
							Std. Dev.	55.3	81.5	301.4	473.2	103.0	1.7	664.6
							COV, %	12.4%	12.2%	16.8%	16.4%	12.0%	20.5%	4.0%
				10%	Optimum	17.3	Mean	602.5	1279.1	3109.1	4530.8	N/A	N/A	N/A
							Std. Dev.	24.0	89.0	142.1	145.2	N/A	N/A	N/A
							COV, %	4.0%	7.0%	4.6%	3.2%	N/A	N/A	N/A
					Optimum	35.2	Mean	307.2	412.0	1154.9	1877.6	560.3	17.5	19189.0
							Std. Dev.	54.0	132.1	161.5	162.2	184.3	1.0	2882.0
							COV, %	17.6%	32.1%	14.0%	8.6%	32.9%	5.6%	15.0%

6.3.19 Plymouth

Table 6.19. Dynamic modulus and creep testing for the Plymouth mixture

								E* (MPa)				Dynamic Creep Testing		
Project	NMAS	Gradation	Traffic	Air Voids	Binder Content	Test Temperature (°C)	Test Statistic	0.1 Hz	1.0 Hz	10.0 Hz	25.0 Hz	FN	Min. Slope	Accumulated Strain at FN
Plymouth	12.5	Dense	>3,000,000	4%	Optimum	19.7	Mean	3642.5	8619.1	19712.6	27204.8	N/A	N/A	N/A
							Std. Dev.	625.3	1965.9	5685.8	5243.5	N/A	N/A	N/A
							COV, %	17.2%	22.8%	28.8%	19.3%	N/A	N/A	N/A
						37.3	Mean	837.1	1514.8	4870.8	8095.9	2093.3	2.9	13899.3
							Std. Dev.	168.9	170.5	384.4	1568.4	360.7	0.5	1233.5
							COV, %	20.2%	11.3%	7.9%	19.4%	17.2%	17.5%	8.9%
				7%	Bump	19.7	Mean	2196.7	5469.7	13107.5	17813.5	N/A	N/A	N/A
							Std. Dev.	144.0	331.7	1850.5	3133.9	N/A	N/A	N/A
							COV, %	6.6%	6.1%	14.1%	17.6%	N/A	N/A	N/A
					Bump	37.3	Mean	636.7	1104.9	3462.4	5556.1	974.0	14.1	22967.3
							Std. Dev.	51.3	104.9	279.3	420.3	482.4	8.2	5319.6
							COV, %	8.1%	9.5%	8.1%	7.6%	49.5%	58.5%	23.2%
				7%	Optimum	19.7	Mean	2860.0	6715.8	17406.4	21691.4	N/A	N/A	N/A
							Std. Dev.	305.4	774.1	1137.7	1844.3	N/A	N/A	N/A
							COV, %	10.7%	11.5%	6.5%	8.5%	N/A	N/A	N/A
					Optimum	37.3	Mean	739.1	1323.4	4183.5	7106.8	960.0	8.0	15134.0
							Std. Dev.	121.7	178.1	764.1	1881.4	208.8	1.5	2796.7
							COV, %	16.5%	13.5%	18.3%	26.5%	21.8%	18.5%	18.5%
				10%	Optimum	19.7	Mean	1881.7	4553.7	10832.1	14109.9	N/A	N/A	N/A
							Std. Dev.	169.9	917.0	1686.1	1428.3	N/A	N/A	N/A
							COV, %	9.0%	20.1%	15.6%	10.1%	N/A	N/A	N/A
					Optimum	37.3	Mean	570.4	973.9	3235.7	4932.0	453.0	22.7	18900.0
							Std. Dev.	85.4	81.8	396.6	680.5	45.6	0.6	1493.4
							COV, %	15.0%	8.4%	12.3%	13.8%	10.1%	2.8%	7.9%

6.3.20 Racine

Table 6.20 Dynamic modulus and creep testing for the Racine mixture

								E* (MPa)				Dynamic Creep Testing		
Project	NMAS	Gradation	Traffic	Air Voids	Binder Content	Test Temperature (°C)	Test Statistic	0.1 Hz	1.0 Hz	10.0 Hz	25.0 Hz	FN	Min. Slope	Accumulated Strain at FN
Racine	12.5	Dense	>3,000,000	4%	Optimum	20.9	Mean	1653.8	3382.8	8809.8	12551.2	N/A	N/A	N/A
							Std. Dev.	306.3	525.6	2107.3	3382.9	N/A	N/A	N/A
							COV, %	18.5%	15.5%	23.9%	27.0%	N/A	N/A	N/A
						39.2	Mean	749.7	1114.9	3150.9	4936.7	5290.7	0.9	12421.7
							Std. Dev.	43.6	84.7	277.9	730.6	1501.3	0.0	3031.0
							COV, %	5.8%	7.6%	8.8%	14.8%	28.4%	4.9%	24.4%
				7%	Bump	20.9	Mean	1191.0	2408.0	6078.8	8294.0	N/A	N/A	N/A
							Std. Dev.	192.1	475.6	705.6	1144.1	N/A	N/A	N/A
							COV, %	16.1%	19.8%	11.6%	13.8%	N/A	N/A	N/A
					Bump	39.2	Mean	559.3	765.6	2002.2	3133.8	1228.0	8.5	20440.3
							Std. Dev.	52.4	51.5	60.4	83.8	490.4	5.1	2907.8
							COV, %	9.4%	6.7%	3.0%	2.7%	39.9%	60.2%	14.2%
				7%	Optimum	20.9	Mean	1423.2	2864.3	6662.9	9247.5	N/A	N/A	N/A
							Std. Dev.	117.9	272.3	631.5	198.7	N/A	N/A	N/A
							COV, %	8.3%	9.5%	9.5%	2.1%	N/A	N/A	N/A
					Optimum	39.2	Mean	651.6	963.8	2689.3	4333.5	1624.0	4.5	16204.3
							Std. Dev.	21.0	92.2	413.8	675.8	485.6	1.0	2834.6
							COV, %	3.2%	9.6%	15.4%	15.6%	29.9%	22.3%	17.5%
				10%	Optimum	20.9	Mean	855.6	1838.9	4306.2	5600.8	N/A	N/A	N/A
							Std. Dev.	24.6	52.8	105.1	261.5	N/A	N/A	N/A
							COV, %	2.9%	2.9%	2.4%	4.7%	N/A	N/A	N/A
					Optimum	39.2	Mean	403.5	559.1	1437.9	2187.3	715.3	16.0	22166.7
							Std. Dev.	34.2	37.5	58.3	104.6	94.6	1.5	1622.6
							COV, %	8.5%	6.7%	4.1%	4.8%	13.2%	9.5%	7.3%

6.3.21 Northfield

Table 6.21. Dynamic modulus and creep testing for the Northfield mixture

								E* (MPa)				Dynamic Creep Testing		
Project	NMAS	Gradation	Traffic	Air Voids	Binder Content	Test Temperature (°C)	Test Statistic	0.1 Hz	1.0 Hz	10.0 Hz	25.0 Hz	FN	Min. Slope	Accumulated Strain at FN
Northfield	12.5	Open	>3,000,000	4%	Optimum	18.4	Mean	868.1	1834.1	4437.2	6974.8	N/A	N/A	N/A
							Std. Dev.	116.4	338.3	1104.6	1283.3	N/A	N/A	N/A
							COV, %	13.4%	18.4%	24.9%	18.4%	N/A	N/A	N/A
						36.5	Mean	385.1	536.5	1425.5	3192.3	2622.7	2.5	17659.7
							Std. Dev.	47.3	61.1	160.5	792.6	888.8	0.5	1367.1
							COV, %	12.3%	11.4%	11.3%	24.8%	33.9%	21.0%	7.7%
				7%	Bump	18.4	Mean	1094.6	2187.2	6478.2	13989.4	N/A	N/A	N/A
							Std. Dev.	147.4	314.7	2207.0	3059.4	N/A	N/A	N/A
							COV, %	13.5%	14.4%	34.1%	21.9%	N/A	N/A	N/A
					Bump	36.5	Mean	448.9	631.8	2528.9	3990.4	4986.7	1.4	20109.0
							Std. Dev.	20.5	50.2	1613.0	1914.4	1146.7	0.1	1871.8
							COV, %	4.6%	7.9%	63.8%	48.0%	23.0%	9.7%	9.3%
				7%	Optimum	18.4	Mean	886.3	1775.4	4146.2	7466.9	N/A	N/A	N/A
							Std. Dev.	124.6	189.9	548.7	628.0	N/A	N/A	N/A
							COV, %	14.1%	10.7%	13.2%	8.4%	N/A	N/A	N/A
					Optimum	36.5	Mean	484.6	703.4	1970.1	3560.5	5840.0	1.1	17121.7
							Std. Dev.	43.0	65.7	131.9	935.3	1304.1	0.4	772.1
							COV, %	8.9%	9.3%	6.7%	26.3%	22.3%	34.0%	4.5%
				10%	Optimum	18.4	Mean	1156.3	2314.4	6125.3	9013.3	N/A	N/A	N/A
							Std. Dev.	26.4	216.4	1152.2	2082.1	N/A	N/A	N/A
							COV, %	2.3%	9.4%	18.8%	23.1%	N/A	N/A	N/A
					Optimum	36.5	Mean	393.2	558.2	1627.8	2897.6	6104.0	1.0	17942.3
							Std. Dev.	18.9	51.0	236.4	503.1	1845.9	0.2	1946.2
							COV, %	4.8%	9.1%	14.5%	17.4%	30.2%	21.8%	10.8%

6.3.22 Pooled Data for Database

Table 6.22. Pooled dynamic modulus and creep testing for dense-graded mixture with an NMAS of 19.0 mm and 300,000 ESAL traffic level

							Pooled E* by Frequency (MPa)				Pooled Dynamic Creep Test Data		
NMAS	Gradation	Traffic	Air Voids, %	Binder Content	Mean Test Temperature, °C	Test Statistic	0.1 Hz	1.0 Hz	10.0 Hz	25.0 Hz	FN	Min. Slope	Accumulated Strain at FN
19	Dense	300,000	4	Optimum	16.6	Mean	1711.9	4513.5	11374.3	18456.8	N/A	N/A	N/A
						Std. Dev.	321.1	872.5	1470.0	2794.6	N/A	N/A	N/A
						COV, %	18.8%	19.3%	12.9%	15.1%	N/A	N/A	N/A
					35.5	Mean	474.8	800.0	2381.5	3849.8	140.7	45.3	10913.0
						Std. Dev.	10.2	54.4	174.9	492.4	18.9	4.1	947.6
						COV, %	2.1%	6.8%	7.3%	12.8%	13.5%	8.9%	8.7%
			7	Bump	16.6	Mean	1330.3	3762.8	10394.8	18857.1	N/A	N/A	N/A
						Std. Dev.	71.6	474.5	461.9	2398.7	N/A	N/A	N/A
						COV, %	5.4%	12.6%	4.4%	12.7%	N/A	N/A	N/A
					35.5	Mean	426.4	697.3	1998.9	2991.9	74.0	165.4	16647.3
						Std. Dev.	64.7	87.1	161.9	347.4	10.0	17.1	1172.5
						COV, %	15.2%	12.5%	8.1%	11.6%	13.5%	10.3%	7.0%
			7	Optimum	16.6	Mean	1438.1	3768.3	8756.4	15191.1	N/A	N/A	N/A
						Std. Dev.	83.8	639.3	1292.3	3973.6	N/A	N/A	N/A
						COV, %	5.8%	17.0%	14.8%	26.2%	N/A	N/A	N/A
					35.5	Mean	383.4	617.7	1984.1	3090.8	75.7	135.8	14743.7
						Std. Dev.	68.0	86.7	185.2	682.0	10.4	12.9	592.0
						COV, %	17.7%	14.0%	9.3%	22.1%	13.8%	9.5%	4.0%
			10	Optimum	16.6	Mean	1114.0	2878.4	7305.7	15268.7	N/A	N/A	N/A
						Std. Dev.	191.4	654.7	1454.2	1990.2	N/A	N/A	N/A
						COV, %	17.2%	22.7%	19.9%	13.0%	N/A	N/A	N/A
					35.5	Mean	290.7	476.2	1370.2	2287.6	37.3	398.2	18501.0
						Std. Dev.	31.7	47.2	114.7	322.5	2.9	53.1	727.5
						COV, %	10.9%	9.9%	8.4%	14.1%	7.7%	13.3%	3.9%

Table 6.23. Pooled dynamic modulus and creep testing for dense-graded mixture with an NMAS of 12.5 mm and 300,000 ESAL traffic level

							Pooled E* (MPa)				Pooled Dynamic Creep Test Data		
NMAS	Gradation	Traffic	Air Voids, %	Binder Content	Mean Test Temperature, ℃	Test Statistic	0.1 Hz	1.0 Hz	10.0 Hz	25.0 Hz	FN	Min. Slope	Accumulated Strain at FN
12.5	Dense	300,000	4	Optimum	17.8	Mean	1649.3	3954.0	8895.4	13431.1	N/A	N/A	N/A
						Std. Dev.	270.1	665.7	1405.1	1558.1	N/A	N/A	N/A
						COV, %	16.4%	16.8%	15.8%	11.6%	N/A	N/A	N/A
					36.2	Mean	415.8	735.8	2432.0	4164.6	179.8	54.2	14878.5
						Std. Dev.	39.7	55.0	236.5	486.5	23.1	4.8	1333.8
						COV, %	9.6%	7.5%	9.7%	11.7%	12.8%	8.9%	9.0%
			7	Bump	17.8	Mean	997.4	2476.0	5923.6	8507.6	N/A	N/A	N/A
						Std. Dev.	68.4	94.5	383.7	393.7	N/A	N/A	N/A
						COV, %	6.9%	3.8%	6.5%	4.6%	N/A	N/A	N/A
					36.2	Mean	265.0	477.2	1465.3	2442.3	98.2	167.7	22018.7
						Std. Dev.	28.4	58.7	153.8	405.8	21.4	33.6	1262.7
						COV, %	10.7%	12.3%	10.5%	16.6%	21.8%	20.0%	5.7%
			7	Optimum	17.8	Mean	1351.3	3341.2	7766.4	11902.8	N/A	N/A	N/A
						Std. Dev.	131.2	341.7	1024.2	1408.6	N/A	N/A	N/A
						COV, %	9.7%	10.2%	13.2%	11.8%	N/A	N/A	N/A
					36.2	Mean	338.0	617.4	2163.0	3373.5	90.7	140.8	17588.5
						Std. Dev.	18.6	50.5	268.2	710.9	14.3	25.0	1310.0
						COV, %	5.5%	8.2%	12.4%	21.1%	15.7%	17.8%	7.4%
			10	Optimum	17.8	Mean	940.7	2312.3	5675.3	8730.8	N/A	N/A	N/A
						Std. Dev.	57.8	63.8	488.2	1557.7	N/A	N/A	N/A
						COV, %	6.1%	2.8%	8.6%	17.8%	N/A	N/A	N/A
					36.2	Mean	259.8	440.9	1355.5	2552.1	54.0	332.3	22963.8
						Std. Dev.	50.9	73.3	173.7	388.6	2.9	50.0	2304.6
						COV, %	19.6%	16.6%	12.8%	15.2%	5.3%	15.0%	10.0%

Table 6.24. Pooled dynamic modulus and creep testing for dense-graded mixture with an NMAS of 19.0 mm and 1,000,000 ESAL traffic level

							Pooled E* (MPa)				Pooled Dynamic Creep Test Data		
NMAS	Gradation	Traffic	Air Voids, %	Binder Content	Mean Test Temperature, ℃	Test Statistic	0.1 Hz	1.0 Hz	10.0 Hz	25.0 Hz	FN	Min. Slope	Accumulated Strain at FN
19	Dense	1,000,000	4	Optimum	18.7	Mean	2106.3	5038.8	11046.2	16028.9	N/A	N/A	N/A
						Std. Dev.	176.9	681.2	1922.6	2674.2	N/A	N/A	N/A
						COV, %	8.4%	13.5%	17.4%	16.7%	N/A	N/A	N/A
					37.2	Mean	662.9	1159.1	2991.7	4854.5	607.3	14.7	13111.8
						Std. Dev.	94.8	150.9	182.9	406.4	100.4	2.7	1137.0
						COV, %	14.3%	13.0%	6.1%	8.4%	16.5%	18.5%	8.7%
			7	Bump	18.7	Mean	1365.2	3171.7	7622.7	11143.4	N/A	N/A	N/A
						Std. Dev.	199.8	484.0	1963.8	2690.5	N/A	N/A	N/A
						COV, %	14.6%	15.3%	25.8%	24.1%	N/A	N/A	N/A
					37.2	Mean	458.7	758.7	1920.1	3190.1	149.0	77.6	17497.2
						Std. Dev.	76.2	127.5	214.8	320.6	21.4	3.0	1483.9
						COV, %	16.6%	16.8%	11.2%	10.1%	14.4%	3.9%	8.5%
			7	Optimum	18.7	Mean	1390.3	3243.6	7263.6	10674.6	N/A	N/A	N/A
						Std. Dev.	187.0	664.7	1769.9	3461.1	N/A	N/A	N/A
						COV, %	13.4%	20.5%	24.4%	32.4%	N/A	N/A	N/A
					37.2	Mean	495.9	854.8	2413.6	3713.1	135.7	76.1	16381.7
						Std. Dev.	73.5	120.2	423.7	495.8	19.0	6.9	1053.8
						COV, %	14.8%	14.1%	17.6%	13.4%	14.0%	9.1%	6.4%
			10	Optimum	18.7	Mean	914.2	2062.3	4990.2	7758.0	N/A	N/A	N/A
						Std. Dev.	64.3	107.4	138.7	897.9	N/A	N/A	N/A
						COV, %	7.0%	5.2%	2.8%	11.6%	N/A	N/A	N/A
					37.2	Mean	535.1	965.4	1871.0	2808.5	70.7	174.7	17711.0
						Std. Dev.	190.0	297.1	228.6	273.5	13.2	19.8	1212.5
						COV, %	35.5%	30.8%	12.2%	9.7%	18.7%	11.4%	6.8%

Table 6.25. Pooled dynamic modulus and creep testing for dense-graded mixture with an NMAS of 12.5 mm and 1,000,000 ESAL traffic level

							Pooled E* (MPa)				Pooled Dynamic Creep Test Data		
NMAS	Gradation	Traffic	Air Voids, %	Binder Content	Mean Test Temperature, ℃	Test Statistic	0.1 Hz	1.0 Hz	10.0 Hz	25.0 Hz	FN	Min. Slope	Accumulated Strain at FN
12.5	Dense	1,000,000	4	Optimum	18.2	Mean	1889.8	4680.4	10470.6	14176.7	N/A	N/A	N/A
						Std. Dev.	182.2	450.4	1466.6	1186.9	N/A	N/A	N/A
						COV, %	9.6%	9.6%	14.0%	8.4%	N/A	N/A	N/A
					36.7	Mean	515.6	978.0	3453.7	5229.1	260.2	32.5	13702.8
						Std. Dev.	16.6	76.9	351.7	838.5	44.7	5.6	2996.3
						COV, %	3.2%	7.9%	10.2%	16.0%	17.2%	17.3%	21.9%
			7	Bump	18.2	Mean	1346.9	3505.4	8052.4	10654.7	N/A	N/A	N/A
						Std. Dev.	206.1	744.1	1972.1	2750.4	N/A	N/A	N/A
						COV, %	15.3%	21.2%	24.5%	25.8%	N/A	N/A	N/A
					36.7	Mean	346.5	624.1	2293.4	3303.6	124.8	107.9	18582.0
						Std. Dev.	68.4	123.8	418.5	639.1	24.0	9.6	2569.8
						COV, %	19.7%	19.8%	18.2%	19.3%	19.3%	8.9%	13.8%
			7	Optimum	18.2	Mean	1172.4	2928.1	6952.2	11576.5	N/A	N/A	N/A
						Std. Dev.	130.9	345.5	712.7	1467.2	N/A	N/A	N/A
						COV, %	11.2%	11.8%	10.3%	12.7%	N/A	N/A	N/A
					36.7	Mean	387.2	727.8	2496.7	3719.2	121.5	99.5	16509.2
						Std. Dev.	73.6	181.8	512.6	578.5	11.5	12.8	1571.0
						COV, %	19.0%	25.0%	20.5%	15.6%	9.5%	12.8%	9.5%
			10	Optimum	18.2	Mean	1017.2	2471.8	6245.4	8835.0	N/A	N/A	N/A
						Std. Dev.	123.7	258.1	682.3	1310.2	N/A	N/A	N/A
						COV, %	12.2%	10.4%	10.9%	14.8%	N/A	N/A	N/A
					36.7	Mean	268.9	467.4	1552.4	2336.5	67.3	291.9	23756.7
						Std. Dev.	32.5	63.7	191.5	353.4	1.4	18.2	704.3
						COV, %	12.1%	13.6%	12.3%	15.1%	2.1%	6.2%	3.0%

Table 6.26. Pooled dynamic modulus and creep testing for open-graded mixture with an NMAS of 25.0 mm and 3,000,000 ESAL traffic level

							Pooled E* (MPa)				Pooled Dynamic Creep Test Data		
NMAS	Gradation	Traffic	Air Voids, %	Binder Content	Mean Test Temperature, ℃	Test Statistic	0.1 Hz	1.0 Hz	10.0 Hz	25.0 Hz	FN	Min. Slope	Accumulated Strain at FN
25	Open	3,000,000	4	Optimum	17.3	Mean	3964.5	10368.2	27417.1	34924.2	N/A	N/A	N/A
						Std. Dev.	635.7	548.5	3327.4	4848.2	N/A	N/A	N/A
						COV, %	16.0%	5.3%	12.1%	13.9%	N/A	N/A	N/A
					35.6	Mean	938.4	1674.3	5297.5	9301.6	2880.0	2.5	16225.3
						Std. Dev.	72.5	266.3	829.9	730.0	524.4	0.5	1020.6
						COV, %	7.7%	15.9%	15.7%	7.8%	18.2%	22.1%	6.3%
			7	Bump	17.3	Mean	2070.7	5258.3	12004.0	14751.1	N/A	N/A	N/A
						Std. Dev.	230.5	343.6	859.6	1238.2	N/A	N/A	N/A
						COV, %	11.1%	6.5%	7.2%	8.4%	N/A	N/A	N/A
					35.6	Mean	471.6	870.6	3320.1	5541.7	774.0	20.1	26157.0
						Std. Dev.	85.2	148.7	704.7	1011.3	101.1	2.6	4543.5
						COV, %	18.1%	17.1%	21.2%	18.2%	13.1%	13.1%	17.4%
			7	Optimum	17.3	Mean	2913.2	6942.3	15695.8	20416.9	N/A	N/A	N/A
						Std. Dev.	622.6	875.5	744.0	1249.8	N/A	N/A	N/A
						COV, %	21.4%	12.6%	4.7%	6.1%	N/A	N/A	N/A
					35.6	Mean	562.8	1032.4	4118.9	6826.6	1387.3	7.1	20829.3
						Std. Dev.	111.9	177.4	1259.2	1893.5	615.5	3.5	6672.6
						COV, %	19.9%	17.2%	30.6%	27.7%	44.4%	49.5%	32.0%
			10	Optimum	17.3	Mean	2158.8	5286.9	13680.9	17857.8	N/A	N/A	N/A
						Std. Dev.	187.2	500.7	1920.7	2226.2	N/A	N/A	N/A
						COV, %	8.7%	9.5%	14.0%	12.5%	N/A	N/A	N/A
					35.6	Mean	509.6	862.9	2999.7	4825.7	447.7	29.7	21742.7
						Std. Dev.	38.3	34.2	170.4	987.1	47.5	1.9	676.1
						COV, %	7.5%	4.0%	5.7%	20.5%	10.6%	6.3%	3.1%

Table 6.27. Pooled dynamic modulus and creep testing for dense-graded mixture with an NMAS of 19.0 mm and 3,000,000 ESAL traffic level

							Pooled E* (MPa)				Pooled Dynamic Creep Test Data		
NMAS	Gradation	Traffic	Air Voids, %	Binder Content	Mean Test Temperature, ℃	Test Statistic	0.1 Hz	1.0 Hz	10.0 Hz	25.0 Hz	FN	Min. Slope	Accumulated Strain at FN
19	Dense	3,000,000	4	Optimum	18.8	Mean	1781.6	4306.5	10278.9	15907.1	N/A	N/A	N/A
						Std. Dev.	183.4	701.4	2178.5	3660.4	N/A	N/A	N/A
						COV, %	10.3%	16.3%	21.2%	23.0%	N/A	N/A	N/A
					36.9	Mean	501.9	926.8	3059.1	5616.5	532.2	24.0	12415.9
						Std. Dev.	63.3	123.2	446.0	915.6	133.7	2.8	1364.3
						COV, %	12.6%	13.3%	14.6%	16.3%	25.1%	11.8%	11.0%
			7	Bump	18.8	Mean	1237.7	2958.2	6917.8	10048.0	N/A	N/A	N/A
						Std. Dev.	156.0	308.9	829.7	1417.9	N/A	N/A	N/A
						COV, %	12.6%	10.4%	12.0%	14.1%	N/A	N/A	N/A
					36.9	Mean	417.0	722.5	2145.1	3525.6	215.1	80.6	17055.7
						Std. Dev.	68.8	111.7	427.3	865.8	19.6	7.9	1221.4
						COV, %	16.5%	15.5%	19.9%	24.6%	9.1%	9.8%	7.2%
			7	Optimum	18.8	Mean	1465.1	3515.8	8304.6	12138.4	N/A	N/A	N/A
						Std. Dev.	197.4	499.7	1024.3	1306.4	N/A	N/A	N/A
						COV, %	13.5%	14.2%	12.3%	10.8%	N/A	N/A	N/A
					36.9	Mean	430.0	762.5	2524.2	4489.5	206.8	78.6	15360.7
						Std. Dev.	64.6	83.6	243.1	597.3	41.4	2.3	1680.0
						COV, %	15.0%	11.0%	9.6%	13.3%	20.0%	2.9%	10.9%
			10	Optimum	18.8	Mean	1077.2	2638.2	6472.8	9697.7	N/A	N/A	N/A
						Std. Dev.	106.4	386.6	1336.9	1743.9	N/A	N/A	N/A
						COV, %	9.9%	14.7%	20.7%	18.0%	N/A	N/A	N/A
					36.9	Mean	346.6	590.4	1875.1	3041.8	86.8	211.9	19014.9
						Std. Dev.	68.5	97.4	586.3	787.6	7.5	16.4	1335.1
						COV, %	19.8%	16.5%	31.3%	25.9%	8.7%	7.7%	7.0%

Table 6.28. Pooled dynamic modulus and creep testing for dense-graded mixture with an NMAS of 12.5 mm and 3,000,000 ESAL traffic level

							Pooled E* (MPa)				Pooled Dynamic Creep Test Data		
NMAS	Gradation	Traffic	Air Voids, %	Binder Content	Mean Test Temperature, ℃	Test Statistic	0.1 Hz	1.0 Hz	10.0 Hz	25.0 Hz	FN	Min. Slope	Accumulated Strain at FN
12.5	Dense	3,000,000	4	Optimum	17.5	Mean	2339.0	5179.9	11317.9	14398.1	N/A	N/A	N/A
						Std. Dev.	255.9	419.1	1301.4	2158.5	N/A	N/A	N/A
						COV, %	10.9%	8.1%	11.5%	15.0%	N/A	N/A	N/A
					36.2	Mean	618.1	1188.4	4026.1	5793.1	2649.3	37.3	12574.7
						Std. Dev.	143.8	211.9	828.3	997.5	528.4	11.3	1464.3
						COV, %	23.3%	17.8%	20.6%	17.2%	19.9%	30.2%	11.6%
			7	Bump	17.5	Mean	1740.1	4068.3	8660.5	11045.1	N/A	N/A	N/A
						Std. Dev.	260.5	548.9	632.0	877.6	N/A	N/A	N/A
						COV, %	15.0%	13.5%	7.3%	7.9%	N/A	N/A	N/A
					36.2	Mean	465.0	874.7	2721.6	4564.2	563.8	148.2	19722.0
						Std. Dev.	78.3	147.3	703.1	1435.8	313.5	69.0	3352.5
						COV, %	16.8%	16.8%	25.8%	31.5%	55.6%	46.5%	17.0%
			7	Optimum	17.5	Mean	1646.0	3908.8	8713.8	12282.7	N/A	N/A	N/A
						Std. Dev.	249.0	568.8	1111.2	2418.3	N/A	N/A	N/A
						COV, %	15.1%	14.6%	12.8%	19.7%	N/A	N/A	N/A
					36.2	Mean	457.7	879.0	3068.0	4560.5	358.9	118.8	17147.2
						Std. Dev.	144.4	215.1	552.0	998.4	91.9	30.4	1493.2
						COV, %	31.6%	24.5%	18.0%	21.9%	25.6%	25.6%	8.7%
			10	Optimum	17.5	Mean	1187.4	2923.9	7444.0	10110.1	N/A	N/A	N/A
						Std. Dev.	117.3	278.2	567.5	1303.6	N/A	N/A	N/A
						COV, %	9.9%	9.5%	7.6%	12.9%	N/A	N/A	N/A
					36.2	Mean	327.6	597.6	1904.3	3155.3	200.3	234.6	25676.3
						Std. Dev.	64.1	121.3	309.1	524.3	56.1	73.5	8920.6
						COV, %	19.6%	20.3%	16.2%	16.6%	28.0%	31.3%	34.7%

Table 6.29. Pooled dynamic modulus and creep testing for dense-graded mixture with an NMAS of 19.0 mm and >3,000,000 ESAL traffic level

							Pooled E* (MPa)				Pooled Dynamic Creep Test Data		
NMAS	Gradation	Traffic	Air Voids, %	Binder Content	Mean Test Temperature, ℃	Test Statistic	0.1 Hz	1.0 Hz	10.0 Hz	25.0 Hz	FN	Min. Slope	Accumulated Strain at FN
19	Dense	>3,000,000	4	Optimum	17.9	Mean	2870.9	6672.6	13928.7	17597.9	N/A	N/A	N/A
						Std. Dev.	656.2	1440.6	2262.2	2214.6	N/A	N/A	N/A
						COV, %	22.9%	21.6%	16.2%	12.6%	N/A	N/A	N/A
					35.9	Mean	736.0	1564.7	4153.4	6487.2	3000.5	1.6	12142.7
						Std. Dev.	86.0	154.0	268.2	545.8	570.0	0.5	679.2
						COV, %	11.7%	9.8%	6.5%	8.4%	19.0%	30.7%	5.6%
			7	Bump	17.9	Mean	2080.9	4905.9	10407.9	13086.0	N/A	N/A	N/A
						Std. Dev.	40.2	284.7	1797.6	2835.7	N/A	N/A	N/A
						COV, %	1.9%	5.8%	17.3%	21.7%	N/A	N/A	N/A
					35.9	Mean	520.0	984.9	2816.4	4497.0	2596.5	5.6	15611.5
						Std. Dev.	105.0	177.4	355.8	661.1	460.6	1.3	754.5
						COV, %	20.2%	18.0%	12.6%	14.7%	17.7%	22.3%	4.8%
			7	Optimum	17.9	Mean	1700.4	3997.5	8467.2	11680.8	N/A	N/A	N/A
						Std. Dev.	126.6	319.3	708.0	1440.7	N/A	N/A	N/A
						COV, %	7.4%	8.0%	8.4%	12.3%	N/A	N/A	N/A
					35.9	Mean	671.9	1182.2	2856.4	4168.7	1766.8	3.0	13292.5
						Std. Dev.	63.5	86.3	211.8	370.9	330.3	0.7	1454.2
						COV, %	9.4%	7.3%	7.4%	8.9%	18.7%	24.0%	10.9%
			10	Optimum	17.9	Mean	1682.1	3611.5	7448.7	9693.5	N/A	N/A	N/A
						Std. Dev.	487.9	1102.8	2246.3	2684.0	N/A	N/A	N/A
						COV, %	29.0%	30.5%	30.2%	27.7%	N/A	N/A	N/A
					35.9	Mean	465.6	835.9	2241.9	3530.2	1160.3	22.7	19239.5
						Std. Dev.	117.4	199.2	463.0	593.5	402.9	4.2	2839.9
						COV, %	25.2%	23.8%	20.7%	16.8%	34.7%	18.3%	14.8%

Table 6.30. Pooled dynamic modulus and creep testing for open-graded mixture with an NMAS of 19.0 mm and >3,000,000 ESAL traffic level

							Pooled E* (MPa)				Pooled Dynamic Creep Test Data		
NMAS	Gradation	Traffic	Air Voids, %	Binder Content	Mean Test Temperature, ℃	Test Statistic	0.1 Hz	1.0 Hz	10.0 Hz	25.0 Hz	FN	Min. Slope	Accumulated Strain at FN
19	Open	>3,000,000	4	Optimum	19.0	Mean	3857.6	9768.8	20501.9	26066.9	N/A	N/A	N/A
						Std. Dev.	516.2	982.4	2802.6	3735.4	N/A	N/A	N/A
						COV, %	13.4%	10.1%	13.7%	14.3%	N/A	N/A	N/A
					37.5	Mean	603.2	1240.6	5317.4	8942.5	2365.3	2.3	13094.3
						Std. Dev.	157.9	437.7	2328.7	3113.3	1176.3	1.2	1431.0
						COV, %	26.2%	35.3%	43.8%	34.8%	49.7%	52.5%	10.9%
			7	Bump	19.0	Mean	3281.0	8090.4	16007.9	19866.1	N/A	N/A	N/A
						Std. Dev.	420.2	1192.5	3002.7	3504.3	N/A	N/A	N/A
						COV, %	12.8%	14.7%	18.8%	17.6%	N/A	N/A	N/A
					37.5	Mean	474.1	975.7	3378.0	5629.0	1076.0	10.2	21902.0
						Std. Dev.	66.4	188.4	803.5	2115.8	335.6	4.3	4264.1
						COV, %	14.0%	19.3%	23.8%	37.6%	31.2%	42.3%	19.5%
			7	Optimum	19.0	Mean	2586.9	7055.6	16404.3	20837.2	N/A	N/A	N/A
						Std. Dev.	296.7	920.2	1980.5	2077.1	N/A	N/A	N/A
						COV, %	11.5%	13.0%	12.1%	10.0%	N/A	N/A	N/A
					37.5	Mean	466.7	940.1	3267.4	4899.8	1024.7	9.0	17924.3
						Std. Dev.	56.1	122.7	581.6	937.7	364.5	4.0	1140.9
						COV, %	12.0%	13.1%	17.8%	19.1%	35.6%	44.5%	6.4%
			10	Optimum	19.0	Mean	2706.0	7106.7	15883.6	20204.5	N/A	N/A	N/A
						Std. Dev.	963.4	2226.2	4442.1	5723.3	N/A	N/A	N/A
						COV, %	35.6%	31.3%	28.0%	28.3%	N/A	N/A	N/A
					37.5	Mean	529.6	980.7	3504.2	6173.9	579.7	20.0	22173.3
						Std. Dev.	173.8	206.6	461.8	1545.7	76.0	3.4	1246.3
						COV, %	32.8%	21.1%	13.2%	25.0%	13.1%	17.0%	5.6%

Table 6.31. Pooled dynamic modulus and creep testing for dense-graded mixture with an NMAS of 12.5 mm and >3,000,000 ESAL traffic level

							Pooled E* (MPa)				Pooled Dynamic Creep Test Data		
NMAS	Gradation	Traffic	Air Voids, %	Binder Content	Mean Test Temperature, ℃	Test Statistic	0.1 Hz	1.0 Hz	10.0 Hz	25.0 Hz	FN	Min. Slope	Accumulated Strain at FN
12.5	Dense	>3,000,000	4	Optimum	19.3	Mean	2169.9	4876.4	11672.0	16679.5	N/A	N/A	N/A
						Std. Dev.	346.5	882.2	2915.6	3578.9	N/A	N/A	N/A
						COV, %	16.0%	18.1%	25.0%	21.5%	N/A	N/A	N/A
					37.2	Mean	693.7	1121.4	3299.1	5259.7	4029.3	1.5	12713.7
						Std. Dev.	102.2	124.4	364.4	928.7	949.1	0.2	2082.1
						COV, %	14.7%	11.1%	11.0%	17.7%	23.6%	13.5%	16.4%
			7	Bump	19.3	Mean	1398.9	3180.4	7732.7	10845.1	N/A	N/A	N/A
						Std. Dev.	152.1	351.5	1110.6	1882.9	N/A	N/A	N/A
						COV, %	10.9%	11.1%	14.4%	17.4%	N/A	N/A	N/A
					37.2	Mean	541.5	817.6	2446.2	3935.2	906.1	12.4	19427.1
						Std. Dev.	67.6	81.5	317.3	522.3	401.1	5.3	5073.5
						COV, %	12.5%	10.0%	13.0%	13.3%	44.3%	42.9%	26.1%
			7	Optimum	19.3	Mean	1776.8	3978.5	10219.7	13420.1	N/A	N/A	N/A
						Std. Dev.	202.3	493.2	1002.0	1355.1	N/A	N/A	N/A
						COV, %	11.4%	12.4%	9.8%	10.1%	N/A	N/A	N/A
					37.2	Mean	612.1	985.5	2888.9	4777.8	1147.3	7.0	15936.9
						Std. Dev.	66.0	117.3	493.1	1010.1	265.8	1.4	2098.6
						COV, %	10.8%	11.9%	17.1%	21.1%	23.2%	20.1%	13.2%
			10	Optimum	19.3	Mean	1113.2	2557.2	6082.5	8080.5	N/A	N/A	N/A
						Std. Dev.	72.8	352.9	644.5	611.7	N/A	N/A	N/A
						COV, %	6.5%	13.8%	10.6%	7.6%	N/A	N/A	N/A
					37.2	Mean	427.0	648.3	1942.9	2999.0	576.2	18.7	20085.2
						Std. Dev.	57.9	83.8	205.5	315.7	108.2	1.0	1999.3
						COV, %	13.5%	12.9%	10.6%	10.5%	18.8%	5.6%	10.0%

Table 6.32. Pooled dynamic modulus and creep testing for open-graded mixture with an NMAS of 12.5 mm and >3,000,000 ESAL traffic level

							Pooled E* (MPa)				Pooled Dynamic Creep Test Data		
NMAS	Gradation	Traffic	Air Voids, %	Binder Content	Mean Test Temperature, ℃	Test Statistic	0.1 Hz	1.0 Hz	10.0 Hz	25.0 Hz	FN	Min. Slope	Accumulated Strain at FN
12.5	Open	>3,000,000	4	Optimum	18.4	Mean	868.1	1834.1	4437.2	6974.8	N/A	N/A	N/A
						Std. Dev.	116.4	338.3	1104.6	1283.3	N/A	N/A	N/A
						COV, %	13.4%	18.4%	24.9%	18.4%	N/A	N/A	N/A
					36.5	Mean	385.1	536.5	1425.5	3192.3	2622.7	2.5	17659.7
						Std. Dev.	47.3	61.1	160.5	792.6	888.8	0.5	1367.1
						COV, %	12.3%	11.4%	11.3%	24.8%	33.9%	21.0%	7.7%
			7	Bump	18.4	Mean	1094.6	2187.2	6478.2	13989.4	N/A	N/A	N/A
						Std. Dev.	147.4	314.7	2207.0	3059.4	N/A	N/A	N/A
						COV, %	13.5%	14.4%	34.1%	21.9%	N/A	N/A	N/A
					36.5	Mean	448.9	631.8	2528.9	3990.4	4986.7	1.4	20109.0
						Std. Dev.	20.5	50.2	1613.0	1914.4	1146.7	0.1	1871.8
						COV, %	4.6%	7.9%	63.8%	48.0%	23.0%	9.7%	9.3%
			7	Optimum	18.4	Mean	886.3	1775.4	4146.2	7466.9	N/A	N/A	N/A
						Std. Dev.	124.6	189.9	548.7	628.0	N/A	N/A	N/A
						COV, %	14.1%	10.7%	13.2%	8.4%	N/A	N/A	N/A
					36.5	Mean	484.6	703.4	1970.1	3560.5	5840.0	1.1	17121.7
						Std. Dev.	43.0	65.7	131.9	935.3	1304.1	0.4	772.1
						COV, %	8.9%	9.3%	6.7%	26.3%	22.3%	34.0%	4.5%
			10	Optimum	18.4	Mean	1156.3	2314.4	6125.3	9013.3	N/A	N/A	N/A
						Std. Dev.	26.4	216.4	1152.2	2082.1	N/A	N/A	N/A
						COV, %	2.3%	9.4%	18.8%	23.1%	N/A	N/A	N/A
					36.5	Mean	393.2	558.2	1627.8	2897.6	6104.0	1.0	17942.3
						Std. Dev.	18.9	51.0	236.4	503.1	1845.9	0.2	1946.2
						COV, %	4.8%	9.1%	14.5%	17.4%	30.2%	21.8%	10.8%

6.3.23 Statistical Analysis

Statistical Analysis Software (SAS) was used to determine the effects of traffic level, NMAS, gradation, air voids and binder content on flow number (FN) and accumulated microstrain (AMS) at flow number. The general linear model (GLM), using a 95% level of confidence ($\alpha = 0.05$), was used to determine if the above factors affect flow number and accumulated microstrain at flow number. The GLM provides a Type I and Type III sum of squares error using an F-statistic and p-value, which is analogous to performing a multiple analysis of variance (ANOVA). Multiple comparisons using least squares difference (LSD) t-tests were performed on traffic level, NMAS, air voids, and binder content to determine if there were statistical differences within a given factor. A 0.05 level of significance was used for the multiple comparison procedure.

Table 6.33 and Table 6.34 show FN and AMS as a function of traffic level, NMAS, gradation, air voids and asphalt content, respectively. Table 6.33 shows that traffic level, NMAS, gradation, and air voids are statistically significant variables in the model. The table also illustrates that different levels within a factor are statistically significant. All levels within the traffic level are statistically significant, except when comparing 1,000,000 ESAL HMA mixtures to 300,000 ESAL mixtures. Also, the data show that there are no statistical differences in NMAS levels, except when comparing 19.0 mm and 12.5 mm mixtures. This is due to the fact that only one 25.0 mm mixture was sampled and the majority of the mixtures were 12.5 mm or 19.0 mm mixtures. The population data set is slightly unbalanced. Also, the statistics demonstrate that there are differences between open-graded and dense-graded mixtures. The multiple comparison procedure also identifies statistically significant differences between 4.0% and 7.0% and between 4.0% and 10.0% air void levels. No statistical difference was seen between field mixes at optimum binder content and those at a 0.3% binder bump.

Table 6.34 shows that NMAS, gradation, air voids, and asphalt content are statistically significant variables in the model. The table also illustrates that different levels within a factor are statistically significant. All levels within the traffic level are statistically significant, except when comparing 1,000,000 ESAL HMA mixtures to 300,000 ESAL mixtures. Also, the data show that there are statistical differences in all NMAS levels. Also, the statistics show that there are differences between open-graded and dense-graded mixtures. The multiple comparison procedure also identifies statistically significant differences in all air void levels. Statistical

differences were seen between field mixes at optimum binder content and those at a 0.3% binder bump. The statistical analysis indicates that flow number may be used for quality control purposes, and accumulated microstrain at flow number may be used for quality assurance purposes.

Table 6.33. GLM and LSD results for flow number test results

Model	FN=f(traffic, NMAS, gradation, air voids, asphalt content)			
	Independent Variables	F-Statistic	p-value	
	Traffic	39.58	<0.0001	
	NMAS	5.54	0.0044	
	Gradation	17.40	<0.0001	
	Air Voids	16.76	<0.0001	
	Asphalt Content	0.00	0.9651	
	R^2	0.43		
	COV	123.4		

Traffic Comparisons	Results at 0.05 level of significance
>3,000,000 vs. 3,000,000	Statistically Significant
>3,000,000 vs. 1,000,000	Statistically Significant
>3,000,000 vs. 300,000	Statistically Significant
3,000,000 vs. 1,000,000	Statistically Significant
3,000,000 vs. 300,000	Statistically Significant
1,000,000 vs. 300,000	Not Statistically Significant

NMAS Comparisons	Results at 0.05 level of significance
25mm vs. 12.5mm	Not Statistically Significant
25mm vs. 19.0mm	Not Statistically Significant
12.5mm vs.19.0mm	Statistically Significant

Gradation Comparison	Results at 0.05 level of significance
Dense vs. Open	Statistically Significant

Air Voids Comparisons	Results at 0.05 level of significance
4.0% vs. 7.0%	Statistically Significant
4.0% vs. 10.0%	Statistically Significant
7.0% vs. 10.0%	Not Statistically Significant

Asphalt Content Comparison	Results at 0.05 level of significance
Optimum vs. Binder Bump	Not Statistically Significant

Table 6.34. GLM and LSD results for accumulated microstrain at flow number test results

Model	AMS=f(traffic, NMAS, gradation, air voids, asphalt content)			
	Independent Variables	F-Statistic	p-value	
	Traffic	1.62	0.1858	
	NMAS	15.97	<0.0001	
	Gradation	8.41	0.0041	
	Air Voids	79.23	<0.0001	
	Asphalt Content	19.33	<0.0001	
	R^2	0.48		
	COV	20.0		

Traffic Comparisons	Results at 0.05 level of significance
>3,000,000 vs. 3,000,000	Not Statistically Significant
>3,000,000 vs. 1,000,000	Not Statistically Significant
>3,000,000 vs. 300,000	Not Statistically Significant
3,000,000 vs. 1,000,000	Not Statistically Significant
3,000,000 vs. 300,000	Not Statistically Significant
1,000,000 vs. 300,000	Not Statistically Significant

NMAS Comparisons	Results at 0.05 level of significance
25mm vs. 12.5mm	Statistically Significant
25mm vs. 19.0mm	Statistically Significant
12.5mm vs.19.0mm	Statistically Significant

Gradation Comparison	Results at 0.05 level of significance
Dense vs. Open	Statistically Significant

Air Voids Comparisons	Results at 0.05 level of significance
4.0% vs. 7.0%	Statistically Significant
4.0% vs. 10.0%	Statistically Significant
7.0% vs. 10.0%	Statistically Significant

Asphalt Content Comparison	Results at 0.05 level of significance
Optimum vs. Binder Bump	Statistically Significant

Tables 6.35 through 6.42 show the results of E* as a function of traffic level, NMAS, gradation, air voids, and binder content while blocking on test temperature and frequency. Tables 6.35 through 6.38 show the statistical results for the intermediate test temperature and all frequencies. All four statistical analyses arrive at almost the same conclusions. Traffic level, NMAS, and air voids are statistically significant variables in the model. Gradation appears to be statistically significant, but only at 25.0 Hz. The multiple comparison procedure found that all levels of NMAS, gradation, and air voids are statistically significant. There was no statistical significance when comparing optimum binder content to binder bump. The majority of the traffic levels were found to be statistically significant, except when comparing >3,000,000 to 3,000,000 ESALs and 1,000,000 to 300,000 ESALs. This could be a function of the mix design, where higher traffic mixtures require additional amounts of manufactured sand, which results in higher

FAA values and larger percentages in crushed materials for the coarse aggregates. Tables 6.39 through 6.42 show the statistical results for the high test temperature and all frequencies. All four statistical analyses arrive at almost the same conclusions. Traffic level, NMAS, gradation, and air voids are statistically significant variables in the model. Gradation is not statistically significant at 10.0 or 25.0 Hz. The multiple comparison procedure found that, most of the time, all levels of NMAS, gradation, air voids, and binder content are statistically significant. There were some cases with NMAS, gradation, and binder content where the results changed due to test frequency. The majority of the traffic levels were found to be statistically significant. Some differences were found; these differences were frequency dependent.

Table 6.35. GLM and LSD results for E* test results at intermediate temperature and 0.1 Hz

Model	E* at Int. Temp. and 0.1 Hz=f(traffic, NMAS, gradation, air voids, asphalt content)			
	Independent Variables	F-Statistic	p-value	
	Traffic	7.31	0.0001	
	NMAS	17.46	<0.0001	
	Gradation	1.52	0.2192	
	Air Voids	26.22	<0.0001	
	Asphalt Content	0.19	0.6635	
	R^2	0.31		
	COV	45.6		

Traffic Comparisons	Result at 0.05 level of significance
>3,000,000 vs. 3,000,000	Not Statistically Significant
>3,000,000 vs. 1,000,000	Statistically Significant
>3,000,000 vs. 300,000	Statistically Significant
3,000,000 vs. 1,000,000	Statistically Significant
3,000,000 vs. 300,000	Statistically Significant
1,000,000 vs. 300,000	Not Statistically Significant

NMAS Comparisons	Result at 0.05 level of significance
25mm vs. 12.5mm	Statistically Significant
25mm vs. 19.0mm	Statistically Significant
12.5mm vs.19.0mm	Statistically Significant

Gradation Comparison	Result at 0.05 level of significance
Dense vs. Open	Statistically Significant

Air Voids Comparisons	Result at 0.05 level of significance
4.0% vs. 7.0%	Statistically Significant
4.0% vs. 10.0%	Statistically Significant
7.0% vs. 10.0%	Statistically Significant

Asphalt Content Comparison	Result at 0.05 level of significance
Optimum vs. Binder Bump	Not Statistically Significant

Table 6.36. GLM and LSD results for E* test results at intermediate temperature and 1.0 Hz

Model	E* at Int. Temp. and 1.0 Hz=f(traffic, NMAS, gradation, air voids, asphalt content)		
	Independent Variables	F-Statistic	p-value
	Traffic	5.33	0.0014
	NMAS	23.79	<0.0001
	Gradation	3.70	0.0554
	Air Voids	26.50	<0.0001
	Asphalt Content	0.17	0.6818
	R^2	0.33	
	COV	45.0	

Traffic Comparisons	Result at 0.05 level of significance
>3,000,000 vs. 3,000,000	Not Statistically Significant
>3,000,000 vs. 1,000,000	Statistically Significant
>3,000,000 vs. 300,000	Statistically Significant
3,000,000 vs. 1,000,000	Statistically Significant
3,000,000 vs. 300,000	Statistically Significant
1,000,000 vs. 300,000	Not Statistically Significant

NMAS Comparisons	Result at 0.05 level of significance
25mm vs. 12.5mm	Statistically Significant
25mm vs. 19.0mm	Statistically Significant
12.5mm vs.19.0mm	Statistically Significant

Gradation Comparison	Result at 0.05 level of significance
Dense vs. Open	Statistically Significant

Air Voids Comparisons	Result at 0.05 level of significance
4.0% vs. 7.0%	Statistically Significant
4.0% vs. 10.0%	Statistically Significant
7.0% vs. 10.0%	Statistically Significant

Asphalt Content Comparison	Result at 0.05 level of significance
Optimum vs. Binder Bump	Not Statistically Significant

Table 6.37. GLM and LSD results for E* test results at intermediate temperature and 10.0 Hz

Model	E* at Int. Temp. and 10.0 Hz=f(traffic, NMAS, gradation, air voids, asphalt content)		
	Independent Variables	F-Statistic	p-value
	Traffic	5.20	0.0017
	NMAS	32.41	<0.0001
	Gradation	3.50	0.0624
	Air Voids	27.00	<0.0001
	Asphalt Content	0.39	0.5351
	R^2	0.36	
	COV	41.2	

Traffic Comparisons	Result at 0.05 level of significance
>3,000,000 vs. 3,000,000	Not Statistically Significant
>3,000,000 vs. 1,000,000	Statistically Significant
>3,000,000 vs. 300,000	Statistically Significant
3,000,000 vs. 1,000,000	Statistically Significant
3,000,000 vs. 300,000	Statistically Significant
1,000,000 vs. 300,000	Not Statistically Significant

NMAS Comparisons	Result at 0.05 level of significance
25mm vs. 12.5mm	Statistically Significant
25mm vs. 19.0mm	Statistically Significant
12.5mm vs.19.0mm	Statistically Significant

Gradation Comparison	Result at 0.05 level of significance
Dense vs. Open	Statistically Significant

Air Voids Comparisons	Result at 0.05 level of significance
4.0% vs. 7.0%	Statistically Significant
4.0% vs. 10.0%	Statistically Significant
7.0% vs. 10.0%	Statistically Significant

Asphalt Content Comparison	Result at 0.05 level of significance
Optimum vs. Binder Bump	Not Statistically Significant

Table 6.38. GLM and LSD results for E* test results at intermediate temperature and 25.0 Hz

Model	E* at Int. Temp. and 25.0 Hz=f(traffic, NMAS, gradation, air voids, asphalt content)			
	Independent Variables	F-Statistic	p-value	
	Traffic	2.31	0.0766	
	NMAS	30.73	<0.0001	
	Gradation	5.72	0.0176	
	Air Voids	29.92	<0.0001	
	Asphalt Content	1.14	0.2862	
	R^2	0.36		
	COV	36.9		

Traffic Comparisons	Result at 0.05 level of significance
>3,000,000 vs. 3,000,000	Not Statistically Significant
>3,000,000 vs. 1,000,000	Statistically Significant
>3,000,000 vs. 300,000	Not Statistically Significant
3,000,000 vs. 1,000,000	Statistically Significant
3,000,000 vs. 300,000	Not Statistically Significant
1,000,000 vs. 300,000	Not Statistically Significant

NMAS Comparisons	Result at 0.05 level of significance
25mm vs. 12.5mm	Statistically Significant
25mm vs. 19.0mm	Statistically Significant
12.5mm vs.19.0mm	Statistically Significant

Gradation Comparison	Result at 0.05 level of significance
Dense vs. Open	Statistically Significant

Air Voids Comparisons	Result at 0.05 level of significance
4.0% vs. 7.0%	Statistically Significant
4.0% vs. 10.0%	Statistically Significant
7.0% vs. 10.0%	Statistically Significant

Asphalt Content Comparison	Result at 0.05 level of significance
Optimum vs. Binder Bump	Not Statistically Significant

Table 6.39. GLM and LSD results for E* test results at high temperature and 0.1 Hz

Model	E* at High Temp. and 0.1 Hz=f(traffic, NMAS, gradation, air voids, asphalt content)		
	Independent Variables	F-Statistic	p-value
	Traffic	14.71	<0.0001
	NMAS	8.76	0.0002
	Gradation	8.64	0.0036
	Air Voids	28.93	<0.0001
	Asphalt Content	2.38	0.1240
	R^2	0.35	
	COV	33.0	

Traffic Comparisons	Result at 0.05 level of significance
>3,000,000 vs. 3,000,000	Statistically Significant
>3,000,000 vs. 1,000,000	Statistically Significant
>3,000,000 vs. 300,000	Statistically Significant
3,000,000 vs. 1,000,000	Not Statistically Significant
3,000,000 vs. 300,000	Statistically Significant
1,000,000 vs. 300,000	Statistically Significant

NMAS Comparisons	Result at 0.05 level of significance
25mm vs. 12.5mm	Statistically Significant
25mm vs. 19.0mm	Statistically Significant
12.5mm vs.19.0mm	Statistically Significant

Gradation Comparison	Result at 0.05 level of significance
Dense vs. Open	Not Statistically Significant

Air Voids Comparisons	Result at 0.05 level of significance
4.0% vs. 7.0%	Statistically Significant
4.0% vs. 10.0%	Statistically Significant
7.0% vs. 10.0%	Statistically Significant

Asphalt Content Comparison	Result at 0.05 level of significance
Optimum vs. Binder Bump	Statistically Significant

Table 6.40. GLM and LSD results for E* test results at high temperature and 1.0 Hz

Model	E* at High Temp. and 1.0 Hz=f(traffic, NMAS, gradation, air voids, asphalt content)			
	Independent Variables	F-Statistic	p-value	
	Traffic	9.52	<0.0001	
	NMAS	7.96	0.0004	
	Gradation	5.31	0.0220	
	Air Voids	27.68	<0.0001	
	Asphalt Content	2.18	0.1410	
	R^2	0.31		
	COV	39.3		

Traffic Comparisons	Result at 0.05 level of significance
>3,000,000 vs. 3,000,000	Not Statistically Significant
>3,000,000 vs. 1,000,000	Statistically Significant
>3,000,000 vs. 300,000	Statistically Significant
3,000,000 vs. 1,000,000	Not Statistically Significant
3,000,000 vs. 300,000	Statistically Significant
1,000,000 vs. 300,000	Statistically Significant

NMAS Comparisons	Result at 0.05 level of significance
25mm vs. 12.5mm	Statistically Significant
25mm vs. 19.0mm	Statistically Significant
12.5mm vs.19.0mm	Statistically Significant

Gradation Comparison	Result at 0.05 level of significance
Dense vs. Open	Not Statistically Significant

Air Voids Comparisons	Result at 0.05 level of significance
4.0% vs. 7.0%	Statistically Significant
4.0% vs. 10.0%	Statistically Significant
7.0% vs. 10.0%	Statistically Significant

Asphalt Content Comparison	Result at 0.05 level of significance
Optimum vs. Binder Bump	Statistically Significant

Table 6.41. GLM and LSD results for E* test results at high temperature and 10.0 Hz

Model	E* at High Temp. and 10.0 Hz=f(traffic, NMAS, gradation, air voids, asphalt content)			
	Independent Variables	F-Statistic	p-value	
	Traffic	8.28	<0.0001	
	NMAS	7.22	0.0009	
	Gradation	0.07	0.7888	
	Air Voids	28.61	<0.0001	
	Asphalt Content	2.48	0.1167	
	R^2	0.29		
	COV	42.2		

Traffic Comparisons	Result at 0.05 level of significance
>3,000,000 vs. 3,000,000	Not Statistically Significant
>3,000,000 vs. 1,000,000	Statistically Significant
>3,000,000 vs. 300,000	Statistically Significant
3,000,000 vs. 1,000,000	Statistically Significant
3,000,000 vs. 300,000	Statistically Significant
1,000,000 vs. 300,000	Not Statistically Significant

NMAS Comparisons	Result at 0.05 level of significance
25mm vs. 12.5mm	Statistically Significant
25mm vs. 19.0mm	Statistically Significant
12.5mm vs.19.0mm	Not Statistically Significant

Gradation Comparison	Result at 0.05 level of significance
Dense vs. Open	Statistically Significant

Air Voids Comparisons	Result at 0.05 level of significance
4.0% vs. 7.0%	Statistically Significant
4.0% vs. 10.0%	Statistically Significant
7.0% vs. 10.0%	Statistically Significant

Asphalt Content Comparison	Result at 0.05 level of significance
Optimum vs. Binder Bump	Not Statistically Significant

Table 6.42. GLM and LSD results for E* test results at high temperature and 25.0 Hz

Model	E* at High Temp. and 25.0 Hz=f(traffic, NMAS, gradation, air voids, asphalt content)			
	Independent Variables	F-Statistic	p-value	
	Traffic	10.74	<0.0001	
	NMAS	11.08	<0.0001	
	Gradation	1.37	0.2426	
	Air Voids	34.79	<0.0001	
	Asphalt Content	2.01	0.1573	
	R^2	0.34		
	COV	39.0		

Traffic Comparisons	Result at 0.05 level of significance
>3,000,000 vs. 3,000,000	Not Statistically Significant
>3,000,000 vs. 1,000,000	Statistically Significant
>3,000,000 vs. 300,000	Not Statistically Significant
3,000,000 vs. 1,000,000	Statistically Significant
3,000,000 vs. 300,000	Not Statistically Significant
1,000,000 vs. 300,000	Not Statistically Significant

NMAS Comparisons	Result at 0.05 level of significance
25mm vs. 12.5mm	Statistically Significant
25mm vs. 19.0mm	Statistically Significant
12.5mm vs.19.0mm	Statistically Significant

Gradation Comparison	Result at 0.05 level of significance
Dense vs. Open	Statistically Significant

Air Voids Comparisons	Result at 0.05 level of significance
4.0% vs. 7.0%	Statistically Significant
4.0% vs. 10.0%	Statistically Significant
7.0% vs. 10.0%	Statistically Significant

Asphalt Content Comparison	Result at 0.05 level of significance
Optimum vs. Binder Bump	Not Statistically Significant

CHAPTER 7. AASHTO M-E PDG SIMULATIONS

7.1 Pavement Design

In addition to analyzing the results of the dynamic modulus and flow number testing, the pavement designs were analyzed using the actual constructed pavement structure and traffic information supplied by WisDOT. The measured dynamic modulus values were used as direct inputs in the Level 1 design, whereas the other pavement layers used either a Level 2 or 3 design input, depending upon the available information. The Mechanistic-Empirical Pavement Design (ME-PDG) Guide, Version 0.75, and the WisPave software were used to analyze the pavement structures. Several assumptions had to be made during the pavement analysis because not all of the information was available. Some information was gathered using soil survey books from the various counties in Wisconsin, if subgrade soil information was not provided by WisDOT. These assumptions are explained where applicable. The performance criteria that were used as default values in the Design Guide software are presented in Table 7.1.

Table 7.1. Design guide software performance criteria

Distress	Performance criteria
Permanent deformation AC layer only (mm)	6.0
Permanent deformation total pavement (mm)	19.0
IRI (mm/km)	2,715.0
Longitudinal cracking (m/500)	305.0
Alligator cracking (%)	25.0

The ensuing sections describe the pavement design analysis that was conducted for each mix as part of this project.

7.1.1 Brule

The Brule E-0.3 19.0 mm pavement design consisted of 127.0 mm (5.0 in) of HMA on 254.0 mm (10 in) of crushed aggregate base course (CABC) on 304.8 mm (12 in) of a granular base on a subgrade of A-7 soil. The main composition of an A-7 soil is highly plastic clay, under the AASHTO soil classification system. A level 1 analysis was used for the 19.0 mm NMAS layer utilizing the dynamic modulus test results shown in the previous chapter. A modulus value of 275.8 MPa (40 ksi) was used for the CABC layer. A plasticity index of 1, with 10% passing the #200 sieve, 30% passing the #4 sieve, and a D60 of 2 mm were also used as inputs for the crushed gravel. The D60 refers to the grain size that corresponds to 60% passing (Coduto 1999). A modulus value of 275.8 MPa (40 ksi) was used for the granular base layer. The subgrade was reported to have a support value of 3.0 and, using the Design Guide software, yielded an analogous modulus value of 20.8 MPa (3.02 ksi). This layer was divided into a 152.4 mm (6 in) layer, followed by an identical semi-infinite layer. The subgrade support value refers to the in-situ strength of a fine-grained soil (Coduto 1999). A plasticity index of 3, with 60% passing the #200 sieve, 90% passing the #4 sieve, and a D60 of 0.05 mm were also used as inputs for the subgrade. The plasticity index refers to the range of moisture contents that compose the plastic state (Cuduto 1999).

The traffic data, shown in Table 7.2, were supplied by WisDOT and show that this particular roadway is not expected to have a considerable amount of truck traffic.

Table 7.2. Traffic characteristics—Brule E-0.3 19.0-mm

Traffic characteristic	
AADT (veh./day)	599.00
Growth (%)	1.37
Percentage of traffic greater than class 4	6.30
AADTT (trucks/day)	38.00
Truck traffic distribution	
2D (%)	1.80
3-SU (%)	0.90
2S-1 (%)	0.60
2S-2 (%)	0.60
3S-2 (%)	2.40
2-S1-2 (%)	0.00

The AADT refers to average annual daily traffic and is determined through traffic counts. The AADTT refers to average annual daily truck traffic for vehicles larger than a passenger vehicle. The truck traffic distribution nomenclature used in Table 7.6 was that used by WisDOT. The Wisconsin Asphalt Pavement Association has provided running definitions for the truck classifications listed as follows:

- 2D: WISDOT designation for a heavy single unit truck with two axles and 6 tires.
- 3SU: WISDOT designation for a heavy single unit truck with three axles.
- 2S-1: WISDOT designation for a heavy tractor-semitrailer truck with three axles.
- 2S-2: WISDOT designation for a heavy tractor-semitrailer with four axles.
- 3S-2: WISDOT designation for a heavy tractor-semitrailer with five or more axles.
- 2-S1-2: WISDOT designation for a heavy tractor-semitrailer-trailer combination with five or more axles. The 2-S1-2 is also known as a Double-Bottom truck.

A new climatic station had to be interpolated for the exact location of this project. A latitude of 46.33 degrees and a longitude of -91.34 degrees were used, along with an estimated elevation of 206.3 m (677 ft) and an annual depth to the water table of 0.9 m (3 ft). The water table information was derived from soil surveys from the United States Department of Agriculture for Douglas County, WI (2000).

The aforementioned values were inputted into the Design Guide software where applicable and a total of 20 simulations were conducted. The simulations were run at varying layer thicknesses to determine the effects on pavement distress for 4.0%, 7.0%, and 10.0% air voids, along with the asphalt binder content increase of 0.3% at 7.0% air voids. Figures 7.1 through 7.5 show the effects of changes in the HMA's layer thickness on permanent deformation, in the AC layer only and in the entire pavement structure, as well as the effects these changes had on IRI, longitudinal cracking, and alligator cracking. The nomenclature used in the following figures shows the air void content as a number (4.0%, 7.0%, and 10.0%) followed by the asphalt binder content (optimum, "opt.," or +0.3% asphalt binder content, "bu."). The criterion stipulated in Table 7.1 is shown on each figure.

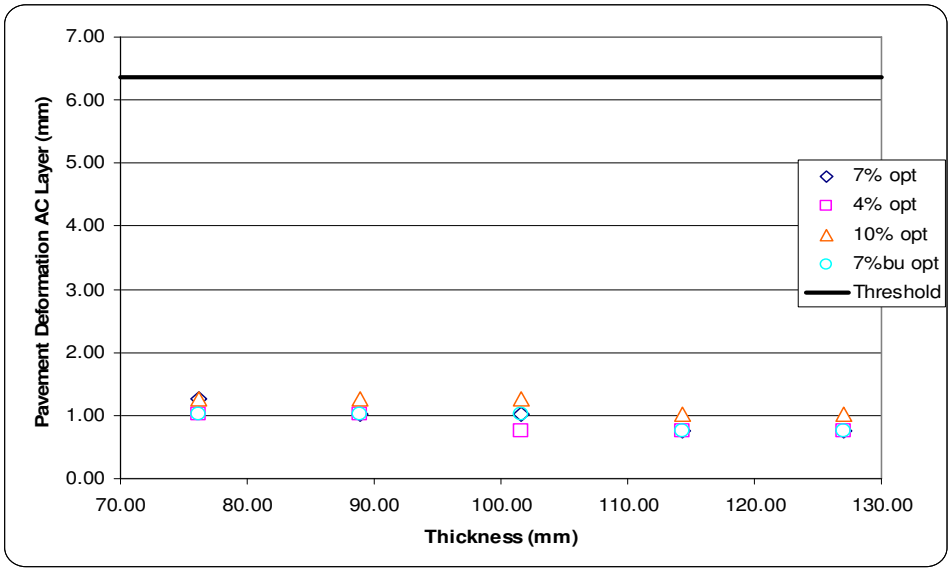

Figure 7.1. Brule permanent deformation in AC layer

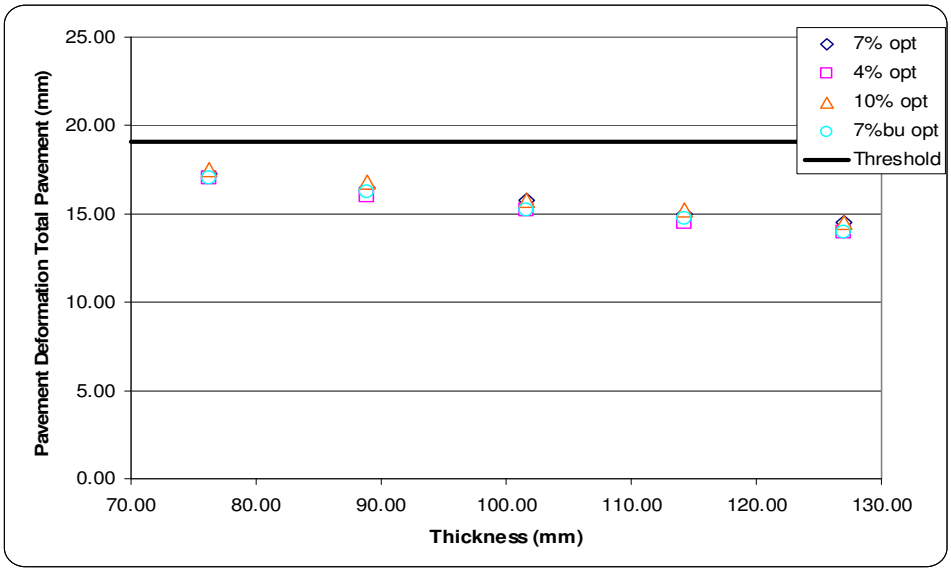

Figure 7.2. Brule permanent deformation in total pavement

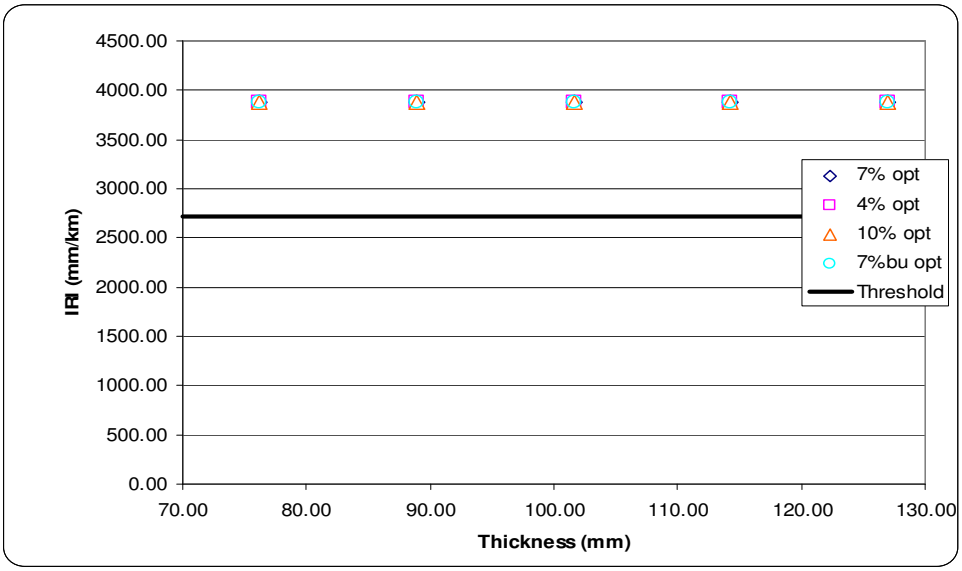

Figure 7.3. Brule IRI

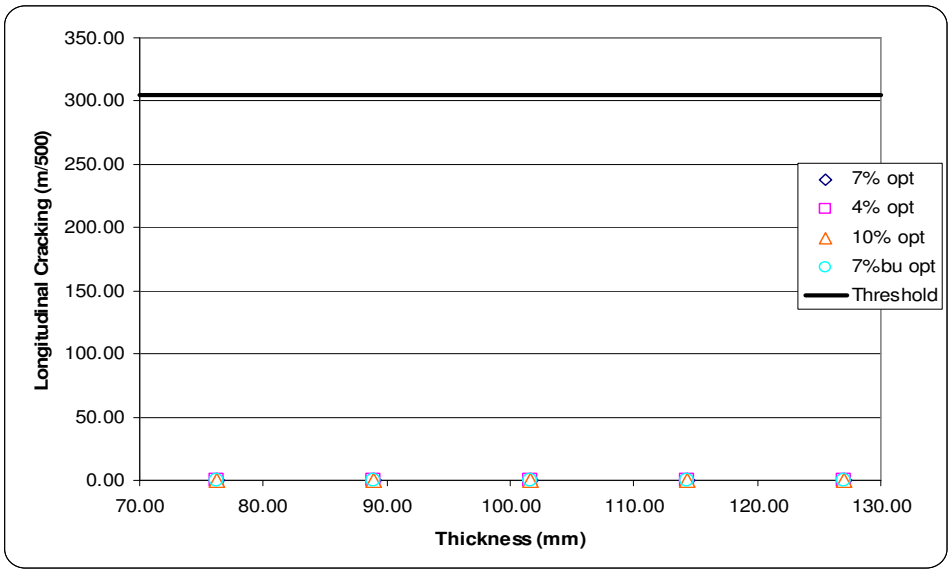

Figure 7.4. Brule longitudinal cracking

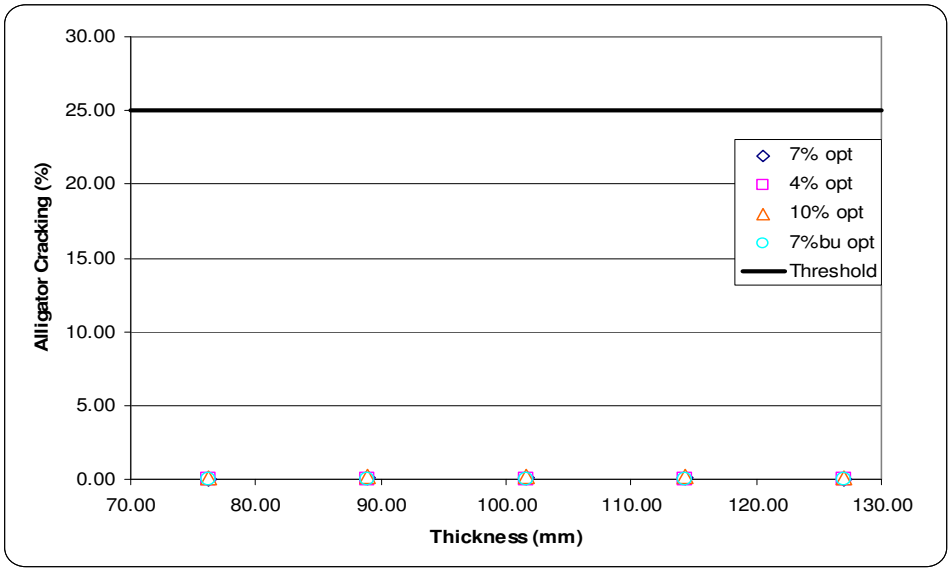

Figure 7.5. Brule alligator cracking

The findings show that all three air void levels and the binder bump at 7.0% air voids performed the same in terms of all of the distresses considered. In terms of rutting in the AC layer, alligator, and longitudinal cracking, there is minimal distress for each the four levels considered. Examining the permanent deformation was rather difficult, as most of the predictions fall near each other, indicating that the pavement is relatively insensitive to changes in air voids or asphalt content. However, there is a tendency for the 10% air void pavement to have slightly larger rutting in the AC surface layer. For total permanent deformation, there is decreasing distress with increasing pavement thickness; however, it is difficult to determine which of the four categories performed best.

Again, IRI appears to be insensitive to changes in the air void content, asphalt binder content, and the pavement thickness. The predicted pavement IRI is significantly greater than the performance criteria used in the Design Guide software of 2,715 mm/km.

7.1.2 Baraboo

The Baraboo E-0.3 12.5 mm pavement design consisted of 101.6 mm (4.0 in) of HMA on a subgrade of A-4 soil. Under the AASHTO soil classification system, the main composition of A-4 soil is silt. A level 1 analysis was used for the 12.5 mm NMAS layer, utilizing the dynamic modulus test results shown in the previous chapter. The subgrade was reported to have a support

value of 4.0 and, using the Design Guide software, yielded an analogous modulus value of 30.1 MPa (4.4 ksi). This layer was divided into a 152.4 mm (6 in) layer followed by an identical semi-infinite layer. The subgrade support value refers to the in-situ strength of a fine-grained soil (Coduto 1999). A plasticity index of 3, with 60% passing the #200 sieve, 90% passing the #4 sieve, and a D60 of 0.05 mm were also used as inputs for the subgrade (Coduto 1999).

The traffic data, shown in Table 7.3, were supplied by WisDOT and show that this particular roadway is not expected to have a considerable amount of truck traffic.

Table 7.3. Traffic characteristics—Baraboo E-0.3 12.5 mm

Traffic characteristic	
AADT (veh./day)	2,011.00
Growth (%)	1.37
Percentage of traffic greater than class 4	4.10
AADTT (trucks/day)	82.00
Truck traffic distribution	
2D (%)	1.00
3-SU (%)	1.00
2S-1 (%)	0.40
2S-2 (%)	0.40
3S-2 (%)	1.30
2-S1-2 (%)	0.00

A new climatic station had to be interpolated for the exact location of this project. A latitude of 43.28 degrees and a longitude of -89.43 degrees were used, along with an estimated elevation of 261.2 m (857 ft) and an annual depth to the water table of 18.3 m (60 ft). The water table information was derived from the soil surveys from the United States Department of Agriculture for Sauk County, WI (2000).

The aforementioned values were inputted into the Design Guide software, where applicable, and a total of 36 simulations were conducted. The simulations were run at varying layer thicknesses to determine the effects on pavement distress for 4.0%, 7.0%, and 10.0% air voids, along with the asphalt binder content increase of 0.3% at 7.0% air voids. Figures 7.6 through 7.10 show the effects of changes in the HMA's layer thickness on permanent deformation, in the AC layer only and the entire pavement structure, as well as the effects on IRI, longitudinal cracking, and alligator cracking. The nomenclature used in the following figures

shows the air void content as a number (4.0%, 7.0%, and 10.0%) followed by the asphalt binder content (optimum, "opt.," or +0.3% asphalt binder content, "bu."). The criterion stipulated in Table 7.1 is shown on each figure.

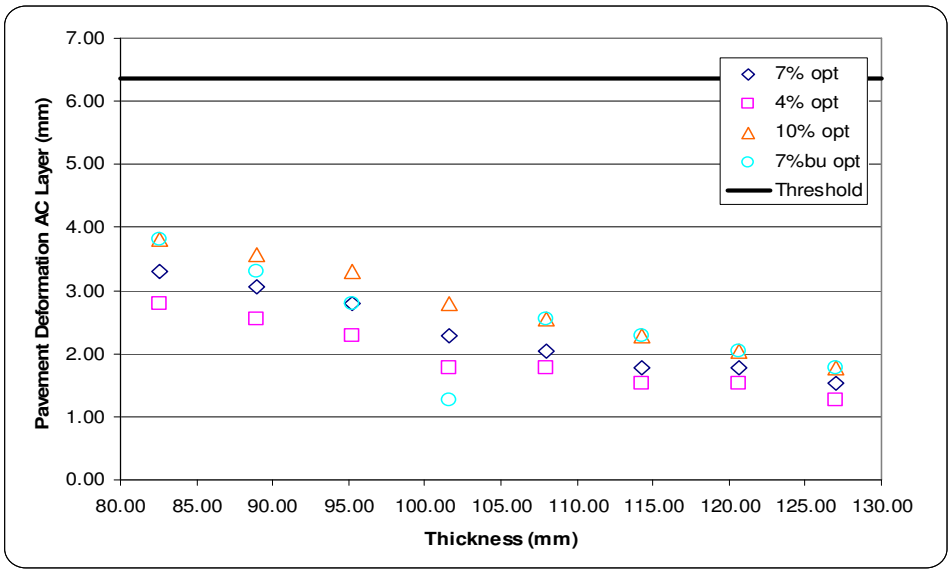

Figure 7.6. Baraboo permanent deformation in AC layer

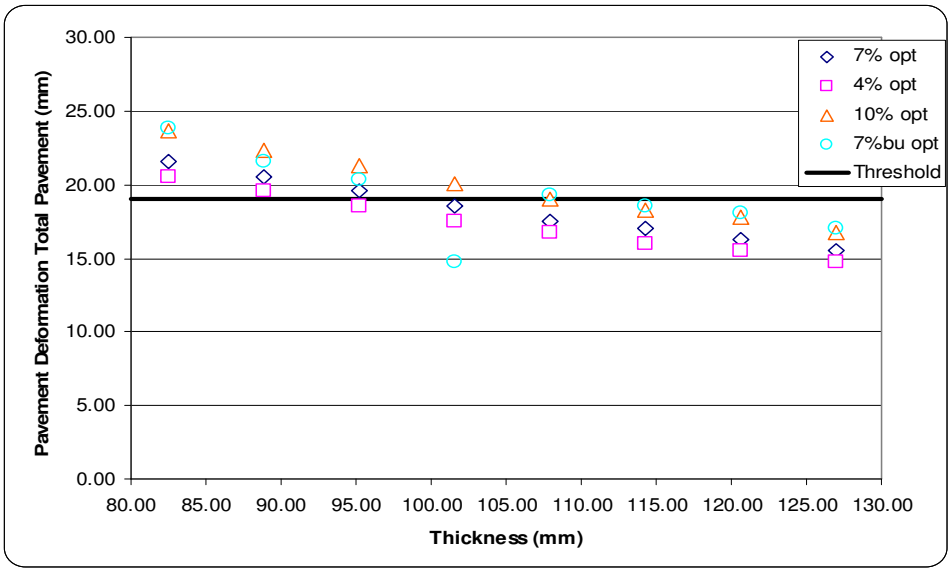

Figure 7.7. Baraboo permanent deformation in total pavement

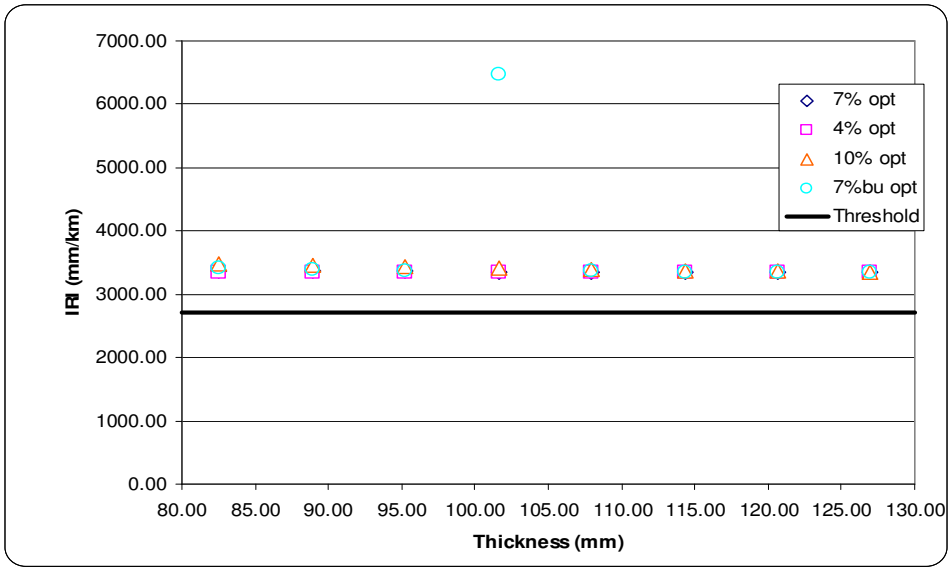

Figure 7.8. Baraboo IRI

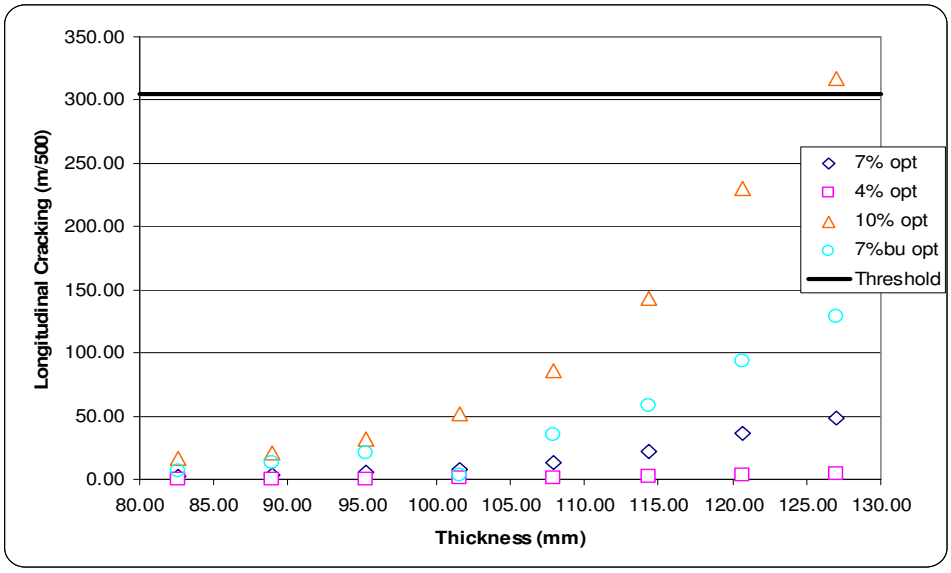

Figure 7.9. Baraboo longitudinal cracking

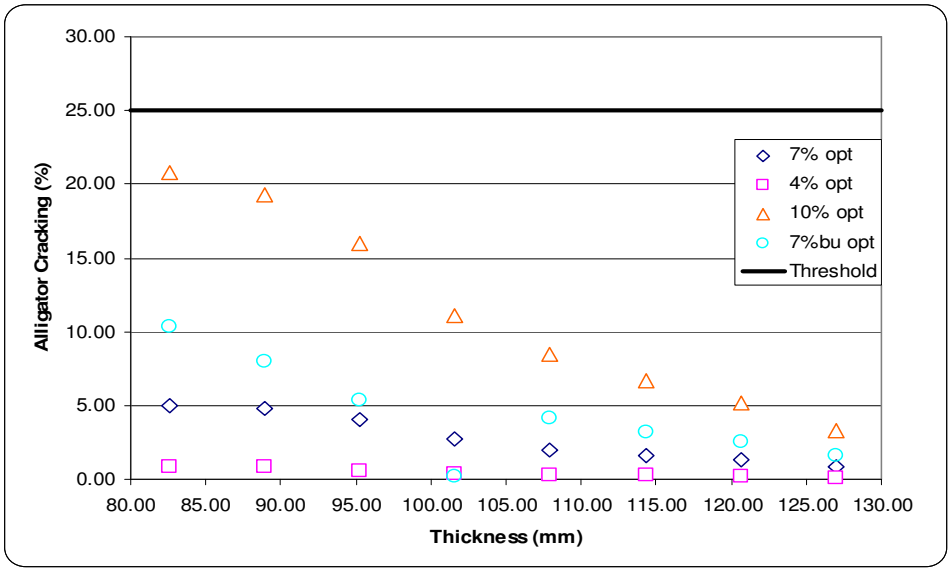

Figure 7.10. Baraboo alligator cracking

The findings show that the low air voids (4.0%) had the best performing configuration in terms of all of the distresses considered. The respective predicted distress gets progressively worse as the air void content increases. The pavement design with the optimum asphalt binder content has a higher predicted resistance to all of the distresses considered in comparison to the pavement design with the asphalt content increase.

In most instances, the high air void content (10.0%) pavement design expectedly results in the highest predicted permanent deformation, while the low air void content (4.0%) results in the lowest. Figures 7.6 and 7.7 show that the permanent deformation decreases with increasing pavement thickness and that permanent deformation is sensitive to changes in air void levels and asphalt content.

Again, IRI appears to be insensitive to changes in the air void content, asphalt binder content, and pavement thickness. The predicted pavement IRI is significantly greater than the performance criteria used in the Design Guide software of 2,715 mm/km.

Figure 7.9 indicates that the examined thicknesses are sufficient to mitigate longitudinal cracking at all air void levels, except at a pavement thickness of 127 mm and 10% air voids. Figure 7.10 shows that alligator cracking is sensitive to changes in air voids, asphalt content, and pavement thickness. As pavement thickness increases, alligator cracking decreases; as air voids increases, alligator cracking increases; and as binder content increases, alligator cracking

increases. Typically, as binder content increases, the HMA is more flexible; thus, the trend showing that alligator cracking increases as binder content increases goes against previous research and rules of thumb.

7.1.3 Hurley

The Hurley E-0.3 12.5 mm pavement design consisted of 44.5 mm (1.75 in) of HMA on an unknown existing HMA pavement and granular base. Therefore, it was assumed that the unknown existing HMA and granular base had thicknesses of 127.0 mm (5 in) and 304.8 mm (12 in), respectively, on a subgrade of A-4 soil. Under the AASHTO soil classification system, the main composition of an A-4 soil is silt. A level 1 analysis was used for the 12.5 mm NMAS layer, utilizing the dynamic modulus test results shown in the previous chapter. A level 3 mix design was used for the existing HMA layer, with typical material properties of a HMA base mixture. A modulus value of 275.8 MPa (40 ksi) was used for the crushed gravel layer; this particular layer was divided into two identical 152.4 mm (6 in layers). The reason for this division was that previous simulations with the Design Guide software had problems handling the thick layers. A plasticity index of 1, with 10% passing the #200 sieve, 30% passing the #4 sieve, and a D60 of 2 mm were also used as inputs for the crushed gravel. The subgrade was reported to have a support value of 5.2 and, using the Design Guide software, yielded an analogous modulus value of 204.4 MPa (29.6 ksi). This layer was divided into a 152.4 mm (6 in) layer followed by an identical semi-infinite layer. A plasticity index of 3, with 60% passing the #200 sieve, 90% passing the #4 sieve, and a D60 of 0.05 mm were also used as inputs for the subgrade.

The traffic data, shown in Table 7.4, were supplied by WisDOT and show that this particular roadway is not expected to have a considerable amount of truck traffic.

Table 7.4. Traffic characteristics—Hurley E-0.3 12.5 mm

Traffic characteristic	
AADT (veh./day)	2,000.00
Growth (%)	1.37
Percentage of traffic greater than class 4	4.10
AADTT (trucks/day)	82.00
Truck traffic distribution	
2D (%)	1.00
3-SU (%)	1.00
2S-1 (%)	0.40
2S-2 (%)	0.40
3S-2 (%)	1.30
2-S1-2 (%)	0.00

A new climatic station had to be interpolated for the exact location of this project. A latitude of 46.27 degrees and a longitude of -90.11 degrees were used, along with an estimated elevation of 261.2 m (857 ft) and an annual depth to the water table of 0.9 m (3 ft). The water table information was derived from the soil surveys from the United States Department of Agriculture for Iron County, WI (2000).

The aforementioned values were inputted into the Design Guide software, where applicable, and a total of 36 simulations were conducted. The simulations were run at varying layer thicknesses to determine the effects on pavement distress for 4.0%, 7.0%, and 10.0% air voids, along with the asphalt binder content increase of 0.3% at 7.0% air voids. Figures 7.11 through 7.15 show the effects of changes in the HMA's layer thickness on permanent deformation, in the AC layer only and the entire pavement structure, as well as effects on IRI, longitudinal cracking, and alligator cracking. The nomenclature used in the following figures shows the air void content as a number (4.0%, 7.0%, and 10.0%) followed by the asphalt binder content (optimum, "opt.," or +0.3% asphalt binder content "bu."). The criterion stipulated in Table 7.1 is shown on each figure.

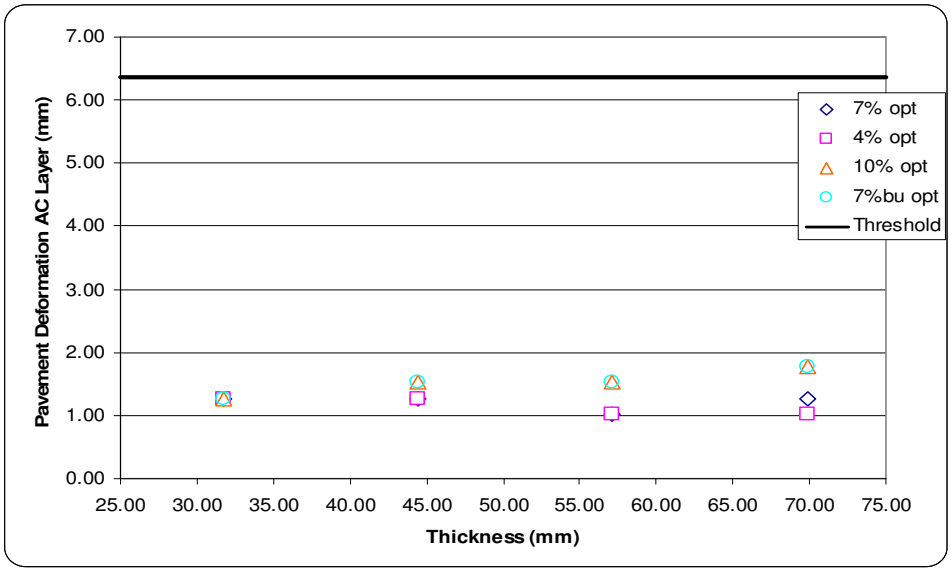

Figure 7.11. Hurley permanent deformation in AC layer

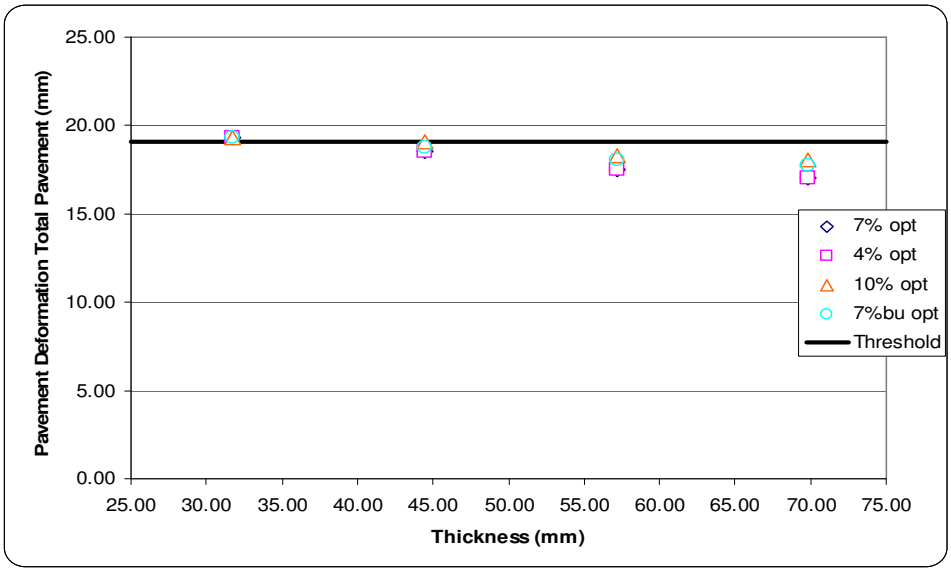

Figure 7.12. Hurley permanent deformation in total pavement

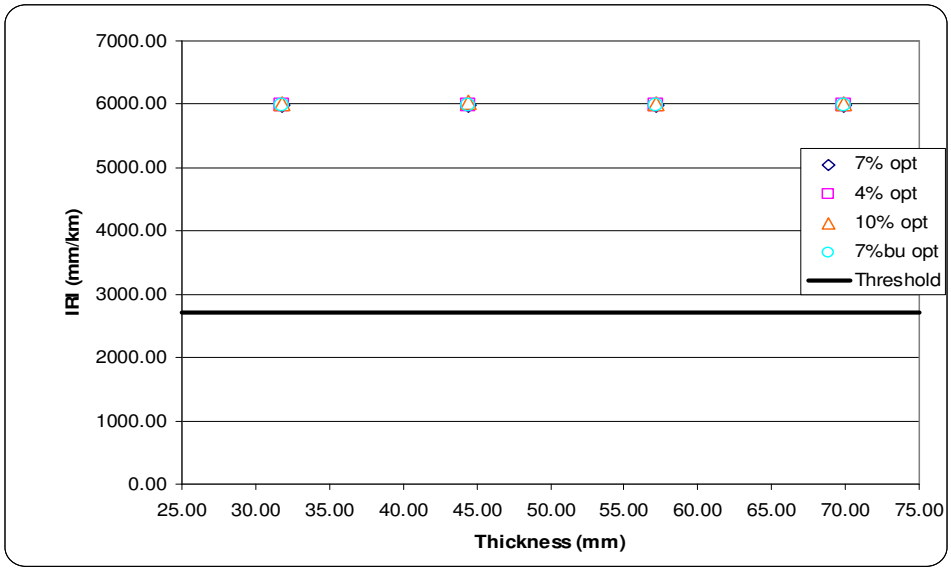

Figure 7.13. Hurley IRI

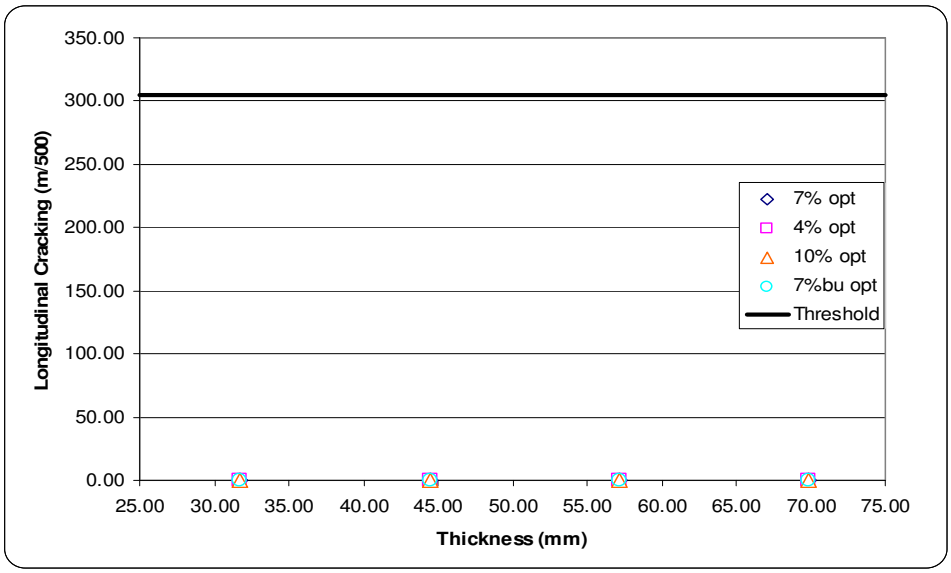

Figure 7.14. Hurley longitudinal cracking

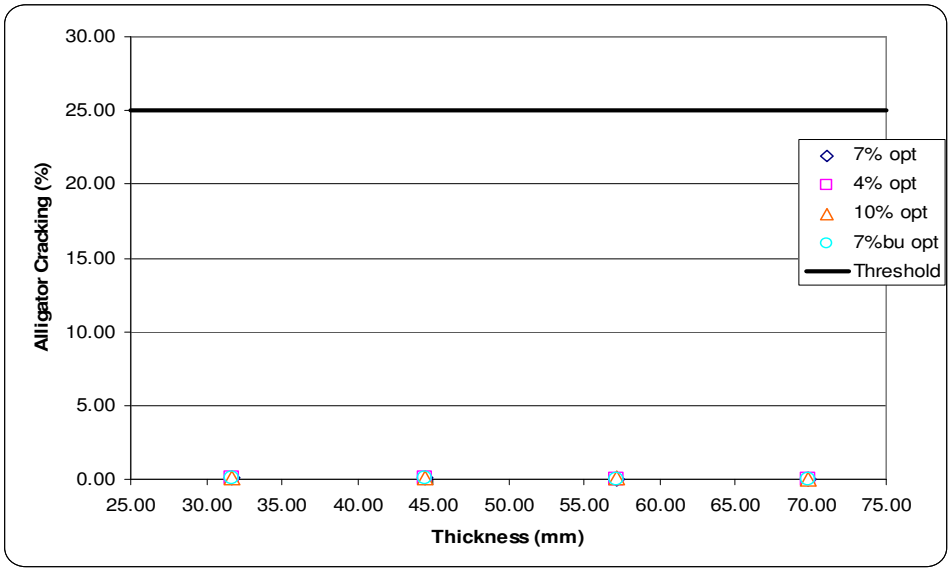

Figure 7.15. Hurley alligator cracking

The findings show that all three air void levels and the binder bump at 7.0% air voids performed the same in terms of all of the distresses considered. In terms of alligator and longitudinal cracking, there is minimal distress for each of the four levels considered. Examining the permanent deformation was rather difficult, as most of the predictions fall near each other, indicating that the pavement is relatively insensitive to changes in air voids or asphalt content. However, there is a tendency for the 10% air void pavement and 7% air void pavement plus binder bump to have slightly larger rutting in the AC surface layer. There are mixed results with the rutting in the AC layer simulations, in that, at 10% air voids and 7% air voids plus binder, there is a reverse trend in which permanent deformation increases with increasing pavement thickness. Typically, as pavement thickness increases, permanent deformation decreases. For total permanent deformation there is decreasing distress with increasing pavement thickness; however, it is difficult to determine which of the four categories performed the best.

Again, IRI appears to be insensitive to changes in the air void content, asphalt binder content, and the pavement thickness. The predicted pavement IRI is significantly greater than the performance criteria used in the Design Guide software of 2,715 mm/km.

7.1.4 Cascade

The Cascade E-1 19.0 mm pavement design consisted of 158.8 mm (6.25 in) of HMA on 330.2 mm (13 in) of CABC on 406.4 mm (16 in) of breaker run on a subgrade of A-6 soil. Under the AASHTO soil classification system, the main composition of an A-6 soil is a lean clay. A level 1 analysis was used for the 19.0 mm NMAS layer, utilizing the dynamic modulus test results shown in the previous chapter. A modulus value of 275.8 MPa (40 ksi) was used for the CABC and breaker run layer; this particular layer was divided into two identical 165.1 mm (6.5 in layers) and 203.2 mm (8.0 in layers). The reason for this division was that previous simulations with the Design Guide software had problems handling the thick layers. A plasticity index of 1, with 10% passing the #200 sieve, 30% passing the #4 sieve, and a D60 of 2 mm were also used as inputs for the CABC. The subgrade was reported to have a support value of 4.2 and, using the Design Guide software, yielded an analogous modulus value of 28.3 MPa (4.1 ksi); this layer was divided into a 152.4 mm (6 in) layer followed by an identical semi-infinite layer. A plasticity index of 3, with 60% passing the #200 sieve, 90% passing the #4 sieve, and a D60 of 0.05 mm were also used as inputs for the subgrade.

The traffic data, shown in Table 7.5, were supplied by WisDOT and show that this particular roadway is not expected to have a considerable amount of truck traffic.

Table 7.5. Traffic characteristics—Cascade E-1 19.0 mm

Traffic characteristic	
AADT (veh./day)	3,800.00
Growth (%)	1.16
Percentage of traffic greater than class 4	20.10
AADTT (trucks/day)	764.00
Truck traffic distribution	
2D (%)	2.90
3-SU (%)	4.50
2S-1 (%)	2.00
2S-2 (%)	2.00
3S-2 (%)	8.30
2-S1-2 (%)	0.40

A new climatic station had to be interpolated for the exact location of this project. A latitude of 43.38 degrees and a longitude of -87.82 degrees were used, along with an estimated elevation of 226.5 m (743 ft) and an annual depth to the water table of 1.5 m (5.0 ft). The water table information was derived from the soil surveys from the United States Department of Agriculture for Sheboygan County, WI (2000).

The aforementioned values were inputted into the Design Guide software, where applicable, and a total of 36 simulations were conducted. The simulations were run at varying layer thicknesses to determine the effects on pavement distress for 4.0%, 7.0%, and 10.0% air voids, along with the asphalt binder content increase of 0.3% at 7.0% air voids. Figures 7.16 through 7.20 show the effects of changes in the HMA's layer thickness on permanent deformation, in the AC layer only and the entire pavement structure, as well as the effects on IRI, longitudinal cracking, and alligator cracking. The nomenclature used in the following figures shows the air void content as a number (4.0%, 7.0%, and 10.0%) followed by the asphalt binder content (optimum, "opt.," or +0.3% asphalt binder content, "bu."). The criterion stipulated in Table 7.1 is shown on each figure.

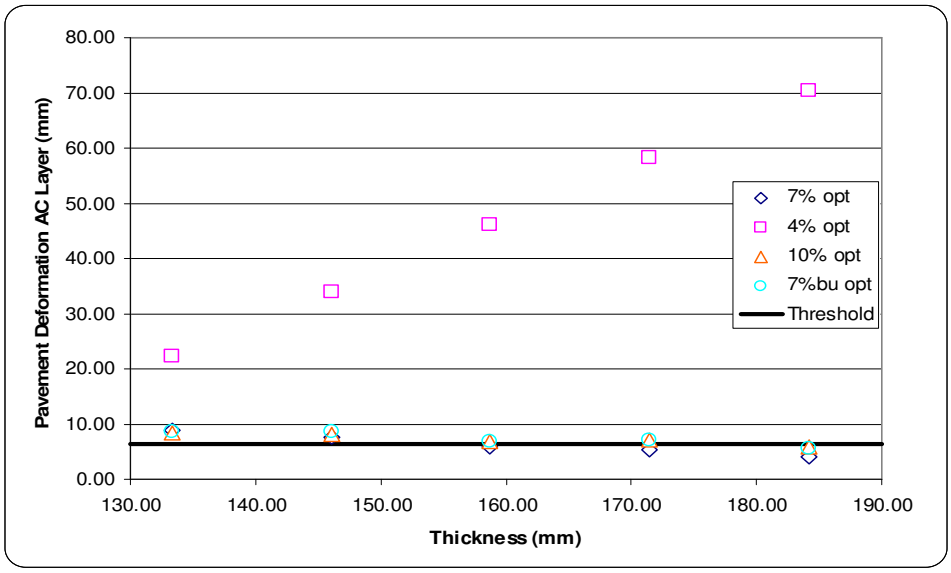

Figure 7.16. Cascade permanent deformation in AC layer

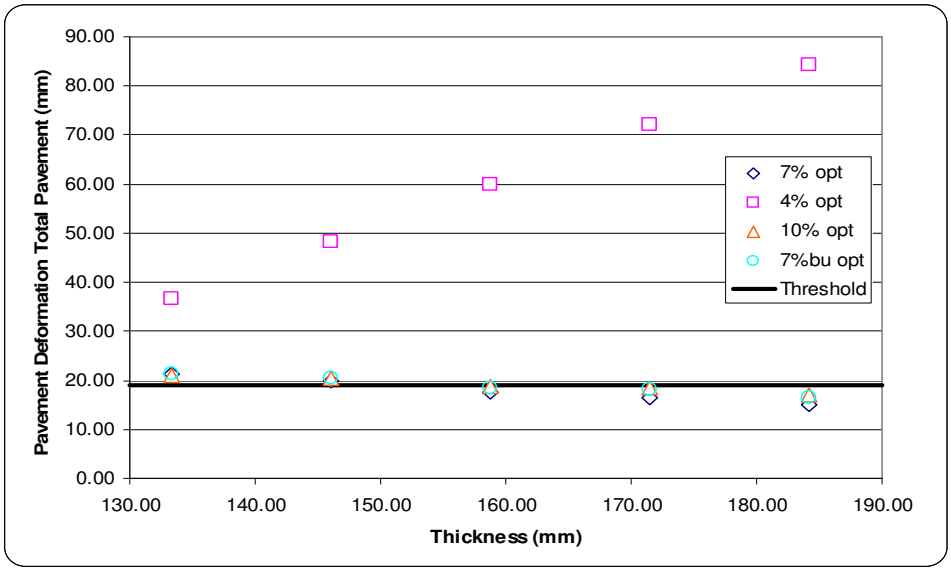

Figure 7.17. Cascade permanent deformation in total pavement

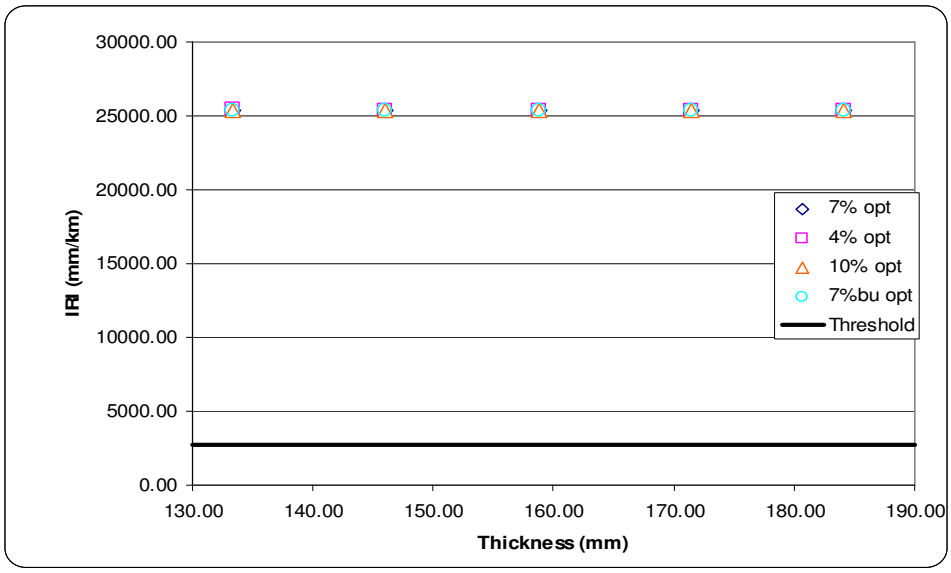

Figure 7.18. Cascade IRI

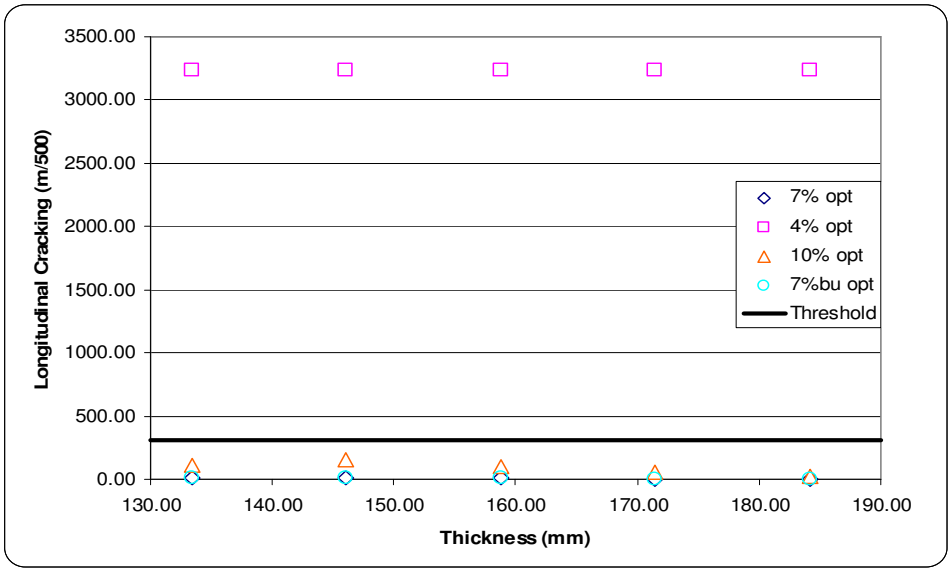

Figure 7.19. Cascade longitudinal cracking

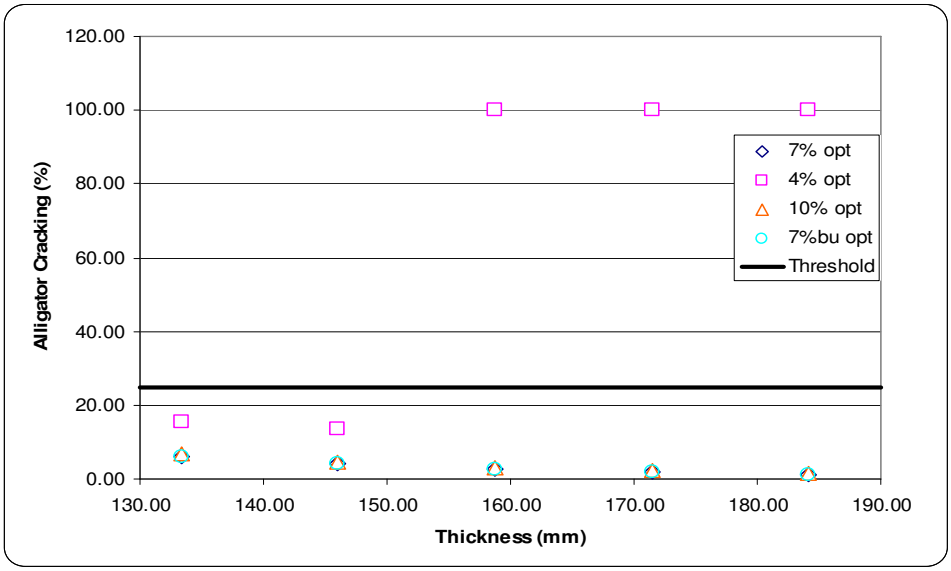

Figure 7.20. Cascade alligator cracking

The findings show that the low air voids (4.0%) were the worst performing configuration in terms of all of the distresses considered. The respective predicted distress gets progressively better as the air void content increases and as pavement thickness increases. The pavement design with the asphalt binder content increase performed the same in comparison to the pavement design with the optimum asphalt content.

It was also interesting to see, at the 4.0% air void configuration, that as thickness increased, permanent deformation increased. All simulations examining permanent deformation, except for the 4.0% air voids, were close to the threshold value of 6.0 mm and 19.0 mm for the rutting in the AC layer and total permanent deformation, respectively. The predicted permanent deformation values for the AC layer and total pavement seem a bit unrealistic based on their magnitudes.

Again, IRI appears to be insensitive to changes in the air void content, asphalt binder content, and pavement thickness. The predicted pavement IRI is significantly greater than the performance criteria used in the Design Guide software of 2,715 mm/km.

In terms of longitudinal and alligator cracking, the 4% air void level was the most sensitive to changes in air voids. The failure criterion for longitudinal cracking is 300m/500, and the 4% air void level failed at each pavement thickness. The failure criterion for alligator cracking is 25 percent. The first two simulations passed for the 4% air void level; however, once the surface thickness increased beyond 150mm, the thicker pavements did not meet performance expectations for alligator cracking.

7.1.5 Bloomville

The Bloomville E-1 19.0 mm pavement design consisted of 114.3 mm (4.5 in) of HMA on 304.8 mm (12 in) of crushed gravel on a subgrade of A-4 soil. Under the AASHTO soil classification system, the main composition of an A-4 soil is silt. A level 1 analysis was used for the 19.0 mm NMAS layer, utilizing the dynamic modulus test results shown in the previous chapter. A modulus value of 275.8 MPa (40 ksi) was used for the crushed gravel layer; this particular layer was divided into two identical 152.4 mm (6 in layers). The reason for this division was that previous simulations with the Design Guide software had problems handling the thick layers. A plasticity index of 1, with 10% passing the #200 sieve, 30% passing the #4 sieve, and a D60 of 2 mm were also used as inputs for the crushed gravel. The subgrade was reported to have a support value of 5.2 and, using the Design Guide software, yielded an analogous modulus value of 204.4 MPa (29.6 ksi). This layer was divided into a 152.4 mm (6 in) layer followed by an identical semi-infinite layer. A plasticity index of 3, with 60% passing the #200 sieve, 90% passing the #4 sieve, and a D60 of 0.05 mm were also used as inputs for the subgrade.

The traffic data, shown in Table 7.6, were supplied by WisDOT and show that this particular roadway is not expected to have a considerable amount of truck traffic.

Table 7.6. Traffic characteristics—Bloomville E-1 19.0 mm

Traffic characteristic	
AADT (veh./day)	3,800.00
Growth (%)	1.37
Percentage of traffic greater than class 4	6.00
AADTT (trucks/day)	228.00
Truck traffic distribution	
2D (%)	1.50
3-SU (%)	1.50
2S-1 (%)	0.70
2S-2 (%)	0.70
3S-2 (%)	1.30
2-S1-2 (%)	0.30

A new climatic station had to be interpolated for the exact location of this project. A latitude of 45.18 degrees and a longitude of -89.18 degrees were used, along with an estimated elevation of 362.4 m (1189 ft) and an annual depth to the water table of 1.8 m (6 ft). The water table information was derived from the soil surveys from the United States Department of Agriculture for Lincoln County, WI (2000).

The aforementioned values were inputted into the Design Guide software, where applicable, and a total of 36 simulations were conducted. The simulations were run at varying layer thicknesses to determine the effects on pavement distress for 4.0%, 7.0%, and 10.0% air voids, along with the asphalt binder content increase of 0.3% at 7.0% air voids. Figures 7.21 through 7.25 show the effects of changes in the HMA's layer thickness on permanent deformation, in the AC layer only and the entire pavement structure, as well as the effects on IRI, longitudinal cracking, and alligator cracking. The nomenclature used in the following figures shows the air void content as a number (4.0%, 7.0%, and 10.0%) followed by the asphalt binder content (optimum, "Opt.," or +0.3% asphalt binder content, "Bump"). The criterion stipulated in Table 7.1 is shown on each figure.

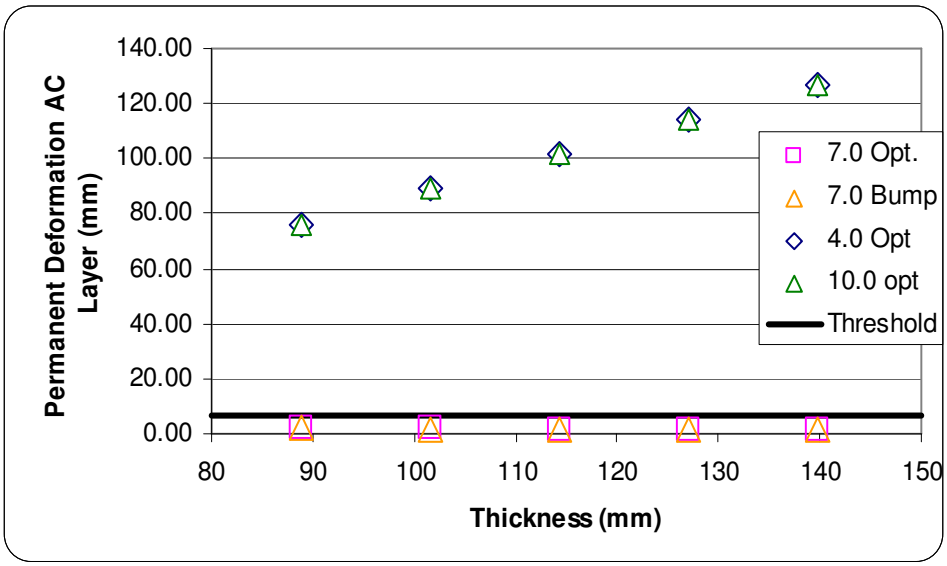

Figure 7.21. Bloomville permanent deformation in AC layer

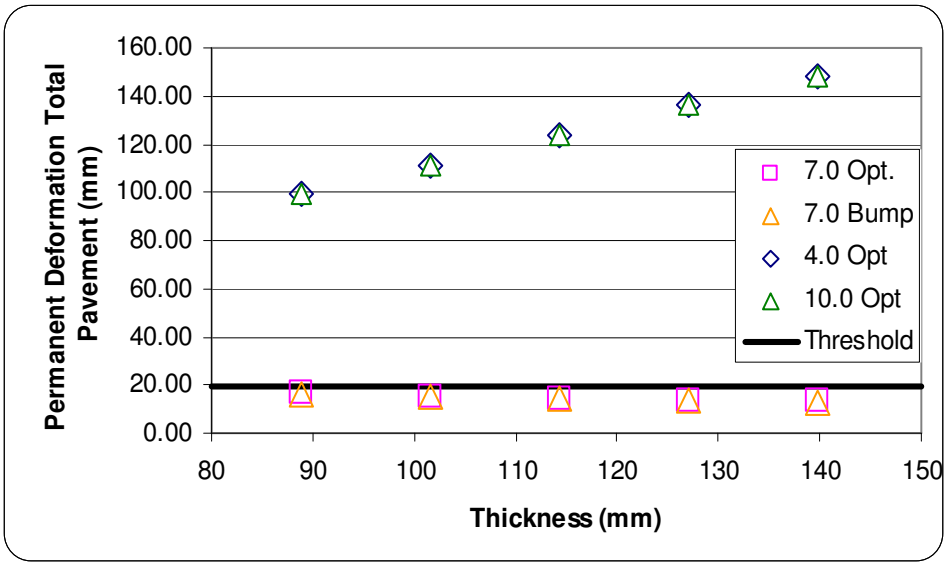

Figure 7.22. Bloomville permanent deformation in total pavement

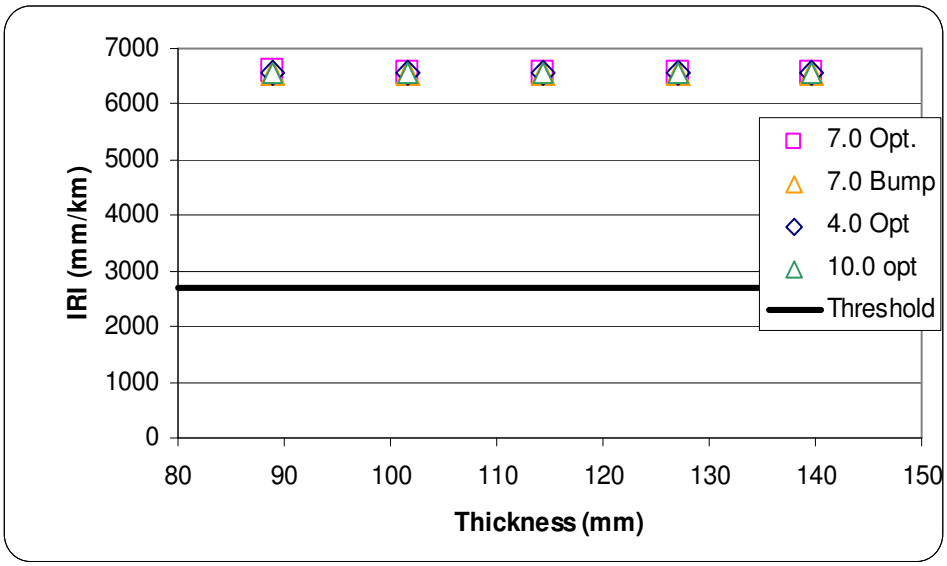

Figure 7.23. Bloomville IRI

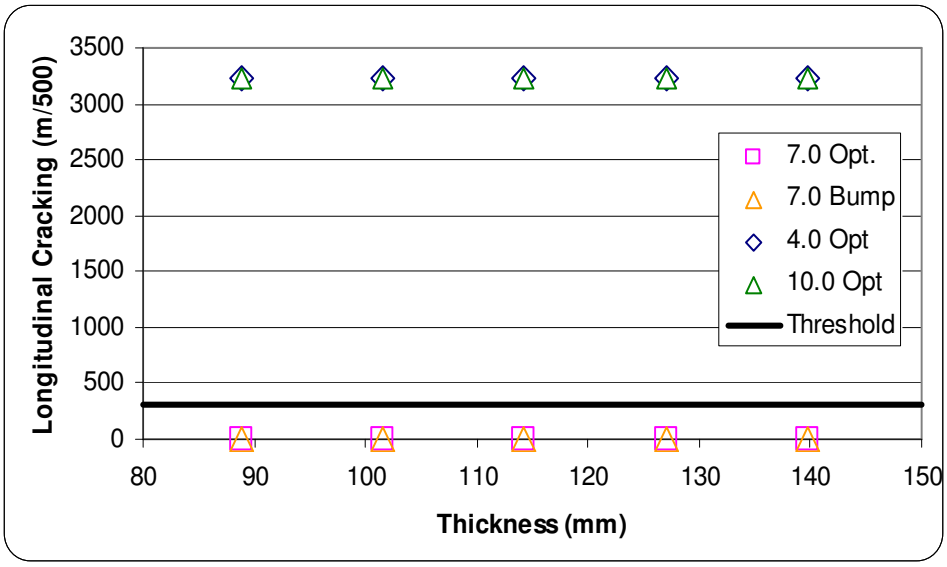

Figure 7.24. Bloomville longitudinal cracking

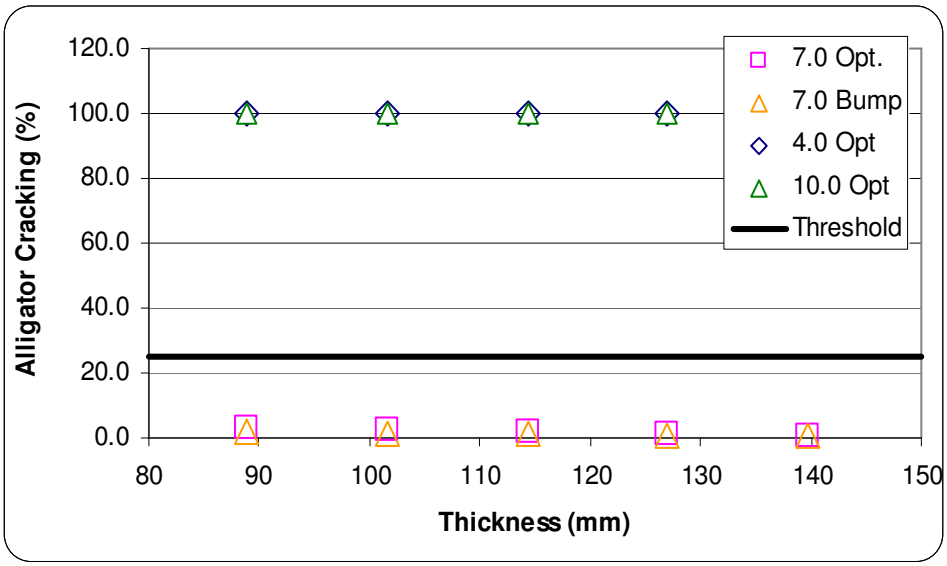

Figure 7.25. Bloomville alligator cracking

Confusing results are shown in Figures 7.21 and 7.22. As thickness increases for the 4% and 10% air voids, permanent deformation increases. There is excessive rutting in the AC layer and total pavement which does not make any sense. Also, the 7% air voids at optimum and 7% air voids at binder bump performed the best in terms of all predicted distresses.

The analysis indicated that the IRI was insensitive to changes in the air void content, asphalt binder content, and thickness. The overall IRI number at the pavement design thickness exceeded the performance criteria used in the Design Guide software of 2,715 mm/km.

Again the data shows that the predicted distresses for the 7% air voids at optimum and 7% air voids at binder bump performed the best in terms of longitudinal and alligator cracking. Also, Figures 7.24 and 7.25 show that longitudinal and alligator cracking are insensitive to changes in thickness.

7.1.6 Medford

The Medford E-1 12.5 mm pavement design consisted of 88.9 mm (3.5 in) of HMA on 50.8 to 101.6 mm (2 to 4 in) of existing HMA on 152.5 to 203.2 mm (6 to 8 in) of granular base on a subgrade of A-4 soil. Under the AASHTO soil classification system, the main composition of an A-4 soil is silt. A level 1 analysis was used for the 12.5. mm NMAS layer, utilizing the dynamic modulus test results shown in the previous chapter. A level 3 mix design was used for

the existing HMA layer, utilizing properties consistent with a HMA base mixture. A modulus value of 275.8 MPa (40 ksi) was used for the granular base layer. A plasticity index of 1, with 10% passing the #200 sieve, 30% passing the #4 sieve, and a D60 of 2 mm were also used as inputs for the crushed gravel The subgrade was reported to have a support value of 4.0 and, using the Design Guide software yielded an analogous modulus value of 30.3 MPa (4.4 ksi); this layer was divided into a 152.4 mm (6 in) layer followed by an identical semi-infinite layer. A plasticity index of 3, with 60% passing the #200 sieve, 90% passing the #4 sieve, and a D60 of 0.05 mm were also used as inputs for the subgrade. The traffic data, shown in Table 7.7, were supplied by WisDOT and show that this particular roadway is not expected to have a considerable amount of truck traffic.

Table 7.7. Traffic characteristics—Medford E-1 12.5 mm

Traffic characteristic	
AADT (veh./day)	800.00
Growth (%)	2.00
Percentage of traffic greater than class 4	10.00
AADTT (trucks/day)	80.00
Truck traffic distribution	
2D (%)	2.00
3-SU (%)	1.00
2S-1 (%)	2.50
2S-2 (%)	2.50
3S-2 (%)	2.00
2-S1-2 (%)	0.00

A new climatic station had to be interpolated for the exact location of this project. A latitude of 45.08 degrees and a longitude of -90.20 degrees were used, along with an estimated elevation of 240.5 m (789 ft) and an annual depth to the water table of 1.2 m (4 ft). The water table information was derived from the soil surveys from the United States Department of Agriculture for Taylor County, WI (2000).

The aforementioned values were inputted into the Design Guide software, where applicable, and a total of 36 simulations were conducted. The simulations were run at varying layer thicknesses to determine the effects on pavement distress for 4.0%, 7.0%, and 10.0% air voids, along with the asphalt binder content increase of 0.3% at 7.0% air voids. Figures 7.26

through 7.30 show the effects of changes in the HMA's layer thickness on permanent deformation, in the AC layer only and the entire pavement structure, as well as the effects on IRI, longitudinal cracking, and alligator cracking. The nomenclature used in the following figures shows the air void content as a number (4.0%, 7.0%, and 10.0%) followed by the asphalt binder content (optimum, "opt.," or +0.3% asphalt binder content, "bu."). The criterion stipulated in Table 7.1 is shown on each figure.

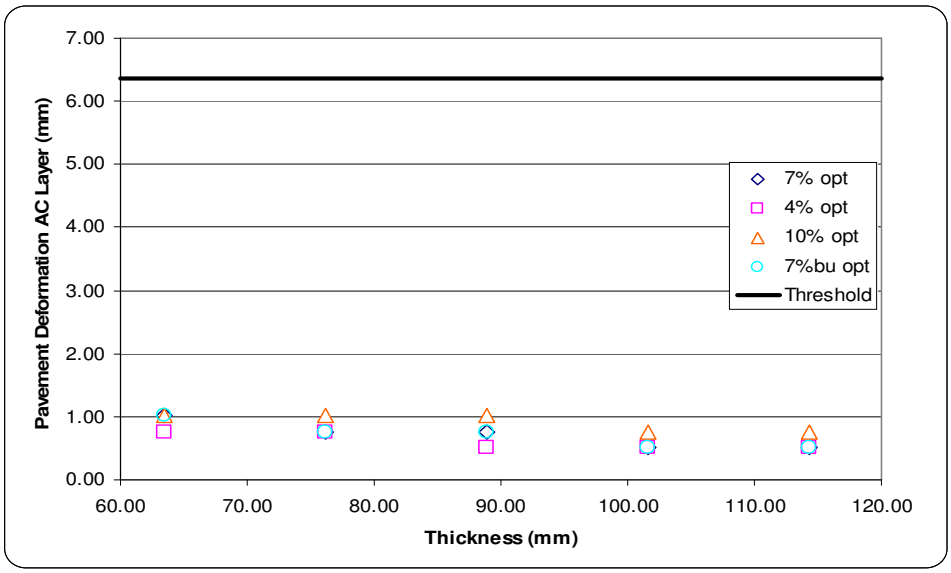

Figure 7.26. Medford permanent deformation in AC layer

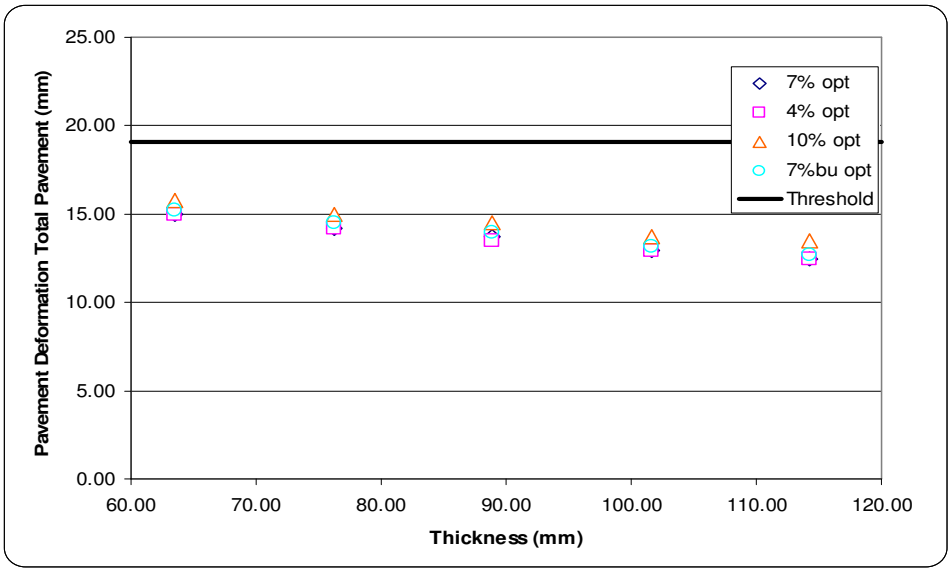

Figure 7.27. Medford permanent deformation in total pavement

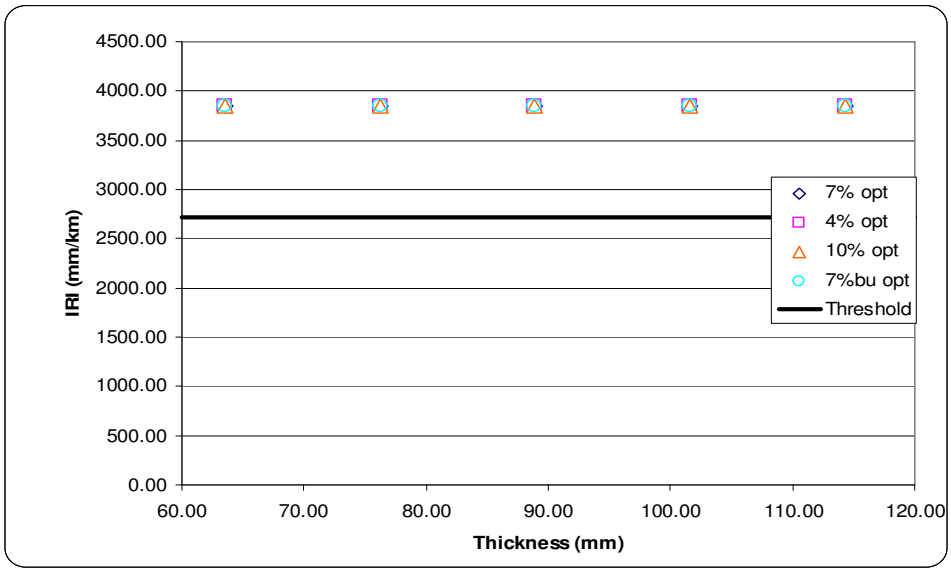

Figure 7.28. Medford IRI

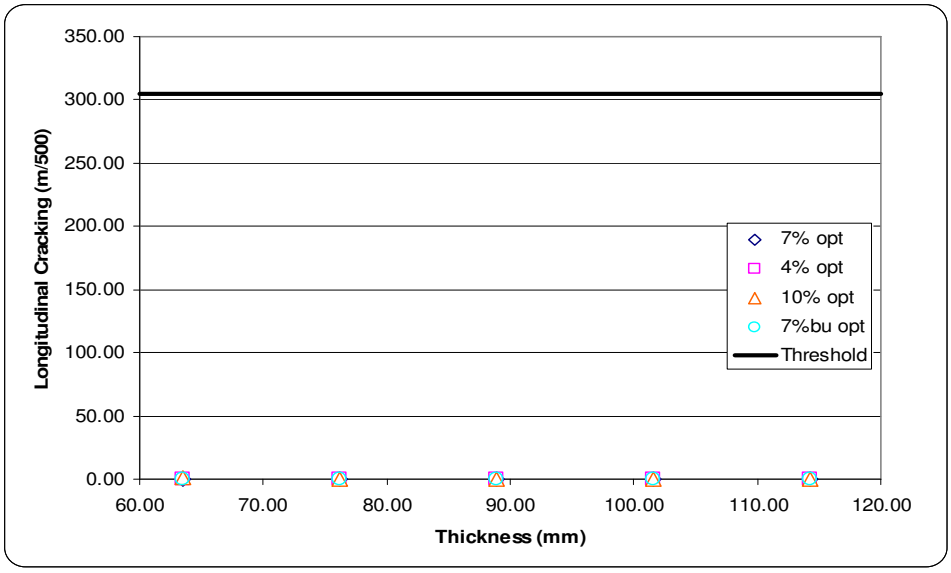

Figure 7.29. Medford longitudinal cracking

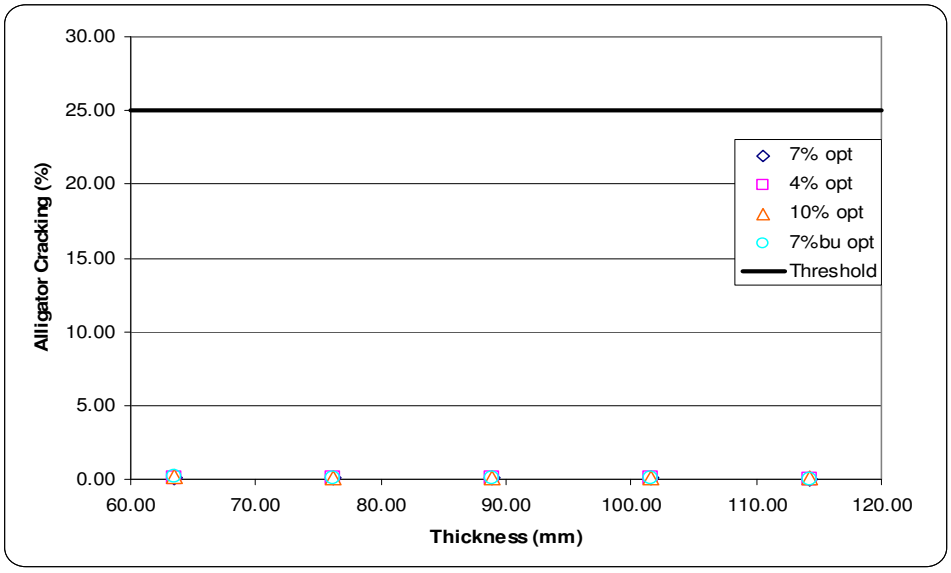

Figure 7.30. Medford alligator cracking

The findings show that all three air void levels and the binder bump at 7.0% air voids performed the same in terms of all of the distresses considered. In terms of rutting in the AC layer, alligator, and longitudinal cracking, there is minimal distress for each the four levels considered. Examining the permanent deformation was rather difficult, as most of the predictions fall near each other, indicating that the pavement is relatively insensitive to changes in air voids or asphalt content. However, there is a tendency for the 10% air void pavement to have slightly larger rutting in the AC surface layer. For total permanent deformation, there is decreasing distress with increasing pavement thickness; however, it is difficult to determine which of the four categories considered performed the best. The predicted distresses for permanent deformation in the AC, total permanent deformation, alligator cracking and longitudinal cracking are all below the threshold value for the simulations.

Again, IRI appears to be insensitive to changes in the air void content, asphalt binder content, and the pavement thickness. The predicted pavement IRI is significantly greater than the performance criteria used in the Design Guide software of 2,715 mm/km.

7.1.7 Wautoma

The Wautoma E-1 12.5 mm pavement design consisted of 69.85 mm (2.75 in) of HMA on 114.3 mm (4.5 in) of existing HMA on a subgrade of A-2-7 soil. Under the AASHTO soil

classification system, the main composition of an A-2-7 soil is sand. A level 1 analysis was used for the 12.5 mm NMAS layer, utilizing the dynamic modulus test results shown in the previous chapter. A level 3 mix design was performed on the existing HMA layer, utilizing typical material volumetric and gradation properties. The subgrade was reported to have a support value of 5.5 and, using the Design Guide software, yielded an analogous modulus value of 52.4 MPa (7.6 ksi); this layer was divided into a 152.4 mm (6 in) layer followed by an identical semi-infinite layer. A plasticity index of 3, with 60% passing the #200 sieve, 90% passing the #4 sieve, and a D60 of 0.05 mm were also used as inputs for the subgrade.

The traffic data, shown in Table 7.8, were supplied by WisDOT and show that this particular roadway is not expected to have a considerable amount of truck traffic.

Table 7.8. Traffic characteristics—Wautoma E-1 12.5 mm

Traffic characteristic	
AADT (veh./day)	3,800.00
Growth (%)	1.37
Percentage of traffic greater than class 4	8.60
AADTT (trucks/day)	327.00
Truck traffic distribution	
2D (%)	2.30
3-SU (%)	1.40
2S-1 (%)	1.10
2S-2 (%)	1.10
3S-2 (%)	2.60
2-S1-2 (%)	0.10

A new climatic station had to be interpolated for the exact location of this project. A latitude of 44.37 degrees and a longitude of -89.12 degrees were used, along with an estimated elevation of 247.8 m (813 ft) and an annual depth to the water table of 1.8 m (6 ft). The water table information was derived from the soil surveys from the United States Department of Agriculture for Waushara County, WI (2000).

The aforementioned values were inputted into the Design Guide software, where applicable, and a total of 36 simulations were conducted. The simulations were run at varying layer thicknesses to determine the effects on pavement distress for 4.0%, 7.0%, and 10.0% air voids, along with the asphalt binder content increase of 0.3% at 7.0% air voids. Figures 7.31 through 7.35 show the effects of changes in the HMA's layer thickness on permanent

deformation, in the AC layer only and the entire pavement structure, as well as the effects on IRI, longitudinal cracking, and alligator cracking. The nomenclature used in the following figures shows the air void content as a number (4.0%, 7.0%, and 10.0%) followed by the asphalt binder content (optimum, "Opt.," or +0.3% asphalt binder content, "Bump"). The criterion stipulated in Table 7.1 is shown on each figure.

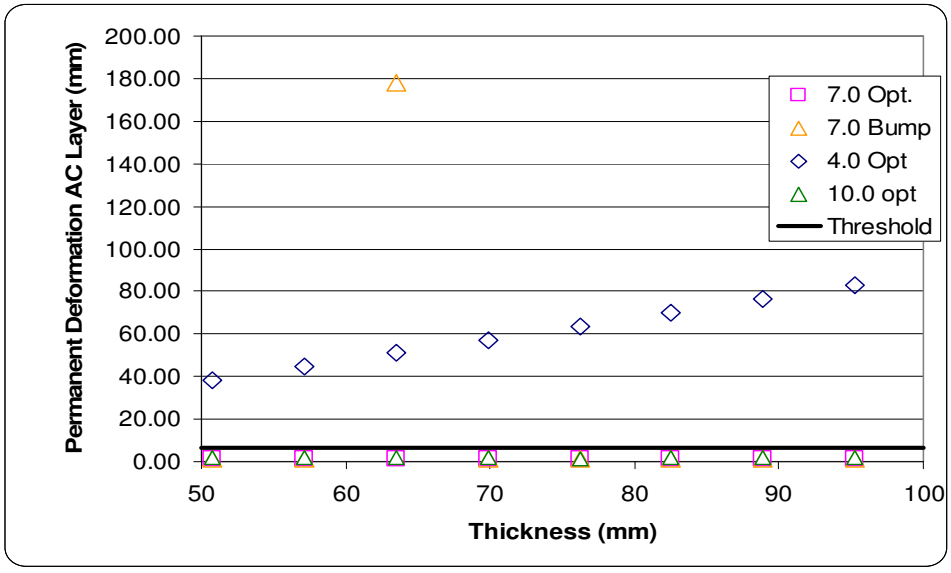

Figure 7.31. Wautoma permanent deformation in AC layer

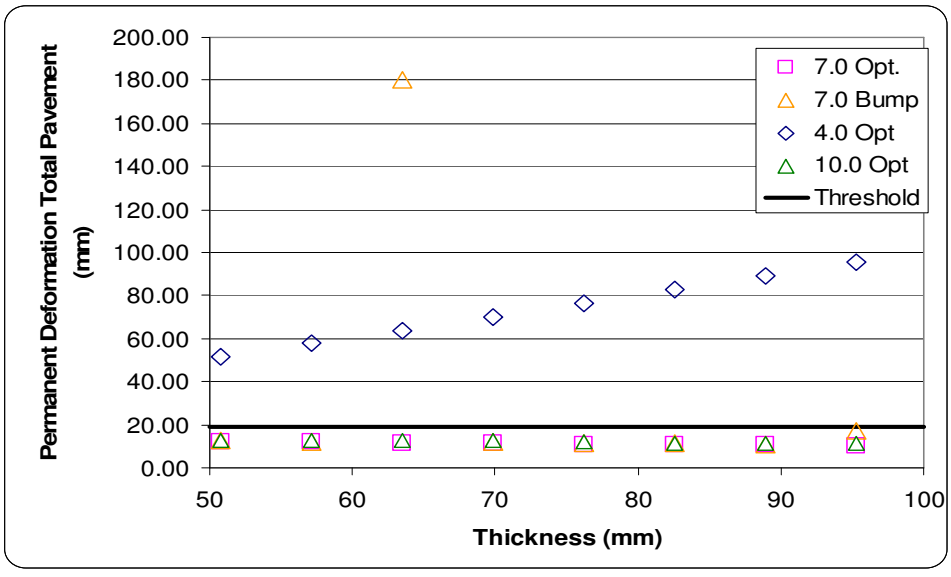

Figure 7.32. Wautoma permanent deformation in total pavement

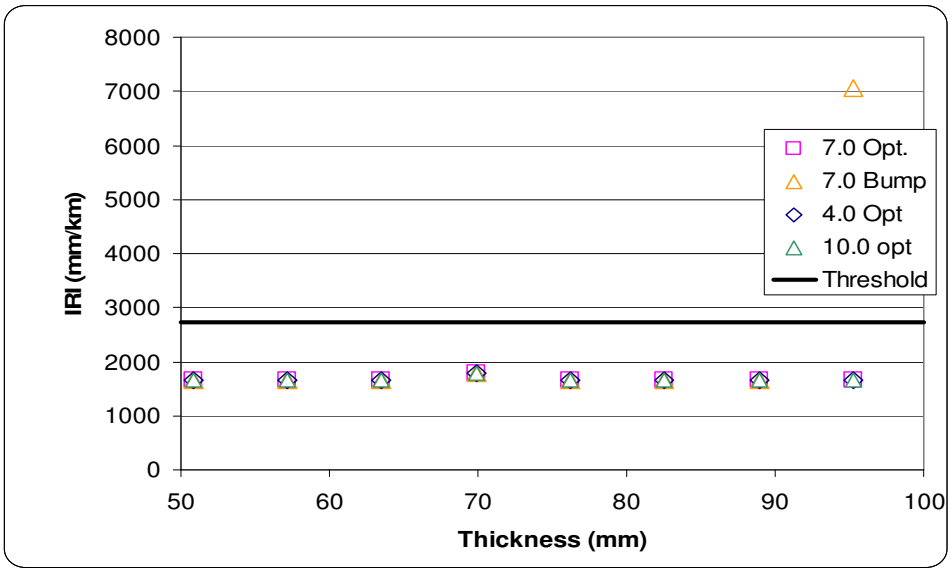

Figure 7.33. Wautoma IRI

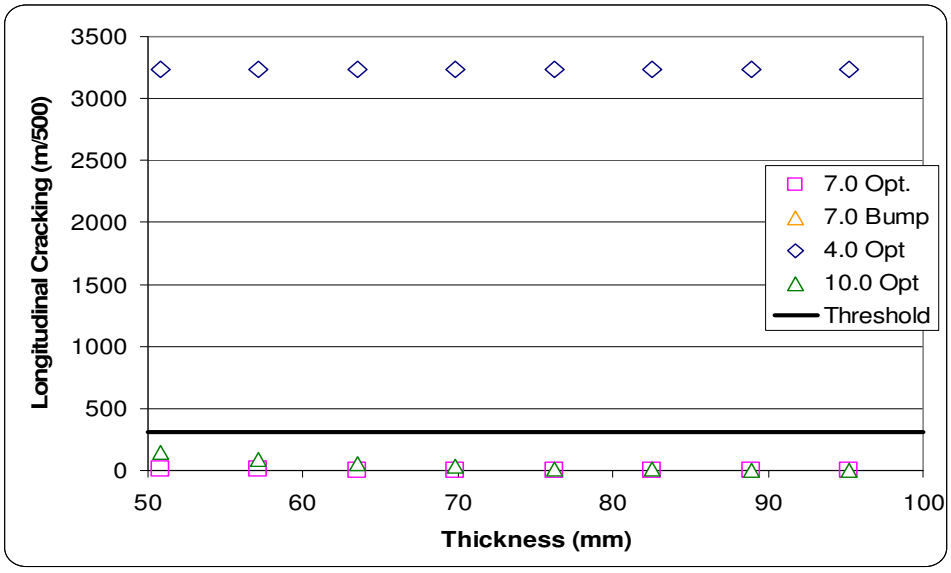

Figure 7.34. Wautoma longitudinal cracking

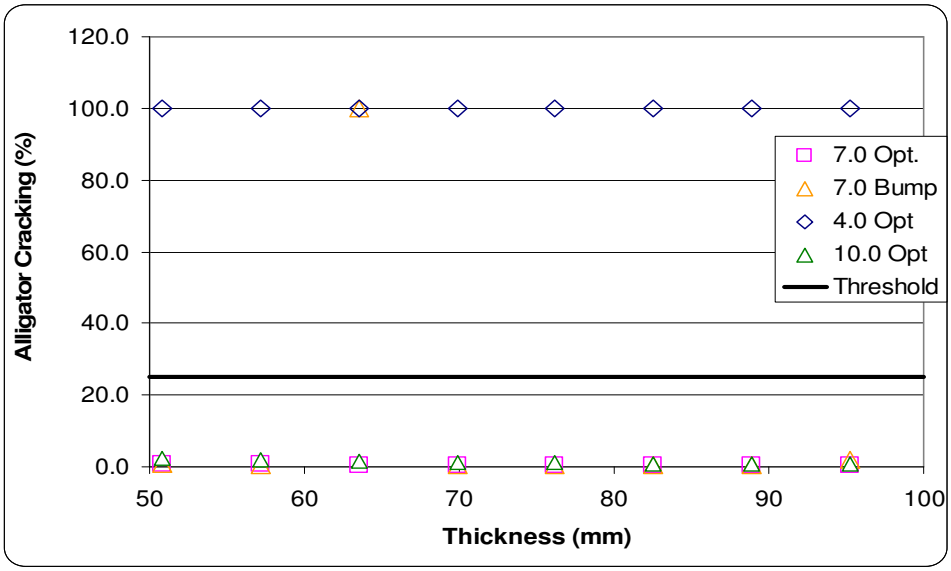

Figure 7.35. Wautoma alligator cracking

The findings show that the low air voids (4.0%) were the worst performing configuration in terms of all of the distresses considered. The respective predicted distress gets progressively better as the air void content increases and as pavement thickness increases. The pavement design with the asphalt binder content increase performed the same in comparison to the pavement design with the optimum asphalt content.

It was also interesting to see, at the 4.0% air void configuration, that as thickness increased, permanent deformation increased. All simulations examining permanent deformation, except for the 4.0% air voids, were close to the threshold value of 6.0 mm and 19.0 mm for the rutting in the AC layer and total permanent deformation, respectively. The predicted permanent deformation values for the AC layer and total pavement seem a bit unrealistic based on their magnitudes.

IRI appears to be insensitive to changes in the air void content, asphalt binder content, and the pavement thickness. The predicted pavement IRI is significantly lower than the performance criteria used in the Design Guide software of 2,715 mm/km.

In terms of longitudinal and alligator cracking, the 4% air void level was the most sensitive to changes in air voids. The failure criterion for longitudinal cracking is 300m/500, and the 4% air void level failed at each pavement thickness. The failure criterion for alligator

cracking is 25 percent. All simulations performed at the 4% air void level did not meet the criteria.

7.1.8 Tomahawk

The Tomahawk E-3 25.0 mm pavement design consisted of 215.9 mm (8.5 in) of HMA on a subgrade of A-4 soil. Under the AASHTO soil classification system, the main composition of an A-4 soil is silt. A level 1 analysis was used for the 25.0 mm NMAS layer, utilizing the dynamic modulus test results shown in the previous chapter. The subgrade was reported to have a support value of 4.1 and, using the Design Guide software, yielded an analogous modulus value of 31.2 MPa (4.5 ksi); this layer was divided into a 152.4 mm (6 in) layer followed by an identical semi-infinite layer. A plasticity index of 3, with 60% passing the #200 sieve, 90% passing the #4 sieve, and a D60 of 0.05 mm were also used as inputs for the subgrade.

The traffic data, shown in Table 7.9, were supplied by WisDOT and show that this particular roadway is not expected to have a considerable amount of truck traffic.

Table 7.9. Traffic characteristics—Tomahawk E-3 25.0 mm

Traffic characteristic	
AADT (veh./day)	3,619.00
Growth (%)	1.37
Percentage of traffic greater than class 4	8.70
AADTT (trucks/day)	315.00
Truck traffic distribution	
2D (%)	2.20
3-SU (%)	0.60
2S-1 (%)	0.40
2S-2 (%)	0.40
3S-2 (%)	5.00
2-S1-2 (%)	0.10

A new climatic station had to be interpolated for the exact location of this project. A latitude of 45.28 degrees and a longitude of -89.43 degrees were used, along with an estimated elevation of 226.4 m (743 ft) and an annual depth to the water table of 1.8 m (6 ft). The water

table information was derived from the soil surveys from the United States Department of Agriculture for Oneida County, WI (2000).

The aforementioned values were inputted into the Design Guide software, where applicable, and a total of 36 simulations were conducted. The simulations were run at varying layer thicknesses to determine the effects on pavement distress for 4.0%, 7.0%, and 10.0% air voids, along with the asphalt binder content increase of 0.3% at 7.0% air voids. Figures 7.36 through 7.40 show the effects of changes in the HMA's layer thickness on permanent deformation, in the AC layer only and the entire pavement structure, as well as the effects on IRI, longitudinal cracking, and alligator cracking. The nomenclature used in the following figures shows the air void content as a number (4.0%, 7.0%, and 10.0%) followed by the asphalt binder content (optimum, "opt.," or +0.3% asphalt binder content, "bu."). The criterion stipulated in Table 7.1 is shown on each figure.

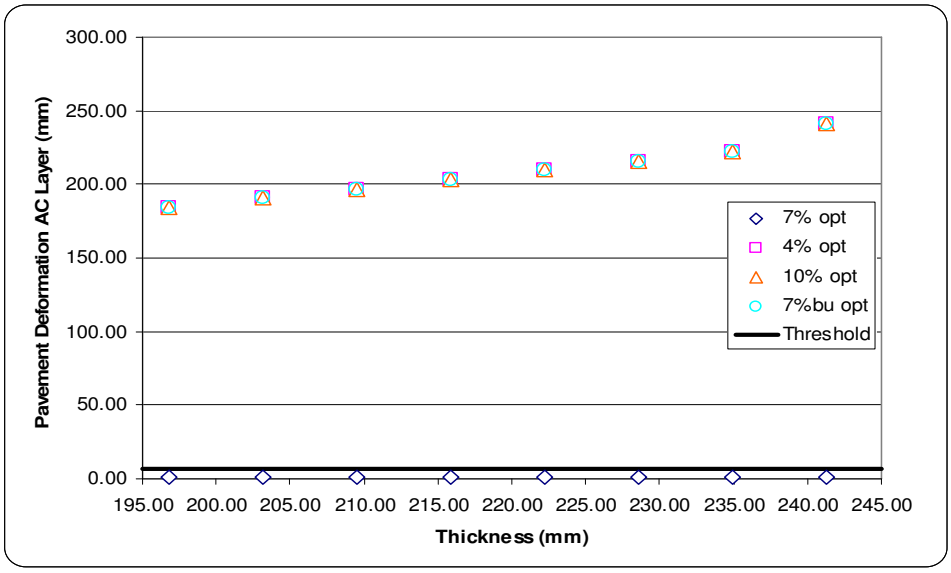

Figure 7.36. Tomahawk permanent deformation in AC layer

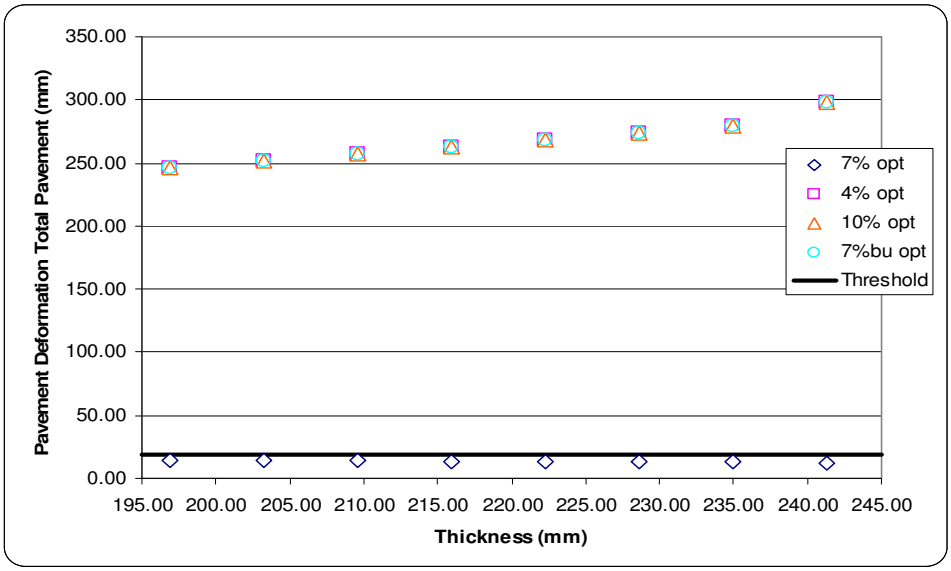

Figure 7.37. Tomahawk permanent deformation in total pavement

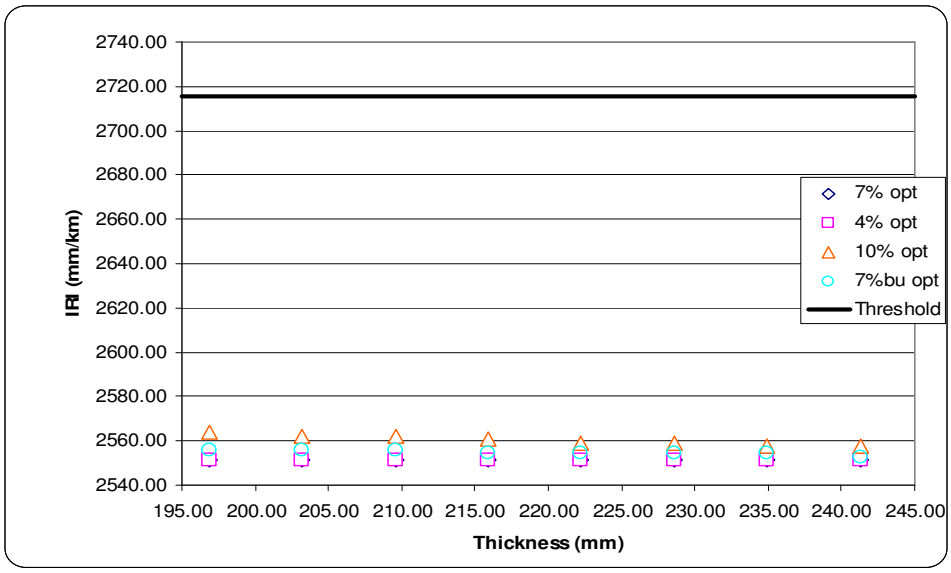

Figure 7.38. Tomahawk IRI

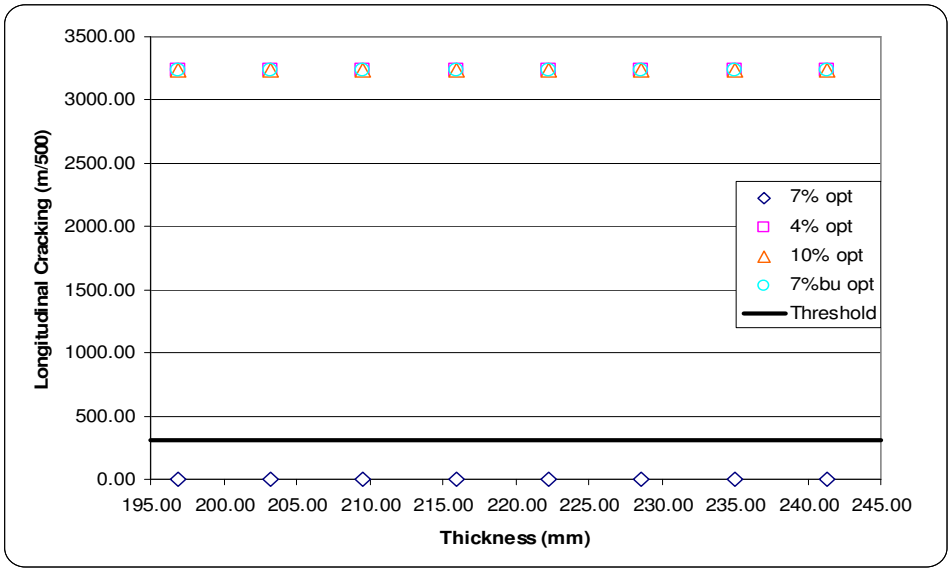

Figure 7.39. Tomahawk longitudinal cracking

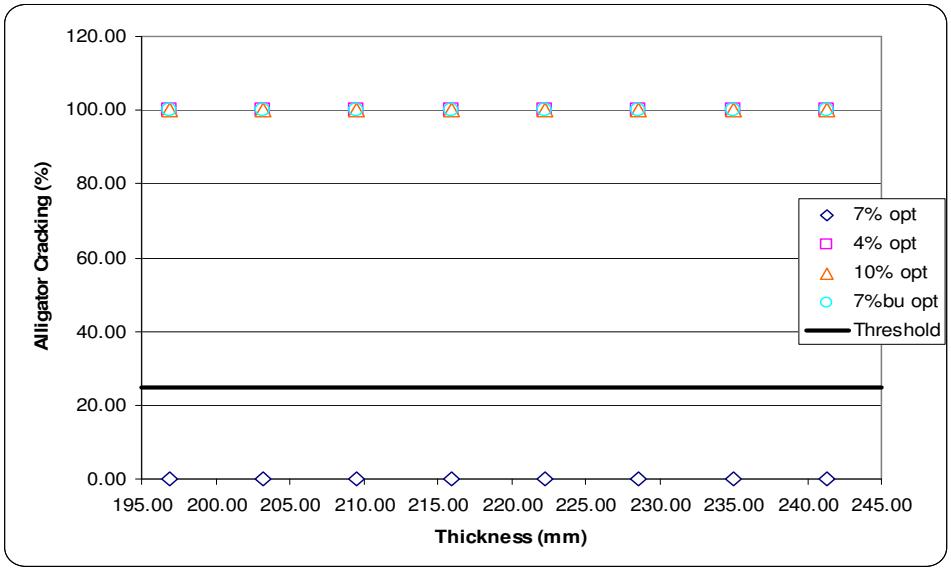

Figure 7.40. Tomahawk alligator cracking

The findings show that the as-built air voids (7.0%) had the highest performing configuration in terms of all of the distresses considered. The respective predicted distress gets progressively worse as the air void content increases or binder content increases. It was also interesting to see, at the 4.0% and 10.0% air void configurations and the 7.0% air void plus binder bump configuration, that as thickness increased, permanent deformation increased. The

predicted permanent deformation values for the AC layer and total pavement seem a bit unrealistic based on their magnitudes.

Again, IRI appears to be insensitive to changes in the air void content, asphalt binder content, and pavement thickness. The predicted pavement IRI is significantly lower than the performance criterion used in the Design Guide software of 2,715 mm/km.

In terms of longitudinal and alligator cracking, the 4.0% and 10.0% air void level and the 7.0% air void level plus binder bump were the most sensitive to changes in air voids. The failure criterion for longitudinal cracking is 300m/500, and these three configurations did not achieve this performance level at each pavement thickness. The failure criterion for alligator cracking is 25%. All simulations performed at these configurations did not meet this criteria.

7.1.9 Waunakee

The Waunakee E-3 19.0 mm pavement design consisted of 158.75 mm (6.25 in) of HMA on 304.8 mm (12 in) of crushed gravel on a subgrade of A-2-4 soil. The main composition of an A-2-4 soil is sandy-silt, under the AASHTO soil classification system. A level 1 analysis was used for the 19.0 mm NMAS layer, utilizing the dynamic modulus test results shown in the previous chapter. A modulus value of 275.8 MPa (40 ksi) was used for the crushed gravel layer; this particular layer was divided into two identical 152.4 mm (6 in layers). The reason for this division was that previous simulations with the Design Guide software had problems handling the thick layers. A plasticity index of 1, with 10% passing the #200 sieve, 30% passing the #4 sieve, and a D60 of 2 mm were also used as inputs for the crushed gravel. The subgrade support value was not provided, so an assumed value of 3.0 was used and, using the Design Guide software, this yielded an analogous modulus value of 20.7 MPa (3 ksi). This layer was divided into a 152.4 mm (6 in) layer, followed by an identical semi-infinite layer. A plasticity index of 3, with 60% passing the #200 sieve, 90% passing the #4 sieve, and a D60 of 0.05 mm were also used as inputs for the subgrade.

The traffic data, shown in Table 7.10, were supplied by WisDOT and show that this particular roadway is not expected to have a considerable amount of truck traffic.

Table 7.10. Traffic characteristics—Waunakee E-3 19.0 mm

Traffic characteristic	
AADT (veh./day)	4,792.00
Growth (%)	1.37
Percentage of traffic greater than class 4	12.20
AADTT (trucks/day)	585.00
Truck traffic distribution	
2D (%)	2.50
3-SU (%)	1.50
2S-1 (%)	1.60
2S-2 (%)	1.60
3S-2 (%)	4.70
2-S1-2 (%)	0.30

A new climatic station had to be interpolated for the exact location of this project. A latitude of 43.11 degrees and a longitude of -89.27 degrees were used, along with an estimated elevation of 226.5 m (743 ft) and an annual depth to the water table of 1.8 m (6 ft). The water table information was derived from the soil surveys from the United States Department of Agriculture for Dane County, WI (2000).

The aforementioned values were inputted into the Design Guide software, where applicable, and a total of 36 simulations were conducted. The simulations were run at varying layer thicknesses to their determine the effects on pavement distress for 4.0%, 7.0%, and 10.0% air voids, along with the asphalt binder content increase of 0.3% at 7.0% air voids. Figures 7.41 through 7.45 show the effects of changes in the HMA's layer thickness on permanent deformation, in the AC layer only and the entire pavement structure, as well as the effects on IRI, longitudinal cracking, and alligator cracking. The nomenclature used in the following figures shows the air void content as a number (4.0%, 7.0%, and10.0%) followed by the asphalt binder content (optimum, "opt.," or +0.3% asphalt binder content, "bu."). The criterion stipulated in Table 7.1 is shown on each figure.

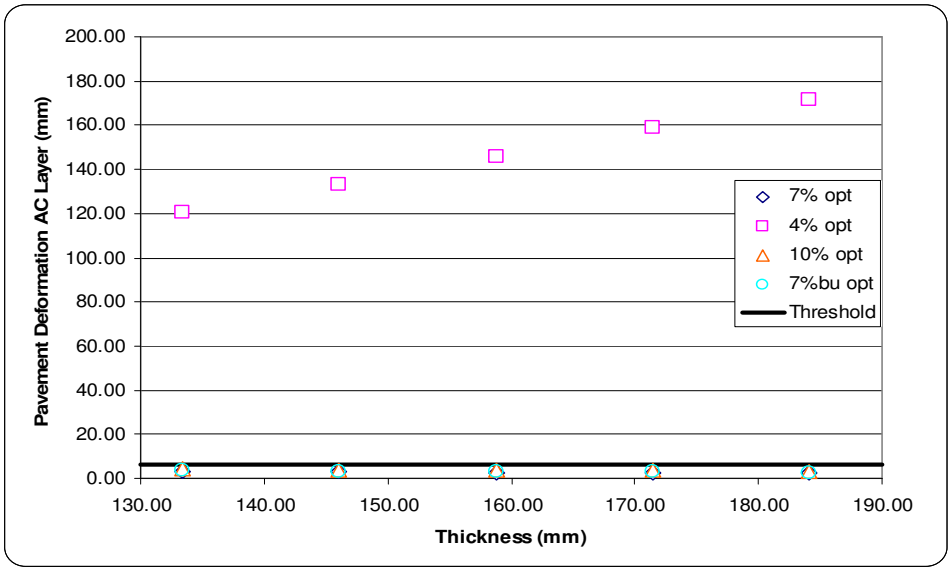

Figure 7.41. Waunakee permanent deformation in AC layer

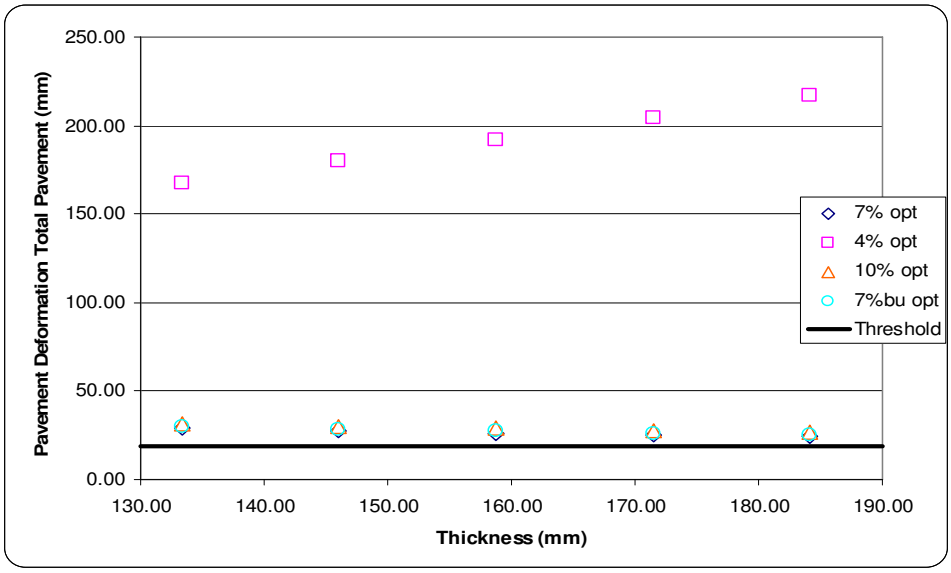

Figure 7.42. Waunakee permanent deformation in total pavement

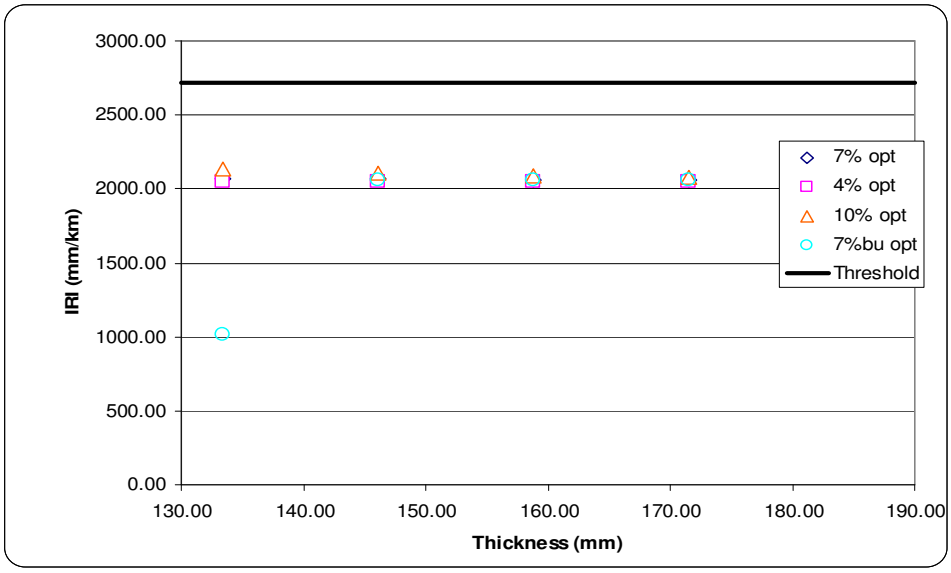

Figure 7.43. Waunakee IRI

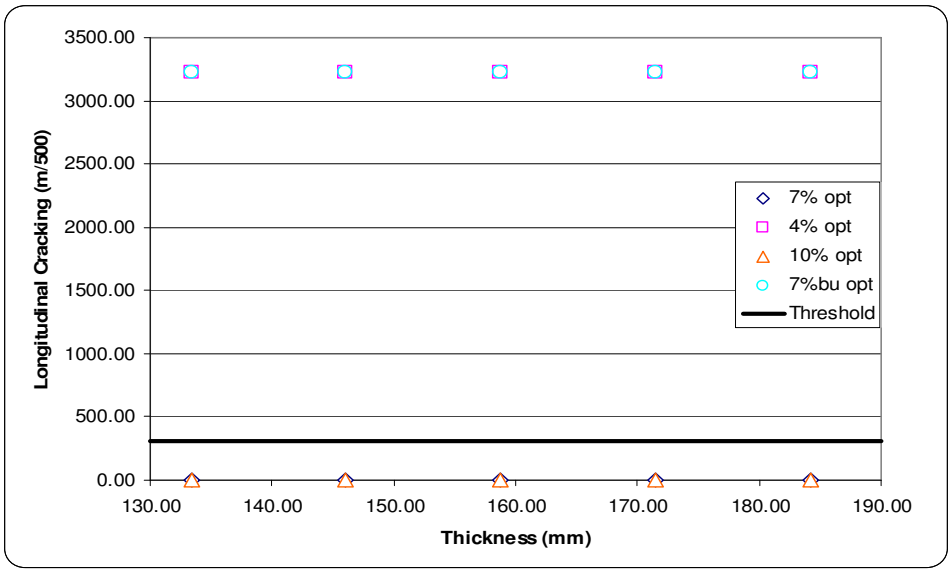

Figure 7.44. Waunakee longitudinal cracking

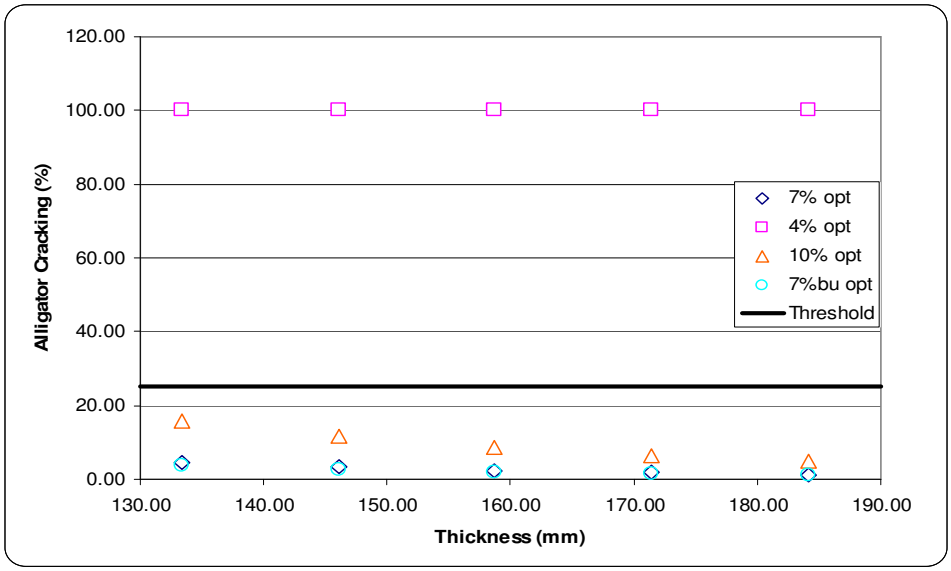

Figure 7.45. Waunakee alligator cracking

The findings show that the low air voids (4.0%) were the worst performing configuration in terms of all of the distresses considered. The respective predicted distress gets progressively better as the air void content increases and as pavement thickness increases. The pavement design with the asphalt binder content increase performed the same in comparison to the pavement design with the optimum asphalt content.

It was also interesting to see, at the 4.0% air void configuration, that as thickness increased, permanent deformation increased. All simulations that examined permanent deformation, except for the 4.0% air voids, were close to the threshold value of 6.0 mm and 19.0 mm for the rutting in the AC layer and total permanent deformation, respectively. The predicted permanent deformation values for the AC layer and total pavement seem a bit unrealistic based on their magnitudes.

Again, IRI appears to be insensitive to changes in the air void content, asphalt binder content, and the pavement thickness. The predicted pavement IRI is significantly lower than the performance criterion used in the Design Guide software of 2,715 mm/km.

In terms of longitudinal cracking, the 4.0% air void level and 7.0% air void level plus binder bump were the most sensitive to changes in air voids. The failure criteria for longitudinal cracking is 300 m/500, and the 4.0% air void level and 7.0% air void level plus binder bump did not achieve this performance criteria at each pavement thickness. The M-E PDG predicted that

3,250 m/500 of the pavement will have longitudinal cracking for the 4.0% air void and 7.0% air void level plus binder bump mix.

The failure criterion for alligator cracking is 25%. The 4.0% air void level did not achieve the performance criteria at every simulation. The M-E PDG predicted that 100% of the pavement will have alligator cracking for the 4.0% air void mix.

7.1.10 Mosinee

The Mosinee E-3 19.0 mm pavement design consisted of 44.45 mm (1.75 in) of HMA on 177.8 mm (7 in) of existing asphalt pavement on an A-4 soil subgrade. The main composition of an A-4 soil is silt, under the AASHTO soil classification system. The HMA design thickness of 44.5 mm (1.75 in) was suspect for this pavement. As a rule of thumb, the thickness should be three times the NMAS of the mixture; thus, the thickness should be at least 57.0 mm (2.24 in) through recommended construction practice. However, this was the information that was provided by WisDOT and, thus, is used in the analysis. It was assumed that the entire HMA layer consisted of the 19.0 mm mixture, as no other information from WisDOT contradicts this assumption. A level 1 analysis is used for the 19.0 mm NMAS layer, utilizing the dynamic modulus test results; these results can be found above in the previous chapter. The existing pavement layer was designed using a level 3 analysis and using the gradation and volumetric information from the JMF for this specific project at 4.0% air voids. The A-4 subgrade was listed as having a subgrade support value of 4.2 and the Design Guide software was used to determine an analogous modulus value of 238.2 MPa (34.6 ksi). A plasticity index of 3, with 60% passing the #200 sieve, 90% passing the #4 sieve, and a D60 of 0.05 mm were also used as inputs for the subgrade.

A breakdown of the truck traffic as well as the AADT for the roadway was supplied by WisDOT. The Design Guide software was then used to determine the analogous average annual

daily truck traffic (AADTT), which was found to be 893. The truck traffic composition and the AADT can be found in Tab.e 7.11.

Table 7.11. Traffic characteristics—Mosinee E-3 19.0 mm

Traffic characteristic	
AADT (veh./day)	6,868.00
Growth (%)	1.37
Percentage of traffic greater than class 4	13.00
AADTT (trucks/day)	893.00
Truck traffic distribution	
2D (%)	2.30
3-SU (%)	1.00
2S-1 (%)	0.70
2S-2 (%)	0.70
3S-2 (%)	8.20
2-S1-2 (%)	0.10

The Wausau, WI climatic file was used for the climatic input, as the actual mix was placed on US-153 in the Wausau city limits. The ground water table was estimated to be at a depth of 1.829 m (6 ft) or greater, based on the information from the soils surveys from the United States Department of Agriculture (2000) for Marathon County, WI.

Nine simulations were run for each of the air voids and asphalt binder contents, amounting to a total of 36 simulations. Figures 7.46 through 7.50 show the effects of changes in the HMA's layer thickness on permanent deformation, in the AC layer only and the entire pavement structure, as well as the effects on IRI, longitudinal cracking, and alligator cracking. The nomenclature used in the following figures shows the air void content as a number (4.0%, 7.0%, and 10.0%) followed by the asphalt binder content (optimum, "opt.," or +0.3% asphalt binder content, "Bump").

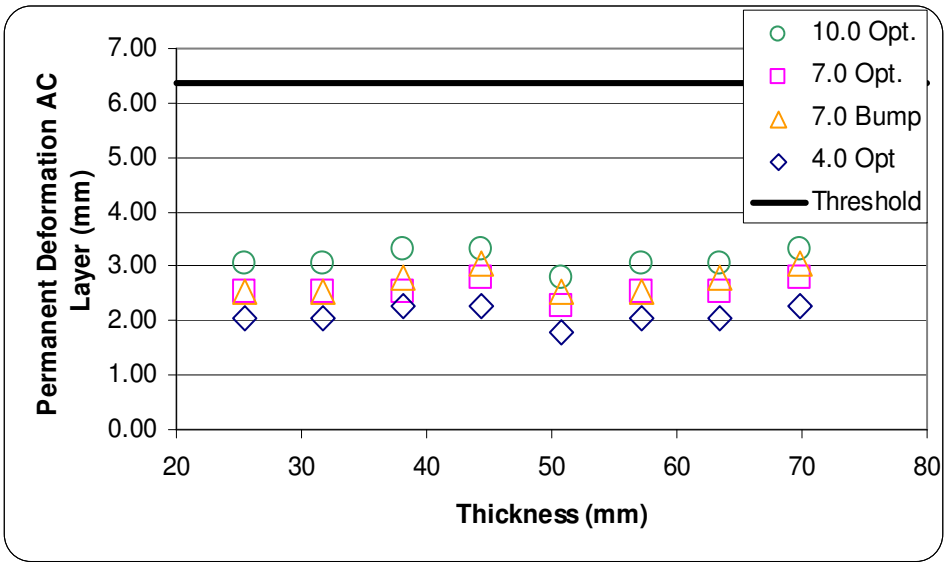

Figure 7.46. Mosinee permanent deformation in AC layer

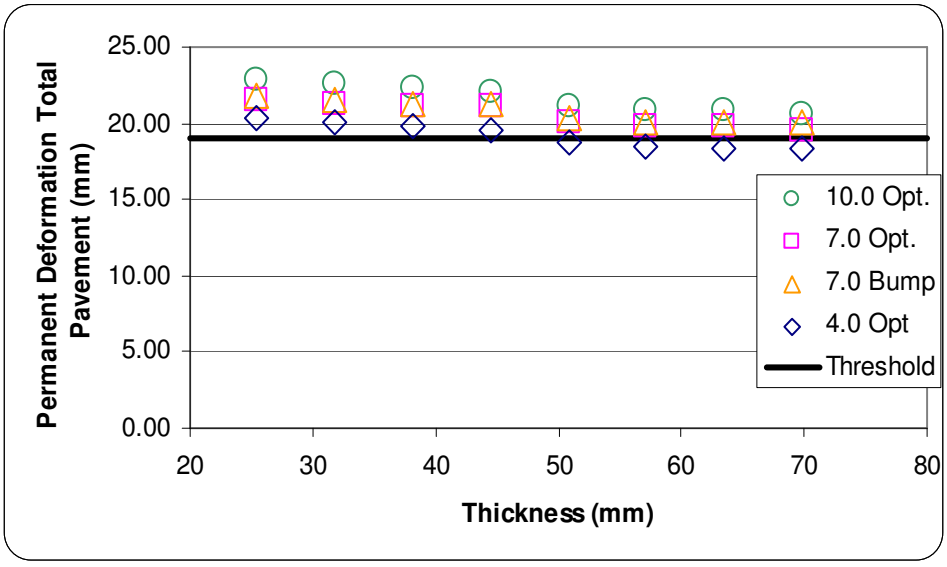

Figure 7.47. Mosinee permanent deformation in total pavement

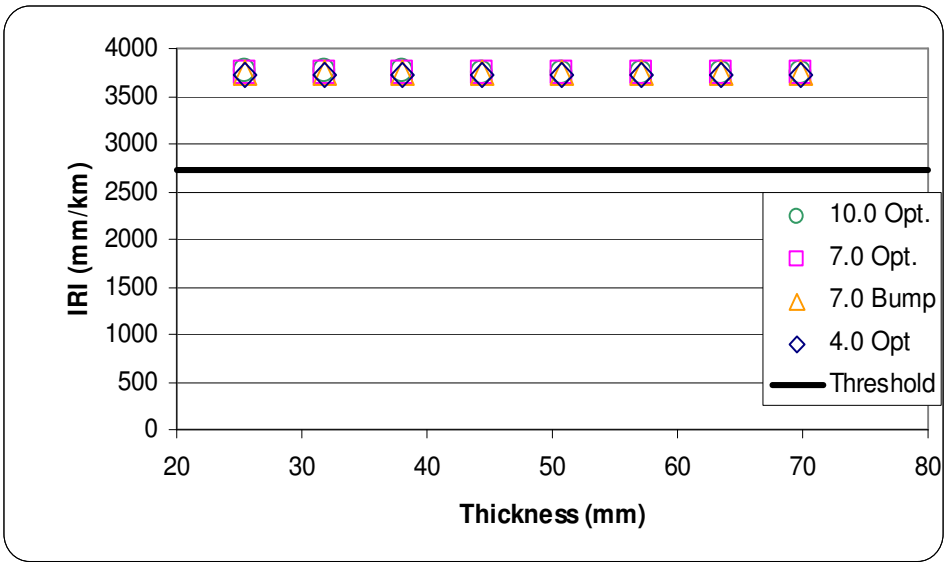

Figure 7.48. Mosinee IRI

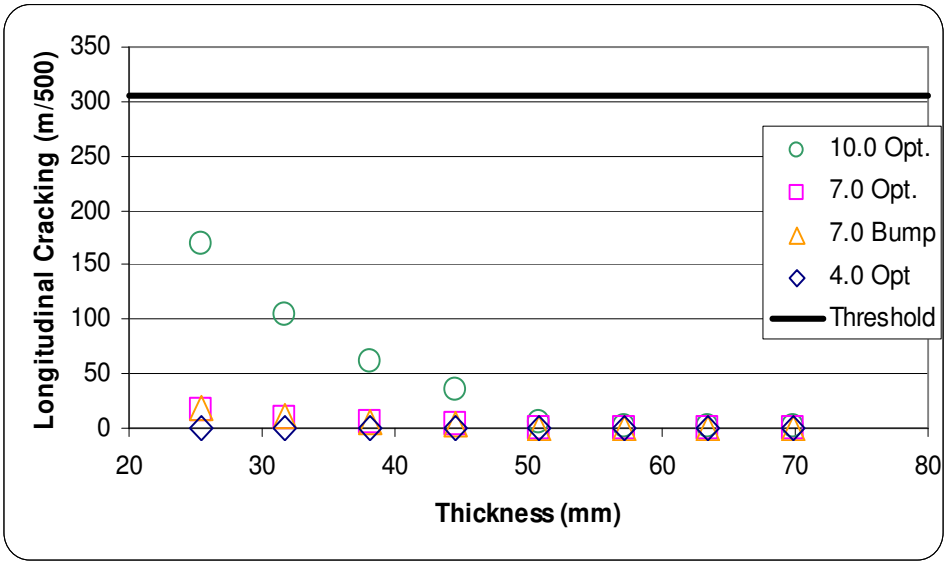

Figure 7.49. Mosinee longitudinal cracking

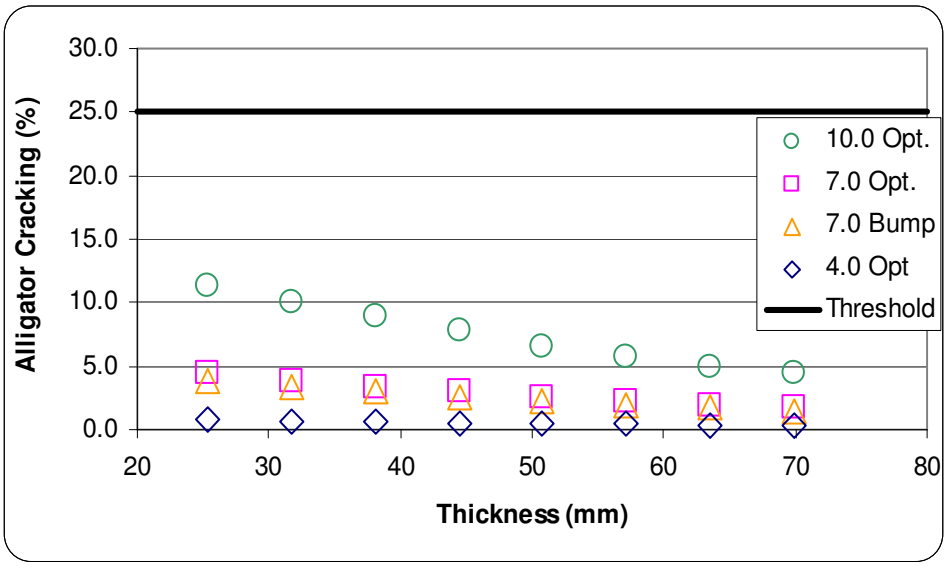

Figure 7.50. Mosinee alligator cracking

The findings show that the low air voids (4.0%) had the highest performing configuration in terms of all of the distresses considered. The respective predicted distress gets progressively worse as the air void content increases. The pavement design with the asphalt binder content increase had a higher predicted resistance to all of the distresses considered, in comparison to the pavement design with the optimum asphalt content. In most instances, the high air void content (10.0%) pavement design expectedly resulted in the highest predicted permanent deformation while the low air void content (4.0%) had the lowest.

Again, IRI appears to be insensitive to changes in the air void content, asphalt binder content, and pavement thickness. The predicted pavement IRI is significantly greater than the performance criterion used in the Design Guide software of 2,715 mm/km.

Figures 7.49 and 7.50 indicate that the thicknesses examined are sufficient to mitigate longitudinal and alligator cracking for each of the air void levels and binder content levels considered. The performance criteria used by the Design Guide software was 305 m/500 and 25% for longitudinal and alligator cracking. Increasing the thickness would, in effect, decrease longitudinal and alligator cracking.

7.1.11 Cumberland

The Cumberland E-3 19.0-mm pavement design consisted 177.8-mm (7.0-in) of HMA on 177.8-mm (7-in) of nominal mill and relay blended with 1" to ¼" aggregate on 228.6-mm (9-in)

of breaker run and/or rubblized concrete on a subgrade of A-4 soil. The main composition of an A-4 soil is silt, under the AASHTO soil classification system. A level 1 analysis was used for the 19.0 mm NMAS layer, utilizing the dynamic modulus test results shown in the previous chapter. A modulus value of 275.8 MPa (40 ksi) was used for the mill and blended aggregate. A modulus value of 380 MPa (55 ksi) was used for the breaker run and/or rubblized concrete. A plasticity index of 1, with 10% passing the #200 sieve, 30% passing the #4 sieve, and a D60 of 2 mm were also used as inputs for layers 2 and 3. The subgrade was reported to have a support value of 3.9 and, using the Design Guide software, yielded an analogous modulus value of 29.0 MPa (4.2 ksi); this layer was divided into a 152.4 mm (6 in) layer followed by an identical semi-infinite layer. A plasticity index of 3, with 60% passing the #200 sieve, 90% passing the #4 sieve, and a D60 of 0.05- mm were also used as inputs for the subgrade.

The traffic data, shown in Table 7.12, were supplied by WisDOT and show that this particular roadway is not expected to have a considerable amount of truck traffic.

Table 7.12. Traffic characteristics—Cumberland E-3 19.0-mm

Traffic characteristic	
AADT (veh./day)	5,353.00
Growth (%)	1.37
Percentage of traffic greater than class 4	12.20
AADTT (trucks/day)	653.00
Truck traffic distribution	
2D (%)	2.50
3-SU (%)	1.50
2S-1 (%)	1.60
2S-2 (%)	1.60
3S-2 (%)	4.70
2-S1-2 (%)	0.30

A new climatic station had to be interpolated for the exact location of this project. A latitude of 45.32 degrees and a longitude of -92.01 degrees were used, along with an estimated elevation of 240.5 m (789 ft) and an annual depth to the water table of 0.91 m (3 ft). The water table information was derived from the soil surveys from the United States Department of Agriculture for Barron County, WI (2000).

The aforementioned values were inputted into the Design Guide software, where applicable, and a total of 36 simulations were conducted. The simulations were run at varying

layer thicknesses to their determine the effects on pavement distress for 4.0%, 7.0%, and 10.0% air voids, along with the asphalt binder content increase of 0.3% at 7.0% air voids. Figures 7.51 through 7.55 show the effects of changes in the HMA's layer thickness on permanent deformation, in the AC layer only and the entire pavement structure, as well as the effects on IRI, longitudinal cracking, and alligator cracking. The nomenclature used in the following figures shows the air void content as a number (4.0%, 7.0%, and 10.0%) followed by the asphalt binder content (optimum, "Opt.," or +0.3% asphalt binder content, "Bump"). The criterion stipulated in Table 7.1 is shown on each figure.

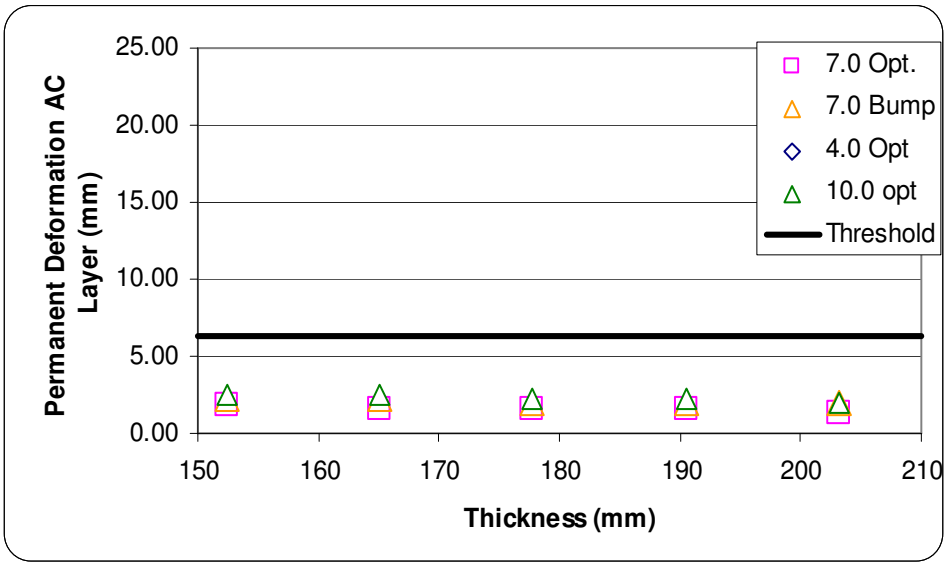

Figure 7.51. Cumberland permanent deformation in AC layer

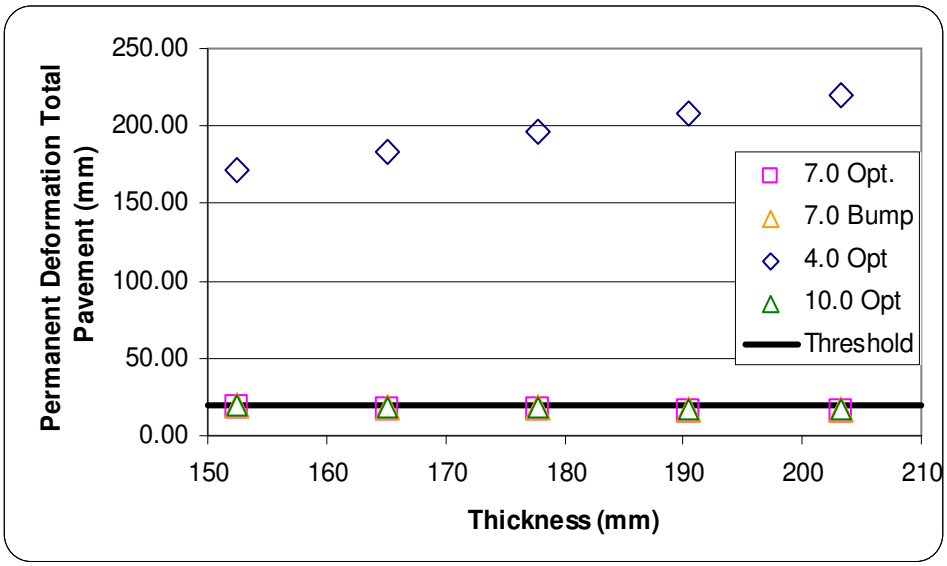

Figure 7.52. Cumberland permanent deformation in total pavement

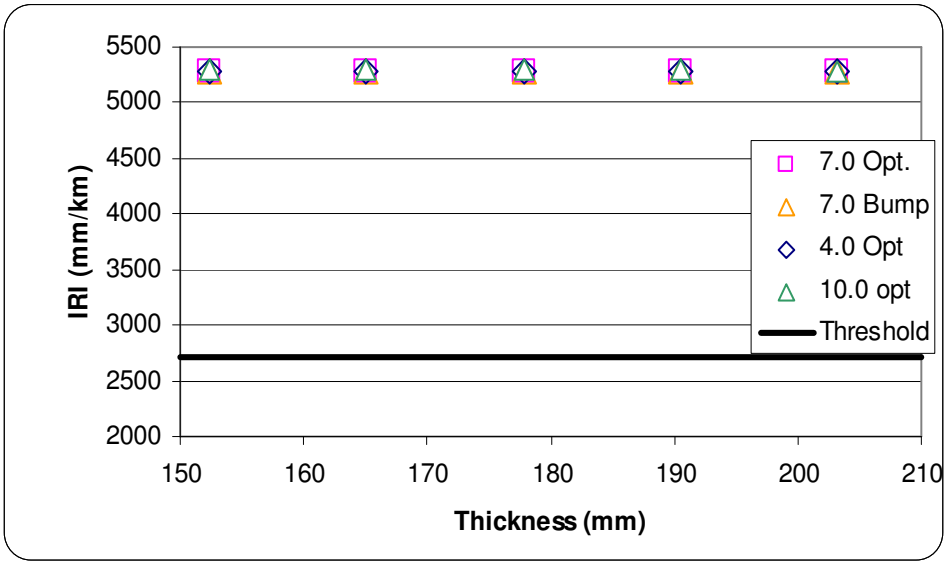

Figure 7.53. Cumberland IRI

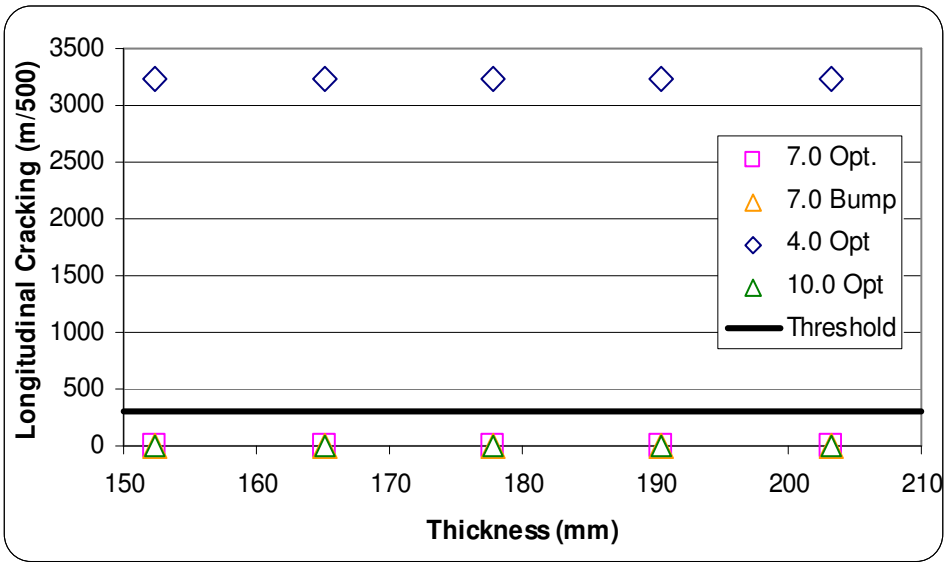

Figure 7.54. Cumberland longitudinal cracking

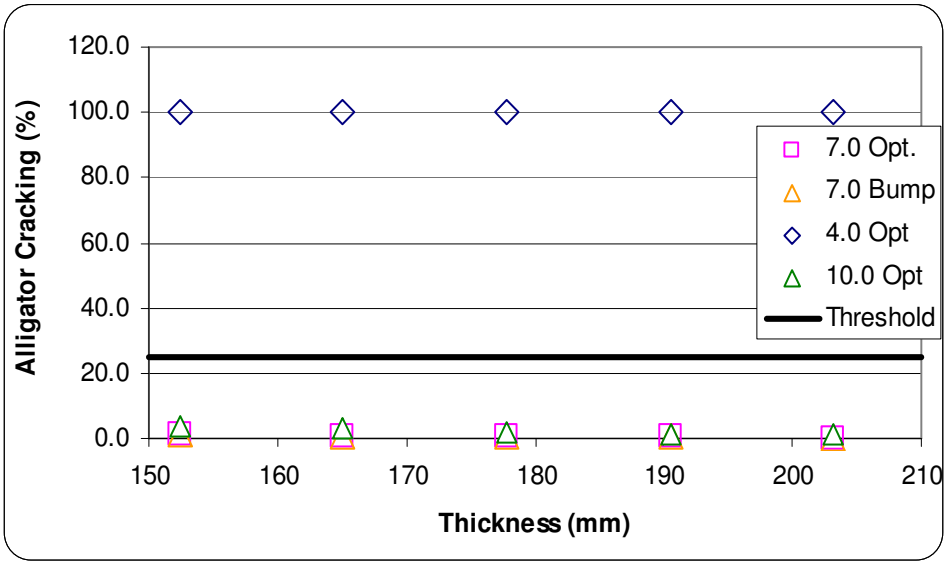

Figure 7.55. Cumberland alligator cracking

The findings show that the low air voids (4.0%) were the worst performing configuration in terms of all of the distresses considered. The respective predicted distress gets progressively better as the air void content increases and as pavement thickness increases. The pavement design with the asphalt binder content increase performed the same in comparison to the pavement design with the optimum asphalt content.

It was also interesting to see, at the 4.0% air void configuration, that as thickness increased, total permanent deformation increased. All simulations examining total permanent

deformation, except for the 4.0% air voids, were close to the threshold value of 19.0 mm. The predicted total permanent deformation values seem a bit unrealistic based on their magnitudes.

IRI appears to be insensitive to changes in the air void content, asphalt binder content, and pavement thickness. The predicted pavement IRI is significantly greater than the performance criteria used in the Design Guide software of 2,715 mm/km.

In terms of longitudinal and alligator cracking, the 4.0% air void level was the most sensitive to changes in air voids. The failure criterion for longitudinal cracking is 300 m/500; the 4.0% air void level did not achieve the criteria at each pavement thickness. The failure criterion for alligator cracking is 25%. All simulations performed at the 4.0% air void level did not meet the intended criteria.

7.1.12 Hayward

The Hayward E-3 12.5 mm pavement design consisted of 127.0 mm (5.0 in) of HMA on 177.8 mm (7.0 in) of pulverized HMA on 304.8 mm (12 in) of granular base on a subgrade of A-4 soil. The main composition of an A-4 soil is silt, under the AASHTO soil classification system. A level 1 analysis was used for the 19.0 mm NMAS layer, utilizing the dynamic modulus test results shown in the previous chapter. A modulus value of 379.2 MPa (55 ksi) and 275.8 MPa (40 ksi) was used for the pulverized HMA layer and granular subbase layer, respectively. The granular subbase layer was divided into two identical 152.4 mm (6 in layers). The reason for this division was that previous simulations with the Design Guide software had problems handling the thick layers. A plasticity index of 1, with 10% passing the #200 sieve, 30% passing the #4 sieve, and a D60 of 2 mm were also used as inputs for the pulverized HMA and subbase layers. The subgrade was reported to have a support value of 3.9 and, using the Design Guide software, yielded an analogous modulus value of 29.0 MPa (4.2 ksi); this layer was divided into a 152.4 mm (6 in) layer followed by an identical semi-infinite layer. A plasticity index of 3, with 60% passing the #200 sieve, 90% passing the #4 sieve, and a D60 of 0.05 mm were also used as inputs for the subgrade.

The traffic data, shown in Table 7.13, were supplied by WisDOT and show that this particular roadway is not expected to have a considerable amount of truck traffic.

Table 7.13. Traffic characteristics—Hayward E-3 12.5 mm

Traffic characteristic	
AADT (veh./day)	9,621.00
Growth (%)	1.37
Percentage of traffic greater than class 4	15.60
AADTT (trucks/day)	1501.00
Truck Traffic Distribution	
2D (%)	4.30
3-SU (%)	1.10
2S-1 (%)	2.10
2S-2 (%)	2.10
3S-2 (%)	6.00
2-S1-2 (%)	0.00

A new climatic station had to be interpolated for the exact location of this project. A latitude of 46.00 degrees and a longitude of -91.29 degrees were used, along with an estimated elevation of 484.6 m (1590 ft) and an annual depth to the water table of 0.91 m (3 ft). The water table information was derived from the soil surveys from the United States Department of Agriculture for Sawyer County, WI (2000).

The aforementioned values were inputted into the Design Guide software, where applicable, and a total of 36 simulations were conducted. The simulations were run at varying layer thicknesses to their determine the effects on pavement distress for 4.0%, 7.0%, and 10.0% air voids, along with the asphalt binder content increase of 0.3% at 7.0% air voids. Figures 7.56 through 7.60 show the effects of changes in the HMA's layer thickness on permanent deformation, in the AC layer only and the entire pavement structure, as well as the effects on IRI, longitudinal cracking, and alligator cracking. The nomenclature used in the following figures shows the air void content as a number (4.0%, 7.0%, and 10.0%) followed by the asphalt binder content (optimum, "Opt.," or +0.3% asphalt binder content, "Bump"). The criterion stipulated in Table 7.1 is shown on each figure.

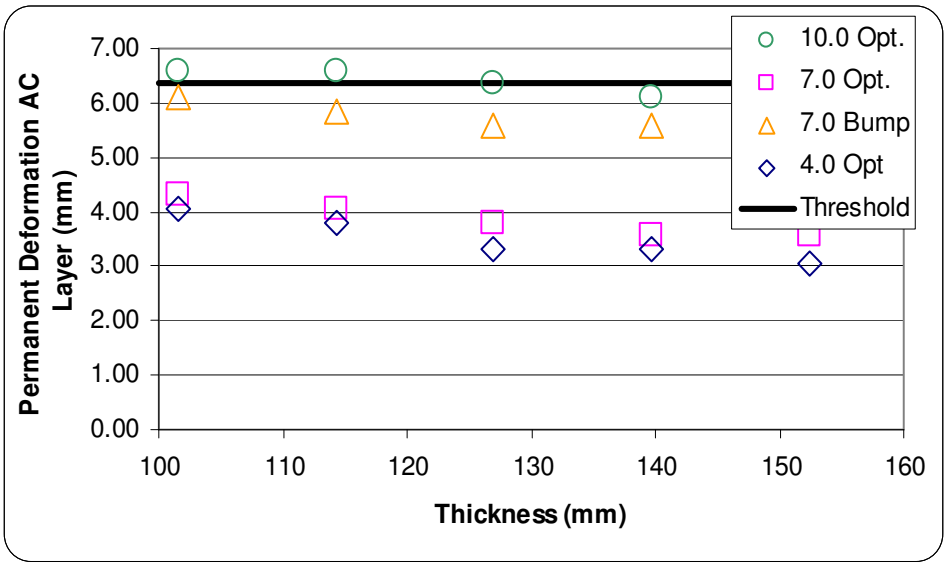

Figure 7.56. Hayward permanent deformation in AC layer

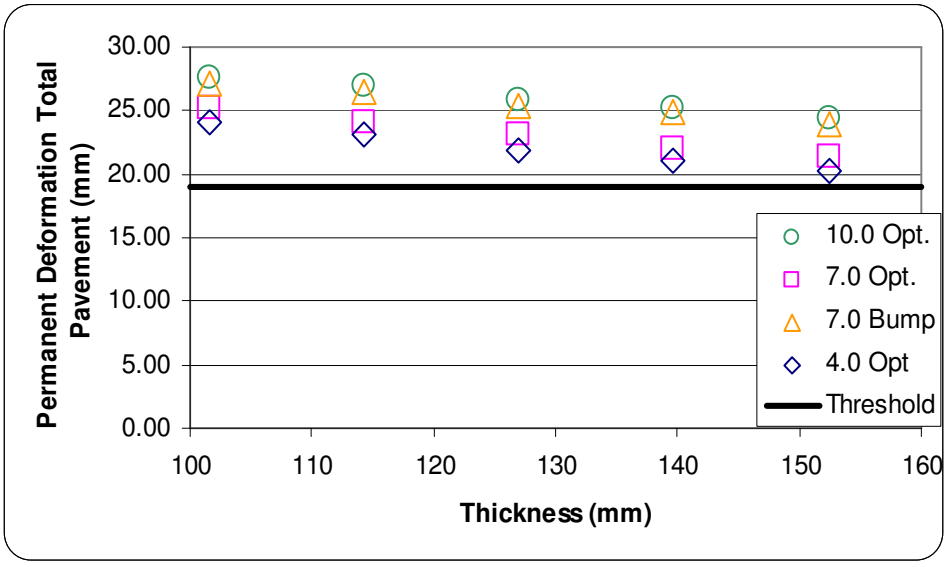

Figure 7.57. Hayward permanent deformation in total pavement

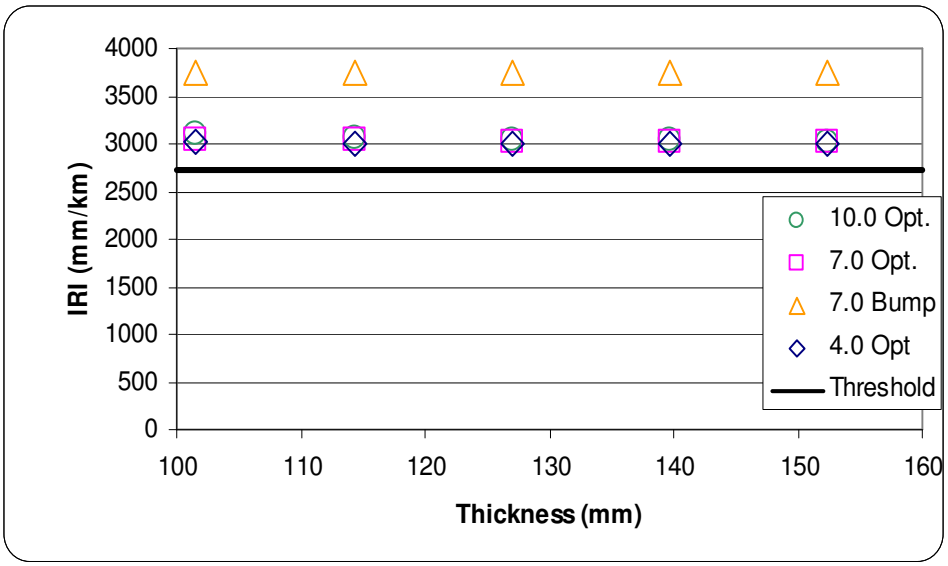

Figure 7.58. Hayward IRI

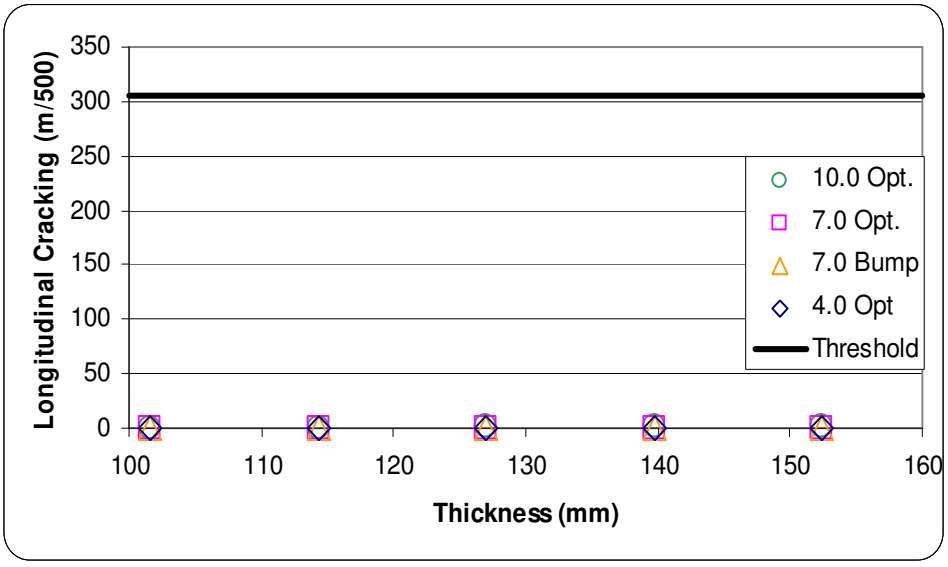

Figure 7.59. Hayward longitudinal lracking

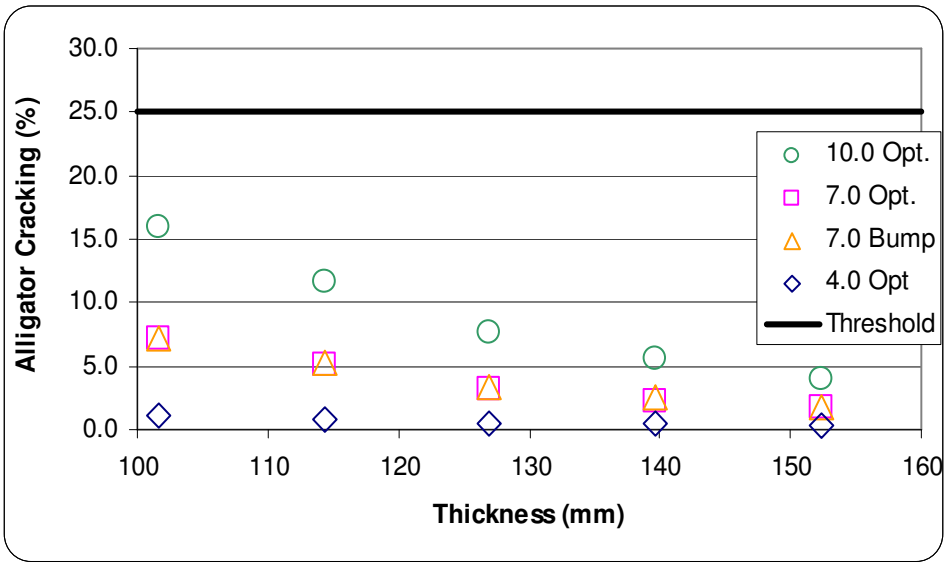

Figure 7.60. Hayward alligator cracking

The findings show that the low air voids (4.0%) had the best performing configuration in terms of all of the distresses considered. The respective predicted distress gets progressively worse as the air void content increases. The pavement design with the optimum asphalt binder content had a higher predicted resistance to all of the distresses considered, in comparison to the pavement design with the asphalt content increase.

In most instances, the high air void content (10.0%) pavement design expectedly resulted in the highest predicted permanent deformation while the low air void content (4.0%) had the lowest. Figures 7.56 and 7.57 show that permanent deformation decreases with increasing pavement thickness and that permanent deformation is sensitive to changes in air void levels and asphalt content. It was noted that all four cases failed the M-E PDG criteria for total permanent deformation.

Again, IRI appears to be insensitive to changes in the air void content, asphalt binder content, and pavement thickness. The predicted pavement IRI is significantly greater than the performance criterion used in the Design Guide software of 2,715 mm/km.

Figure 7.59 indicates that the thicknesses examined are sufficient to mitigate longitudinal cracking at all air void levels. Figure 7.60 shows that alligator cracking is sensitive to changes in air voids, asphalt content, and pavement thickness. As pavement thickness increases, alligator cracking decreases; as air voids increases, alligator cracking increases; and as binder content increases, alligator cracking increases. Typically, as binder content increases, the HMA is more

flexible; thus, the trend showing that alligator cracking increases as binder content increases goes against previous research and rules of thumb. Figure 7.60 shows that, at a 7.0% air void level, there is no difference in predicted alligator cracking at optimum binder content versus a binder bump.

7.1.13 Wausau

The Wausau E-3 12.5 mm pavement design consisted of 114.3 mm (4.5 in) of HMA on 304.8 mm (12 in) of crushed gravel on a subgrade of A-3 soil. The main composition of an A-4 soil is sandy-silt, under the AASHTO soil classification system. A level 1 analysis was used for the 12.5 mm NMAS layer, utilizing the dynamic modulus test results shown in the previous chapter. A modulus value of 275.8 MPa (40 ksi) was used for the crushed gravel layer; this particular layer was divided into two identical 152.4 mm (6 in layers). The reason for this division was that previous simulations with the Design Guide software had problems handling the thick layers. A plasticity index of 1, with 10% passing the #200 sieve, 30% passing the #4 sieve, and a D60 of 2 mm were also used as inputs for the crushed gravel. The subgrade was reported to have a support value of 5.2 and, using the Design Guide software, yielded an analogous modulus value of 204.4 MPa (29.6 ksi); this layer was divided into a 152.4 mm (6 in) layer followed by an identical semi-infinite layer. A plasticity index of 3, with 60% passing the #200 sieve, 90% passing the #4 sieve, and a D60 of 0.05 mm were also used as inputs for the subgrade.

The traffic data, shown in Table 7.14, were supplied by WisDOT and show that this particular roadway is not expected to have a considerable amount of truck traffic.

Table 7.14. Traffic characteristics—Wausau E-3 12.5 mm

Traffic characteristic	
AADT (veh./day)	3,800.00
Growth (%)	1.37
Percentage of traffic greater than class 4	6.00
AADTT (trucks/day)	228.00
Truck traffic distribution	
2D (%)	1.50
3-SU (%)	1.50
2S-1 (%)	0.70
2S-2 (%)	0.70
3S-2 (%)	1.30
2-S1-2 (%)	0.30

A new climatic station had to be interpolated for the exact location of this project. A latitude of 44.56 degrees and a longitude of -89.38 degrees were used, along with an estimated elevation of 362.4 m (1189 ft) and an annual depth to the water table of 1.8 m (6 ft). The water table information was derived from the soil surveys from the United States Department of Agriculture for Marathon County, WI (2000).

The aforementioned values were inputted into the Design Guide software, where applicable, and a total of 36 simulations were conducted. The simulations were run at varying layer thicknesses to their determine the effects on pavement distress for 4.0%, 7.0%, and 10.0% air voids, along with the asphalt binder content increase of 0.3% at 7.0% air voids. Figures 7.61 through 7.65 show the effects of changes in the HMA's layer thickness on permanent deformation, in the AC layer only and the entire pavement structure, as well as the effects on IRI, longitudinal cracking, and alligator cracking. The nomenclature used in the following figures shows the air void content as a number (4.0%, 7.0%, and 10.0%) followed by the asphalt binder content (optimum, "Opt.," or +0.3% asphalt binder content, "Bump"). The criterion stipulated in Table 7.1 is shown on each figure.

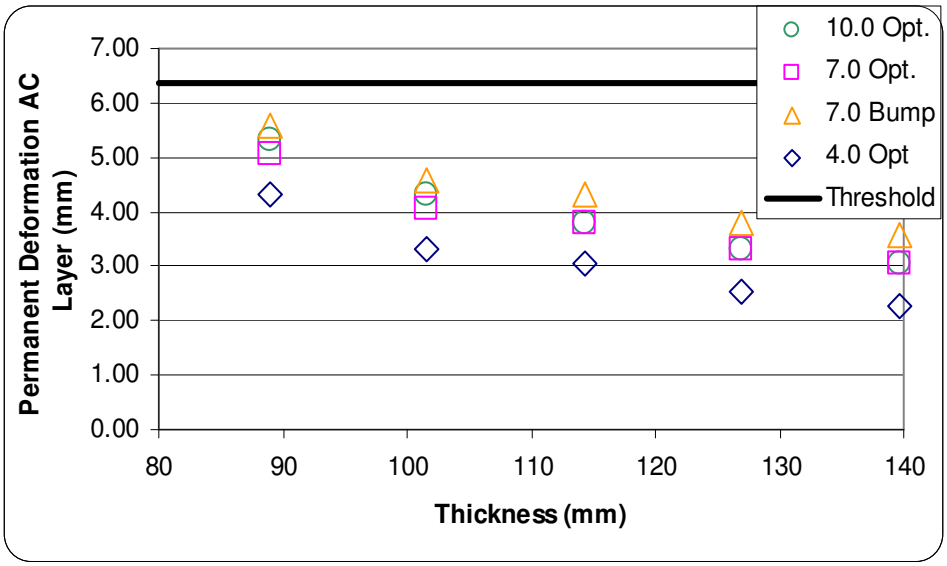

Figure 7.61. Wausau permanent deformation in AC layer

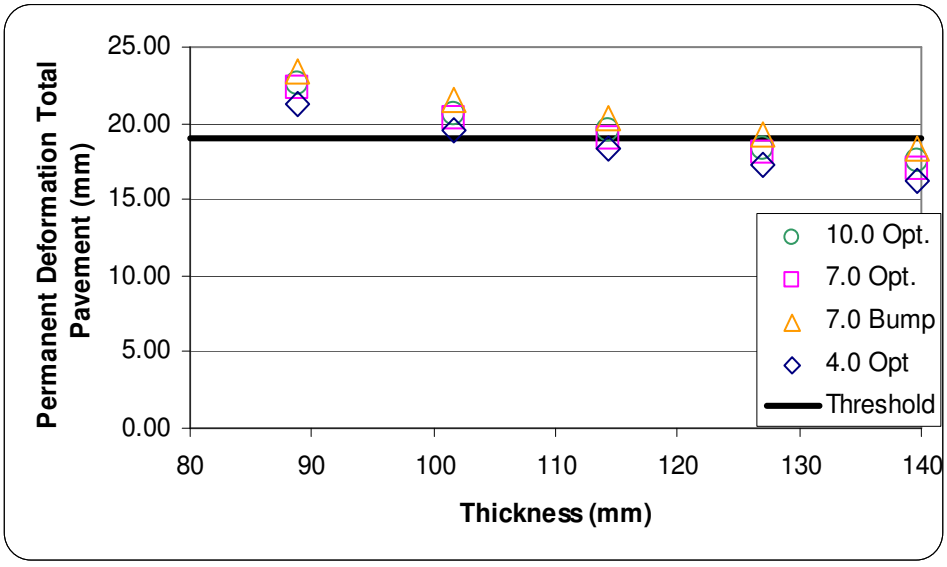

Figure 7.62. Wausau permanent deformation in total pavement

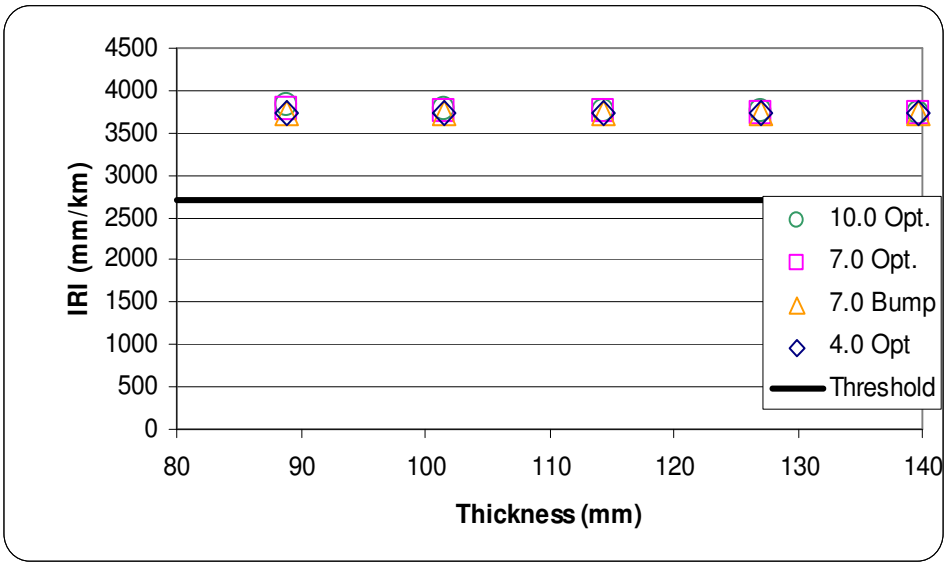

Figure 7.63. Wausau IRI

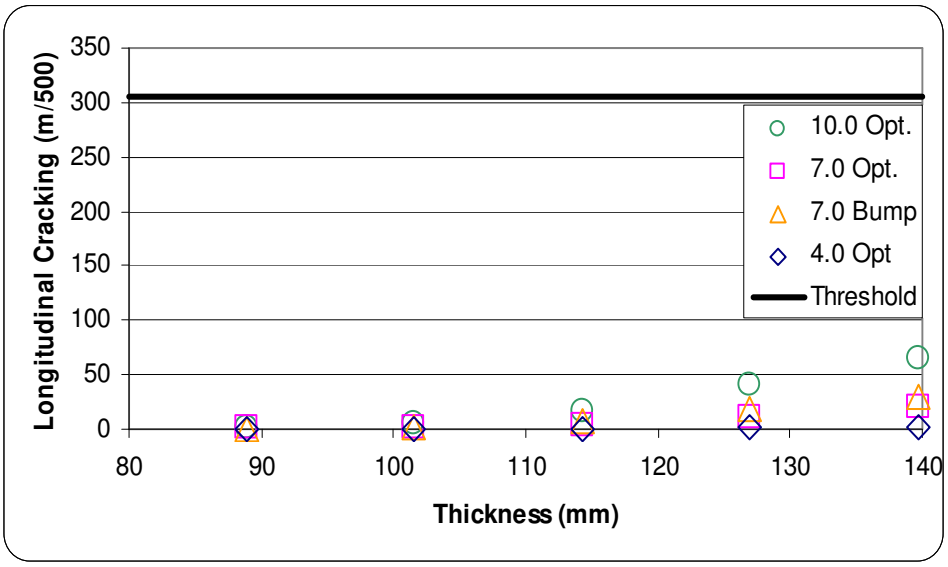

Figure 7.64. Wausau longitudinal cracking

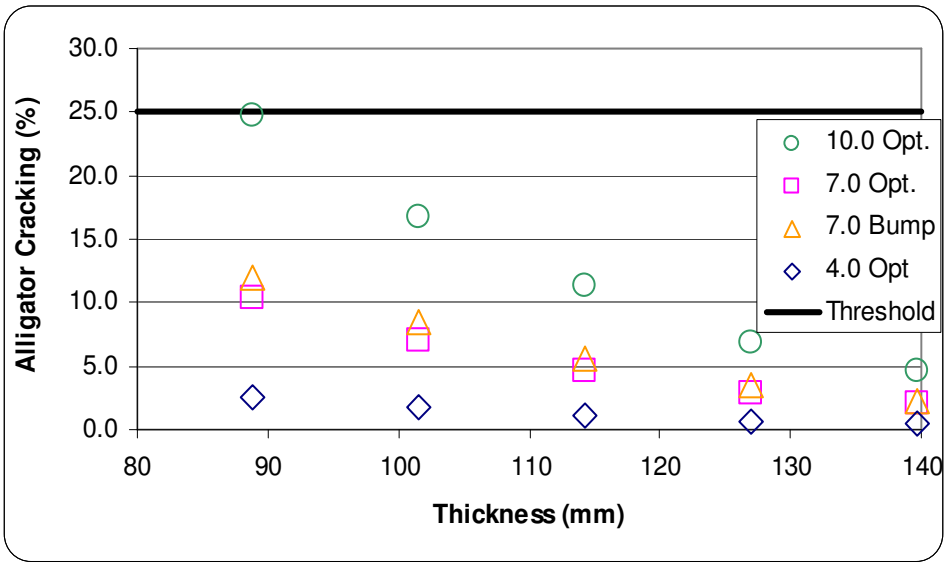

Figure 7.65. Wausau alligator cracking

The findings show that the low air voids (4.0%) had the best performing configuration in terms of all of the distresses considered. The respective predicted distress gets progressively worse as the air void content increases. The pavement design with the optimum asphalt binder content had a higher predicted resistance to all of the distresses considered, in comparison to the pavement design with the asphalt content increase.

In most instances, the high air void content (10.0%) pavement design expectedly resulted in the highest predicted permanent deformation while the low air void content (4.0%) with had the lowest. Figures 7.61 and 7.62 show that permanent deformation decreases with increasing pavement thickness and that permanent deformation is sensitive to changes in air void levels and asphalt content.

Again, IRI appears to be insensitive to changes in the air void content, asphalt binder content, and the pavement thickness. The predicted pavement IRI is significantly greater than the performance criterion used in the Design Guide software of 2,715 mm/km.

Figure 7.64 indicates that the thicknesses examined are sufficient to mitigate longitudinal cracking at all air void levels. However, as pavement thickness increases, there is an increase in longitudinal cracking. Figure 7.65 shows that alligator cracking is sensitive to changes in air voids, asphalt content, and pavement thickness. As pavement thickness increases, alligator cracking decreases; as air voids increases, alligator cracking increases; and as binder content increases, alligator cracking increases. Typically, as binder content increases, the HMA is more

flexible; thus, the trend showing that alligator cracking increases as binder content increases goes against previous research and rules of thumb. Figure 7.60 shows that, at a 7.0% air void level, there is no difference in predicted alligator cracking at optimum binder content versus a binder bump.

7.1.14 Hurley

The Hurley E-3 12.5 mm pavement design consisted 101.6 mm (4.0 in) of HMA on 127.0 mm (5 in) of sulfur extended HMA on 304.8 mm (12 in) select borrow on a subgrade of A-4 soil. The main composition of an A-4 soil is sil, under the AASHTO soil classification system. A level 1 analysis was used for the 19.0 mm NMAS layer, utilizing the dynamic modulus test results shown in the previous chapter. A level 3 analysis was used on the sulfur extended HMA, for which default values were inputted for gradation and volumetric characteristics. A modulus value of 103.4 MPa (15 ksi) was used for the select borrow layer; this particular layer was divided into two identical 152.4 mm (6 in layers). The reason for this division was that previous simulations with the Design Guide software had problems handling the thick layers. A plasticity index of 1, with 10% passing the #200 sieve, 30% passing the #4 sieve, and a D60 of 2 mm were also used as inputs for the crushed gravel. The subgrade was reported to have a support value of 4.6 and, using the Design Guide software, yielded an analogous modulus value of 37.5 MPa (5.4 ksi); this layer was divided into a 152.4 mm (6 in) layer followed by an identical semi-infinite layer. A plasticity index of 3, with 60% passing the #200 sieve, 90% passing the #4 sieve, and a D60 of 0.05 mm were also used as inputs for the subgrade.

The traffic data, shown in Table 7.15, were supplied by WisDOT and show that this particular roadway is not expected to have a considerable amount of truck traffic.

Table 7.15. Traffic characteristics—Hurley E-3 12.5 mm

Traffic characteristic	
AADT (veh./day)	4,970.00
Growth (%)	1.17
Percentage of traffic greater than class 4	14.00
AADTT (trucks/day)	696.00
Truck traffic distribution	
2D (%)	2.90
3-SU (%)	1.70
2S-1 (%)	1.80
2S-2 (%)	1.80
3S-2 (%)	5.40
2-S1-2 (%)	0.30

A new climatic station had to be interpolated for the exact location of this project. A latitude of 46.27 degrees and a longitude of -90.11 degrees were used, along with an estimated elevation of 261.2 m (857 ft) and an annual depth to the water table of 0.91 m (3 ft). The water table information was derived from the soil surveys from the United States Department of Agriculture for Iron County, WI (2000).

The aforementioned values were inputted into the Design Guide software, where applicable, and a total of 36 simulations were conducted. The simulations were run at varying layer thicknesses to their determine the effects on pavement distress for 4.0%, 7.0%, and 10.0% air voids, along with the asphalt binder content increase of 0.3% at 7.0% air voids. Figures 7.66 through 7.70 show the effects of changes in the HMA's layer thickness on permanent deformation, in the AC layer only and the entire pavement structure, as well as the effects on IRI, longitudinal cracking, and alligator cracking. The nomenclature used in the following figures shows the air void content as a number (4.0%, 7.0%, and 10.0%) followed by the asphalt binder content (optimum, "opt.," or +0.3% asphalt binder content, "bu."). The criterion stipulated in Table 7.1 is shown on each figure.

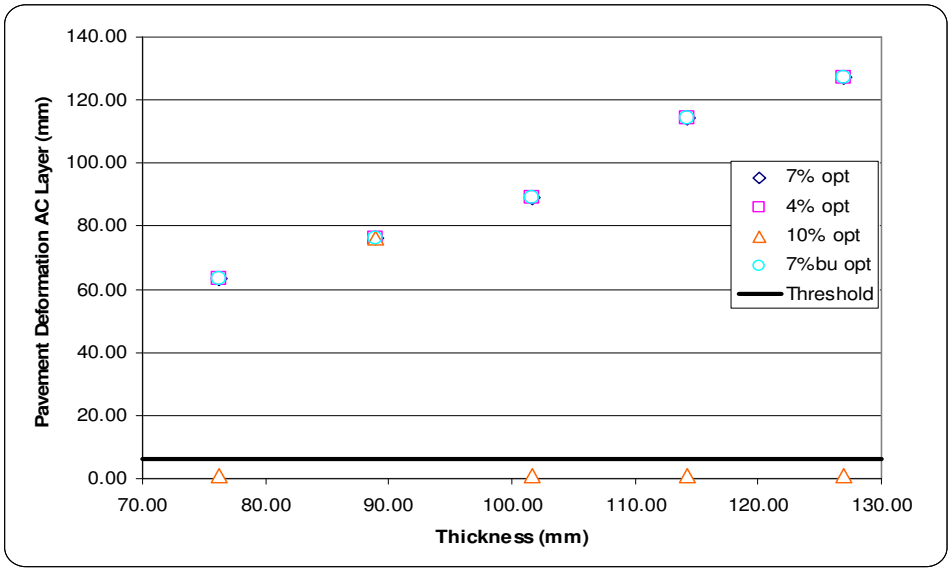

Figure 7.66. Hurley permanent deformation in AC layer

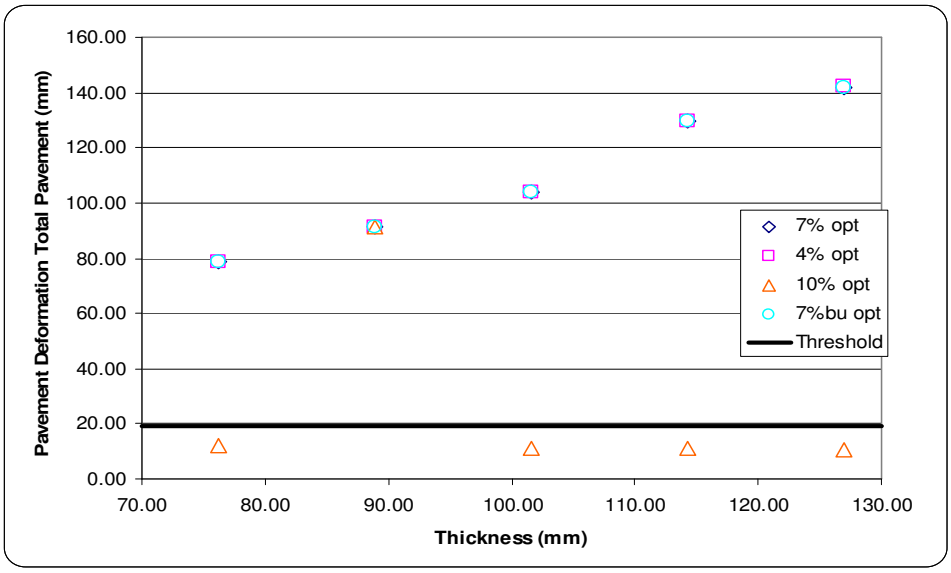

Figure 7.67. Hurley permanent deformation in total pavement

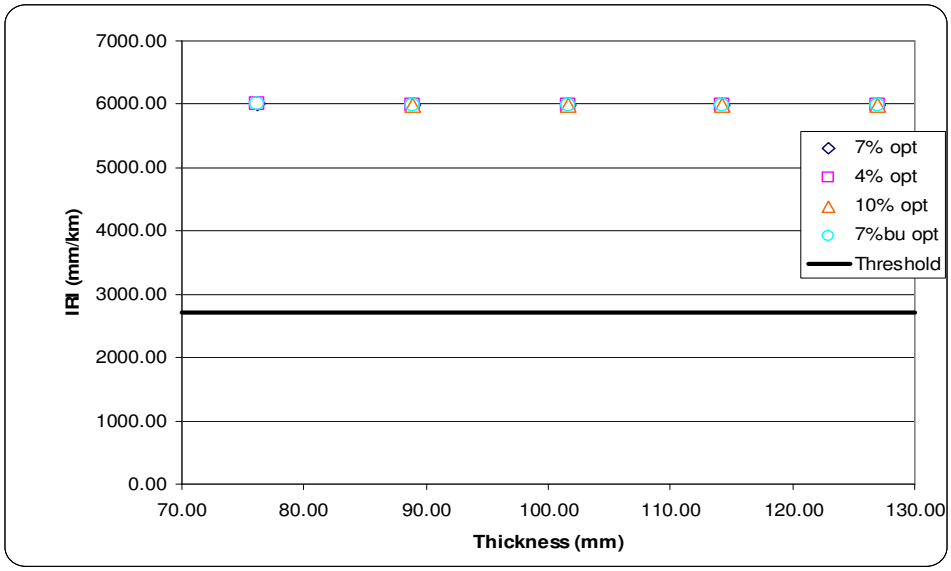

Figure 7.68. Hurley IRI

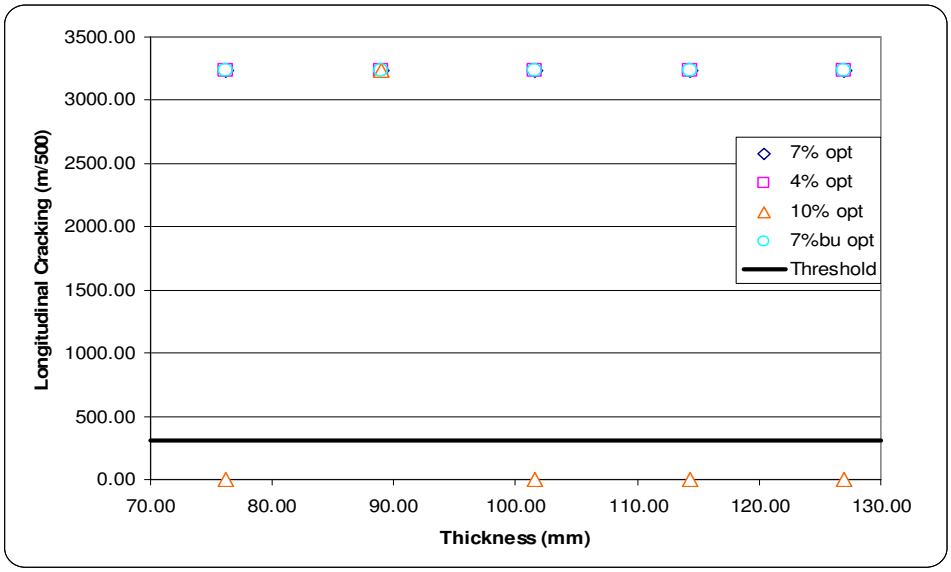

Figure 7.69. Hurley longitudinal cracking

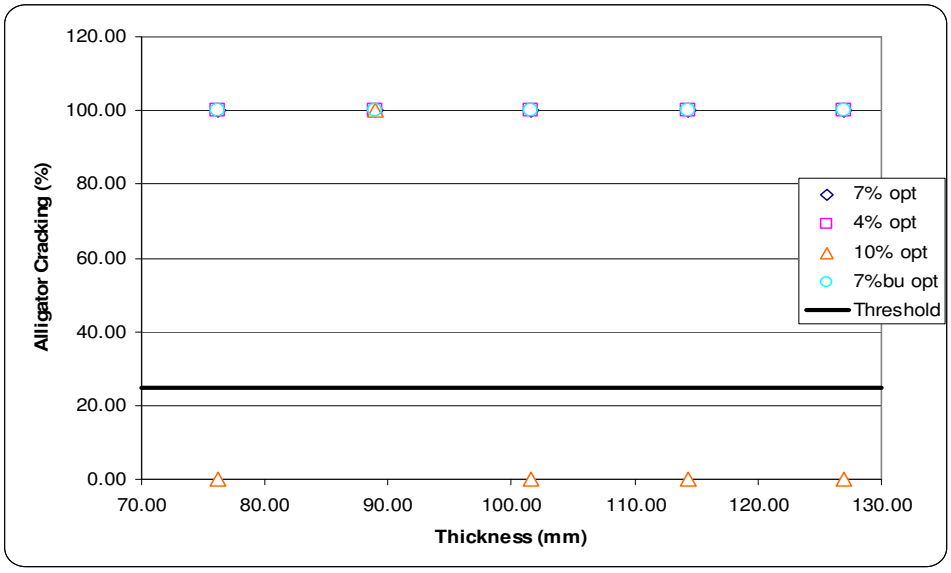

Figure 7.70. Hurley alligator cracking

The findings show that the high air voids (10.0%) had the best performing configuration in terms of all of the distresses considered at three out of the five simulations. In most instances, the high air void content (10.0%) pavement design expectedly resulted in the lowest predicted permanent deformation while the low air void content (4.0%) had the highest. Examining the permanent deformation was rather difficult, as most of the predictions fall near each other, indicating that the pavement is relatively insensitive to changes in air voids or asphalt content, except at the 10% air void levels.

Again, IRI appears to be insensitive to changes in the air void content, asphalt binder content, and the pavement thickness. The predicted pavement IRI is significantly greater than the performance criterion used in the Design Guide software of 2,715 mm/km.

Figures 7.69 and 7.70 indicate that the thicknesses examined may not be sufficient to mitigate longitudinal and alligator cracking, unless the pavement is compacted to 10% air voids and greater than 100 mm thick AC surface layer. The performance criterion used by the Design Guide software was 305 m/500 for longitudinal cracking and 25% for alligator cracking. Increasing the thickness would, in effect, decrease longitudinal cracking. By iteration, the pavement thickness would need to be at least 100 mm (3.75 in) thick to bring the pavement within the performance criteria for a pavement with 10.0% air voids at the optimum asphalt binder content.

7.1.15 Antigo

The Antigo E-10 12.5 pavement design consisted of 50.8 mm (2.0 in) of E-10 HMA on 101.6 mm (4.0 in) of a 19.0 mm E-10 on 355.6 to 457.2 mm (14 to 18 in) of crushed gravel on a subgrade of A-6 soil. The main composition of an A-6 soil is clay, under the AASHTO soil classification system. A level 1 analysis was used for both the 12.5 and 19.0 mm NMAS layers, utilizing the dynamic modulus test results shown in the previous chapter. A modulus value of 275.8 MPa (40 ksi) was used for the crushed gravel layer; this particular layer was divided into two identical 203.2 mm (8 in layers). The reason for this division was that previous simulations with the Design Guide software had problems handling the thick layers. A plasticity index of 1, with 10% passing the #200 sieve, 30% passing the #4 sieve, and a D60 of 2 mm were also used as inputs for the crushed gravel. The subgrade was reported to have a support value of 4.1 and, using the Design Guide software, yielded an analogous modulus value of 31.2 MPa (4.5 ksi); this layer was divided into a 152.4 mm (6 in) layer followed by an identical semi-infinite layer. A plasticity index of 3, with 60% passing the #200 sieve, 90% passing the #4 sieve, and a D60 of 0.05 mm were also used as inputs for the subgrade.

The traffic data, shown in Table 7.16, were supplied by WisDOT and show that this particular roadway is not expected to have a considerable amount of truck traffic.

Table 7.16. Traffic characteristics—Antigo E-10 12.5 and 19.0 mm

Traffic characteristic	
AADT (veh./day)	9,829.00
Growth (%)	1.37
Percentage of traffic greater than class 4	9.10
AADTT (trucks/day)	894.00
Truck traffic distribution	
2D (%)	2.80
3-SU (%)	1.10
2S-1 (%)	1.10
2S-2 (%)	1.10
3S-2 (%)	3.00
2-S1-2 (%)	0.00

A new climatic station had to be interpolated for the exact location of this project. A latitude of 44.79 degrees and a longitude of -89.01 degrees were used, along with an estimated elevation of 362.4 m (1189 ft) and an annual depth to the water table of 1.8 m (6 ft). The water table information was derived from the soil surveys from the United States Department of Agriculture for Langlade County, WI (2000).

The aforementioned values were inputted into the Design Guide software, where applicable, and a total of 36 simulations were conducted. The simulations were run at varying layer thicknesses to their determine the effects on pavement distress for 4.0%, 7.0%, and 10.0% air voids, along with the asphalt binder content increase of 0.3% at 7.0% air voids. Figures 7.71 through 7.75 show the effects of changes in the HMA's layer thickness on permanent deformation, in the AC layer only and the entire pavement structure, as well as the effects on IRI, longitudinal cracking, and alligator cracking. The nomenclature used in the following figures shows the air void content as a number (4.0%, 7.0%, and 10.0%) followed by the asphalt binder content (optimum, "opt.," or +0.3% asphalt binder content, "bu."). The criterion stipulated in Table 7.1 is shown on each figure.

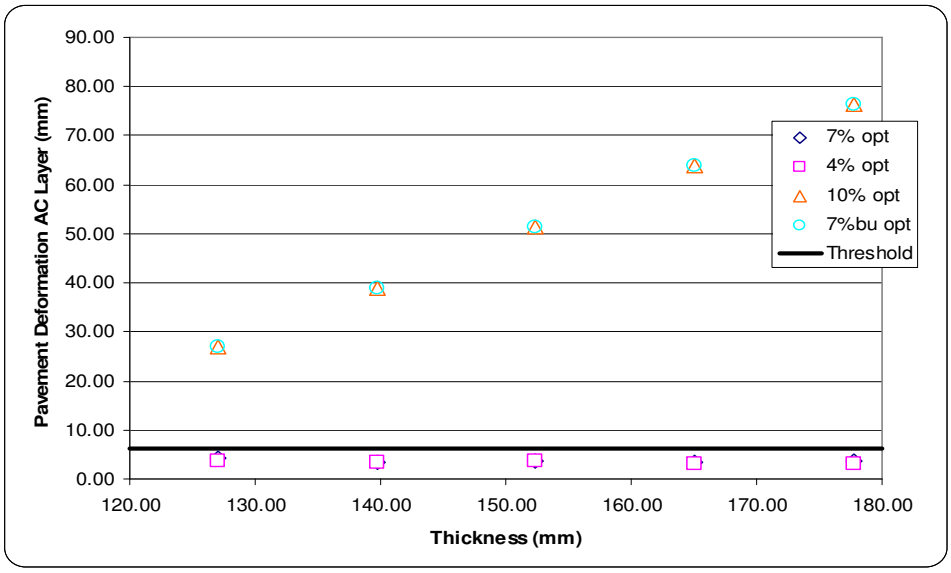

Figure 7.71. Antigo permanent deformation in AC layer

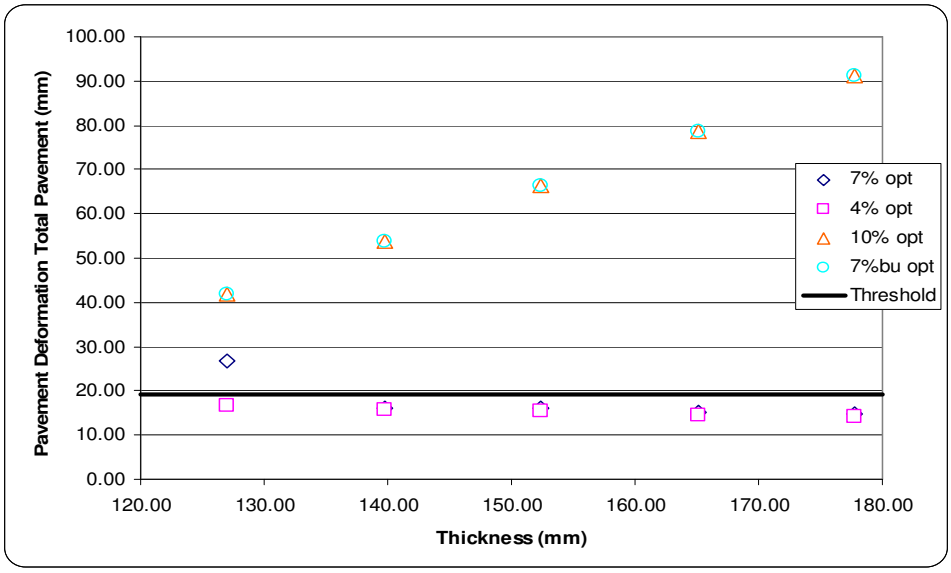

Figure 7.72. Antigo permanent deformation in total pavement

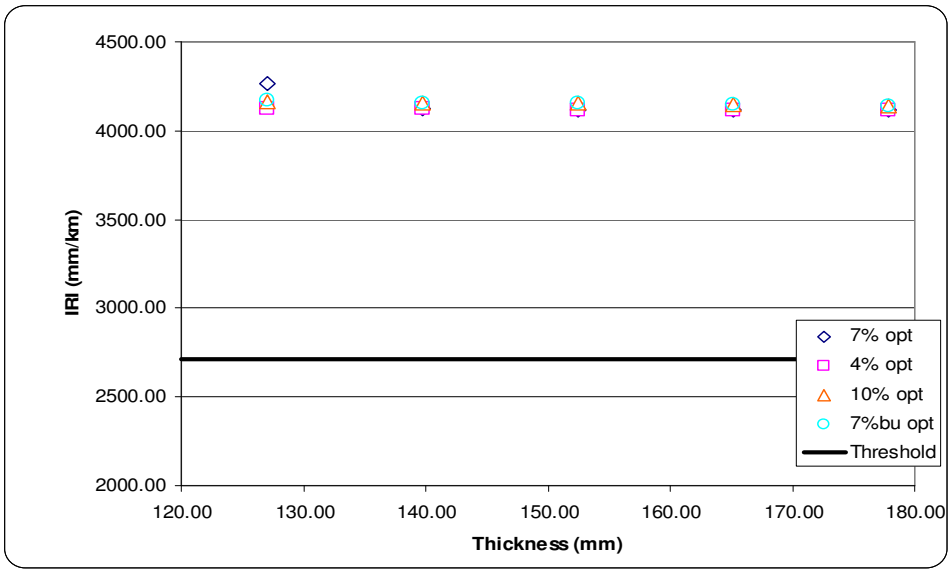

Figure 7.73. Antigo IRI

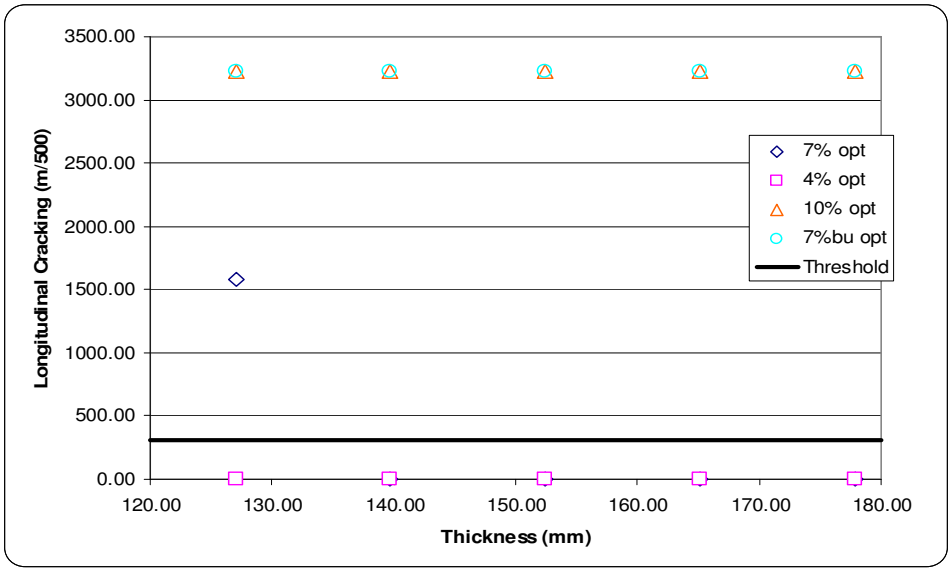

Figure 7.74. Antigo longitudinal cracking

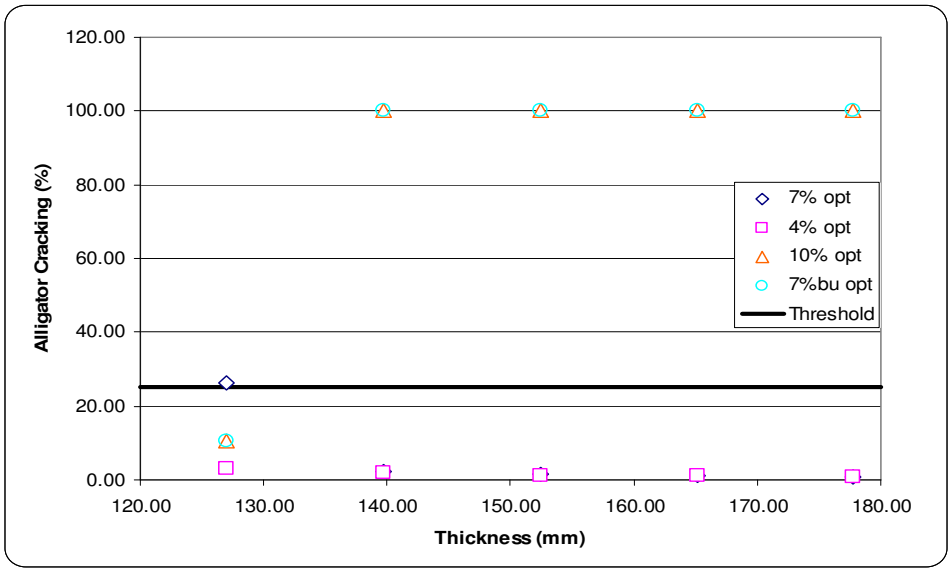

Figure 7.75. Antigo alligator cracking

The findings show that the low air voids (4.0%) and as-built air voids (7.0%) at optimum binder content had the best performing configuration in terms of all of the distresses considered. The respective predicted distress gets progressively worse as the air void content increases to 10.0% or at an air level of 7.0% and a binder bump. The pavement design with the optimum asphalt binder content had a higher predicted resistance to all of the distresses considered, in comparison to the pavement design with the asphalt content increase. In most instances, the high

air void content (10.0%) pavement design expectedly resulted in the highest predicted permanent deformation while the low air void content (4.0%) had the lowest.

Again, IRI appears to be insensitive to changes in the air void content, asphalt binder content, and the pavement thickness. The predicted pavement IRI is significantly greater than the performance criteria used in the Design Guide software of 2,715 mm/km.

Figure 7.74 and 7.75 indicates that the thicknesses examined may not be sufficient to mitigate longitudinal and alligator cracking unless the pavement is compacted to less than 4.0% air voids and 7.0% air voids at the optimum asphalt content. The performance criterion used by the Design Guide software was 305 m/500. Increasing the thickness would, in effect, decrease longitudinal cracking. By iteration, the pavement thickness would need to be at least 130 mm thick to bring the pavement within the performance criteria for a pavement with 4.0% and 7.0% air voids at the optimum asphalt binder content.

7.1.16 Northfield

The Northfield pavement is an extremely complex design structure and is not typical. The design consisted of 44.5 mm (1.75 in) of a 12.5 mm NMAS SMA on 57.2 mm (2.25 in) of 19.0 mm dense-graded HMA on 254.0 mm (10 in) of continuously reinforced concrete pavement (CRCP) on 25.4 mm (1.0 in) of HMA on 228.6 mm (9 in) of joint reinforced concrete pavement (JRCP) on an A-4 subgrade. The main composition of an A-4 soil is silt under the AASHTO soil classification system. The composition of this pavement made it difficult to analyze and, in fact, the Design Guide software was unable to process the pavement design as constructed. The difficulties with the pavement analysis were further compounded by the 19.0 mm mixture having a high dynamic modulus, which was found previously to cause problems with the software. Many approaches were developed in an attempt to tackle the problems that were occurring for this pavement and, in most instances, they failed. The final pavement structure that was used to simulate the aforementioned pavement consisted of the two as-is HMA layers on a 25.4 mm (1 in) high modulus subgrade on bedrock. The SMA layer was inputted as a level 1 design. A level 1 analysis was used for the 19.0 mm NMAS layer, utilizing the dynamic modulus results. The thin subgrade used a modulus 1724 MPa (200 ksi) with a plasticity index of 1, with 3% passing the #200 sieve, 20% passing the #4 sieve, and a D60 of 8 mm. It was realized that this subgrade would not exist, but was necessary in order to analyze the pavement and was meant to act as a

stiff layer, similar to concrete. The bedrock had a modulus of 5171 MPa (750 ksi), Poisson's ratio of 0.15, and unit weight of 22 kN/m^3 (140 pcf).

The traffic characteristics, shown in Table 7.17, were supplied by WisDOT and, as can be seen by the truck traffic distribution, this section constitutes a major trunk line.

Table 7.17. Traffic characteristics— Northfield E-30 19.0mm

Traffic characteristic	
AADT (veh./day)	11,550.00
Growth (%)	1.11
Percentage of traffic greater than class 4	38.10
AADTT (trucks/day)	4,401.00
Truck traffic distribution	
2D (%)	3.10
3-SU (%)	0.70
2S-1 (%)	1.20
2S-2 (%)	1.20
3S-2 (%)	29.10
2-S1-2 (%)	2.80

A new climatic station had to be interpolated for the exact location of this project. A latitude of 44.27 degrees and longitude of -91.20 degrees were used, along with an estimated elevation of 213.4 m (700 ft) and an annual depth to the water table of 1.829 m (6 ft). This information was derived from the soil survey made by the United States Department of Agriculture for Jackson County, WI (1990).

The aforementioned values were inputted into the Design Guide software, where applicable, and a total of 36 simulations were conducted. The simulations were run at varying layer thicknesses to their determine the effects on pavement distress for 4.0%, 7.0%, and 10.0% air voids along with the asphalt binder content increase of 0.3% at 7.0% air voids. Figures 7.76 through 7.80 show the effects of changes in the HMA's layer thickness on permanent deformation, in the AC layer only and the entire pavement structure, as well as the effects on IRI, longitudinal cracking, and alligator cracking. The nomenclature used in the following figures shows the air void content as a number (4.0%, 7.0%, and 10.0%) followed by the asphalt binder content (optimum, "Opt.," or +0.3% asphalt binder content, "bu."). The criterion stipulated in Table 7.1 is shown on each figure.

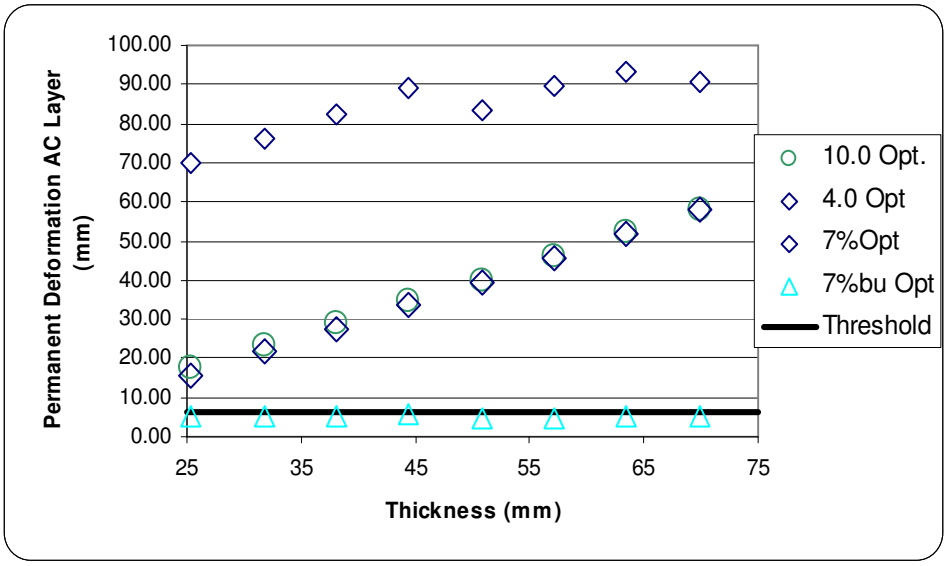

Figure 7.76. Northfield permanent deformation in AC layer

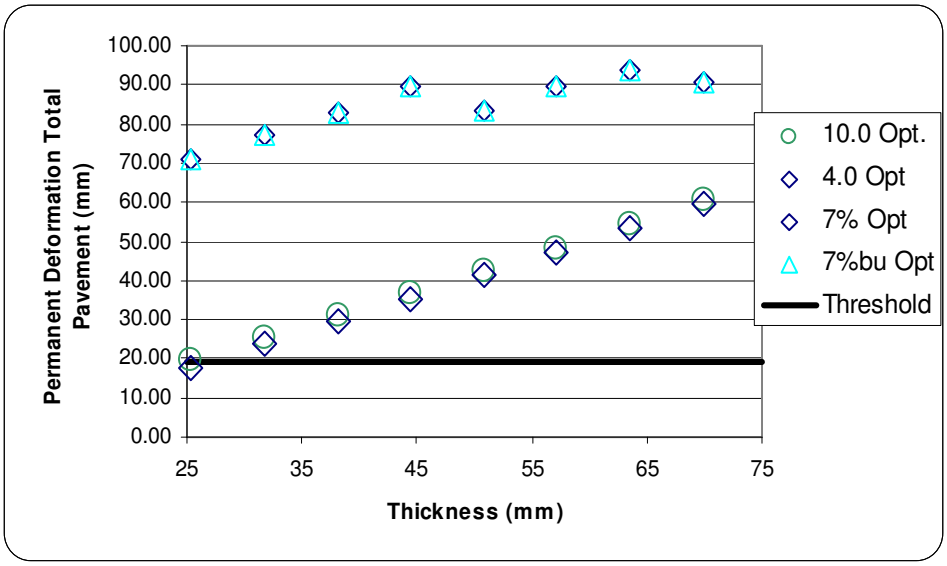

Figure 7.77. Northfield permanent deformation in total pavement

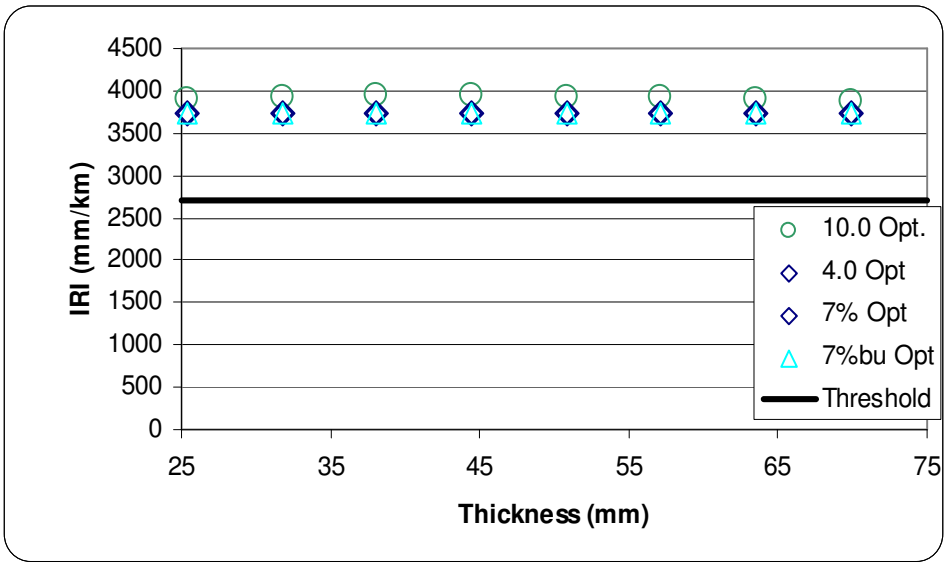

Figure 7.78. Northfield IRI

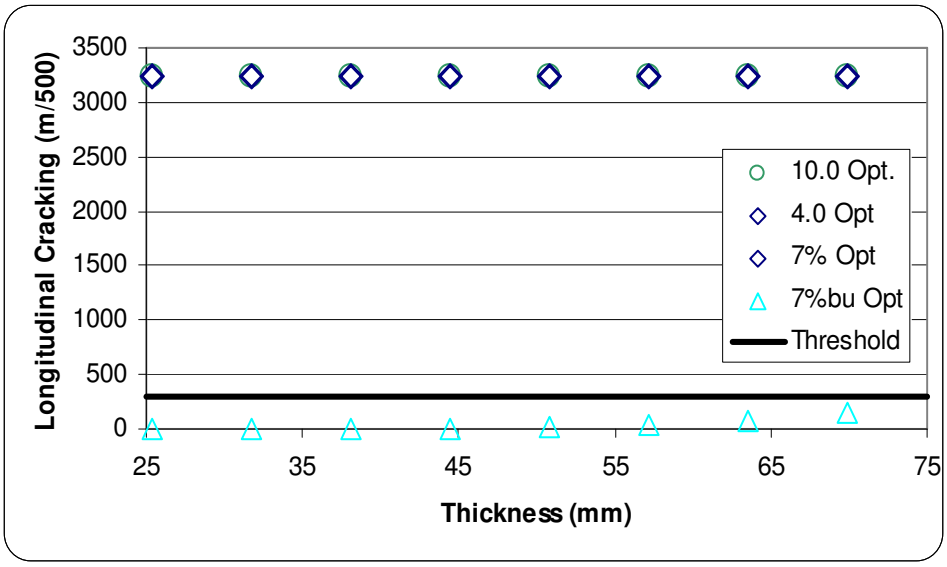

Figure 7.79. Northfield longitudinal cracking

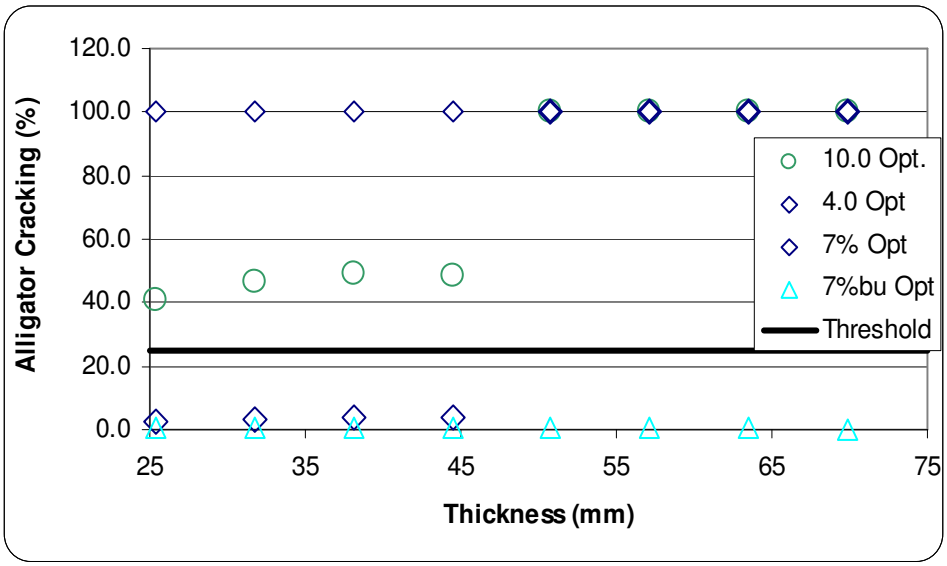

Figure 7.80. Northfield alligator cracking

There are several issues associated with the simulations for the Northfield project. First, the project has a very complicated pavement structure. It consists of a JRCP with a HMA layer on top, with a CRCP layer with an E30 mixture, with an SMA mixture on the surface. The simulations in Figures 7.76 to 7.80 are suspect because the proper pavement structure could not be inputted into the M-E PDG. The concrete layers had to be changed into a bedrock layer in order for the M-E PDG to work. Also, the dynamic modulus data for the SMA material are suspect because each specimen was compacted to 300 gyrations. It was impossible to compact samples to the target air voids. In addition, SMA mixtures are typically tested using a confining pressure. Any conclusions that can be drawn from the Northfield project will be left up to the reader of this document.

7.1.17 Wisconsin Rapids

The Wisconsin Rapids E-10 19.0 mm pavement design consisted of 152.4 mm (6.0 in) of HMA on 203.2 mm (8.0 in) of open-graded base course on 152.4 mm (6.0 in) of crushed aggregate base course on 304.8 to 457.2 mm (12 to 18-in) of granular subbase on a subgrade of A-4 soil. The main composition of an A-4 soil is silt, under the AASHTO soil classification system. A level 1 analysis was used for the 19.0 mm NMAS layer, utilizing the dynamic modulus test results shown in the previous chapter. A modulus value of 275.8 MPa (40 ksi) was

used for both the open-graded base course and crushed aggregate base course layers. A modulus value of 103.4 MPa (15 ksi) was used for the granular subbase layer; this particular layer was divided into two identical 190.5 mm (7.5 in layers). The reason for this division was that previous simulations with the Design Guide software had problems handling the thick layers. A plasticity index of 1, with 10% passing the #200 sieve, 30% passing the #4 sieve, and a D60 of 2 mm were also used as inputs for the open-graded base course and crushed gravel. The subgrade was reported to have a support value of 3.9 and, using the Design Guide software, yielded an analogous modulus value of 29.0 MPa (4.2 ksi); this layer was divided into a 152.4 mm (6 in) layer followed by an identical semi-infinite layer. A plasticity index of 3, with 60% passing the #200 sieve, 90% passing the #4 sieve, and a D60 of 0.05 mm were also used as inputs for the subgrade.

The traffic data, shown in Table 7.18, were supplied by WisDOT and show that this particular roadway is not expected to have a considerable amount of truck traffic.

Table 7.18. Traffic characteristics—Wisconsin Rapids E-10 19.0 mm

Traffic characteristic	
AADT (veh./day)	10,175.00
Growth (%)	2.00
Percentage of traffic greater than class 4	11.70
AADTT (trucks/day)	1,190.00
Truck traffic distribution	
2D (%)	2.90
3-SU (%)	2.30
2S-1 (%)	2.10
2S-2 (%)	2.10
3S-2 (%)	1.90
2-S1-2 (%)	0.40

A new climatic station had to be interpolated for the exact location of this project. A latitude of 44.22 degrees and a longitude of -89.50 degrees were used, along with an estimated elevation of 307.2 m (1008-ft) and an annual depth to the water table of 1.8 m (6 ft). The water table information was derived from the soil surveys from the United States Department of Agriculture for Marathon County, WI (2000).

The aforementioned values were inputted into the Design Guide software, where applicable, and a total of 36 simulations were conducted. The simulations were run at varying layer thicknesses to their determine the effects on pavement distress for 4.0%, 7.0%, and 10.0% air voids, along with the asphalt binder content increase of 0.3% at 7.0% air voids. Figures 7.81 through 7.85 show the effects of changes in the HMA's layer thickness on permanent deformation, in the AC layer only and the entire pavement structure, as well as the effects on IRI, longitudinal cracking, and alligator cracking. The nomenclature used in the following figures shows the air void content as a number (4.0%, 7.0%, and 10.0%) followed by the asphalt binder content (optimum, "opt.," or +0.3% asphalt binder content, "bu."). The criterion stipulated in Table 7.1 is shown on each figure.

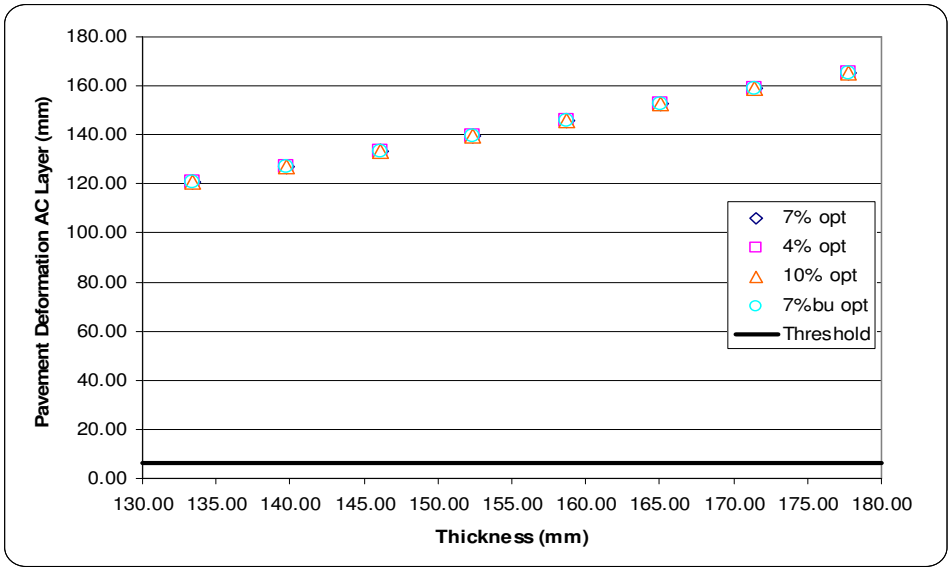

Figure 7.81. Wisconsin Rapids permanent deformation in AC layer

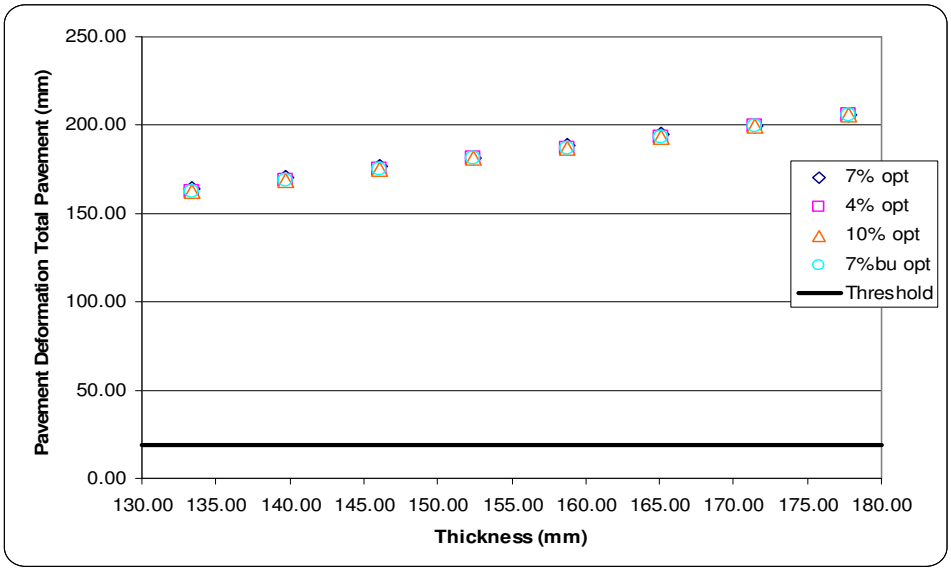

Figure 7.82. Wisconsin Rapids permanent deformation in total pavement

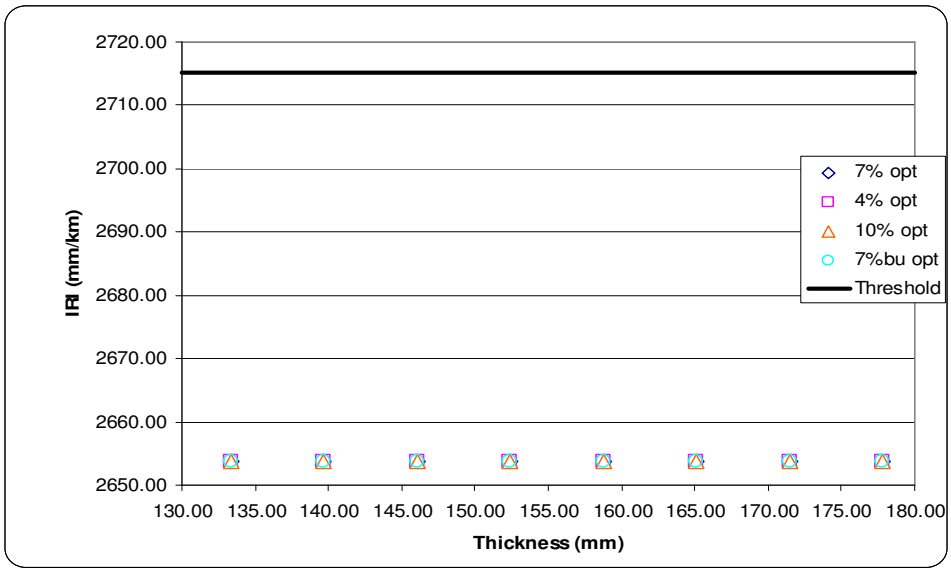

Figure 7.83. Wisconsin Rapids IRI

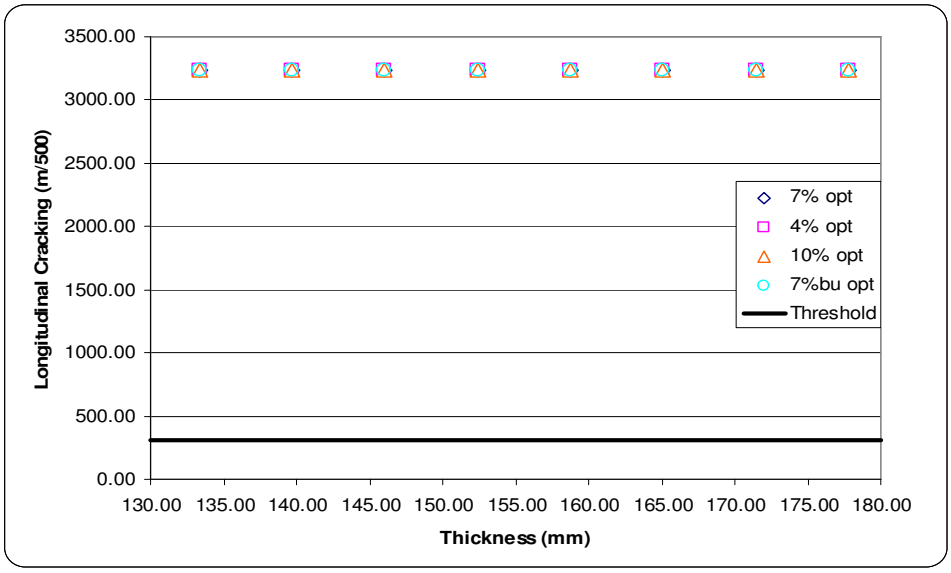

Figure 7.84. Wisconsin Rapids longitudinal cracking

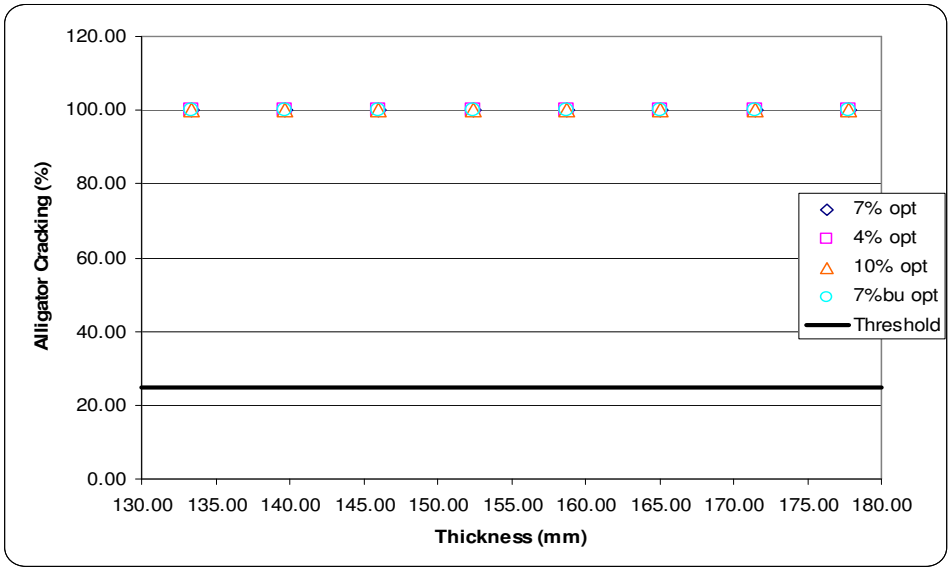

Figure 7.85. Wisconsin Rapids alligator cracking

The findings show that all four cases had the best performing configuration in terms of all of the distresses considered. The M-E PDG criteria were exceeded in all distress types, except for IRI. For surface permanent deformation and total permanent deformation, as thickness increases, permanent deformation increases. It was also noted that the predicted permanent deformation in Figures 7.81 and 7.82 is unrealistic.

7.1.18 Plymouth

The Plymouth E-10 12.5 mm pavement design consisted of 63.5 mm (2.5 in) of HMA on 127.0 mm (5 in) of existing HMA on 330.2 mm (13 in) of crushed gravel on a subgrade of A-4 soil. The main composition of an A-4 soil is silt, under the AASHTO soil classification system. A level 1 analysis was used for the 12.5 mm NMAS layer , utilizing the dynamic modulus test results shown in the previous chapter. A level 3 analysis was used for the existing HMA layer, which utilizes gradation and volumetric properties of the in-service HMA pavement. A modulus value of 275.8 MPa (40 ksi) was used for the crushed gravel layer; this particular layer was divided into two identical 165.1 mm (6.5 in layers). The reason for this division was that previous simulations with the Design Guide software had problems handling the thick layers. A plasticity index of 1, with 10% passing the #200 sieve, 30% passing the #4 sieve, and a D60 of 2 mm were also used as inputs for the crushed gravel. The subgrade was reported to have a support value of 4.25 and, using the Design Guide software, yielded an analogous modulus value of 33.0 MPa (4.7 ksi); this layer was divided into a 152.4 mm (6 in) layer followed by an identical semi-infinite layer. A plasticity index of 3, with 60% passing the #200 sieve, 90% passing the #4 sieve, and a D60 of 0.05 mm were also used as inputs for the subgrade.

The traffic data, shown in Table 7.19, were supplied by WisDOT and show that this particular roadway is not expected to have a considerable amount of truck traffic.

Table 7.19. Traffic characteristics—Plymouth E-10 12.5 mm

Traffic characteristic	
AADT (veh./day)	9,800.00
Growth (%)	1.51
Percentage of traffic greater than class 4	20.10
AADTT (trucks/day)	1,970.00
Truck traffic distribution	
2D (%)	2.90
3-SU (%)	4.50
2S-1 (%)	2.00
2S-2 (%)	2.00
3S-2 (%)	8.30
2-S1-2 (%)	0.40

A new climatic station had to be interpolated for the exact location of this project. A latitude of 43.45 degrees and a longitude of -87.58 degrees were used, along with an estimated elevation of 261.2 m (857 ft) and an annual depth to the water table of 0.91 m (3 ft). The water table information was derived from the soil surveys from the United States Department of Agriculture for Sheboygan County, WI (2000).

The aforementioned values were inputted into the Design Guide software, where applicable, and a total of 36 simulations were conducted. The simulations were run at varying layer thicknesses to their determine the effects on pavement distress for 4.0%, 7.0%, and 10.0% air voids, along with the asphalt binder content increase of 0.3% at 7.0% air voids. Figures 7.86 through 7.90 show the effects of changes in the HMA's layer thickness on permanent deformation, in the AC layer only and the entire pavement structure, as well as the effects on IRI, longitudinal cracking, and alligator cracking. The nomenclature used in the following figures shows the air void content as a number (4.0%, 7.0%, and 10.0%) followed by the asphalt binder content (optimum, "opt.," or +0.3% asphalt binder content, "bu."). The criterion stipulated in Table 7.1 is shown on each figure.

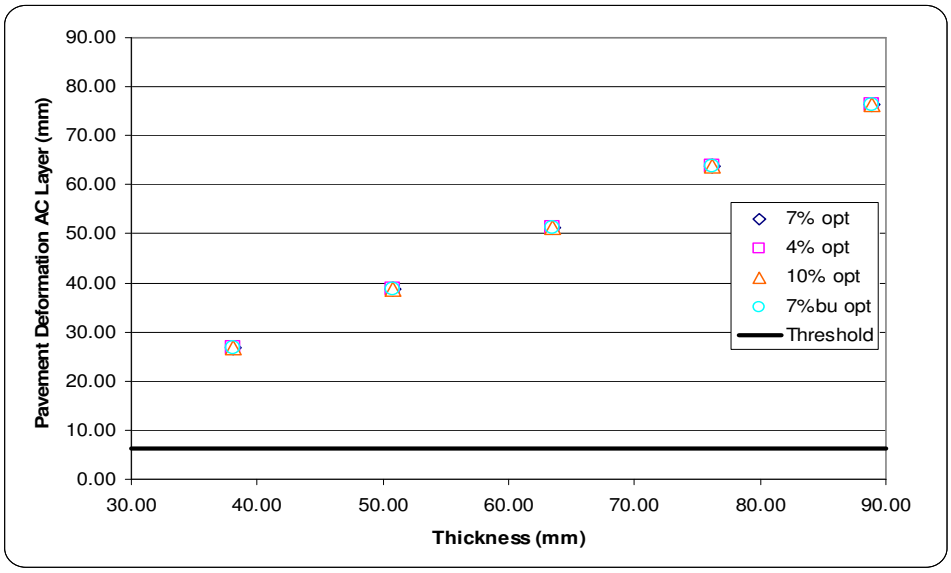

Figure 7.86. Plymouth permanent deformation in AC layer

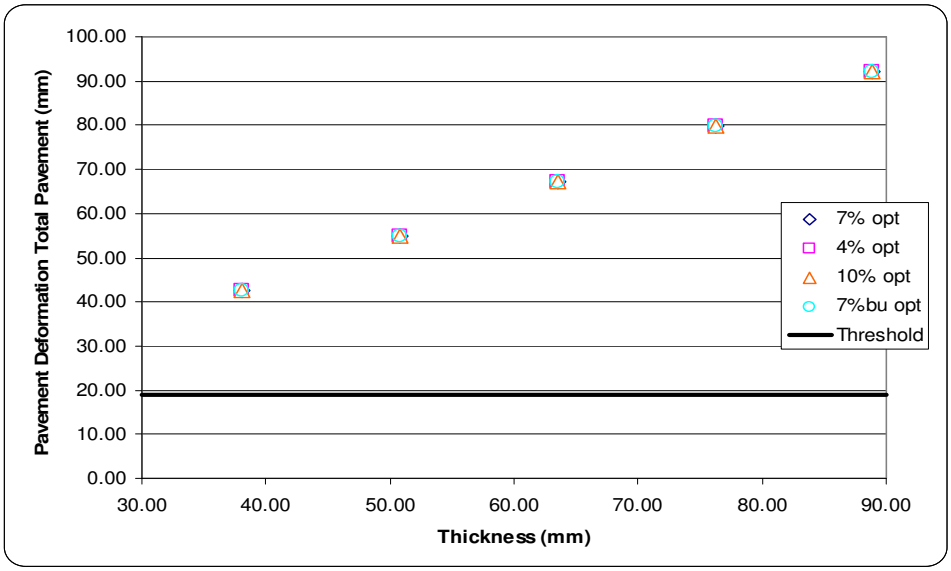

Figure 7.87. Plymouth permanent deformation in total pavement

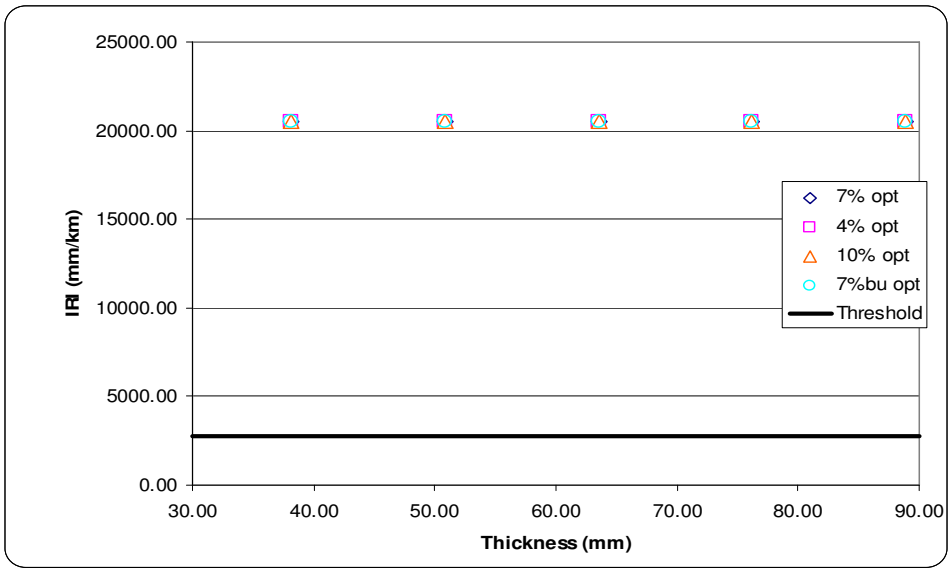

Figure 7.88. Plymouth IRI

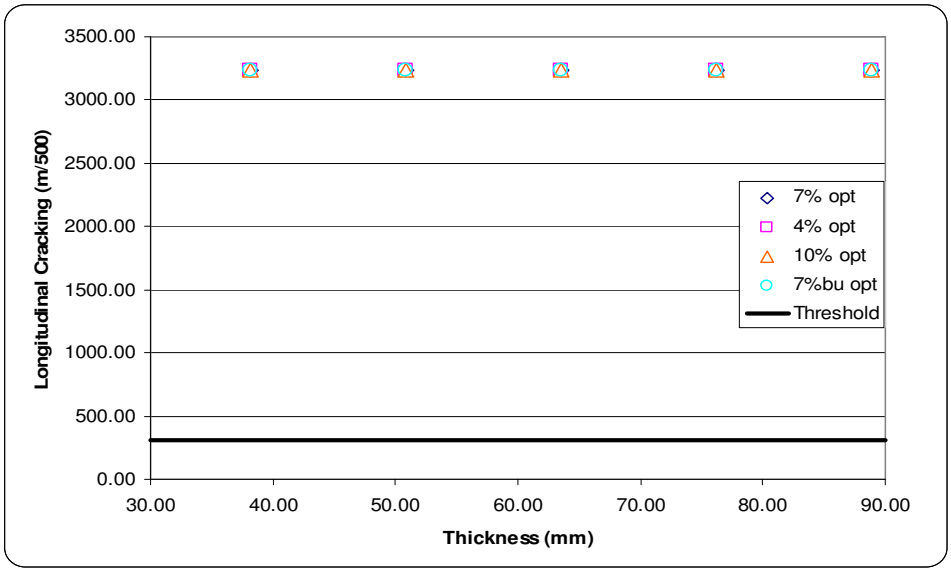

Figure 7.89. Plymouth longitudinal cracking

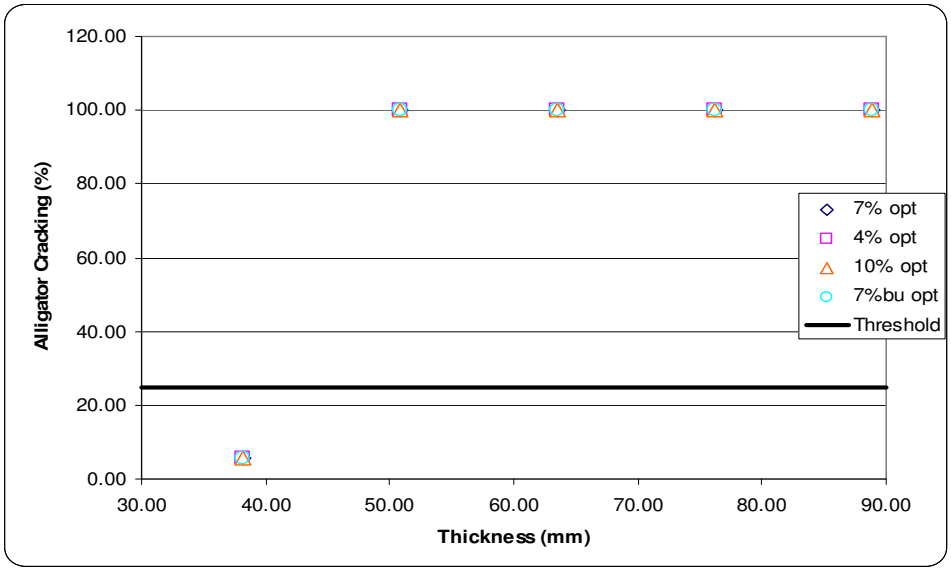

Figure 7.90. Plymouth alligator cracking

The findings show that all four cases had the best performing configuration in terms of all of the distresses considered. The M-E PDG criteria were exceeded in all distress types, except for IRI. For surface permanent deformation and total permanent deformation, as thickness increases, permanent deformation increases. It was also noted that the predicted permanent deformation in Figures 7.86 and 7.87 is unrealistic.

7.1.19 Racine

The Racine E-10 12.5 mm pavement design consisted of 76.2 mm (3.0 in) of HMA on a subgrade of A-4 soil. The main composition of an A-4 soil is silt, under the AASHTO soil classification system. A level 1 analysis was used for the 12.5 mm NMAS layer, utilizing the dynamic modulus test results shown in the previous chapter. The subgrade was reported to have a support value of 3.7 and, using the Design Guide software, yielded an analogous modulus value of 26.9 MPa (3.9 ksi); this layer was divided into a 152.4 mm (6 in) layer followed by an identical semi-infinite layer. A plasticity index of 3, with 60% passing the #200 sieve, 90% passing the #4 sieve, and a D60 of 0.05 mm were also used as inputs for the subgrade.

The traffic data, shown in Table 7.20, were supplied by WisDOT and show that this particular roadway is not expected to have a considerable amount of truck traffic.

Table 7.20. Traffic characteristics—Bloomville E-1 19.0 mm

Traffic characteristic	
AADT (veh./day)	10,000.00
Growth (%)	1.49
Percentage of traffic greater than class 4	13.00
AADTT (trucks/day)	1,300.00
Truck traffic distribution	
2D (%)	1.10
3-SU (%)	0.20
2S-1 (%)	0.40
2S-2 (%)	0.40
3S-2 (%)	9.90
2-S1-2 (%)	1.00

A new climatic station had to be interpolated for the exact location of this project. A latitude of 44.43 degrees and a longitude of -87.47 degrees were used, along with an estimated elevation of 269.7 m (885 ft) and an annual depth to the water table of 1.2 m (4 ft). The water table information was derived from the soil surveys from the United States Department of Agriculture for Kenosha County, WI (2000).

The aforementioned values were inputted into the Design Guide software, where applicable, and a total of 36 simulations were conducted. The simulations were run at varying layer thicknesses to their determine the effects on pavement distress for 4.0%, 7.0%, and 10.0% air voids, along with the asphalt binder content increase of 0.3% at 7.0% air voids. Figures 7.91 through 7.95 show the effects of changes in the HMA's layer thickness on permanent deformation, in the AC layer only and the entire pavement structure, as well as the effects on IRI, longitudinal cracking, and alligator cracking. The nomenclature used in the following figures shows the air void content as a number (4.0%, 7.0%, and 10.0%) followed by the asphalt binder content (optimum, "opt.," or +0.3% asphalt binder content, "bu."). The criterion stipulated in Table 7.1 is shown on each figure.

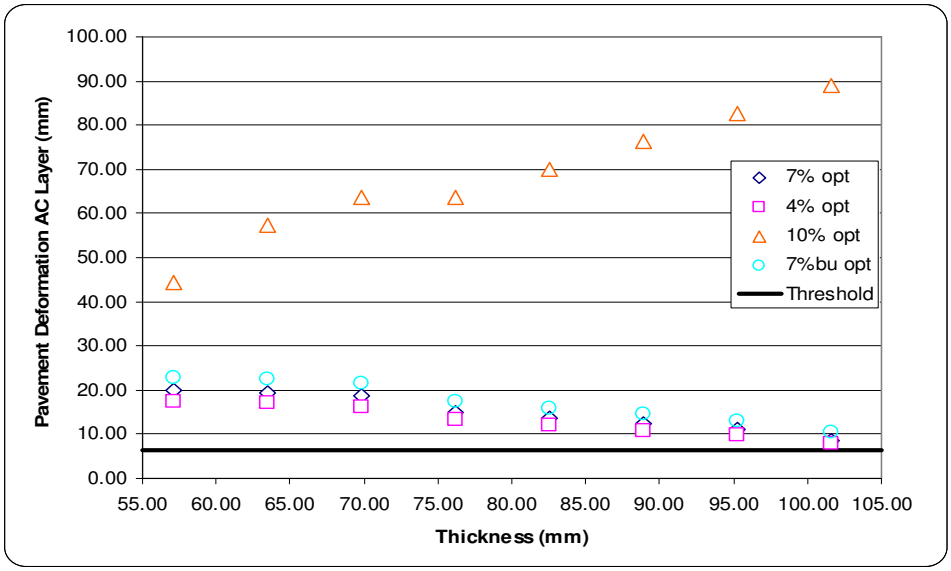

Figure 7.91. Racine permanent deformation in AC layer

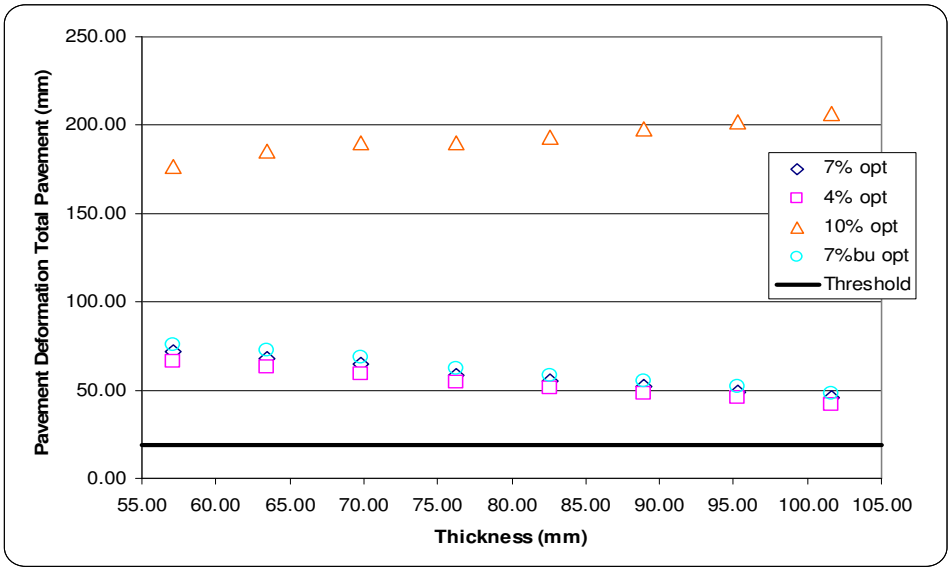

Figure 7.92. Racine permanent deformation in total pavement

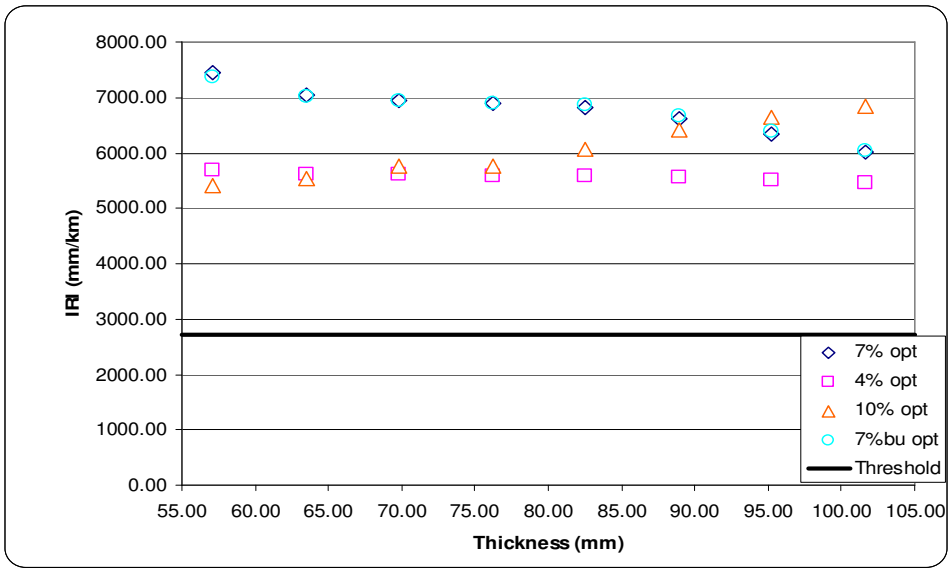

Figure 7.93. Racine IRI

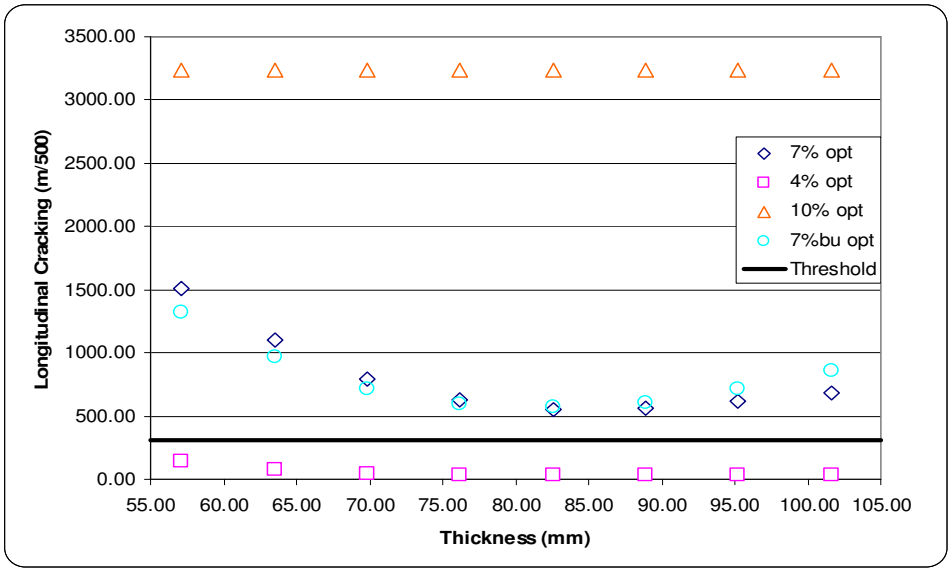

Figure 7.94. Racine longitudinal cracking

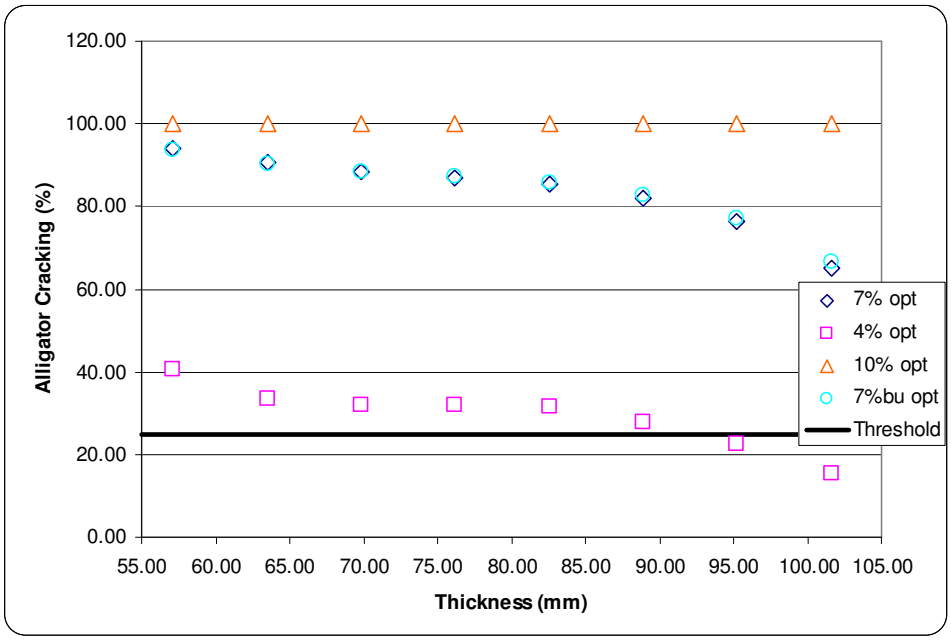

Figure 7.95. Racine alligator cracking

The findings show that the low air voids (4.0%) had the best performing configuration in terms of all of the distresses considered. The respective predicted distress gets progressively worse as the air void content increases. The pavement design with the asphalt binder content

increase had a higher predicted resistance to all of the distresses considered, in comparison to the pavement design with the optimum asphalt content.

In most instances the high air void content (10.0%) pavement design expectedly resulted in the highest predicted permanent deformation, while the low air void content (4.0%) had the lowest. Examining the permanent deformation was rather difficult, as most of the predictions fall near each other, indicating that the pavement is relatively insensitive to changes in air voids or asphalt content.

For this mixture, IRI appears to be sensitive to changes in the air void content, asphalt binder content, and pavement thickness. The predicted pavement IRI is significantly greater than the performance criterion used in the Design Guide software of 2,715 mm/km.

Figures 7.94 and 7.95 indicate that the thicknesses examined may not be sufficient to mitigate longitudinal and alligator cracking, unless the pavement is compacted to less than 4% air voids and the thickness is greater than 10 2mm. The performance criteria used by the Design Guide software was 305 m/500. Increasing the thickness would, in effect, decrease longitudinal cracking. By iteration, the pavement thickness would need to be at least 102 mm to bring the pavement within the performance criteria for a pavement with 4.0% air voids at the optimum asphalt binder content.

7.1.20 WisPave Results

The WisPave software, which uses the 1972 AASHTO design guide, was used for comparison with the forthcoming AASHTO M-E pavement Design Guide. Figure 7.96 shows the as-built structural numbers versus the required structural numbers. In many cases, the as-built or design and bid structural number exceeds the required structural number.

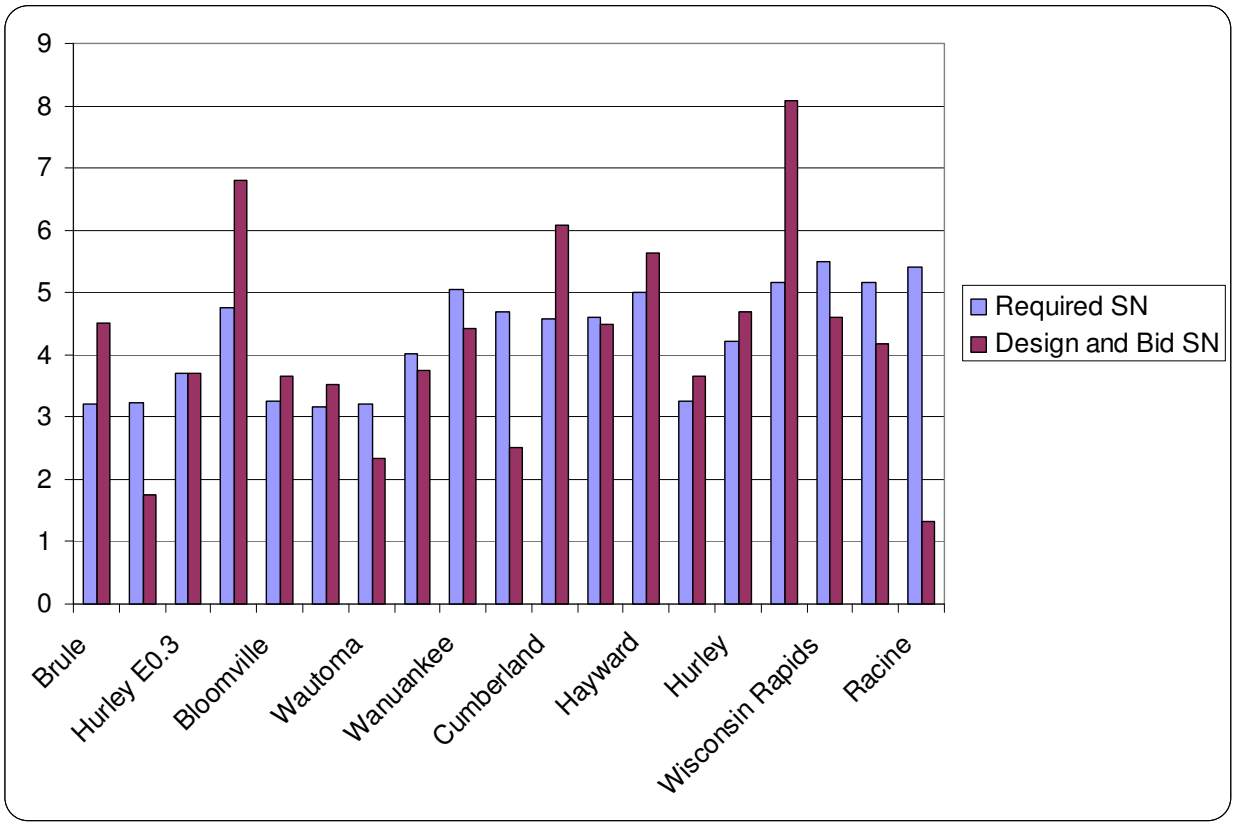

Figure 7.96. WisPave results for required and as builts

7.1.21 Comparison of M-E PDG versus WisPave

The results of both analyses using both M-E PDG and WisPave for the designed and bid structural numbers corresponding with pavement thickness are summarized in Tables 7.21 through 7.24; the shaded cells highlight the design sections that did not achieve the performance criteria as shown in the tables. The following can be concluded when comparing the results of both programs:

- Of the 19 projects analyzed, nine did not meet the WisPave performance criteria. These nine projects are the same, regardless of variation in the percent air voids or the asphalt content.
- At 7% air voids and optimum asphalt content, eight projects did not meet performance expectations under the M-E PDG out of the 19 projects analyzed. Five

of these eight projects were predicted to not achieve WisPave performance criteria, while the remaining three were not.

- At 4% air voids and optimum asphalt content, 13 projects did not achieve the M-E PDG performance criteria out of the 19 projects analyzed. Seven of these 13 projects were predicted to not meet WisPave performance expectations, while the remaining six were not.
- At 10% air voids and optimum asphalt content, 12 projects did not achieve performance expectations under the M-E PDG out of the 19 projects analyzed. Eight of these 12 projects were predicted to not achieve WisPave performance expectations, while the remaining four were not.
- At 7% air voids and adding 0.3%AC to the optimum asphalt content, eleven projects did not achieve performance expectations under the M-E PDG out of the 19 projects analyzed. Seven of these eleven projects were predicted to not achieve performance expectations using WisPave, while the remaining four were not.

Table 7.21. As-built design using 7% air voids at optimum AC using Level 1 design

Project	New HMA Thickness	MEPDG				WisPave	
		AC Surface Down Cracking (Long. Cracking) (ft/500):	AC Bottom Up Cracking (Alligator Cracking) (%):	Permanent Deformation (AC Only) (in):	Permanent Deformation (Total Pavement) (in):	Required SN	Designed & Bid SN
Brule	4"	0	0.1	0.04	0.62	3.22	4.52
Baraboo	4"	26.8	2.7	0.09	0.73	**3.23**	**1.76**
Hurley E0.3	1.75"	0	0.1	0.05	0.73	3.71	3.70
Cascade	6.25"	26.2	2.6	0.23	0.69	4.76	6.81
Bloomville	4.5"	5	1.7	0.07	0.58	3.26	3.66
Medford	3.5"	0	0.1	0.03	0.54	3.16	3.52
Wautoma	2.75"	6	0.5	0.06	0.45	**3.2**	**2.34**
Tomahawk	8.5	0	0	0.02	0.53	**4.01**	**3.74**
Wanuankee	6.25"	0.1	2.3	0.11	**1.03**	**5.04**	**4.43**
Mosinee	1.75"	9.2	3	0.11	**0.83**	**4.68**	**2.52**
Cumberland	7"	0	0.6	0.06	0.66	4.58	6.09
Antigo	2" E10 12.5mm 4" E10 19.0 mm	5.9	1.4	0.15	0.63	**4.59**	**4.48**
Hayward	5"	1.6	3.2	0.15	**0.91**	5.01	5.63
Wausau	4.5"	14.6	4.7	0.15	0.75	3.26	3.66
Hurley	4"	**10600**	**100**	**3.50**	**4.10**	4.22	4.69
Northfield	1.75" SMA 2.25" E30	**10600**	**100**	**3.50**	**3.52**	5.16	8.08
Wisconsin Rapids	6"	**10600**	**100**	**5.50**	**7.13**	**5.5**	**4.6**
Plymouth	2.5"	**10600**	**100**	**2.02**	**2.64**	**5.17**	**4.17**
Racine	3"	**2050**	**86.9**	**0.58**	**2.30**	**5.4**	**1.32**
Criteria	**N/A**	**1000**	**25**	**0.25**	**0.75**	**Designed & Bid SN>Required SN**	

Table 7.22. As-built design using 4% air voids at optimum AC using Level 1 design

Project	New HMA Thickness	MEPDG				WisPave	
		AC Surface Down Cracking (Long. Cracking) (ft/500):	AC Bottom Up Cracking (Alligator Cracking) (%):	Permanent Deformation (AC Only) (in):	Permanent Deformation (Total Pavement) (in):	Required SN	Designed & Bid SN
Brule	4"	0	0	0.03	0.60	3.22	4.52
Baraboo	4"	2.7	0.4	0.07	0.69	**3.23**	**1.76**
Hurley E0.3	1.75"	0	0.1	0.05	0.73	3.71	3.70
Cascade	6.25"	**10600**	**100**	**1.81**	**2.36**	4.76	6.81
Bloomville	4.5"	**10600**	**100**	**4.00**	**4.87**	3.26	3.66
Medford	3.5"	0	0.1	0.02	0.53	3.16	3.52
Wautoma	2.75"	**10600**	**100**	**2.25**	**2.77**	**3.2**	**2.34**
Tomahawk	8.5	**10600**	**100**	**8.00**	**10.35**	**4.01**	**3.74**
Wanuankee	6.25"	**10600**	**100**	**5.75**	**7.56**	**5.04**	**4.43**
Mosinee	1.75"	0.2	0.5	0.09	**0.77**	**4.68**	**2.52**
Cumberland	7"	**10600**	**100**	**6.50**	**7.71**	4.58	6.09
Antigo	2" E10 12.5mm 4" E10 19.0 mm	1.1	1.3	0.14	0.61	**4.59**	**4.48**
Hayward	5"	0.1	0.5	0.13	**0.86**	5.01	5.63
Wausau	4.5"	2.4	1.1	0.12	0.72	3.26	3.66
Hurley	4"	**10600**	**100**	**3.50**	**4.10**	4.22	4.69
Northfield	1.75" SMA 2.25" E30	**10600**	4	**1.32**	**1.39**	5.16	8.08
Wisconsin Rapids	6"	**10600**	**100**	**5.50**	**7.13**	**5.5**	**4.6**
Plymouth	2.5"	**10600**	**100**	**2.02**	**2.64**	**5.17**	**4.17**
Racine	3"	115	**32.1**	**0.52**	**2.13**	**5.4**	**1.32**
Criteria	**N/A**	**1000**	**25**	**0.25**	**0.75**	**Designed & Bid SN>Required SN**	

Table 7.23. As-built design using 10% air voids at optimum AC using Level 1 design

Project	New HMA Thickness	MEPDG				WisPave	
		AC Surface Down Cracking (Long. Cracking) (ft/500):	AC Bottom Up Cracking (Alligator Cracking) (%):	Permanent Deformation (AC Only) (in):	Permanent Deformation (Total Pavement) (in):	Required SN	Designed & Bid SN
Brule	4"	0	0.2	0.05	0.62	3.22	4.52
Baraboo	4"	169	11.1	0.11	**0.79**	**3.23**	**1.76**
Hurley E0.3	1.75"	0	0.1	0.06	0.75	3.71	3.70
Cascade	6.25"	335	3	0.27	0.74	4.76	6.81
Bloomville	4.5"	**10600**	**100**	**4.00**	**4.87**	3.26	3.66
Medford	3.5"	0.1	0.1	0.04	0.57	3.16	3.52
Wautoma	2.75"	113	1.3	0.08	0.50	**3.2**	**2.34**
Tomahawk	8.5	**10600**	**100**	**8.00**	**10.35**	**4.01**	**3.74**
Wanuankee	6.25"	1.6	8.5	0.15	**1.13**	**5.04**	**4.43**
Mosinee	1.75"	116	7.8	0.13	**0.87**	**4.68**	**2.52**
Cumberland	7"	0.4	2	0.09	0.70	4.58	6.09
Antigo	2" E10 12.5mm 4" E10 19.0 mm	**10600**	**100**	**2.02**	**2.61**	**4.59**	**4.48**
Hayward	5"	4.2	7.6	0.25	**1.02**	5.01	5.63
Wausau	4.5"	53.5	11.3	0.15	**0.77**	3.26	3.66
Hurley	4"	0	0	0.03	0.44	4.22	4.69
Northfield	1.75" SMA 2.25" E30	**10600**	**48.6**	**1.36**	**1.45**	5.16	8.08
Wisconsin Rapids	6"	**10600**	**100**	**5.50**	**7.13**	**5.5**	**4.6**
Plymouth	2.5"	**10600**	**100**	**2.02**	**2.64**	**5.17**	**4.17**
Racine	3"	**10600**	**100**	**2.50**	**7.47**	**5.4**	**1.32**
Criteria	**N/A**	**1000**	**25**	**0.25**	**0.75**	**Designed & Bid SN>Required SN**	

Table 7.24. As-built design using 7% air voids at 0.3% plus optimum AC using Level 1 design

Project	New HMA Thickness	MEPDG				WisPave	
		AC Surface Down Cracking (Long. Cracking) (ft/500):	AC Bottom Up Cracking (Alligator Cracking) (%):	Permanent Deformation (AC Only) (in):	Permanent Deformation (Total Pavement) (in):	Required SN	Designed & Bid SN
Brule	4"	0	0	0.04	0.60	3.22	4.52
Baraboo	4"	9.3	0.2	0.05	0.58	**3.23**	**1.76**
Hurley E0.3	1.75"	0	0.1	0.06	0.74	3.71	3.70
Cascade	6.25"	28.6	2.7	**0.27**	**0.73**	4.76	6.81
Bloomville	4.5"	2.4	1	0.07	0.57	3.26	3.66
Medford	3.5"	0	0.1	0.03	0.55	3.16	3.52
Wautoma	2.75"	6.6	0.4	0.06	0.47	**3.2**	**2.34**
Tomahawk	8.5	**10600**	**100**	**8.00**	**10.35**	**4.01**	**3.74**
Wanuankee	6.25"	0.1	2	0.12	**1.07**	**5.04**	**4.43**
Mosinee	1.75"	11.4	2.6	0.12	**0.84**	**4.68**	**2.52**
Cumberland	7"	0.1	0.6	0.08	0.71	4.58	6.09
Antigo	2" E10 12.5mm 4" E10 19.0 mm	**10600**	**100**	**2.02**	**2.61**	**4.59**	**4.48**
Hayward	5"	1.9	3.4	0.22	**1.00**	5.01	5.63
Wausau	4.5"	22.5	5.6	0.17	**0.80**	3.26	3.66
Hurley	4"	**10600**	**100**	**3.50**	**4.10**	4.22	4.69
Northfield	1.75" SMA 2.25" E30	21.2	0.8	0.22	0.27	5.16	8.08
Wisconsin Rapids	6"	**10600**	**100**	**5.50**	**7.13**	**5.5**	**4.6**
Plymouth	2.5"	**10600**	**100**	**2.02**	**2.64**	**5.17**	**4.17**
Racine	3"	**1960**	**87.1**	**0.68**	**2.45**	**5.4**	**1.32**
Criteria	**N/A**	**1000**	**25**	**0.25**	**0.75**	**Designed & Bid SN>Required SN**	

CHAPTER 8. CONCLUSIONS

The mechanistic-empirical pavement design procedure has been developed to the point where it is ready for understanding and verification by outside researchers prior to implementation by owners/agencies. The work outlined in this report has formed a basis that WisDOT will use to evaluate the newly-developed design approach.

The objectives of this project were to examine hot mix asphalt mixtures that are typically used in the state of Wisconsin in terms of traffic level, gradation, and nominal maximum aggregate size. Additionally, volumetric properties of the pavement were considered (air voids and asphalt content).

The HMA that was sampled from Wisconsin was split and compacted to the project parameters, and three specimens were sawed/cored to the testing geometries for each factor considered. The same specimen was tested throughout the testing sequence for both intermediate and high temperature dynamic modulus and flow number. The conclusions of the results reported herein are as follows:

- The increase in asphalt binder content by 0.3% was actually found to increase the dynamic modulus at the intermediate and high test temperatures. This result was based on the testing that was conducted and was contradictory to previous research and the hypothesis that was put forth for this project. This result should be used with caution and requires further review.
- The binder content variation did not have a statistical effect on flow number.
- Based on the limited results presented herein, the asphalt binder grade appears to have a greater impact on performance in the Superpave™ SPT than does aggregate angularity.
- Dynamic modulus values generally decreased with an increase in mixture air voids. This trend was observed at the four different test frequencies at both test temperatures. An increase in air voids also generally resulted in a decrease in flow number values for the mixtures tested.
- The nominal maximum aggregate size was found to be a statistically important factor affecting dynamic modulus and flow number test results.

- Dynamic modulus and flow number were shown to increase with traffic level, coinciding with an increase in aggregate angularity and with a decrease in air voids. This confirms the hypotheses regarding these two factors. However, the 3 million and 30 million ESAL levels provided better dynamic modulus values than the 10 million ESAL level. This suggests the combination of aggregate and volumetric design criteria (number of design gyrations) may produce the differences in the expected differences in performance of the 10 million ESAL level.
- The dynamic modulus values generally increased with an increase in the loading frequency; this result was expected.
- Accumulated microstrain at flow number, as opposed to the use of flow number, appears to be a promising measure for comparing the quality of specimens within a specific mixture. However, the flow number appears to be better at comparing the performance between mixtures. These findings suggest flow number may be preferred for mix design, whereas the accumulated microstrain may be preferred for quality control and quality assurance testing.
- The 1972 AASHTO Pavement Design Guide provided sufficient designs to resist permanent deformation. However, the 1972 guide's thicknesses generally were thinner than what the newer M-E PDG would identify as appropriate for resisting longitudinal cracking for 3 and 10 million ESAL traffic levels.
- The identification of traffic characteristics (number and types of trucks) and the forecast traffic volume is critical for performance of pavement structures for higher volume highways (3 million and 10 million ESALs).
- The M-E PDG is still a work in progress. Most of the predictive models need further refinement. At the time of this project, only Version 0.8 was available; currently, version 1.0 is available.
- The M-E PDG calibration factors for the models should be calibrated for the state of Wisconsin; the state should not use the nationally-calibrated values.

CHAPTER 9. RECOMMENDATIONS

Extensive testing has been conducted as part of this research project. This testing has brought to light many issues are involved in the implementation of the Superpave™ SPT. These issues should be addressed prior to the implementation of Superpave™ SPT by owners/agencies and industry. Additional research is needed, as discussed in the following points:

- All of the mixtures sampled for this project have been tested. Testing needs to continue to examine the effects of NMAS and to make the analysis more robust through the inclusion of more results with regard to 25.0 mm mixtures.
- Further testing should examine asphalt binder content changes greater than +0.3%. The testing in this study was not significant enough to statistically demonstrate any differences between asphalt binder contents or the effects of asphalt binder content changes. However, greater asphalt binder content changes would not be practical in the field, as construction limits are set at ±0.3% of the optimum value stated in the JMF.
- Additional testing should examine the effects of laboratory- versus field-prepared specimens to validate the use of the SSPT as both a design and QC/QA test.
- Further testing should be conducted on the method of preparation (sawed/cored and compacted to the test geometry), as it pertains to the NMAS of the mixture as well as gradation type. Further testing could validate the conclusion that the method of preparation does not matter. An additional factor for specimen preparation would be to consider specimens that were compacted to 150 mm in diameter and height and then were only cored. This type of preparation would provide a quality surface in which to mount the LVDTs to the sides of the specimen.
- Additional research should examine the application of accumulated micro-strain as a means of comparison within a mixture type to changes in volumetric properties.
- Further studies should examine the implications of using the latest version of the M-E PDG (version 1.0), as changes to the guide have occurred since version 0.8, which was used for this study.

- All of the pavement designs considered in this study were rehabilitated; examination of pre-existing distresses were not considered.
- The M-E PDG does not address complex pavement structures utilizing multiple layers of PCC and HMA.
- The M-E PDG assumes consistent subgrade properties when in fact subgrade variability exists.
- Further research should monitor the field performance of the mixes so that localized calibration of the M-E PDG can be done.

REFERENCES

Akhter, G. F. and M.W. Witczak, "Sensitivity of Flexible Pavement Performance to Bituminous Mix Properties," Washington D.C.: Transportation Research Board (Transportation Research Record 1034) pp. 70-79, 1985.

"An Introduction to Aggregate Testing", Materials Certification and Training Program, Transportation Institute, Michigan Technological University, 2002.

Anderson, R.M., R.J. Cominsky, and B.M. Killingsworth, "Sensitivity of Superpave Mixture Tests to Changes in Mixture Components," Journal of the Association of Asphalt Paving Technologists, Vol. 67, pp.153-188, 1998.

Annual Book of ASTM Standards, American Society for Testing and Materials (ASTM), Vol. 04.03, 2003.

Asphalt Institute, "Superpave Mix Design Series No. 2 (SP-2)", 1996.

Ayyub, B.M., R.H. McCuen, Probability, Statistics, and Reliability for Engineers and Scientists 2nd Ed., Chapman & Hall/CRC, Boca Raton, FL, 2003.

Azari, H., R. McCuen, and K. Stuart, "The Effect of Vertical Inhomogeneity on Compressive Properties of Asphalt Mixtures," Journal of the Association of Asphalt Paving Technologists, Vol. 73, pp.121-146, 2004.

Basyouny, M.M. and M.W. Witczak, "Verification of the Calibrated Fatigue Cracking Models for the 2002 Design Guide," Journal of the Association of Asphalt Paving Technologists, 2005.

Basyouny, M.M., M.W. Witczak, and S. El-Badawy, "Verification for the Calibrated Permanent Deformation Models for the 2002 Design Guide," Journal of the Association of Asphalt Paving Technologists, 2005.

Birgisson, B, G. Sholar, and R. Roque, "Evaluation of Predicted Dynamic Modulus for Florida Mixtures," Washington D.C.: Transportation Research Board (Transportation Research Record 84th Annual Meeting) pp. 1-21, 2005.

Bonaquist, R., D. Christensen, W. Stump III, and C. Antle, "Simple Performance Tester for Superpave Mixture Design," Interim Report for NCHRP 9-29, Advanced Asphalt Technologies, LLC, Sterling VA, September 2001.

Bonaquist, R., Personal Conversation, Fall 2004.

Brown, E.R., P.S. Kandhal, and J. Zhang, "Performance Testing for Hot Mix Asphalt," National Center for Asphalt Technology (NCAT) Report 2001-05, 2001.

Brown, E.R.,R.B. Mallick, J.E. Haddock, and J. Bukowski, "Performance of Stone Matrix Asphalt (SMA) Mixtures in the United States," Journal of the Association of Asphalt Paving Technologists, Vol. 66, pp.426-457, 1997.

Brown, S.F. and M.S. Snaith, "The Permanent Deformation Characteristics of a Dense Bitumen Macadam Subjected to Repeated Loading," Journal of the Association of Asphalt Paving Technologists, Vol. 43, pp.224-252, 1974.

Brown, S. F. and K. E. Cooper, "The Mechanical Properties of Bituminous Materials for Road Bases and Basecourses," Journal of the Association of Asphalt Paving Technologists, Vol. 53, pp.415-439, 1984.

Brown, S. F. and J. M. Gibb. "Validation Experiments for Permanent Deformation Testing of Bituminous Mixtures," Journal of the Association of Asphalt Paving Technologists, Vol.65, pp.255-299, 1996.

Burmister, D.M., "The Theory of Stresses and Displacement in Layered Systems and Applications to the Design of Airport Runways," Highway Research Record, Vol. 23, pp. 126-148, 1943.

Buttlar, W.G., R. Roque, and B. Reid, "Automated Procedure for Generation of Creep Compliance Master Curve for Asphalt Mixtures," Washington D.C.: Transportation Research Board (Transportation Research Record 1630) pp. 28-36, 1998.

Christensen, D., Personal Conversation, Fall 2004.

Clyne, T.R., X. Li, M.O. Marasteanu, and E.L. Skok, "Dynamic and Resilient Modulus of MN/DOT Asphalt Mixtures," Minnesota Department of Transportation, MN/RC-2003-09, 2003.

Coduto, D.P., Geotechnical Engineering: Principles and Practices, Prentice Hall, Upper Saddle River, New Jersey, 1999.

Coffman, B.S., D.C. Kraft, and J. Tamayo, "A Comparison of Calculated and Measured Deflections for the AASHO Test Road," Proceedings of the Association of Asphalt Paving Technologists, Vol.33, pp.54-91, 1964.

Collop, A.C., A. Scarpas, C. Kasbergen, and A. de Bondt, "Development and Finitie Element Implementation of Stress-Dependent Elastoviscoplastic Constitutive Model with Damage for Asphalt", Washington D.C.: Transportation Research Board (Transportation Research Record 1832) pp. 96-104, 2003.

Crockford, W.W., C. Berthelot, B. Tritt, and C. Sinadinos, "Rapid Triaxial Test," Journal of the Association of Asphalt Paving Technologists, Vol.71, pp.712-724, 2001.

DATAPAVE, http://www.datapave.com, LTPP DataPave Online, 2004.

Dougan, C.E., J.E. Stephens, J. Mahoney, and G. Hansen, "E* - DYNAMIC MODULUS Test Protocol – Problems and Solutions," Connecticut Transportation Institute, Report CT-SPR-0003084-F-03-3, 2003.

Dukatz, E., "Aggregate Production for Superpave HMA," The Superpave Asphalt Research Program, The University of Texas at Austin, 1996.

Epps, A.L. and A.J. Hand, "A Comparison of HMA Field Performance and Laboratory Volumetric Sensitivities," Journal of the Association of Asphalt Paving Technologists, Vol.70, pp.675-711, 2001.

Epps, J.A., R.B. Leahy, T. Mitchell, C. Ashmore, S. Seeds, S. Alavi, and C.L. Monismith, "WesTrack – The Road to Performance-Related Specifications," International Conference on Accelerated Pavement Testing, Reno, NV, 1999.

Foster, C.R. and R.G. Ahlvin, "Stresses and Deflections Induced by a Uniform Circular Load," Highway Research Board, Vol. 33, pp. 467-470, 1954.

Guide for Mechanistic-Empirical Design of New and Rehabilitated Pavement Structures, National Cooperative Highway Research Program, NCHRP 1-37A, March 2004.

Hills, J.F., "The Creep of Asphalt Mixes," Journal of the Institute of Petroleum, V59, No. 570, 1973.

Hills, J.F., D. Brien, and P.J. van de Loo, "The Correlation of Rutting and Creep Test on Asphalt Mixes," Journal of the Institute of Petroleum, Paper IP 74-001, 1974.

Huang, Y.H, Pavement Analysis and Design, Prentice Hall, Upper Saddle River, New Jersey, 2003.

Jones, A., "Tables of Stresses in Three-Layered Elastic Systems," Washington D.C.: Highway Research Board (1025), pp. 176-214, 1962.

Kaloush, K.E. and M.W. Witczak, " Tertiary Flow Characteristics of Asphalt Mixtures," Journal of the Association of Asphalt Paving Technologists, Vol. 71, pp.248-276, 2002.

Kerkhoven, R.E. and G.M. Dormon, "Some Considerations on the California Bearing Ratio Method for the Design of Flexible Pavement," Shell Bitumen Monograph No. 1, 1953.

Krutz, N.C. and P.E. Sebaaly, "The Effects of Aggregate Gradation on Permanent Deformation of Asphalt Concrete," Journal of the Association of Asphalt Paving Technologists, Vol.62, pp.450-480, 1993.

Kutner, M.H., C.J. Nachtheim, and J. Neter, Applied Regression Models, McGraw Hill/Irwin, 2004.

Levene, H. (1960). In Contributions to Probability and Statistics: Essays in Honor of Harold Hotelling, I. Olkin et al. eds., Stanford University Press, pp. 278-292.

Lytton, R.L., J. Uzan, E.G. Femando, R. Roque, D. Hiltunen, and S.M. Stoffels, "Development and Validation of Performance Prediction Models and Specifications for Asphalt Binders and Paving Mixes", Strategic Highway Research Program 357, National Research Council, Washington D.C., 1993.

Mahoney, J. and J. Stephens, "Connecticut Superpave Gyratory Round Robin – 2003," Connecticut Transportation Institute, Report CAP Lab 1-2003, 2003.

Mallick, R.B., R. Ahlrich, and E.R. Brown, "Potential of Dynamic Creep to Predict Rutting," Engineering Properties of Asphalt Mixtures and the Relationship to their Performance,

ASTM STP 1265, G.A. Huber and D.S. Decker Eds., American Society for Testing and Materials, Philadelphia, 1995.

McClave, J.T. and T. Sinich, Statistics 9th Ed., Prentice Hall, Upper Saddle River, NJ, 2003.

McGhee, K. H. "Summary of Proposed 2002 Pavement Design Guide," National Highway Cooperative Research Program 1-37A, 1999.

Mirza, M.W. and M.W. Witczak, "Development of a Global Aging System for Short and Long Term Aging of Asphalt Cements," Journal of the Association of Asphalt Paving Technologists, Vol.64, pp.393-430, 1995.

Mohammad, L.N., Z. Wu, L. Myers, S. Cooper, and C. Abadie, "A Practical Look at the Simple Performance Tests: Louisiana's Experience," Journal of the Association of Asphalt Paving Technologists, 2005.

Molenaar, A.A.A. and Ch. A.P.M. Van Gurp, "Structural Performance Model and Overlay Design Method for Asphalt Concrete Pavements," Washington D.C.: Transportation Research Board (Transportation Research Record 888) pp. 31-37, 1982.

Monismith, C.L. and A.A. Tayabali "Permanent Deformation (Rutting) Considerations in Asphalt Concrete Pavement Actions," Journal of the Association of Asphalt Paving Technologists, Vol. 57 pp. 414-446, 1988.

Myers, L., Federal Highway Administration Engineer, Personal Conversation, Fall 2004.

Newcomb, D.E. and D.H. Timm, "Mechanistic Pavement Design: The Next Wave," Hot Mix Asphalt Technology, pp. 49-51, September/October 2001.

Owen, D.R.J. and E. Hinton, Finite Elements in Plasticity: Theory and Practice, Pineridge Press Limited, Swansea, U.K., 1980.

Papazian, H.S., "The Response of Linear Viscoelastic Materials in the Frequency Domain with Emphasis on Asphaltic Concrete," International Conference on the Structural Design of Asphalt Pavements, University of Michigan, pp. 454-463, 1962.

Peattie, K.R., "Stress and Strain Factors for Three-Layered Elastic Systems," Washington D.C.: Highway Research Board (1025), pp. 214-253, 1962.

Pellinen, T.K and M.W. Witczak, "Stress Dependent Master Curve Construction for Dynamic (Complex) Modulus," Journal of the Association of Asphalt Paving Technologists, Vol. 71, pp.281-309, 2002.

Roberts, F. L. Hot Mix Asphalt Materials, Mixture Design, and Construction, Lanham: NAPA Research and Education Foundation, 1996.

Roberts, F.L., L.N. Mohammad, and L.B. Wang, "History of Hot Mix Asphalt Mixture Design in the United States," American Society of Civil Engineers, Journal of Civil Engineering Materials, July 2002.

Saal R.N.J. and P.S. Pell, "Kolloid-Zeitschrift MI," Heft 1, pp. 61-71, 1960.

Shenoy, A. and P. Romero, "Standardized Procedure for Analysis of Dynamic Modulus $|E^*|$ Data to Predict Asphalt Pavement Distresses," Washington D.C.: Transportation Research Board (Transportation Research Record 1789) pp. 173-182, 2002.

Shook J.F. and B.F. Kallas. "Factors Influencing Dynamic Modulus of Asphalt Concrete," Journal of the Association of Asphalt Paving Technologists, Vol. 38, pp.140-178, 1969.

Soil Survey of Lincoln County Wisconsin, United States Department of Agriculture, 1990.

Soil Survey of Lincoln County Wisconsin, United States Department of Agriculture, 2000.

Soil Survey of Marathon County Wisconsin, United States Department of Agriculture, 2000.

Superpave Mix Design Series No.2 (SP-2), The Asphalt Institute, 1996.

Timm, D., B. Birgisson, and D. Newcomb, "Development of Mechanistic-Empirical Pavement Design in Minnesota," Washington D.C.: Transportation Research Board (Transportation Research Record 1629) pp. 181-188, 1998.

Uzan, J., A. Sides, and M. Perl, "Viscoelastoplastic Model for Predicting Performance of Asphaltic Mixtures," Washington D.C.: Transportation Research Board (Transportation Research Record 1043) pp. 78-89, 1985.

Uzan, J., "Permanent Deformation in Flexible Pavements", American Society of Civil Engineering, Journal of Transportation Engineering, Vol. 130, No. 1, January 1, 2004.

Van Cauwelaert, F., D.R. Alexander, T.D. White, and W.R. Barker, "Multilayer Elastic Program for Backcalculating Layer Moduli in Pavement Evaluation," Nondestructive Testing of Pavements and Backcalculating Moduli , ASTM STP 1026, A.J. Bush III and G.Y. Baladi, American Society for Testing and Materials, Philadelphia, 1989, pp. 171-188.

Van de Loo, P.J., "Creep Testing, a Simple Tool to Judge Asphalt Mix Stability," Proceedings of the Association of Asphalt Paving Technologists, Vol. 43, pp.253-284, 1974.

Vesic, A.S. and L. Domaschuk, "Theoretical Analysis of Structural Behavior of Road Test Flexible Pavements," National Cooperative Highway Research Program, Report 10, 1964.

Wisconsin Department of Transportation: Standard Specifications for Highway and Structure Construction, Wisconsin Department of Transportation, 2002.

Wisconsin State Climatology Office, http://www.aos.wisc.edu/~sco/, 1/7/2005.

Witczak, M. W., R. Bonaquist, H. Von Quintus, and K. Kaloush. "Specimen Geometry and Aggregate Size Effects in Uniaxial Compression and Constant Height Shear Tests," Journal of the Association of Asphalt Paving Technologists, Vol. 69, pp.733-793, 2000.

Witczak, M.W. and O.A. Fonseca, "Revised Predictive Model for Dynamic (Complex) Modulus of Asphalt Mixtures," Washington D.C.: Transportation Research Board (Transportation Research Record 1540) pp. 15-23, 1996.

Witczak, M.W., K.E. Kaloush, and H. Von Quintus, "Pursuit of the Simple Performance Test for Asphalt Mixture Rutting," Journal of the Association of Asphalt Paving Technologists, Vol. 71, pp.671-691, 2002a.

Witczak, M. W., K. Kaloush, T. Pellinen, M. El-Basyouny, and H. Von Quintus, "Simple Performance Test for Superpave Mix Design," National Cooperative Highway Research Program 465, pp.6-100, 2002b.

WSDOT Pavement Guide Vol. 2 Pavement Notes For Design, Evaluation and Rehabilitation, Washington Department of Transportation, February 1995.

Zhou, F. and T. Scullion, "Preliminary Field Validation of Simple Performance Tests for Permanent Deformation: Case Study," Washington D.C.: Transportation Research Board (Transportation Research Record 1832) pp. 209-216, 2003.

Zhou, F., T. Scullion, and L. Sun, "Verification and Modeling of Three-Stage Permanent Deformation Behavior of Asphalt Mixtures," Journal of Transportation Engineering, Vol. 130 Issue 4, pp. 486-494, 2004.

APPENDIX A. PROJECT JMFs

Project: Sauk County - Baraboo USH 12

Project No.:	5300-03-77
Location:	Sauk County
Contractor:	D.L. Gasser
Traffic Volume (ESALs):	300,000
NMAS (mm):	12.5
Mix Type:	Dense
Date:	6/16/2004
G_{se}	2.701
G_{sb}	2.652
G_{sa}	N/A
Absorption (%)	0.8
Sand Equivalency (%)	41.5
Flat & Elongated (%)	4.7
NAA	79.0
1 Face Crush (%)	89.5
2 Face Crush (%)	87.4

Temperatures:

Mixing:	N/A
Compacting:	143

Sieve Size in (mm):	3/4" Gravel	5/8" Quartzite	Blend Sand	Agg Source 4	Agg Source 5	Agg Source 6	Agg Source 7	Mix
1 (25)	100.0	100.0	100.0					100.0
3/4 (19)	100.0	100.0	100.0					100.0
1/2 (12.5)	90.0	91.0	99.0					95.3
3/8 (9.5)	73.0	75.0	94.0					85.2
#4 (4.75)	45.0	47.0	82.0					66.2
#8 (2.36)	31.0	31.0	72.0					54.0
#16 (1.18)	23.0	22.0	67.0					47.4
#30 (0.60)	19.0	16.0	56.0					39.1
#50 (0.30)	14.0	12.0	23.0					18.6
#100 (0.15)	8.4	9.0	5.1					6.7
#200 (0.075)	5.7	6.5	3.0					4.4
Percentages	22%	22%	56%					100%

Asphalt & Additives:

Asphalt Source:	MIF-LaCrosse
Asphalt Grade (PG):	58-28
Asphalt Content (%):	6.0
Specific Gravity:	1.029
Asphalt Additives:	None
Asphalt Additives (%):	N/A

Compactive Effort:

N_{ini}:	6
N_{des}:	40
N_{max}:	60
$\%G_{mm}$ @ N_{ini}:	91.7
$\%G_{mm}$ @ N_{max}:	96.7
CF:	1.020

Volumetrics:

VMA @ N_{des}:	16.2
VFA @ N_{des}:	75.4
AV @ N_{des}:	4.0
F/P_{be}:	0.8
P_{be} (%):	5.3

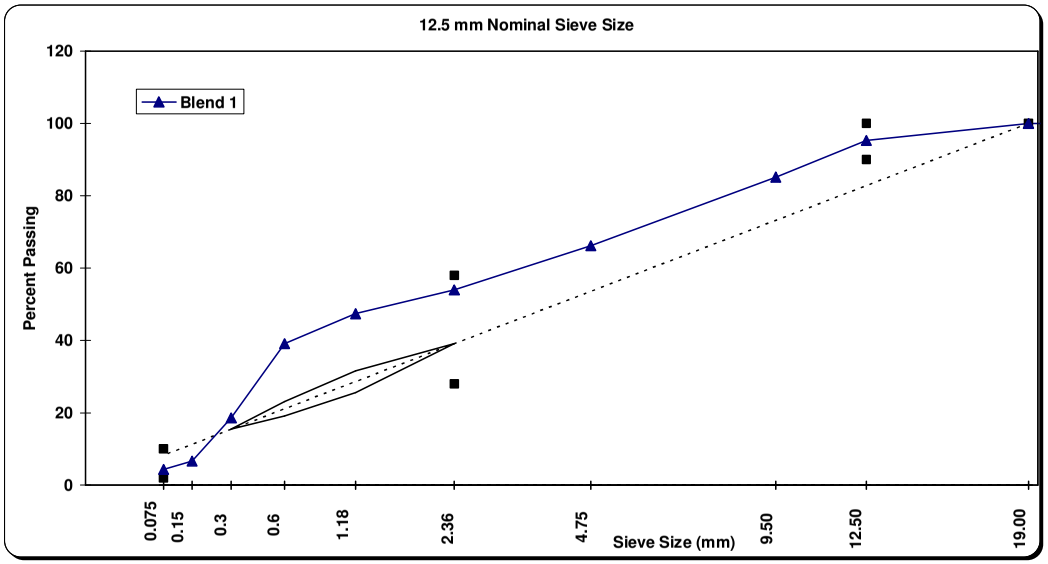

Project: Taylor County Medford WI STH 102

Project No.:	9225-05-70
Location:	Taylor County
Contractor:	American - Mathy
Traffic Volume (ESALs):	1,000,000
NMAS (mm):	12.5
Mix Type:	Dense
Date:	7/8/2004
G_{se}	2.747
G_{sb}	2.697
G_{sa}	N/A
Absorption (%)	1.0
Sand Equivalency (%)	75.0
Flat & Elongated (%)	3.3
NAA	42.9
1 Face Crush (%)	96.5
2 Face Crush (%)	96.4

Temperatures:

Mixing:	N/A
Compacting:	143

Sieve Size in (mm):	11/16" Rock	5/8 Sand	RAP (5.0% AC)	Agg Source 4	Agg Source 5	Agg Source 6	Agg Source 7	Mix
1 (25)	100.0	100.0	100.0					100.0
3/4 (19)	100.0	100.0	100.0					100.0
1/2 (12.5)	89.0	99.0	93.0					94.9
3/8 (9.5)	67.0	91.0	79.0					81.4
#4 (4.75)	39.0	75.0	60.0					60.9
#8 (2.36)	25.0	63.0	49.0					48.3
#16 (1.18)	18.0	48.0	40.0					36.7
#30 (0.60)	13.0	30.0	31.0					24.2
#50 (0.30)	9.0	12.0	20.0					11.8
#100 (0.15)	5.9	3.5	13.0					5.3
#200 (0.075)	3.9	3.2	9.5					4.1
Percentages	35%	55%	10%					100%

Asphalt & Additives:

Asphalt Source:	MIF-LaCrosse
Asphalt Grade (PG):	58-28
Asphalt Content (%):	5.2
Specific Gravity:	1.03
Asphalt Additives:	None
Asphalt Additives (%):	N/A

Compactive Effort:

N_{ini}:	7
N_{des}:	60
N_{max}:	75
$\%G_{mm}$ @ N_{ini}:	90
$\%G_{mm}$ @ N_{max}:	96.8
CF:	1.020

Volumetrics:

VMA @ N_{des}:	15.3
VFA @ N_{des}:	73.9
AV @ N_{des}:	4.0
F/P_{be}:	0.9
P_{be} (%):	4.5

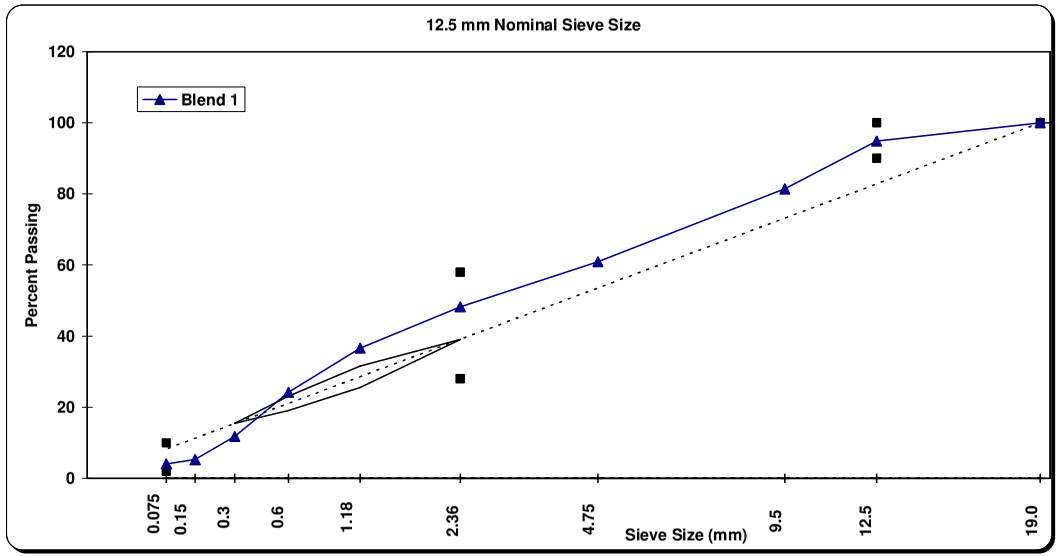

Project: Waushara County Wautoma STH 22

Project No.:	6300-03-60
Location:	Waushara County
Contractor:	Northeast Asphalt
Traffic Volume (ESALs):	1,000,000
NMAS (mm):	12.5
Mix Type:	Dense
Date:	6/20/2004
G_{se}	2.733
G_{sb}	2.713
G_{sa}	2.765
Absorption (%)	0.7
Sand Equivalency (%)	84.0
Flat & Elongated (%)	2.5
NAA	41.0
1 Face Crush (%)	96.7
2 Face Crush (%)	96.0

Temperatures:

Mixing:	N/A
Compacting:	143

Sieve Size in (mm):	Millings	5/8x1/2 Chip	1/2x1/4 Chip	1/4" Screen	Screen Sand	Agg Source 6	Agg Source 7	Mix
1 (25)	100.0	100.0	100.0	100.0	100.0			100.0
3/4 (19)	100.0	100.0	100.0	100.0	100.0			100.0
1/2 (12.5)	96.5	63.7	100.0	100.0	100.0			96.8
3/8 (9.5)	90.8	7.7	81.8	100.0	100.0			87.9
#4 (4.75)	77.6	1.6	8.3	93.6	95.4			66.1
#8 (2.36)	64.5	1.3	2.4	60.8	86.1			52.8
#16 (1.18)	52.2	1.2	2.1	43.3	79.1			44.7
#30 (0.60)	38.5	1.2	1.9	33.6	62.5			34.8
#50 (0.30)	18.3	1.1	1.8	25.0	19.8			15.3
#100 (0.15)	11.0	0.9	1.5	16.5	3.0			6.7
#200 (0.075)	8.1	0.7	1.2	11.3	1.1			4.4
Percentages	18%	7%	22%	20%	33%			100%

Asphalt & Additives:

Asphalt Source:	Koch, Stevens Point
Asphalt Grade (PG):	58-28
Asphalt Content (%):	4.7
Specific Gravity:	1.032
Asphalt Additives:	None
Asphalt Additives (%):	N/A

Compactive Effort:

N_{ini}:	7
N_{des}:	60
N_{max}:	75
$\%G_{mm}$ @ N_{ini}:	91.2
$\%G_{mm}$ @ N_{max}:	96.5
CF:	1.020

Volumetrics:

VMA @ N_{des}:	14.5
VFA @ N_{des}:	72.4
AV @ N_{des}:	4.0
F/P_{be}:	1
P_{be} (%):	4.4

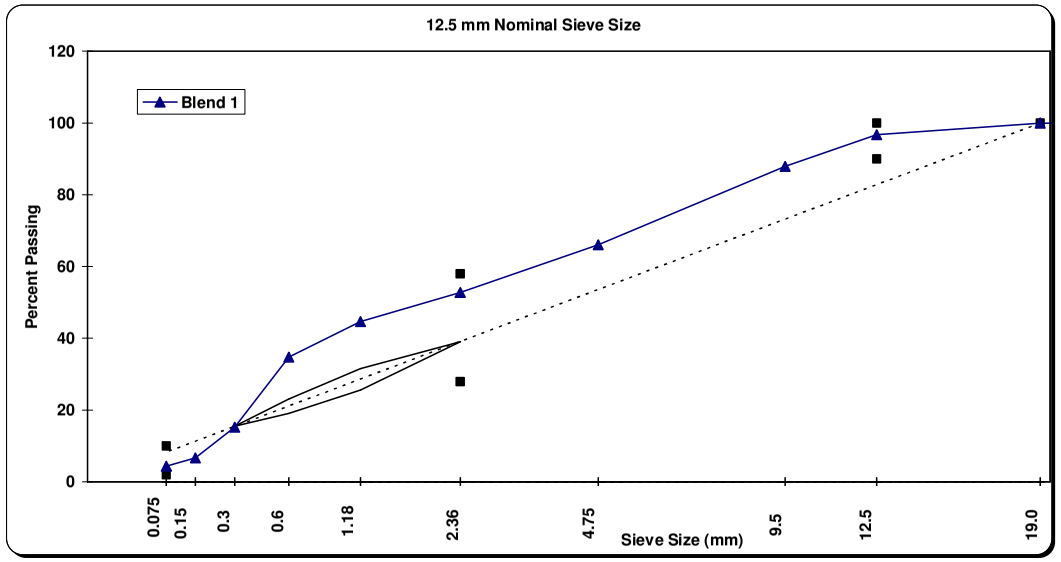

Project:	Iron County Hurley STH 169
Project No.:	9311-13-60
Location:	Iron County
Contractor:	Northwoods Paving
Traffic Volume (ESALs):	300,000
NMAS (mm):	12.5
Mix Type:	Dense
Date:	7/21/2004
G_{se}	2.760
G_{sb}	2.689
G_{sa}	N/A
Absorption (%)	1.3
Sand Equivalency (%)	74.0
Flat & Elongated (%)	4.0
NAA	43.0
1 Face Crush (%)	93.6
2 Face Crush (%)	93.4

Temperatures:

Mixing:	N/A
Compacting:	143

Sieve Size in (mm):	3/4" Rock	5/8x3/8 Rock	3/8 Minus	5/8 Nat Sand	RAP (6.0% AC)	Agg Source 6	Agg Source 7	Mix
1 (25)	100.0	100.0	100.0	100.0	100.0			100.0
3/4 (19)	100.0	100.0	100.0	100.0	100.0			100.0
1/2 (12.5)	78.0	77.0	100.0	99.0	98.0			92.7
3/8 (9.5)	62.0	35.0	100.0	97.0	91.0			83.4
#4 (4.75)	34.0	2.4	73.0	94.0	70.0			62.8
#8 (2.36)	19.0	2.0	48.0	90.0	54.0			49.3
#16 (1.18)	12.0	1.8	28.0	83.0	43.0			38.9
#30 (0.60)	9.0	1.7	18.0	65.0	32.0			29.1
#50 (0.30)	7.0	1.5	13.0	19.0	17.0			13.0
#100 (0.15)	6.0	1.4	9.0	6.7	11.0			7.5
#200 (0.075)	5.0	1.0	7.0	1.0	8.8			4.9
Percentages	20%	10%	25%	25%	20%			100%

Asphalt & Additives:

Asphalt Source:	Murphy
Asphalt Grade (PG):	58-28
Asphalt Content (%):	6.3
Specific Gravity:	1.03
Asphalt Additives:	None
Asphalt Additives (%):	N/A

Compactive Effort:

N_{ini}:	6
N_{des}:	40
N_{max}:	60
$\%G_{mm}$ @ N_{ini}:	90.6
$\%G_{mm}$ @ N_{max}:	96.7
CF:	1.020

Volumetrics:

VMA @ N_{des}:	16.5
VFA @ N_{des}:	75.8
AV @ N_{des}:	4.0
F/P_{be}:	0.9
P_{be} (%):	5.4

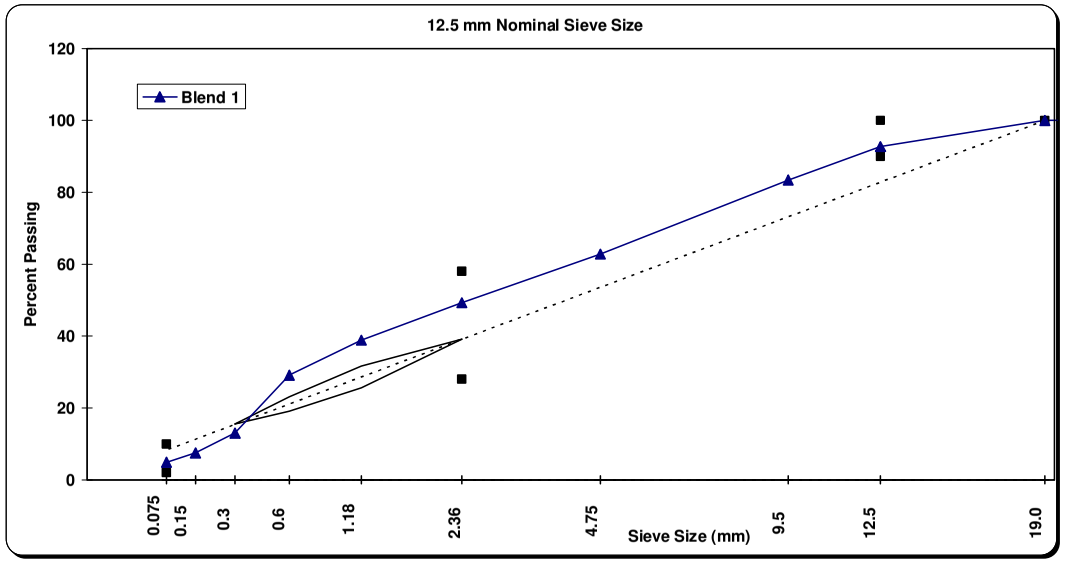

Project: Sawyer County Hayward WI State Highway 77

Project No.:	8520-13-71
Location:	Sawyer County
Contractor:	B. R. Amon
Traffic Volume (ESALs):	3,000,000
NMAS (mm):	12.5
Mix Type:	Dense
Date:	6/3/2004
G_{se}	2.779
G_{sb}	2.728
G_{sa}	N/A
Absorption (%)	0.9
Sand Equivalency (%)	81.0
Flat & Elongated (%)	2.1
NAA	44.0
1 Face Crush (%)	74.7
2 Face Crush (%)	70.4

Temperatures:

Mixing:	148
Compacting:	135

Sieve Size in (mm):	7/8" Stone	5/8" Stone	3/8" Stone	Sand	Dust	RAP	Agg Source 7	Mix
1 (25)	100.0	100.0	100.0	100.0	100.0	100.0		100.0
3/4 (19)	95.8	100.0	100.0	100.0	100.0	100.0		100.0
1/2 (12.5)	18.2	91.9	100.0	100.0	100.0	100.0		98.8
3/8 (9.5)	3.0	25.7	96.0	99.2	100.0	100.0		87.8
#4 (4.75)	2.3	3.3	8.4	89.2	88.6	100.0		62.4
#8 (2.36)	2.2	3.1	4.2	76.1	57.9	100.0		48.4
#16 (1.18)	2.1	3.0	4.0	61.2	41.8	100.0		37.9
#30 (0.60)	2.0	2.9	3.7	37.8	31.4	100.0		25.2
#50 (0.30)	1.8	2.5	3.2	16.5	21.3	100.0		13.3
#100 (0.15)	1.3	1.8	2.5	4.3	12.4	100.0		5.6
#200 (0.075)	1.1	1.6	2.0	3.9	9.4	100.0		4.6
Percentages	0%	15%	17%	43%	25%	0%		100%

Asphalt & Additives:

Asphalt Source:	Murphy
Asphalt Grade (PG):	58-28
Asphalt Content (%):	5.3
Specific Gravity:	1.031
Asphalt Additives:	None
Asphalt Additives (%):	N/A

Compactive Effort:

N_{ini}:	7
N_{des}:	75
N_{max}:	115
$\%G_{mm}$ @ N_{ini}:	89.1
$\%G_{mm}$ @ N_{max}:	96.7
CF:	1.020

Volumetrics:

VMA @ N_{des}:	15.0
VFA @ N_{des}:	73.3
AV @ N_{des}:	4.0
F/P_{be}:	0.99
P_{be} (%):	4.6

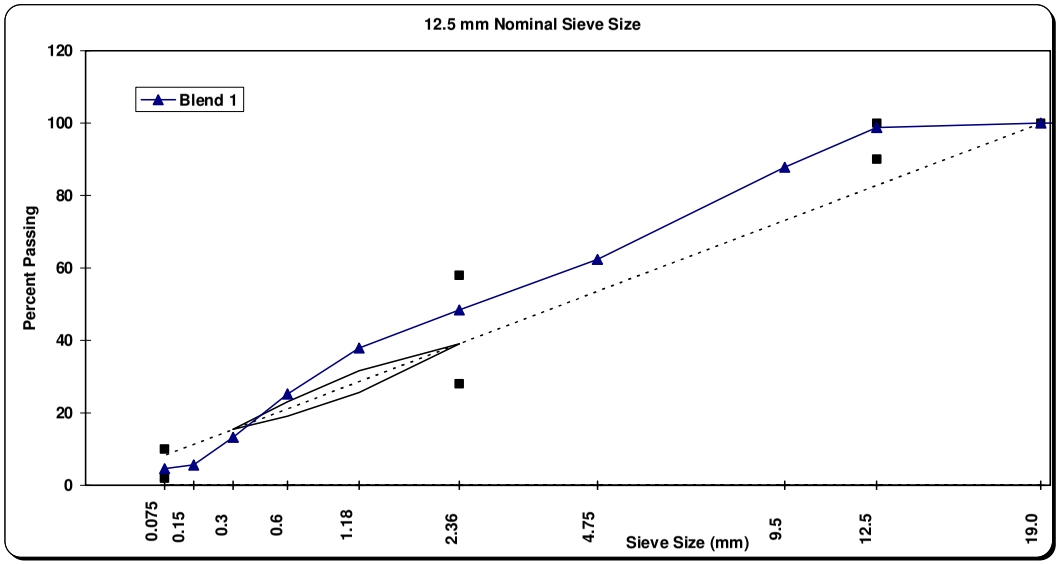

Project: Marathon County Wausau WI CTH 12

Project No.:	6675-00-70
Location:	Marathon County
Contractor:	American - Mathy
Traffic Volume (ESALs):	3,000,000
NMAS (mm):	12.5
Mix Type:	Dense
Date:	6/15/2004
G_{se}	2.698
G_{sb}	2.647
G_{sa}	N/A
Absorption (%)	0.5
Sand Equivalency (%)	87.0
Flat & Elongated (%)	1.8
NAA	43.2
1 Face Crush (%)	96.7
2 Face Crush (%)	96.5

Temperatures:

Mixing:	N/A
Compacting:	143

Sieve Size in (mm):	1/2" Rock	3/8" Rock	3/16 Screening	Blend Sand	Man Sand	RAP (4.0% AC)	Agg Source 7	Mix
1 (25)	100.0	100.0	100.0	100.0	100.0	100.0		100.0
3/4 (19)	100.0	100.0	100.0	100.0	100.0	100.0		100.0
1/2 (12.5)	81.0	100.0	100.0	99.0	100.0	97.0		95.7
3/8 (9.5)	36.0	100.0	100.0	98.0	100.0	90.0		85.8
#4 (4.75)	6.0	29.0	97.0	94.0	100.0	73.0		66.1
#8 (2.36)	3.0	10.0	66.0	88.0	67.0	58.0		48.8
#16 (1.18)	2.2	5.6	42.0	77.0	43.0	47.0		36.2
#30 (0.60)	1.9	4.4	28.0	58.0	24.0	36.0		25.4
#50 (0.30)	1.8	3.5	17.0	10.0	10.0	18.0		9.6
#100 (0.15)	1.5	3.0	11.0	1.2	3.5	11.0		4.8
#200 (0.075)	1.3	2.4	10.0	0.7	1.5	8.0		3.8
Percentages	20%	15%	20%	20%	15%	10%		100%

Asphalt & Additives:

Asphalt Source:	MIF-LaCrosse
Asphalt Grade (PG):	64-22
Asphalt Content (%):	5.9
Specific Gravity:	1.029
Asphalt Additives:	Polymer
Asphalt Additives (%):	N/A

Compactive Effort:

N_{ini}:	7
N_{des}:	75
N_{max}:	115
$\%G_{mm}$ @ N_{ini}:	89.5
$\%G_{mm}$ @ N_{max}:	96.9
CF:	1.020

Volumetrics:

VMA @ N_{des}:	15.9
VFA @ N_{des}:	74.9
AV @ N_{des}:	4.0
F/P_{be}:	0.7
P_{be} (%):	5.2

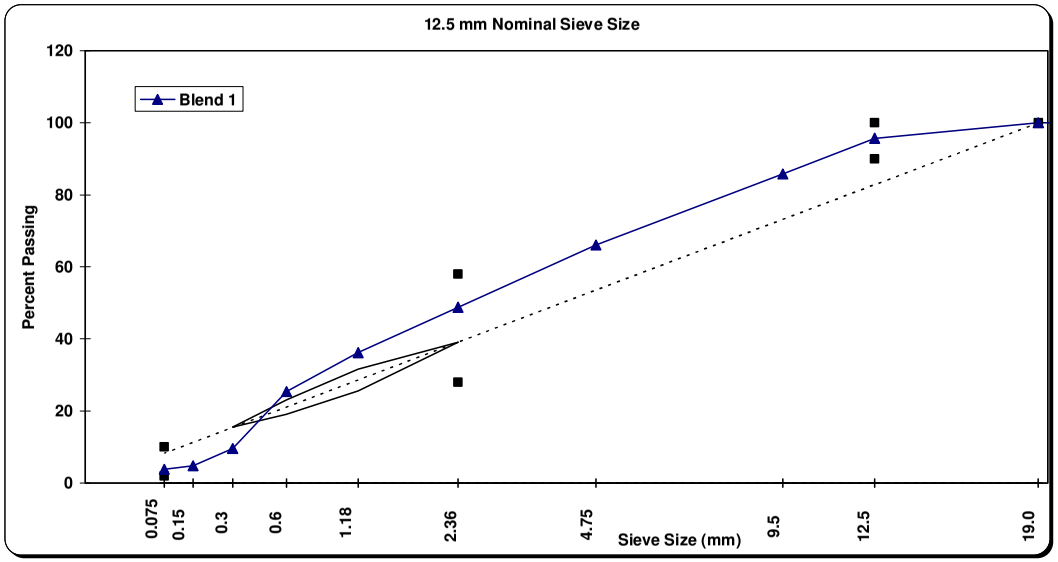

Project: Iron County Hurley WI West County Line - CTH B US 2

Project No.:	1185-02-70
Location:	Iron County
Contractor:	Northwoods Paving
Traffic Volume (ESALs):	3,000,000
NMAS (mm):	12.5
Mix Type:	Dense
Date:	6/24/2004
G_{se}	2.748
G_{sb}	2.696
G_{sa}	N/A
Absorption (%)	1.3
Sand Equivalency (%)	66.0
Flat & Elongated (%)	3.9
NAA	44.0
1 Face Crush (%)	95.4
2 Face Crush (%)	95.3

Temperatures:

Mixing:	
Compacting:	

Sieve Size in (mm):	3/4" Rock	5/8x3/8 Rock	3/8 Minus	5/8 Nat Sand	RAP (5.9% AC)	Agg Source 6	Agg Source 7	Mix
1 (25)	100.0	100.0	100.0	100.0	100.0			100.0
3/4 (19)	100.0	100.0	100.0	100.0	100.0			100.0
1/2 (12.5)	78.0	77.0	100.0	99.0	95.0			93.4
3/8 (9.5)	62.0	35.0	100.0	97.0	90.0			83.0
#4 (4.75)	34.0	2.4	73.0	94.0	75.0			61.4
#8 (2.36)	19.0	2.0	48.0	90.0	50.0			46.1
#16 (1.18)	12.0	1.8	28.0	83.0	40.0			34.8
#30 (0.60)	9.0	1.7	18.0	65.0	30.0			25.5
#50 (0.30)	7.0	1.5	13.0	19.0	25.0			13.4
#100 (0.15)	6.0	1.4	9.0	6.7	17.0			8.1
#200 (0.075)	5.0	1.0	7.0	1.0	12.0			5.3
Percentages	5%	20%	40%	20%	15%			100%

Asphalt & Additives:

Asphalt Source:	MIF-LaCrosse
Asphalt Grade (PG):	64-34
Asphalt Content (%):	5.6
Specific Gravity:	1.029
Asphalt Additives:	Polymer
Asphalt Additives (%):	N/A

Compactive Effort:

N_{ini}:	7
N_{des}:	75
N_{max}:	115
$\%G_{mm}$ @ N_{ini}:	89.3
$\%G_{mm}$ @ N_{max}:	96.7
CF:	1.020

Volumetrics:

VMA @ N_{des}:	15.5
VFA @ N_{des}:	74.2
AV @ N_{des}:	4.0
F/P_{be}:	1.1
P_{be} (%):	4.9

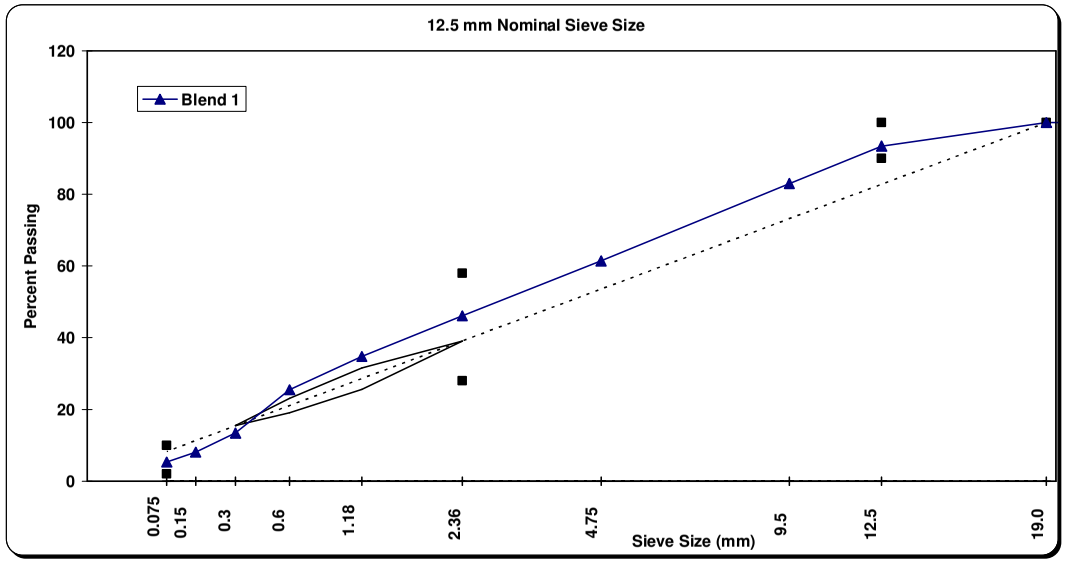

Project: Langlade County Antigo WI City of Antigo

Project No.:	1605-04-70
Location:	Langlade County
Contractor:	Northeast Asphalt
Traffic Volume (ESALs):	10,000,000
NMAS (mm):	12.5
Mix Type:	Dense
Date:	6/2/2004
G_{se}	2.700
G_{sb}	2.690
G_{sa}	2.721
Absorption (%)	0.4
Sand Equivalency (%)	86.0
Flat & Elongated (%)	0.4
NAA	45.2
1 Face Crush (%)	95.4
2 Face Crush (%)	93.8

Temperatures:

Mixing:	N/A
Compacting:	142

Sieve Size in (mm):	5/8"x1/2" Chip	1/2"x1/4" Chip	1/4" Screenings	MFGD Sand	Screened Sand	Agg Source 6	Agg Source 7	Mix
1 (25)	100.0	100.0	100.0	100.0	100.0			100.0
3/4 (19)	100.0	100.0	100.0	100.0	100.0			100.0
1/2 (12.5)	83.4	100.0	100.0	100.0	100.0			98.0
3/8 (9.5)	27.6	85.8	100.0	100.0	99.3			89.6
#4 (4.75)	6.9	10.3	88.5	76.0	84.6			64.5
#8 (2.36)	5.1	6.0	60.4	44.7	68.1			43.9
#16 (1.18)	4.2	4.9	44.2	27.1	55.8			31.7
#30 (0.60)	3.8	4.2	33.3	17.0	37.2			21.5
#50 (0.30)	3.3	3.6	24.5	9.0	15.2			11.6
#100 (0.15)	2.7	3.0	15.7	3.7	6.4			6.0
#200 (0.075)	2.0	2.2	10.2	1.7	3.9			4.1
Percentages	12%	11%	15%	37%	25%			100%

Asphalt & Additives:

Asphalt Source:	CRM Gladstone
Asphalt Grade (PG):	58-34
Asphalt Content (%):	5.0
Specific Gravity:	1.03
Asphalt Additives:	Polymer
Asphalt Additives (%):	N/A

Compactive Effort:

N_{ini}:	8
N_{des}:	100
N_{max}:	160
$\%G_{mm}$ @ N_{ini}:	89
$\%G_{mm}$ @ N_{max}:	97
CF:	1.020

Volumetrics:

VMA @ N_{des}:	14.7
VFA @ N_{des}:	72.8
AV @ N_{des}:	4.0
F/P_{be}:	0.8
P_{be} (%):	4.9

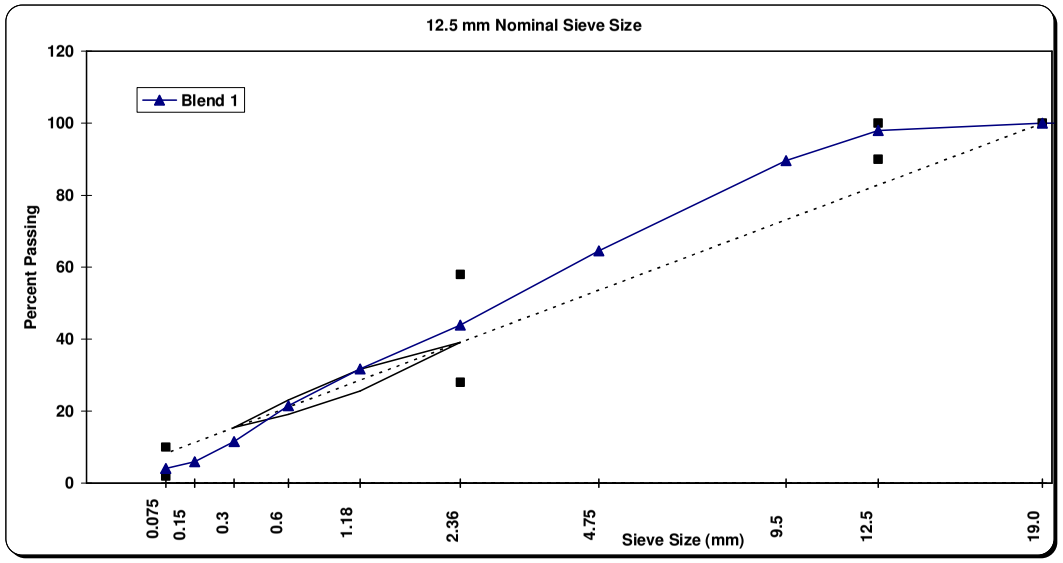

Project: Sheboygan County Plymouth WI STH 23

Project No.:	4840-02-71
Location:	Sheboygan County
Contractor:	Northeast Asphalt
Traffic Volume (ESALs):	10,000,000
NMAS (mm):	12.5
Mix Type:	Dense
Date:	6/8/2004
G_{se}	2.812
G_{sb}	2.768
G_{sa}	2.838
Absorption (%)	0.9
Sand Equivalency (%)	83.7
Flat & Elongated (%)	1.0
NAA	45.4
1 Face Crush (%)	97.0
2 Face Crush (%)	95.0

Temperatures:

Mixing:	N/A
Compacting:	155

Sieve Size in (mm):	5/8x1/2 Chip	1/2x1/4 Chip	Wash Man Sand	Wash Nat Sand	1/4" Screen	Agg Source 6	Agg Source 7	Mix
1 (25)	100.0	100.0	100.0	100.0	100.0			100.0
3/4 (19)	100.0	100.0	100.0	100.0	100.0			100.0
1/2 (12.5)	80.8	100.0	100.0	100.0	100.0			97.9
3/8 (9.5)	14.8	93.9	100.0	100.0	100.0			89.9
#4 (4.75)	2.6	18.1	90.9	90.2	93.7			72.5
#8 (2.36)	2.1	3.4	52.6	72.1	69.7			45.3
#16 (1.18)	2.0	2.8	36.4	54.1	53.8			32.5
#30 (0.60)	1.9	2.6	24.3	37.5	44.7			22.6
#50 (0.30)	1.9	2.5	15.3	19.0	37.4			14.2
#100 (0.15)	1.8	2.3	7.6	5.4	29.1			7.3
#200 (0.075)	1.8	2.1	4.0	2.3	20.4			4.2
Percentages	11%	12%	55%	16%	6%			100%

Asphalt & Additives:

Asphalt Source:	Amoco
Asphalt Grade (PG):	64-22
Asphalt Content (%):	4.9
Specific Gravity:	1.029
Asphalt Additives:	None
Asphalt Additives (%):	N/A

Compactive Effort:

N_{ini}:	8
N_{des}:	100
N_{max}:	160
$\%G_{mm}$ @ N_{ini}:	87.7
$\%G_{mm}$ @ N_{max}:	97
CF:	1.020

Volumetrics:

VMA @ N_{des}:	14.5
VFA @ N_{des}:	72.4
AV @ N_{des}:	4.0
F/P_{be}:	1.0
P_{be} (%):	4.2

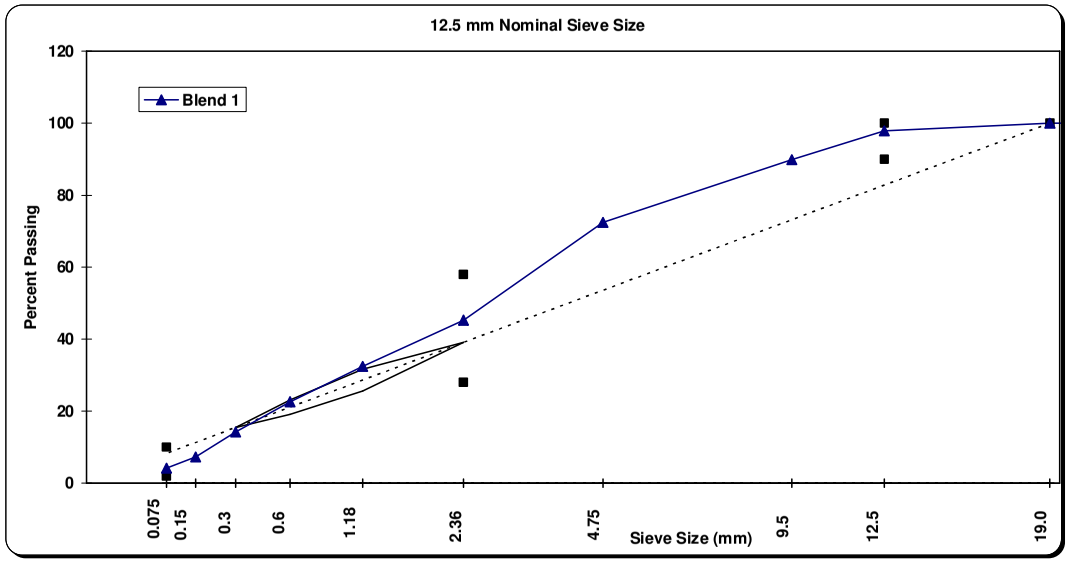

Project: Racine County Racine WI

Project No.:	3230-06-60
Location:	Racine County
Contractor:	Payne & Dolan
Traffic Volume (ESALs):	10,000,000
NMAS (mm):	12.5
Mix Type:	Dense
Date:	10/14/2004
G_{se}	2.723
G_{sb}	2.671
G_{sa}	2.795
Absorption (%)	1.7
Sand Equivalency (%)	93.0
Flat & Elongated (%)	1.0
NAA	45.1
1 Face Crush (%)	95.8
2 Face Crush (%)	95.0

Temperatures:

Mixing:	N/A
Compacting:	160

Sieve Size in (mm):	RAP (3.52% AC)	5/8" Chip	3/8" Chip	Mfg'd Sand	Nat Sand	Agg Source 6	Agg Source 7	Mix
1 (25)	100.0	100.0	100.0	100.0	100.0			100.0
3/4 (19)	100.0	100.0	100.0	100.0	100.0			100.0
1/2 (12.5)	96.5	82.2	100.0	100.0	100.0			97.2
3/8 (9.5)	87.5	33.6	97.9	100.0	100.0			89.1
#4 (4.75)	67.7	4.6	26.2	97.1	86.7			69.2
#8 (2.36)	51.8	3.6	7.6	63.7	69.7			46.8
#16 (1.18)	40.6	3.3	6.5	34.4	52.9			29.2
#30 (0.60)	31.5	3.1	6.1	16.8	32.9			16.8
#50 (0.30)	22.3	3.0	5.7	8.0	12.6			8.4
#100 (0.15)	15.4	2.9	5.3	4.5	6.3			5.2
#200 (0.075)	12.2	2.7	4.5	3.2	4.9			4.1
Percentages	5%	15%	15%	47%	18%			100%

Asphalt & Additives:

Asphalt Source:	CRM Milwaukee
Asphalt Grade (PG):	64-28
Asphalt Content (%):	5.8
Specific Gravity:	1.029
Asphalt Additives:	Polymer
Asphalt Additives (%):	N/A

Compactive Effort:

N_{ini}:	8
N_{des}:	100
N_{max}:	160
$\%G_{mm}$ @ N_{ini}:	87.3
$\%G_{mm}$ @ N_{max}:	97.4
CF:	1.020

Volumetrics:

VMA @ N_{des}:	15.5
VFA @ N_{des}:	74.2
AV @ N_{des}:	4.0
F/P_{be}:	0.8
P_{be} (%):	5.1

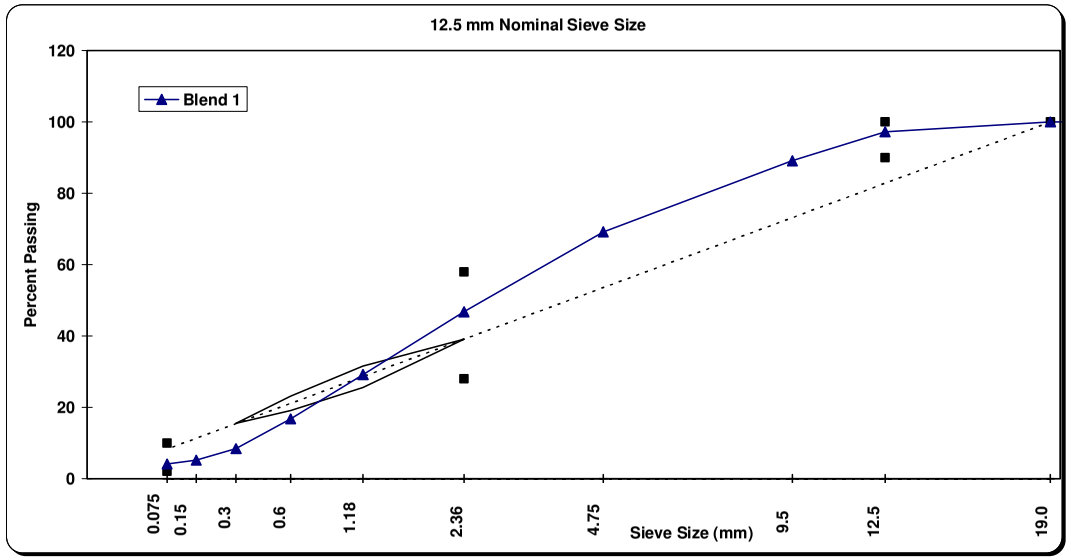

Project: Jackson County Northfield WI I-94 Westbound Northfield to Osseo

Project No.:	1023-04-12
Location:	Jackson County
Contractor:	Mathy - Milestone
Traffic Volume (ESALs):	10,000,000
NMAS (mm):	12.5
Mix Type:	Open
Date:	10/1/2004
G_{se}	2.719
G_{sb}	2.694
G_{sa}	N/A
Absorption (%)	0.6
Sand Equivalency (%)	68.0
Flat & Elongated (%)	18.8
NAA	46.1
1 Face Crush (%)	100.0
2 Face Crush (%)	99.8

Temperatures:

Mixing:	N/A
Compacting:	155

Sieve Size in (mm):	5/8x3/8 Rock	3/8 Minus Rock	3/8" Chip	Fly Ash	Agg Source 5	Agg Source 6	Agg Source 7	Mix
1 (25)	100.0	100.0	100.0	100.0				100.0
3/4 (19)	100.0	100.0	100.0	100.0				100.0
1/2 (12.5)	89.0	100.0	100.0	100.0				92.4
3/8 (9.5)	48.0	100.0	100.0	100.0				64.1
#4 (4.75)	6.9	76.0	41.0	100.0				26.2
#8 (2.36)	4.3	51.0	8.2	100.0				17.5
#16 (1.18)	3.5	35.0	2.6	100.0				14.3
#30 (0.60)	3.0	24.0	1.2	100.0				12.3
#50 (0.30)	2.5	17.0	0.8	99.0				11.0
#100 (0.15)	2.0	12.0	0.6	97.0				9.8
#200 (0.075)	1.5	8.0	0.3	91.0				8.5
Percentages	69%	13%	11%	7%				100%

Asphalt & Additives:

Asphalt Source:	MIF-LaCrosse
Asphalt Grade (PG):	70-22
Asphalt Content (%):	5.9
Specific Gravity:	1.029
Asphalt Additives:	None
Asphalt Additives (%):	N/A

Compactive Effort:

N_{ini}:	8
N_{des}:	100
N_{max}:	160
$\%G_{mm}$ @ N_{ini}:	85.8
$\%G_{mm}$ @ N_{max}:	96.8
CF:	1.020

Volumetrics:

VMA @ N_{des}:	16.9
VFA @ N_{des}:	76.3
AV @ N_{des}:	4.0
F/P_{be}:	1.5
P_{be} (%):	5.5

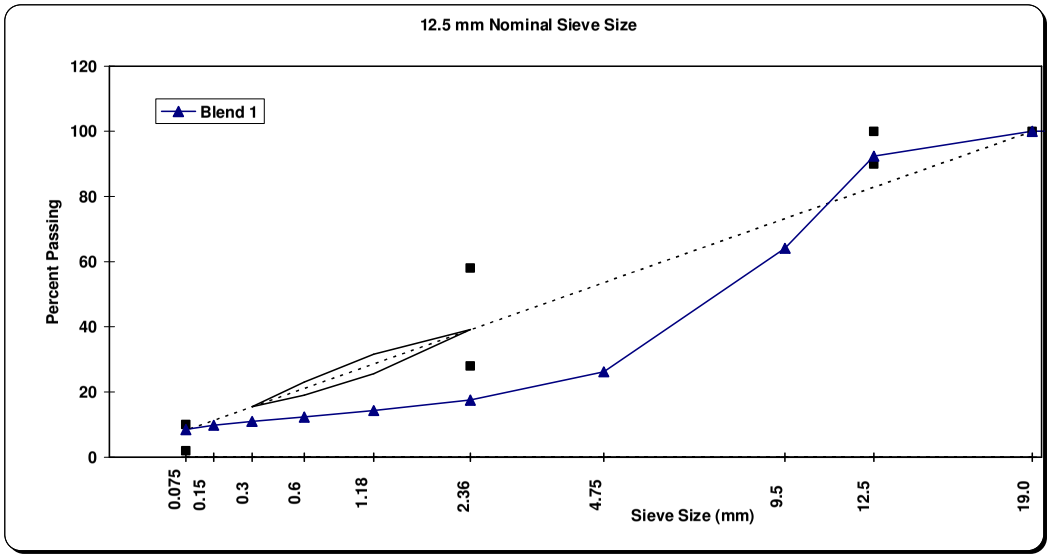

Project: Sheboygan County Cascade WI STH32

Project No.:	4540-14-71
Location:	Sheboygan County
Contractor:	B. R. Amon
Traffic Volume (ESALs):	1,000,000
NMAS (mm):	19.0
Mix Type:	Dense
Date:	8/5/2004
G_{se}	2.759
G_{sb}	2.721
G_{sa}	N/A
Absorption (%)	1.3
Sand Equivalency (%)	89.0
Flat & Elongated (%)	2.1
NAA	42.4
1 Face Crush (%)	71.0
2 Face Crush (%)	0.0

Temperatures:

Mixing:	N/A
Compacting:	143

Sieve Size in (mm):	RAP (4.1%)	7/8" Stone	5/8" Stone	3/8" Stone	Sand	Dust	Agg Source 7	Mix
1 (25)	100.0	100.0	100.0	100.0	100.0	100.0		100.0
3/4 (19)	100.0	97.3	100.0	100.0	100.0	100.0		99.8
1/2 (12.5)	97.9	3.2	59.0	100.0	100.0	100.0		88.8
3/8 (9.5)	92.6	1.7	9.4	87.6	99.7	100.0		81.7
#4 (4.75)	72.5	1.4	2.2	5.0	88.0	91.0		64.0
#8 (2.36)	54.6	1.3	1.8	2.0	71.7	59.4		49.1
#16 (1.18)	41.1	1.2	1.7	1.9	55.6	40.6		37.1
#30 (0.60)	31.9	1.2	1.6	1.8	35.3	30.9		25.4
#50 (0.30)	23.4	1.1	1.6	1.8	12.0	24.1		12.8
#100 (0.15)	16.3	1.1	1.5	1.7	3.2	18.1		6.9
#200 (0.075)	12.0	0.9	1.2	1.4	1.7	13.0		4.8
Percentages	15%	7%	10%	9%	44%	15%		100%

Asphalt & Additives:

Asphalt Source:	Amoco
Asphalt Grade (PG):	58-28
Asphalt Content (%):	4.4
Specific Gravity:	1.026
Asphalt Additives:	None
Asphalt Additives (%):	N/A

Compactive Effort:

N_{ini}:	7
N_{des}:	60
N_{max}:	75
$\%G_{mm}$ @ N_{ini}:	90.3
$\%G_{mm}$ @ N_{max}:	96.4
CF:	1.020

Volumetrics:

VMA @ N_{des}:	13.4
VFA @ N_{des}:	70.9
AV @ N_{des}:	4.0
F/P_{be}:	1.2
P_{be} (%):	3.9

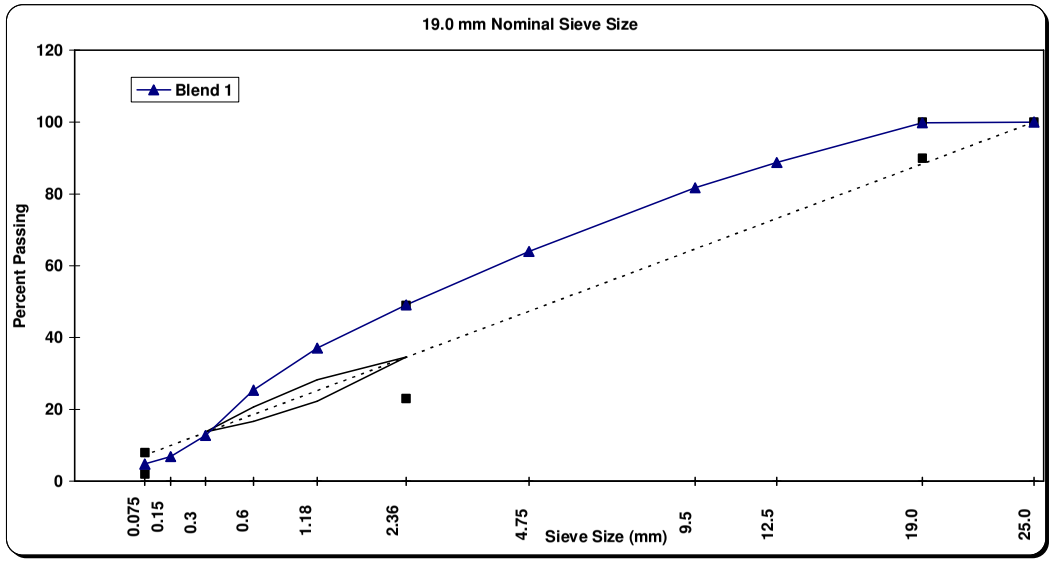

Project: Lincoln County Bloomville WI STH 17

Project No.:	9030-08-70
Location:	Lincoln County
Contractor:	American Asphalt
Traffic Volume (ESALs):	1,000,000
NMAS (mm):	19.0
Mix Type:	Dense
Date:	8/26/2004
G_{se}	2.742
G_{sb}	2.696
G_{sa}	2.742
Absorption (%)	1.2
Sand Equivalency (%)	49.0
Flat & Elongated (%)	1.8
NAA	42.2
1 Face Crush (%)	71.0
2 Face Crush (%)	69.4

Temperatures:

Mixing:	N/A
Compacting:	143

Sieve Size in (mm):	3/4" Rock	Blend Sand	Agg Source 3	Agg Source 4	Agg Source 5	Agg Source 6	Agg Source 7	Mix
1 (25)	100.0	100.0						100.0
3/4 (19)	98.0	100.0						99.2
1/2 (12.5)	70.0	99.0						87.4
3/8 (9.5)	52.0	92.0						76.0
#4 (4.75)	32.0	72.0						56.0
#8 (2.36)	22.0	56.0						42.4
#16 (1.18)	17.0	40.0						30.8
#30 (0.60)	13.0	26.0						20.8
#50 (0.30)	7.0	14.0						11.2
#100 (0.15)	5.0	8.0						6.8
#200 (0.075)	3.5	5.8						4.9
Percentages	40%	60%						100%

Asphalt & Additives:

Asphalt Source:	MIF-LaCrosse
Asphalt Grade (PG):	58-34
Asphalt Content (%):	4.8
Specific Gravity:	1.028
Asphalt Additives:	None
Asphalt Additives (%):	N/A

Compactive Effort:

N_{ini}:	7
N_{des}:	60
N_{max}:	75
$\%G_{mm}$ @ N_{ini}:	89.6
$\%G_{mm}$ @ N_{max}:	96.2
CF:	1.020

Volumetrics:

VMA @ N_{des}:	13.9
VFA @ N_{des}:	71.2
AV @ N_{des}:	4.0
F/P_{be}:	1.2
P_{be} (%):	4.1

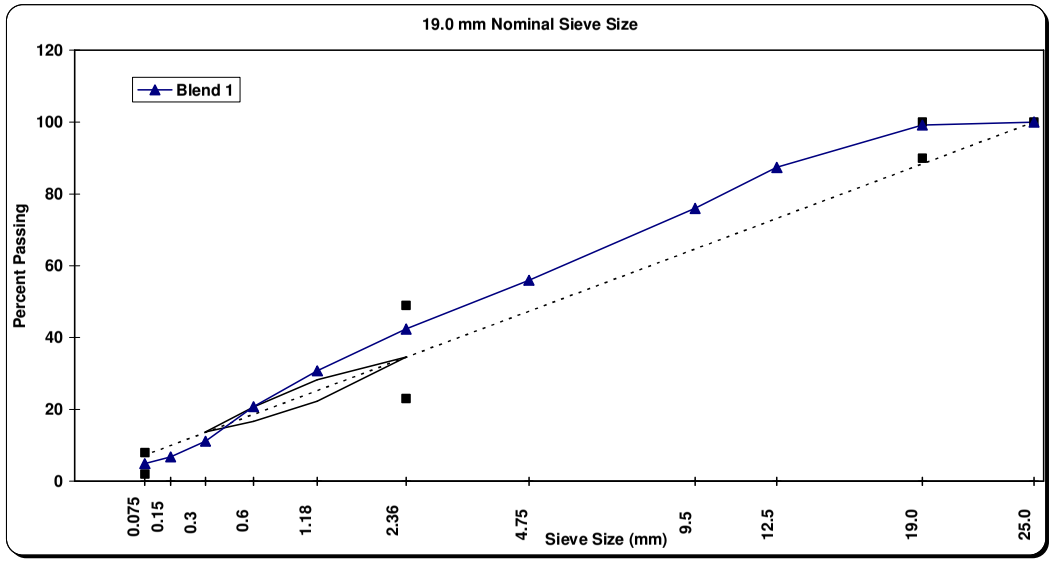

Project: Douglas County Brule WI CTH 13

Project No.:	8510-14-71
Location:	Douglas County
Contractor:	Northwoods Paving
Traffic Volume (ESALs):	300,000
NMAS (mm):	19.0
Mix Type:	Dense
Date:	9/9/2004
G_{se}	2.811
G_{sb}	2.772
G_{sa}	2.811
Absorption (%)	0.9
Sand Equivalency (%)	71.0
Flat & Elongated (%)	2.0
NAA	42.4
1 Face Crush (%)	96.3
2 Face Crush (%)	96.1

Temperatures:

Mixing:	N/A
Compacting:	143

Sieve Size in (mm):	15/16 Rock	3/8 Minus	Nat Sand	RAP (4.4% AC)	Agg Source 5	Agg Source 6	Agg Source 7	Mix
1 (25)	100.0	100.0	100.0	100.0				100.0
3/4 (19)	92.0	100.0	100.0	100.0				97.4
1/2 (12.5)	43.0	100.0	99.0	93.0				79.9
3/8 (9.5)	19.0	100.0	98.0	88.0				70.9
#4 (4.75)	2.0	68.0	96.0	69.0				53.9
#8 (2.36)	1.8	40.0	94.0	57.0				44.5
#16 (1.18)	1.7	26.0	91.0	45.0				38.4
#30 (0.60)	1.6	16.0	78.0	32.0				30.4
#50 (0.30)	1.5	11.0	42.0	21.0				17.7
#100 (0.15)	1.4	7.6	9.0	13.0				6.7
#200 (0.075)	1.0	5.0	2.0	9.0				3.5
Percentages	33%	25%	27%	15%				100%

Asphalt & Additives:

Asphalt Source:	Murphy
Asphalt Grade (PG):	58-28
Asphalt Content (%):	5.4
Specific Gravity:	1.03
Asphalt Additives:	None
Asphalt Additives (%):	N/A

Compactive Effort:

N_{ini}:	6
N_{des}:	40
N_{max}:	60
$\%G_{mm}$ @ N_{ini}:	91.2
$\%G_{mm}$ @ N_{max}:	96.8
CF:	1.020

Volumetrics:

VMA @ N_{des}:	15.8
VFA @ N_{des}:	74.6
AV @ N_{des}:	4.0
F/P_{be}:	0.7
P_{be} (%):	4.9

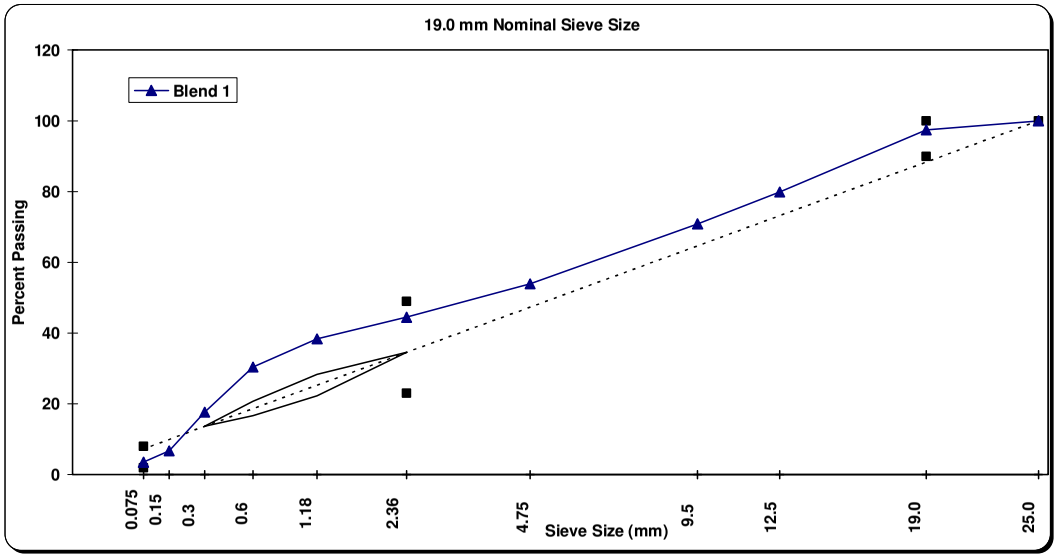

Project: Dane County Waunakee WI STH 113

Project No.:	5992-04-14
Location:	Dane County
Contractor:	Payne & Dolan
Traffic Volume (ESALs):	3,000,000
NMAS (mm):	19.0
Mix Type:	Dense
Date:	6/30/2004
G_{se}	2.737
G_{sb}	2.648
G_{sa}	2.765
Absorption (%)	1.6
Sand Equivalency (%)	80.0
Flat & Elongated (%)	0.0
NAA	43.9
1 Face Crush (%)	100.0
2 Face Crush (%)	100.0

Temperatures:

Mixing:	N/A
Compacting:	142

Sieve Size in (mm):	5/8" Chip	3/8" Chip	1/4" Screenings	Man Sand	Nat Sand	RAP	Agg Source 7	Mix
1 (25)	100.0	100.0	100.0	100.0	100.0	100.0		100.0
3/4 (19)	99.3	100.0	100.0	100.0	100.0	100.0		99.9
1/2 (12.5)	40.0	95.3	99.8	100.0	100.0	98.3		89.6
3/8 (9.5)	16.8	74.7	99.3	99.1	100.0	87.8		81.9
#4 (4.75)	5.0	13.1	83.3	77.9	99.5	65.7		62.1
#8 (2.36)	4.2	7.3	63.6	48.8	84.6	51.3		46.1
#16 (1.18)	4.0	6.4	50.7	28.1	70.7	42.1		34.5
#30 (0.60)	3.9	6.1	42.7	16.2	59.3	36.0		26.9
#50 (0.30)	3.7	5.7	34.6	7.8	32.4	25.6		16.0
#100 (0.15)	3.3	4.8	25.1	4.5	8.4	16.1		7.3
#200 (0.075)	2.5	3.5	15.3	2.5	1.9	10.7		3.8
Percentages	16%	14%	5%	31%	26%	8%		100%

Asphalt & Additives:

Asphalt Source:	Koch
Asphalt Grade (PG):	58-28
Asphalt Content (%):	5.11
Specific Gravity:	1.032
Asphalt Additives:	None
Asphalt Additives (%):	N/A

Compactive Effort:

N_{ini}:	7
N_{des}:	75
N_{max}:	115
$\%G_{mm}$ @ N_{ini}:	89.7
$\%G_{mm}$ @ N_{max}:	96.7
CF:	1.020

Volumetrics:

VMA @ N_{des}:	13.2
VFA @ N_{des}:	69.6
AV @ N_{des}:	4.0
F/P_{be}:	1.1
P_{be} (%):	3.9

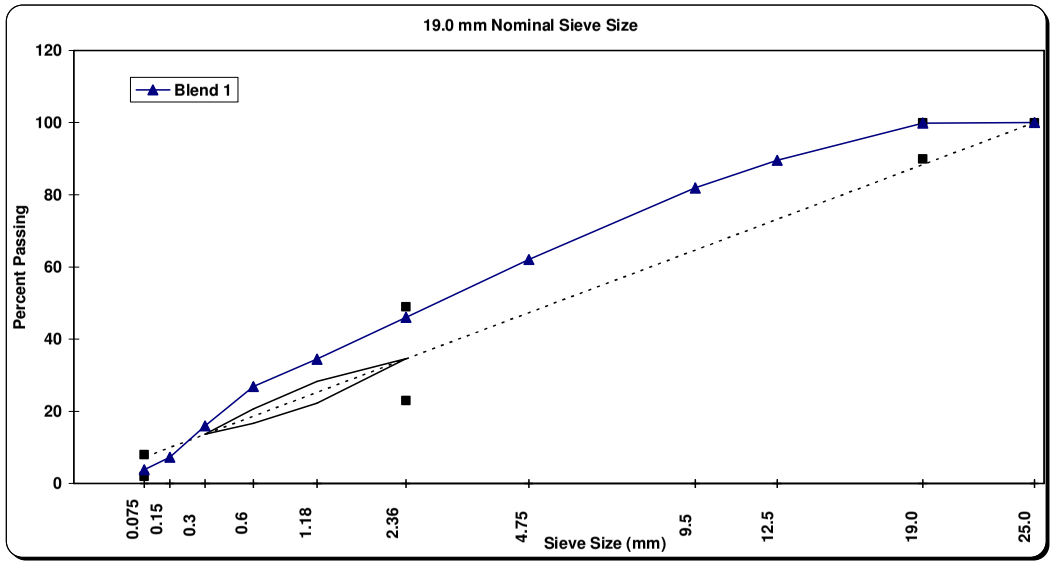

Project: Marathon County Mosinee WI USH 51

Project No.:	6370-00-60
Location:	Marathon County
Contractor:	American - Mathy
Traffic Volume (ESALs):	3,000,000
NMAS (mm):	19.0
Mix Type:	Dense
Date:	7/7/2004
G_{se}	2.699
G_{sb}	2.649
G_{sa}	N/A
Absorption (%)	0.4
Sand Equivalency (%)	88.0
Flat & Elongated (%)	2.1
NAA	43.3
1 Face Crush (%)	97.1
2 Face Crush (%)	97.0

Temperatures:

Mixing:	N/A
Compacting:	143

Sieve Size in (mm):	3/4" Rock	3/8" Rock	3/16 Screen	Blend Sand	Man Sand	RAP (4.0% AC)	Agg Source 7	Mix
1 (25)	100.0	100.0	100.0	100.0	100.0	100.0		100.0
3/4 (19)	98.0	100.0	100.0	100.0	100.0	100.0		99.4
1/2 (12.5)	61.0	100.0	100.0	99.0	100.0	97.0		87.8
3/8 (9.5)	29.0	100.0	100.0	98.0	100.0	90.0		77.3
#4 (4.75)	6.6	29.0	97.0	94.0	100.0	73.0		60.5
#8 (2.36)	3.8	10.0	66.0	88.0	67.0	58.0		45.5
#16 (1.18)	2.9	5.6	42.0	77.0	43.0	47.0		34.3
#30 (0.60)	2.4	4.4	28.0	58.0	24.0	36.0		24.2
#50 (0.30)	2.1	3.5	17.0	10.0	10.0	18.0		8.8
#100 (0.15)	1.8	3.0	11.0	1.2	3.5	11.0		4.4
#200 (0.075)	1.5	2.4	10.0	0.7	1.5	8.0		3.4
Percentages	30%	10%	15%	20%	15%	10%		100%

Asphalt & Additives:

Asphalt Source:	MIF-LaCrosse
Asphalt Grade (PG):	58-28
Asphalt Content (%):	5.0
Specific Gravity:	1.029
Asphalt Additives:	None
Asphalt Additives (%):	N/A

Compactive Effort:

N_{ini}:	7
N_{des}:	75
N_{max}:	115
$\%G_{mm}$ @ N_{ini}:	90.1
$\%G_{mm}$ @ N_{max}:	96.5
CF:	1.020

Volumetrics:

VMA @ N_{des}:	14.9
VFA @ N_{des}:	73.1
AV @ N_{des}:	4.0
F/P_{be}:	0.7
P_{be} (%):	4.3

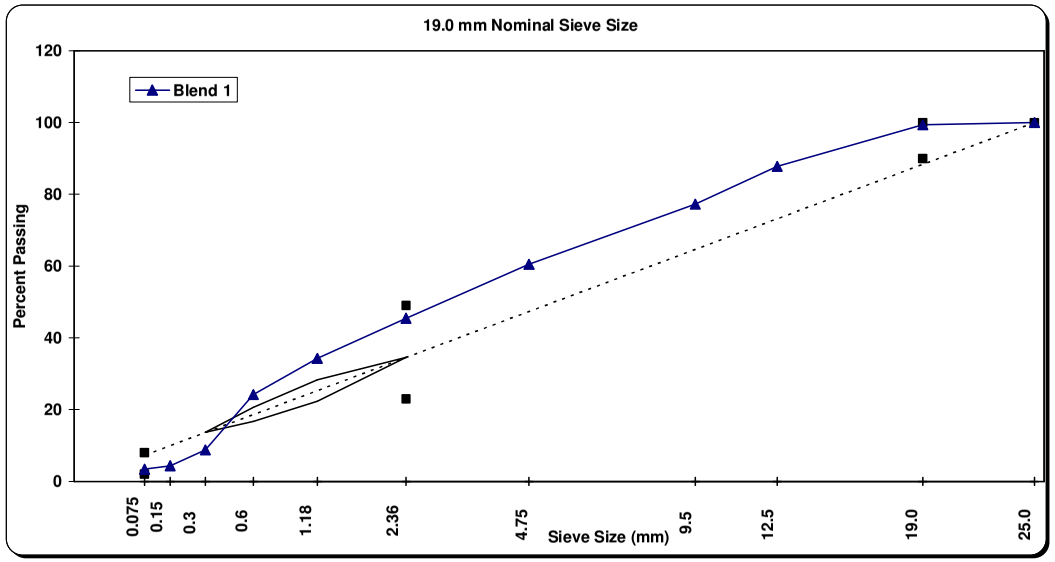

Project: Barron County Cumberland USH 63

Project No.:	1550-17-71
Location:	Barron County
Contractor:	Monarch Paving
Traffic Volume (ESALs):	3,000,000
NMAS (mm):	19.0
Mix Type:	Dense
Date:	9/9/2004
G_{se}	2.781
G_{sb}	2.738
G_{sa}	2.781
Absorption (%)	0.8
Sand Equivalency (%)	74.0
Flat & Elongated (%)	1.7
NAA	43.2
1 Face Crush (%)	63.3
2 Face Crush (%)	61.1

Temperatures:

Mixing:	N/A
Compacting:	143

Sieve Size in (mm):	7/8x3/8 Rock	5/8x3/8 Rock	Man Sand	Nat Sand	RAP (4.2%)	Agg Source 6	Agg Source 7	Mix
1 (25)	100.0	100.0	100.0	100.0	100.0			100.0
3/4 (19)	100.0	100.0	100.0	100.0	98.0			99.5
1/2 (12.5)	52.0	81.0	100.0	98.0	93.0			92.5
3/8 (9.5)	6.5	30.0	100.0	92.0	85.0			80.7
#4 (4.75)	1.2	2.4	67.0	77.0	68.0			60.2
#8 (2.36)	1.0	2.0	42.0	65.0	57.0			47.1
#16 (1.18)	1.0	1.0	28.0	50.0	46.0			35.7
#30 (0.60)	0.9	1.0	21.0	31.0	35.0			24.7
#50 (0.30)	0.9	1.0	14.0	11.0	21.0			12.6
#100 (0.15)	0.8	1.0	9.8	4.6	11.0			6.9
#200 (0.075)	0.8	1.0	6.5	3.1	7.6			4.7
Percentages	7%	9%	25%	34%	25%			100%

Asphalt & Additives:

Asphalt Source:	Koch
Asphalt Grade (PG):	58-28
Asphalt Content (%):	4.6
Specific Gravity:	1.03
Asphalt Additives:	None
Asphalt Additives (%):	N/A

Compactive Effort:

N_{ini}:	7
N_{des}:	75
N_{max}:	115
$\%G_{mm}$ @ N_{ini}:	89.7
$\%G_{mm}$ @ N_{max}:	97.1
CF:	1.020

Volumetrics:

VMA @ N_{des}:	13.5
VFA @ N_{des}:	70.3
AV @ N_{des}:	4.0
F/P_{be}:	1.2
P_{be} (%):	4

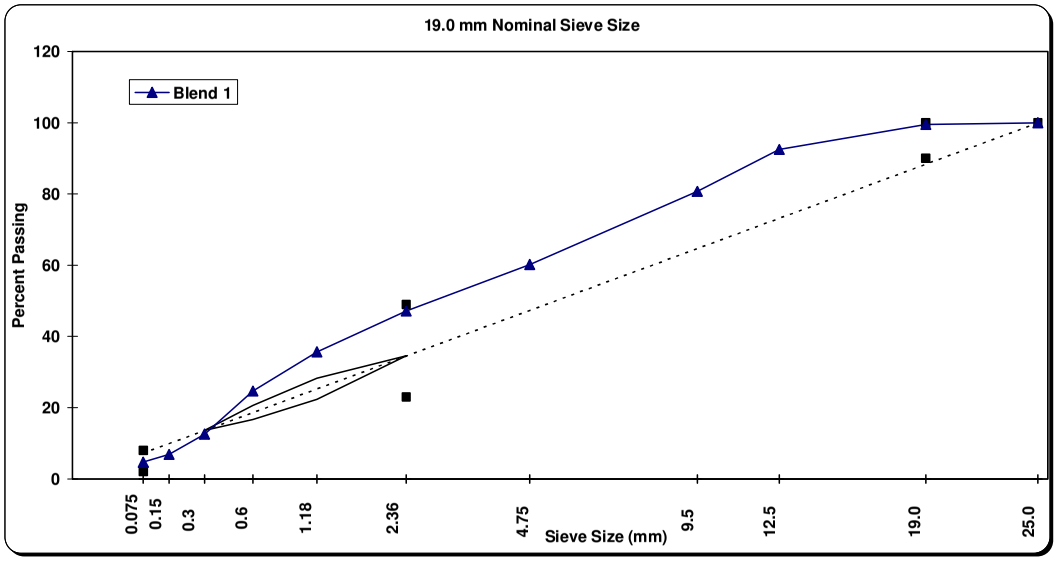

Project: Langlade County Antigo WI City of Antigo

Project No.:	1605-04-70
Location:	Langlade County
Contractor:	Northeast Asphalt
Traffic Volume (ESALs):	10,000,000
NMAS (mm):	19.0
Mix Type:	Dense
Date:	6/15/2004
G_{se}	2.700
G_{sb}	2.688
G_{sa}	2.723
Absorption (%)	0.5
Sand Equivalency (%)	85.0
Flat & Elongated (%)	0.4
NAA	44.9
1 Face Crush (%)	93.8
2 Face Crush (%)	91.5

Temperatures:

Mixing:	N/A
Compacting:	143

Sieve Size in (mm):	3/4" Chip	5/8"x1/2" Chip	1/2"x1/4" Chip	1/4" Screenings	Man Sand	Screened Sand	Agg Source 7	Mix
1 (25)	100.0	100.0	100.0	100.0	100.0	100.0		100.0
3/4 (19)	97.9	100.0	100.0	100.0	100.0	100.0		99.7
1/2 (12.5)	41.8	83.4	100.0	100.0	100.0	100.0		89.6
3/8 (9.5)	13.2	27.6	85.8	100.0	100.0	99.5		78.2
#4 (4.75)	3.5	6.9	10.3	88.5	76.0	84.6		55.3
#8 (2.36)	2.6	5.1	6.0	60.4	44.7	68.1		43.2
#16 (1.18)	2.3	4.2	4.9	44.2	27.1	55.8		28.0
#30 (0.60)	2.2	3.8	4.2	33.3	17.0	37.2		19.1
#50 (0.30)	2.0	3.3	3.6	24.5	9.0	15.2		10.3
#100 (0.15)	1.7	2.7	3.0	15.7	3.7	6.4		5.4
#200 (0.075)	1.3	2.0	2.2	10.2	1.7	3.9		3.9
Percentages	15%	10%	10%	13%	28%	24%		100%

Asphalt & Additives:

Asphalt Source:	CRM Gladstone
Asphalt Grade (PG):	58-34
Asphalt Content (%):	4.3
Specific Gravity:	1.03
Asphalt Additives:	Polymer
Asphalt Additives (%):	N/A

Compactive Effort:

N_{ini}:	8
N_{des}:	100
N_{max}:	160
$\%G_{mm}$ @ N_{ini}:	89
$\%G_{mm}$ @ N_{max}:	96.9
CF:	1.020

Volumetrics:

VMA @ N_{des}:	13.7
VFA @ N_{des}:	70.8
AV @ N_{des}:	4.0
F/P_{be}:	0.951219512
P_{be} (%):	4.1

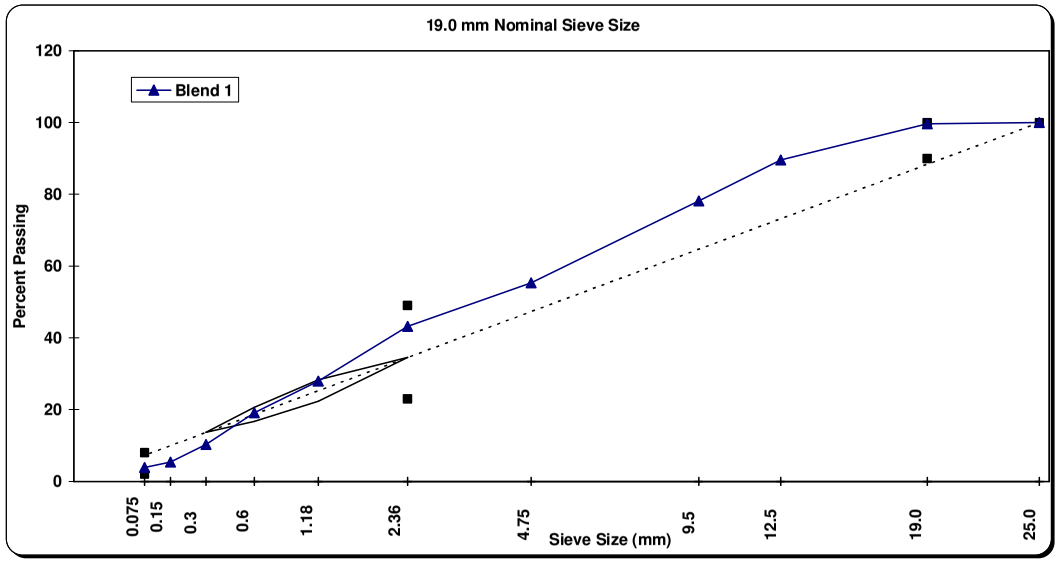

Project: Jackson County Northfield WI I-94 Westbound Northfield to Osseo

Project No.:	1023-04-12
Location:	Jackson County
Contractor:	Mathy - Milestone
Traffic Volume (ESALs):	30,000,000
NMAS (mm):	19.0
Mix Type:	Dense
Date:	9/29/2004
G_{se}	2.648
G_{sb}	2.635
G_{sa}	N/A
Absorption (%)	0.7
Sand Equivalency (%)	75.0
Flat & Elongated (%)	3.7
NAA	45.1
1 Face Crush (%)	100.0
2 Face Crush (%)	93.3

Temperatures:

Mixing:	N/A
Compacting:	155

Sieve Size in (mm):	7/8"x3/8" Rock	3/8" Minus Roc	Washed Sand	Agg Source 4	Agg Source 5	Agg Source 6	Agg Source 7	Mix
1 (25)	100.0	100.0	100.0					100.0
3/4 (19)	99.0	100.0	100.0					99.4
1/2 (12.5)	54.0	100.0	100.0					72.4
3/8 (9.5)	23.0	100.0	100.0					53.8
#4 (4.75)	1.2	76.0	100.0					33.5
#8 (2.36)	0.7	51.0	86.0					24.3
#16 (1.18)	0.6	35.0	78.0					18.7
#30 (0.60)	0.5	24.0	60.0					13.5
#50 (0.30)	0.5	16.0	26.0					7.7
#100 (0.15)	0.5	10.0	4.4					3.7
#200 (0.075)	0.4	8.0	1.4					2.8
Percentages	60%	30%	10%					100%

Asphalt & Additives:

Asphalt Source:	MIF-LaCrosse
Asphalt Grade (PG):	64-28
Asphalt Content (%):	4.5
Specific Gravity:	1.029
Asphalt Additives:	None
Asphalt Additives (%):	N/A

Compactive Effort:

N_{ini}:	8
N_{des}:	100
N_{max}:	160
$\%G_{mm}$ @ N_{ini}:	86.4
$\%G_{mm}$ @ N_{max}:	97.7
CF:	1.020

Volumetrics:

VMA @ N_{des}:	13.9
VFA @ N_{des}:	71.3
AV @ N_{des}:	4.0
F/P_{be}:	0.6
P_{be} (%):	4.3

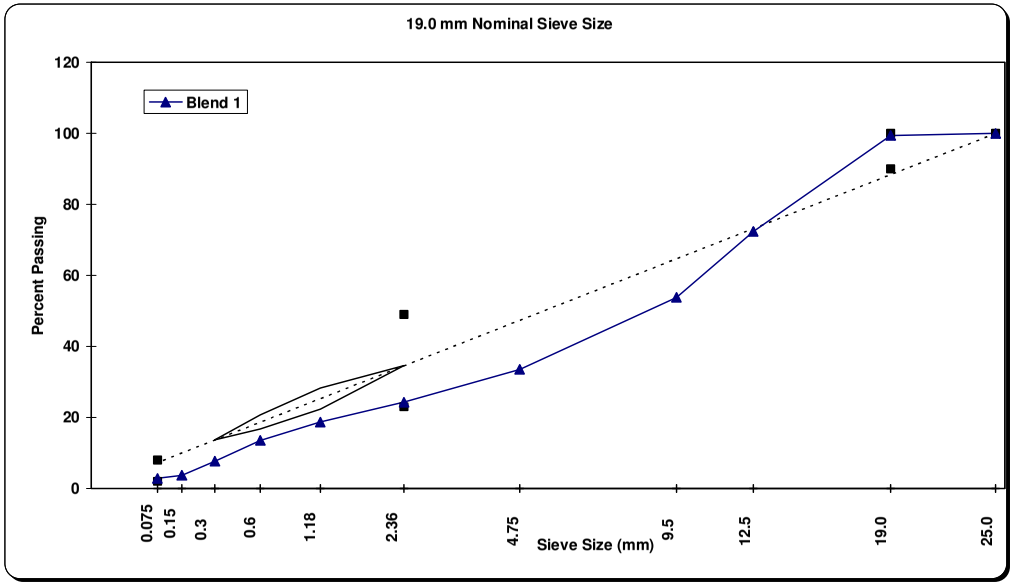

Project: Oneida County Tomahawk USH 8 - Birchwood Drive STH 17

Project No.:	9040-05-70
Location:	Oneida County
Contractor:	American - Mathy
Traffic Volume (ESALs):	3,000,000
NMAS (mm):	25.0
Mix Type:	Open
Date:	6/16/2004
G_{se}	2.723
G_{sb}	2.693
G_{sa}	N/A
Absorption (%)	0.7
Sand Equivalency (%)	N/A
Flat & Elongated (%)	0.7
NAA	43.4
1 Face Crush (%)	80.1
2 Face Crush (%)	70.4

Temperatures:

Mixing:	N/A
Compacting:	142

Sieve Size in (mm):	3/4" Gravel	Blend Sand	RAP (3.8%AC)	Agg Source 4	Agg Source 5	Agg Source 6	Agg Source 7	Mix
1 (25)	100.0	100.0	100.0					100.0
3/4 (19)	72.0	100.0	98.0					81.3
1/2 (12.5)	9.5	99.0	89.0					38.3
3/8 (9.5)	6.0	94.0	83.0					34.1
#4 (4.75)	5.3	81.0	69.0					28.8
#8 (2.36)	5.0	69.0	57.0					24.4
#16 (1.18)	4.8	55.0	47.0					20.4
#30 (0.60)	4.5	39.0	39.0					16.6
#50 (0.30)	3.3	17.0	24.0					9.8
#100 (0.15)	2.1	7.5	13.0					5.4
#200 (0.075)	1.4	4.0	9.0					3.6
Percentages	65%	10%	25%					100%

Asphalt & Additives:

Asphalt Source:	MIF-LaCrosse
Asphalt Grade (PG):	58-28
Asphalt Content (%):	3.4
Specific Gravity:	1.029
Asphalt Additives:	None
Asphalt Additives (%):	N/A

Compactive Effort:

N_{ini}:	7
N_{des}:	75
N_{max}:	115
$\%G_{mm}$ @ N_{ini}:	87.6
$\%G_{mm}$ @ N_{max}:	96.6
CF:	1.020

Volumetrics:

VMA @ N_{des}:	11.2
VFA @ N_{des}:	64.3
AV @ N_{des}:	4.0
F/P_{be}:	1.2
P_{be} (%):	3.0

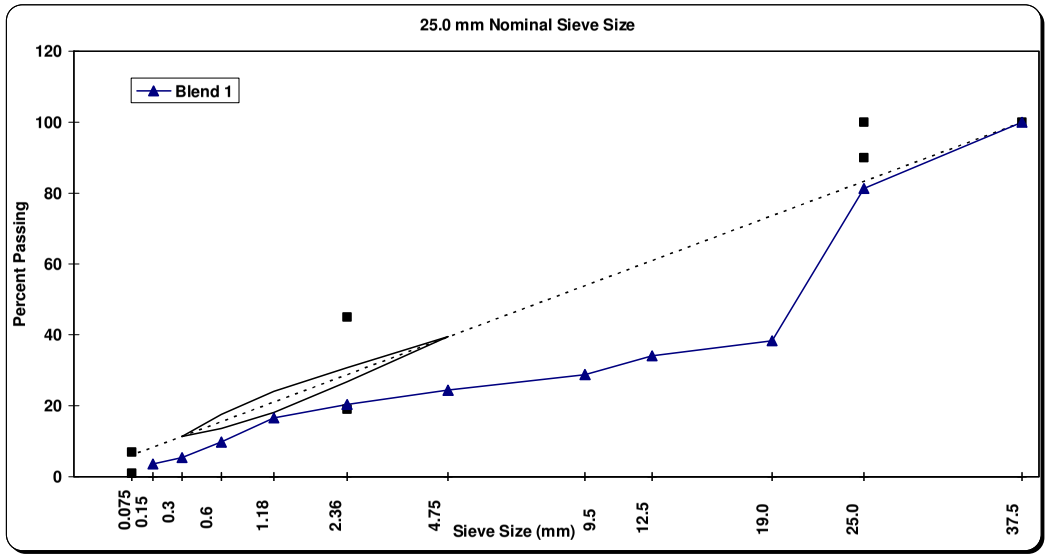

APPENDIX B. SPECIMEN VOLUMETRICS BEFORE SAWING/CORING

Project	Specimen ID	Compacted	AC%	Target AV%	Bulk Specific Gravity					MTSG	Done	Air Voids	Gry. Ht.	Gmb Est.	Actual Corr. Fac.
					Dry Wt.	Submerged Wt.	SSD Wt.	BSG	Done						
Sauk Cty Baraboo 12.5mm E-0.3	BAR-OP-7.0-12.5-E0.3-A	√	-	7.0	6792.8	3859.2	6801.3	2.309	√	2.486	√	7.1	168.4	2.283	1.011
	BAR-OP-7.0-12.5-E0.3-B	√	-	7.0	6796.2	3861.2	6812.3	2.303	√	2.486	√	7.4	169.0	2.276	1.012
	BAR-OP-7.0-12.5-E0.3-C	√	-	7.0	6794.6	3866.3	6805.8	2.311	√	2.486	√	7.0	168.3	2.285	1.012
	BAR-OP-7.0-12.5-E0.3-D	√	-	7.0	6794.7	3863.3	6809	2.307	√	2.486	√	7.2	168.8	2.278	1.013
	BAR-OP-7.0-12.5-E0.3-E	√	-	7.0	6803.1	3865.5	6815.9	2.306	√	2.486	√	7.2	168.9	2.279	1.012
	BAR-OP-7.0-12.5-E0.3-F	√	-	7.0	6800.3	3864.4	6812.9	2.306	√	2.486	√	7.2	168.9	2.278	1.012
	BAR-OP-4.0-12.5-E0.3-A	√	-	4.0	7047.9	4080.1	7055.3	2.369	√	2.486	√	4.7	170.2	2.343	1.011
	BAR-OP-4.0-12.5-E0.3-B	√	-	4.0	7050.3	4078.2	7054.9	2.368	√	2.486	√	4.7	170.4	2.341	1.012
	BAR-OP-4.0-12.5-E0.3-C	√	-	4.0	7050.9	4084.9	7056.5	2.373	√	2.486	√	4.5	170.4	2.342	1.013
	BAR-OP-4.0-12.5-E0.3-D	√	-	4.0	7046	4082.2	7053.8	2.371	√	2.486	√	4.6	170.3	2.341	1.013
	BAR-OP-4.0-12.5-E0.3-E	√	-	4.0	7048.8	4082.1	7054	2.372	√	2.486	√	4.6	170.2	2.344	1.012
	BAR-OP-4.0-12.5-E0.3-F	√	-	4.0	7054.5	4083.6	7059.9	2.370	√	2.486	√	4.6	170.4	2.343	1.012
	BAR-OP-10.0-12.5-E0.3-A	√	-	10.0	6587.6	3709	6617.4	2.265	√	2.486	√	8.9	167.1	2.231	1.015
	BAR-OP-10.0-12.5-E0.3-B	√	-	10.0	6606	3699.8	6629.3	2.255	√	2.486	√	9.3	167.9	2.226	1.013
	BAR-OP-10.0-12.5-E0.3-C	√	-	10.0	6611.5	3717.8	6637.3	2.265	√	2.486	√	8.9	167.4	2.235	1.013
	BAR-OP-10.0-12.5-E0.3-D	√	-	10.0	6602.2	3698	6628.7	2.253	√	2.486	√	9.4	168.0	2.224	1.013
	BAR-OP-10.0-12.5-E0.3-E	√	-	10.0	6598.6	3714.7	6628	2.265	√	2.486	√	8.9	167.3	2.232	1.015
	BAR-OP-10.0-12.5-E0.3-F	√	-	10.0	6607.9	3704.3	6643.3	2.248	√	2.486	√	9.6	168.6	2.218	1.014
	BAR-BU-7.0-12.5-E0.3-A	√	+0.3	7.0	6741.9	3823.5	6754.2	2.300	√	2.474	√	7.0	168.1	2.270	1.014
	BAR-BU-7.0-12.5-E0.3-B	√	+0.3	7.0	6723.3	3813.8	6735.5	2.301	√	2.474	√	7.0	167.5	2.271	1.013
	BAR-BU-7.0-12.5-E0.3-C	√	+0.3	7.0	6777.8	3849.6	6792.1	2.303	√	2.474	√	6.9	169.8	2.259	1.020
	BAR-BU-7.0-12.5-E0.3-D	√	+0.3	7.0	6768.3	3851.3	6782.4	2.309	√	2.474	√	6.7	168.1	2.278	1.013
	BAR-BU-7.0-12.5-E0.3-E	√	+0.3	7.0	6767.6	3847.4	6782.4	2.306	√	2.474	√	6.8	168.6	2.271	1.015
	BAR-BU-7.0-12.5-E0.3-F	√	+0.3	7.0	6756.3	3847.4	6771.9	2.310	√	2.474	√	6.6	167.9	2.277	1.015

Project	Specimen ID	Compacted	AC%	Target AV%	Bulk Specific Gravity					MTSG		Air Voids	Gry. Ht.	Gmb Est.	Actual Corr. Fac.
					Dry Wt.	Submerged Wt.	SSD Wt.	BSG	Done		Done				
Taylor Cty Medford 12.5mm E-1	MED-OP-7.0-12.5-E1-A	√	-	7.0	6850.1	3928.2	6879.4	2.321	√	2.502	√	7.2	168.7	2.298	1.010
	MED-OP-7.0-12.5-E1-B	√	-	7.0	6841.2	3921.2	6870.6	2.320	√	2.502	√	7.3	168.4	2.299	1.009
	MED-OP-7.0-12.5-E1-C	√	-	7.0	6843.9	3930.3	6875	2.324	√	2.502	√	7.1	168.4	2.300	1.011
	MED-OP-7.0-12.5-E1-D	√	-	7.0	6844.9	3940.1	6883.3	2.326	√	2.502	√	7.1	168.6	2.297	1.012
	MED-OP-7.0-12.5-E1-E	√	-	7.0	6847.4	3943.8	6887.8	2.326	√	2.502	√	7.0	168.5	2.300	1.011
	MED-OP-7.0-12.5-E1-F	√	-	7.0	6846.5	3937.6	6877.8	2.329	√	2.502	√	6.9	169.4	2.287	1.018
	MED-OP-4.0-12.5-E1-A	√	-	4.0	7066.1	4122.5	7075.2	2.393	√	2.502	√	4.4	168.5	2.373	1.008
	MED-OP-4.0-12.5-E1-B	√	-	4.0	7069.6	4118.3	7076.3	2.390	√	2.502	√	4.5	168.4	2.376	1.006
	MED-OP-4.0-12.5-E1-C	√	-	4.0	7064.9	4123.4	7074.6	2.394	√	2.502	√	4.3	168.8	2.368	1.011
	MED-OP-4.0-12.5-E1-D	√	-	4.0	7064.6	4123.7	7075.8	2.393	√	2.502	√	4.4	168.9	2.367	1.011
	MED-OP-4.0-12.5-E1-E	√	-	4.0	7075.7	4132.4	7083.6	2.398	√	2.502	√	4.2	168.7	2.373	1.010
	MED-OP-4.0-12.5-E1-F	√	-	4.0	7071.1	4123.5	7079.4	2.392	√	2.502	√	4.4	168.9	2.369	1.010
	MED-OP-10.0-12.5-E1-A	√	-	10.0	6617.4	3778.2	6718.1	2.251	√	2.502	√	10.0	168.7	2.220	1.014
	MED-OP-10.0-12.5-E1-B	√	-	10.0	6617	3768.8	6705.8	2.253	√	2.502	√	10.0	168.4	2.224	1.013
	MED-OP-10.0-12.5-E1-C	√	-	10.0	6616.8	3772.8	6704.8	2.257	√	2.502	√	9.8	168.4	2.223	1.015
	MED-OP-10.0-12.5-E1-D	√	-	10.0	6627.2	3785.2	6719.4	2.259	√	2.502	√	9.7	168.6	2.224	1.015
	MED-OP-10.0-12.5-E1-E	√	-	10.0	6617.3	3789.4	6709.5	2.266	√	2.502	√	9.4	168.5	2.222	1.020
	MED-OP-10.0-12.5-E1-F	√	-	10.0	6617.1	3785.7	6726.4	2.250	√	2.502	√	10.1	169.4	2.210	1.018
	MED-BU-7.0-12.5-E1-A	√	+0.3	7.0	6784.2	3888.6	6817.1	2.317	√	2.489	√	6.9	168.5	2.278	1.017
	MED-BU-7.0-12.5-E1-B	√	+0.3	7.0	6791.3	3880.6	6815.8	2.314	√	2.489	√	7.0	168.4	2.282	1.014
	MED-BU-7.0-12.5-E1-C	√	+0.3	7.0	6815	3905.6	6839.7	2.323	√	2.489	√	6.7	168.8	2.285	1.017
	MED-BU-7.0-12.5-E1-D	√	+0.3	7.0	6807.6	3899.7	6834.7	2.319	√	2.489	√	6.8	168.9	2.281	1.017
	MED-BU-7.0-12.5-E1-E	√	+0.3	7.0	6819	3909.8	6845.8	2.323	√	2.489	√	6.7	168.7	2.287	1.015
	MED-BU-7.0-12.5-E1-F	√	+0.3	7.0	6815.1	3909.6	6847.5	2.320	√	2.489	√	6.8	168.9	2.283	1.016

Project	Specimen ID	Compacted	AC%	Target AV%	Bulk Specific Gravity					MTSG		Air Voids	Gry. Ht.	Gmb Est.	Actual Corr. Fac.
					Dry Wt.	Submerged Wt.	SSD Wt.	BSG	Done		Done				
Waushara Cty Wautoma 12.5mm E-1	OMA-OP-7.0-12.5-E1-A	√	-	7.0	6946.1	3985.5	6960.3	2.335	√	2.532	√	7.8	169.8	2.315	1.009
	OMA-OP-7.0-12.5-E1-B	√	-	7.0	6939.4	3990.8	6956.9	2.340	√	2.532	√	7.6	169.5	2.317	1.010
	OMA-OP-7.0-12.5-E1-C	√	-	7.0	6939.5	3997.6	6957.3	2.345	√	2.532	√	7.4	169.3	2.320	1.011
	OMA-OP-7.0-12.5-E1-D	√	-	7.0	6939	3985	6957.1	2.335	√	2.532	√	7.8	169.4	2.318	1.007
	OMA-OP-7.0-12.5-E1-E	√	-	7.0	6934.2	3990.1	6956.7	2.337	√	2.532	√	7.7	169.6	2.314	1.010
	OMA-OP-7.0-12.5-E1-F	√	-	7.0	6935.7	3991.8	6955.9	2.340	√	2.532	√	7.6	169.5	2.316	1.011
	OMA-OP-4.0-12.5-E1-A	√	-	4.0	7162	4190.9	7166.4	2.407	√	2.532	√	4.9	169.9	2.385	1.009
	OMA-OP-4.0-12.5-E1-B	√	-	4.0	7160.5	4197.4	7165.6	2.412	√	2.532	√	4.7	169.9	2.385	1.012
	OMA-OP-4.0-12.5-E1-C	√	-	4.0	7162.5	4196.4	7167.6	2.411	√	2.532	√	4.8	169.8	2.387	1.010
	OMA-OP-4.0-12.5-E1-D	√	-	4.0	7157.2	4190.6	7161.5	2.409	√	2.532	√	4.8	169.7	2.387	1.009
	OMA-OP-4.0-12.5-E1-E	√	-	4.0	7160.5	4197	7166.3	2.412	√	2.532	√	4.7	169.8	2.386	1.011
	OMA-OP-4.0-12.5-E1-F	√	-	4.0	7160.2	4196.5	7165.4	2.412	√	2.532	√	4.7	169.8	2.386	1.011
	OMA-OP-10.0-12.5-E1-A	√	-	10.0	6721.2	3824.5	6764	2.287	√	2.532	√	9.7	168.3	2.260	1.012
	OMA-OP-10.0-12.5-E1-B	√	-	10.0	6715.9	3822.3	6775.4	2.274	√	2.532	√	10.2	169.2	2.246	1.013
	OMA-OP-10.0-12.5-E1-C	√	-	10.0	6712.3	3802.2	6758.8	2.270	√	2.532	√	10.3	169.0	2.248	1.010
	OMA-OP-10.0-12.5-E1-D	√	-	10.0	6717.2	3795.9	6768.8	2.259	√	2.532	√	10.8	169.8	2.239	1.009
	OMA-OP-10.0-12.5-E1-E	√	-	10.0	6717.2	3791	6766.3	2.258	√	2.532	√	10.8	170.1	2.235	1.010
	OMA-OP-10.0-12.5-E1-F	√	-	10.0	6713.9	3823.3	6779.6	2.271	√	2.532	√	10.3	169.5	2.241	1.013
	OMA-BU-7.0-12.5-E1-A	√	+0.3	7.0	6903.5	3965.6	6921.8	2.335	√	2.521	√	7.4	169.3	2.307	1.012
	OMA-BU-7.0-12.5-E1-B	√	+0.3	7.0	6903.8	3970.3	6920.1	2.340	√	2.521	√	7.2	169.0	2.312	1.012
	OMA-BU-7.0-12.5-E1-C	√	+0.3	7.0	6910.7	3973.4	6931.2	2.336	√	2.521	√	7.3	169.3	2.310	1.011
	OMA-BU-7.0-12.5-E1-D	√	+0.3	7.0	6921	3973.2	6938.4	2.334	√	2.521	√	7.4	169.5	2.311	1.010
	OMA-BU-7.0-12.5-E1-E	√	+0.3	7.0	6926.1	3974.2	6942.8	2.333	√	2.521	√	7.5	169.7	2.310	1.010
	OMA-BU-7.0-12.5-E1-F	√	+0.3	7.0	6928.9	3980.4	6945.6	2.337	√	2.521	√	7.3	169.7	2.311	1.011

Project	Specimen ID	Compacted	AC%	Target AV%	Bulk Specific Gravity					MTSG		Air Voids	Gry. Ht.	Gmb Est.	Actual Corr. Fac.
					Dry Wt.	Submerged Wt.	SSD Wt.	BSG	Done		Done				
Iron Cty Hurley 12.5mm E-3	HUR-OP-7.0-12.5-E0.3-A	√	-	7.0	6813.6	3913.2	6841.4	2.327	√	2.498	√	6.9	168.3	2.291	1.016
	HUR-OP-7.0-12.5-E0.3-B	√	-	7.0	6826.4	3907	6851.5	2.318	√	2.498	√	7.2	169.1	2.284	1.015
	HUR-OP-7.0-12.5-E0.3-C	√	-	7.0	6830.1	3916.3	6865.3	2.316	√	2.498	√	7.3	169.2	2.284	1.014
	HUR-OP-7.0-12.5-E0.3-D	√	-	7.0	6828.9	3909.5	6854.3	2.319	√	2.498	√	7.2	169.0	2.287	1.014
	HUR-OP-7.0-12.5-E0.3-E	√	-	7.0	6827.3	3909.1	6852	2.320	√	2.498	√	7.1	169.0	2.286	1.015
	HUR-OP-7.0-12.5-E0.3-F	√	-	7.0	6830	3919.2	6859.8	2.323	√	2.498	√	7.0	169.1	2.286	1.016
	HUR-OP-4.0-12.5-E0.3-A	√	-	4.0	7045.6	4100.9	7053.4	2.386	√	2.498	√	4.5	169.4	2.354	1.014
	HUR-OP-4.0-12.5-E0.3-B	√	-	4.0	7049.3	4108.4	7055.1	2.392	√	2.498	√	4.2	169.4	2.355	1.016
	HUR-OP-4.0-12.5-E0.3-C	√	-	4.0	7039.6	4096.7	7044.8	2.388	√	2.498	√	4.4	169.2	2.354	1.014
	HUR-OP-4.0-12.5-E0.3-D	√	-	4.0	7049.9	4106.4	7055.5	2.391	√	2.498	√	4.3	169.2	2.358	1.014
	HUR-OP-4.0-12.5-E0.3-E	√	-	4.0	7052.7	4110.6	7059.8	2.391	√	2.498	√	4.3	169.4	2.356	1.015
	HUR-OP-4.0-12.5-E0.3-F	√	-	4.0	7047.8	4107.8	7054.1	2.392	√	2.498	√	4.2	169.4	2.354	1.016
	HUR-OP-10.0-12.5-E0.3-A	√	-	10.0	6607	3750.4	6698.2	2.241	√	2.498	√	10.3	169.3	2.208	1.015
	HUR-OP-10.0-12.5-E0.3-B	√	-	10.0	6607.7	3754.1	6696.4	2.246	√	2.498	√	10.1	169.4	2.207	1.017
	HUR-OP-10.0-12.5-E0.3-C	√	-	10.0	6611.4	3760.5	6691.3	2.256	√	2.498	√	9.7	168.9	2.215	1.018
	HUR-OP-10.0-12.5-E0.3-D	√	-	10.0	6620.9	3750.6	6717.4	2.232	√	2.498	√	10.7	169.8	2.207	1.011
	HUR-OP-10.0-12.5-E0.3-E	√	-	10.0	6608.9	3744.8	6683.7	2.249	√	2.498	√	10.0	168.7	2.217	1.014
	HUR-OP-10.0-12.5-E0.3-F	√	-	10.0	6619.9	3757.5	6703	2.247	√	2.498	√	10.0	169.0	2.217	1.014
	HUR-BU-7.0-12.5-E0.3-A	√	+0.3	7.0	6762.8	3874.5	6793.4	2.317	√	2.476	√	6.4	168.4	2.273	1.020
	HUR-BU-7.0-12.5-E0.3-B	√	+0.3	7.0	6783.4	3886.3	6812	2.319	√	2.476	√	6.4	168.6	2.277	1.018
	HUR-BU-7.0-12.5-E0.3-C	√	+0.3	7.0	6800.8	3890.7	6830.4	2.313	√	2.476	√	6.6	169.0	2.277	1.016
	HUR-BU-7.0-12.5-E0.3-D	√	+0.3	7.0	6772.5	3864.2	6798.1	2.308	√	2.476	√	6.8	168.6	2.273	1.016
	HUR-BU-7.0-12.5-E0.3-E	√	+0.3	7.0	6784.8	3881.3	6807.3	2.319	√	2.476	√	6.3	168.6	2.277	1.018
	HUR-BU-7.0-12.5-E0.3-F	√	+0.3	7.0	6786.8	3878.8	6813.6	2.313	√	2.476	√	6.6	169.1	2.271	1.018

Project	Specimen ID	Compacted	AC%	Target AV%	Bulk Specific Gravity					MTSG		Air Voids	Gry. Ht.	Gmb Est.	Actual Corr. Fac.
					Dry Wt.	Submerged Wt.	SSD Wt.	BSG	Done		Done				
Sawyer Cty Hayward 12.5mm E-3	HAY-OP-7.0-12.5-E3-A	√	-	7.0	6997	4075.6	7016.2	2.379	√	2.543	√	6.4	169.4	2.337	1.018
	HAY-OP-7.0-12.5-E3-B	√	-	7.0	6942	4039.2	6976.6	2.363	√	2.543	√	7.1	168.9	2.326	1.016
	HAY-OP-7.0-12.5-E3-C	√	-	7.0	6990.2	4056.1	7016.8	2.361	√	2.543	√	7.2	170.1	2.325	1.015
	HAY-OP-7.0-12.5-E3-D	√	-	7.0	6973.3	4066.2	7016	2.364	√	2.543	√	7.0	169.6	2.327	1.016
	HAY-OP-7.0-12.5-E3-E	√	-	7.0	6961.6	4031.9	6989.5	2.354	√	2.543	√	7.5	169.9	2.319	1.015
	HAY-OP-7.0-12.5-E3-F	√	-	7.0	7005	4065.9	7035.5	2.359	√	2.543	√	7.2	170.3	2.328	1.013
	HAY-OP-4.0-12.5-E3-A	√	-	4.0	6984.9	4126.2	6995	2.435	√	2.543	√	4.3	164.7	2.400	1.015
	HAY-OP-4.0-12.5-E3-B	√	-	4.0	7205.8	4265	7218.8	2.440	√	2.543	√	4.1	169.7	2.403	1.015
	HAY-OP-4.0-12.5-E3-C	√	-	4.0	7182.8	4248.6	7192.7	2.440	√	2.543	√	4.1	169.3	2.401	1.016
	HAY-OP-4.0-12.5-E3-D	√	-	4.0	7183.7	4245.5	7194	2.436	√	2.543	√	4.2	169.4	2.400	1.015
	HAY-OP-4.0-12.5-E3-E	√	-	4.0	7205.4	4256.1	7214	2.436	√	2.543	√	4.2	169.9	2.400	1.015
	HAY-OP-4.0-12.5-E3-F	√	-	4.0	7207.7	4267.4	7221.6	2.440	√	2.543	√	4.1	169.9	2.401	1.016
	HAY-OP-10.0-12.5-E3-A	√	-	10.0	6794.8	3950.4	6885.1	2.315	√	2.543	√	9.0	169.9	2.263	1.023
	HAY-OP-10.0-12.5-E3-B	√	-	10.0	6816.5	3935.8	6899.1	2.300	√	2.543	√	9.6	169.6	2.274	1.011
	HAY-OP-10.0-12.5-E3-C	√	-	10.0	6792.4	3907.7	6862.7	2.299	√	2.543	√	9.6	168.3	2.284	1.006
	HAY-OP-10.0-12.5-E3-D	√	-	10.0	6818.8	3948.5	6901.1	2.309	√	2.543	√	9.2	168.8	2.286	1.010
	HAY-OP-10.0-12.5-E3-E	√	-	10.0	6802.8	3947.9	6888.1	2.314	√	2.543	√	9.0	169.6	2.270	1.019
	HAY-OP-10.0-12.5-E3-F	√	-	10.0	6744.7	3898.3	6813.8	2.313	√	2.543	√	9.0	167.7	2.276	1.016
	HAY-BU-7.0-12.5-E3-A	√	+0.3	7.0	6783	3931.2	6841.3	2.331	√	2.483	√	6.1	167.6	2.290	1.018
	HAY-BU-7.0-12.5-E3-B	√	+0.3	7.0	6769.2	3921.4	6831.8	2.326	√	2.483	√	6.3	167.1	2.292	1.015
	HAY-BU-7.0-12.5-E3-C	√	+0.3	7.0	6748	3916.6	6819.8	2.324	√	2.483	√	6.4	167.9	2.274	1.022
	HAY-BU-7.0-12.5-E3-D	√	+0.3	7.0	6775.8	3915.5	6844	2.314	√	2.483	√	6.8	168.3	2.278	1.016
	HAY-BU-7.0-12.5-E3-E	√	+0.3	7.0	6770.3	3911.8	6825.7	2.323	√	2.483	√	6.4	168.1	2.279	1.019
	HAY-BU-7.0-12.5-E3-F	√	+0.3	7.0	6788.4	3926.7	6842.3	2.328	√	2.483	√	6.2	167.4	2.295	1.015

Project	Specimen ID	Compacted	AC%	Target AV%	Bulk Specific Gravity					MTSG		Air Voids	Gry. Ht.	Gmb Est.	Actual Corr. Fac.
					Dry Wt.	Submerged Wt.	SSD Wt.	BSG	Done		Done				
Marathon Cty Wausau 12.5mm E-3	WAU-OP-7.0-12.5-E3-A	√	-	7.0	6688.3	3753.5	6713	2.260	√	2.450	√	7.7	169.0	2.240	1.009
	WAU-OP-7.0-12.5-E3-B	√	-	7.0	6697.1	3765.8	6718.2	2.268	√	2.450	√	7.4	169.1	2.241	1.012
	WAU-OP-7.0-12.5-E3-C	√	-	7.0	6692.7	3758.5	6713.8	2.265	√	2.450	√	7.6	170.4	2.223	1.019
	WAU-OP-7.0-12.5-E3-D	√	-	7.0	6697.5	3763.8	6721.9	2.264	√	2.450	√	7.6	169.2	2.240	1.011
	WAU-OP-7.0-12.5-E3-E	√	-	7.0	6689.5	3762.2	6713.3	2.267	√	2.450	√	7.5	169.3	2.236	1.014
	WAU-OP-7.0-12.5-E3-F	√	-	7.0	6688.1	3765.9	6712.8	2.270	√	2.450	√	7.4	169.0	2.239	1.013
	WAU-OP-4.0-12.5-E3-A	√	-	4.0	6958.6	3981.7	6963.7	2.334	√	2.450	√	4.7	169.0	2.330	1.002
	WAU-OP-4.0-12.5-E3-B	√	-	4.0	6933.4	3973.9	6939	2.338	√	2.450	√	4.5	171.0	2.294	1.019
	WAU-OP-4.0-12.5-E3-C	√	-	4.0	6942.9	3977.4	6949.3	2.336	√	2.450	√	4.6	170.1	2.310	1.011
	WAU-OP-4.0-12.5-E3-D	√	-	4.0	6943.5	3975.7	6949.7	2.335	√	2.450	√	4.7	170.6	2.303	1.014
	WAU-OP-4.0-12.5-E3-E	√	-	4.0	6945.5	3982.6	6951.2	2.340	√	2.450	√	4.5	170.5	2.305	1.015
	WAU-OP-4.0-12.5-E3-F	√	-	4.0	6940.7	3978.9	6947.4	2.338	√	2.450	√	4.6	170.5	2.304	1.015
	WAU-OP-10.0-12.5-E3-A	√	-	10.0	6327.5	3536.8	6419.1	2.195	√	2.450	√	10.4	164.9	2.171	1.011
	WAU-OP-10.0-12.5-E3-B	√	-	10.0	6482.6	3621.1	6553.5	2.211	√	2.450	√	9.8	168.0	2.184	1.012
	WAU-OP-10.0-12.5-E3-C	√	-	10.0	6498.6	3645.6	6581.2	2.214	√	2.450	√	9.6	168.7	2.180	1.016
	WAU-OP-10.0-12.5-E3-D	√	-	10.0	6486.4	3629.2	6570.4	2.205	√	2.450	√	10.0	168.5	2.178	1.012
	WAU-OP-10.0-12.5-E3-E	√	-	10.0	6515.5	3644.3	6604.7	2.201	√	2.450	√	10.2	169.3	2.178	1.011
	WAU-OP-10.0-12.5-E3-F	√	-	10.0	6485.7	3636.7	6584.3	2.200	√	2.450	√	10.2	168.9	2.173	1.013
	WAU-BU-7.0-12.5-E3-A	√	+0.3	7.0	6674	3752.3	6700.6	2.264	√	2.436	√	7.1	169.3	2.231	1.015
	WAU-BU-7.0-12.5-E3-B	√	+0.3	7.0	6706.8	3774.5	6737.1	2.264	√	2.436	√	7.1	170.3	2.229	1.016
	WAU-BU-7.0-12.5-E3-C	√	+0.3	7.0	6697.6	3755.8	6725.8	2.255	√	2.436	√	7.4	170.3	2.226	1.013
	WAU-BU-7.0-12.5-E3-D	√	+0.3	7.0	6738.1	3784.9	6759.9	2.265	√	2.436	√	7.0	170.8	2.232	1.015
	WAU-BU-7.0-12.5-E3-E	√	+0.3	7.0	6727.3	3770.9	6754.9	2.254	√	2.436	√	7.5	171.1	2.225	1.013
	WAU-BU-7.0-12.5-E3-F	√	+0.3	7.0	6761.9	3791.5	6793.1	2.253	√	2.436	√	7.5	171.9	2.226	1.012

Project	Specimen ID	Compacted	AC%	Target AV%	Bulk Specific Gravity					MTSG		Air Voids	Gry. Ht.	Gmb Est.	Actual Corr. Fac.
					Dry Wt.	Submerged Wt.	SSD Wt.	BSG	Done		Done				
Iron Cty Hurley 12.5mm E-3	HUR-OP-7.0-12.5-E3-A	√	-	7.0	6789.4	3880	6821.9	2.308	√	2.484	√	7.1	169.4	2.268	1.018
	HUR-OP-7.0-12.5-E3-B	√	-	7.0	6797.6	3901.3	6836.7	2.316	√	2.484	√	6.8	169.4	2.271	1.020
	HUR-OP-7.0-12.5-E3-C	√	-	7.0	6793.1	3890.5	6829.5	2.311	√	2.484	√	6.9	169.5	2.268	1.019
	HUR-OP-7.0-12.5-E3-D	√	-	7.0	6789.7	3888.7	6828.2	2.310	√	2.484	√	7.0	169.4	2.268	1.018
	HUR-OP-7.0-12.5-E3-E	√	-	7.0	6791.9	3888.3	6822.9	2.314	√	2.484	√	6.8	169.3	2.270	1.019
	HUR-OP-7.0-12.5-E3-F	√	-	7.0	6794.6	3902.2	6834.4	2.317	√	2.484	√	6.7	169.4	2.270	1.021
	HUR-OP-4.0-12.5-E3-A	√	-	4.0	6985.3	4071.7	6994.7	2.390	√	2.484	√	3.8	168.0	2.353	1.016
	HUR-OP-4.0-12.5-E3-B	√	-	4.0	6998.6	4077.9	7005.7	2.390	√	2.484	√	3.8	168.4	2.352	1.016
	HUR-OP-4.0-12.5-E3-C	√	-	4.0	6988.8	4077.9	6997.9	2.393	√	2.484	√	3.6	168.1	2.353	1.017
	HUR-OP-4.0-12.5-E3-D	√	-	4.0	6991.9	4083.3	7003.3	2.394	√	2.484	√	3.6	168.3	2.351	1.019
	HUR-OP-4.0-12.5-E3-E	√	-	4.0	6986.7	4085.2	6997.5	2.399	√	2.484	√	3.4	168.1	2.352	1.020
	HUR-OP-4.0-12.5-E3-F	√	-	4.0	7008.1	4078.4	7014.1	2.387	√	2.484	√	3.9	168.6	2.352	1.015
	HUR-OP-10.0-12.5-E3-A	√	-	10.0	6576.5	3724.2	6655.9	2.243	√	2.484	√	9.7	169.2	2.199	1.020
	HUR-OP-10.0-12.5-E3-B	√	-	10.0	6578.6	3743.8	6663.1	2.253	√	2.484	√	9.3	168.9	2.204	1.022
	HUR-OP-10.0-12.5-E3-C	√	-	10.0	6594.6	3736.7	6666	2.251	√	2.484	√	9.4	169.2	2.206	1.021
	HUR-OP-10.0-12.5-E3-D	√	-	10.0	6586.5	3754.3	6670.6	2.259	√	2.484	√	9.1	169.1	2.204	1.025
	HUR-OP-10.0-12.5-E3-E	√	-	10.0	6592.2	3738.7	6675.1	2.245	√	2.484	√	9.6	169.2	2.205	1.018
	HUR-OP-10.0-12.5-E3-F	√	-	10.0	6584.3	3762.4	6675.6	2.260	√	2.484	√	9.0	169.1	2.203	1.026
	HUR-BU-7.0-12.5-E3-A	√	+0.3	7.0	6701.4	3829.8	6736.9	2.305	√	2.472	√	6.7	167.9	2.259	1.021
	HUR-BU-7.0-12.5-E3-B	√	+0.3	7.0	6661.8	3799.9	6694.6	2.301	√	2.472	√	6.9	166.9	2.259	1.019
	HUR-BU-7.0-12.5-E3-C	√	+0.3	7.0	6674.8	3820.6	6704.9	2.314	√	2.472	√	6.4	167.1	2.260	1.024
	HUR-BU-7.0-12.5-E3-D	√	+0.3	7.0	6687.1	3814.6	6720.5	2.301	√	2.472	√	6.9	167.7	2.256	1.020
	HUR-BU-7.0-12.5-E3-E	√	+0.3	7.0	6664.7	3808.2	6697.9	2.306	√	2.472	√	6.7	166.8	2.261	1.020
	HUR-BU-7.0-12.5-E3-F	√	+0.3	7.0	6694.8	3817.7	6727.4	2.301	√	2.472	√	6.9	167.9	2.256	1.020

Project	Specimen ID	Compacted	AC%	Target AV%	Bulk Specific Gravity					MTSG		Air Voids	Gry. Ht.	Gmb Est.	Actual Corr. Fac.
					Dry Wt.	Submerged Wt.	SSD Wt.	BSG	Done		Done				
Langlade Cty Antigo 12.5mm E-10	ANT-OP-7.0-12.5-E10-A	√	-	7.0	6996.9	4048.3	7010.6	2.362	√	2.551	√	7.4	170.2	2.326	1.015
	ANT-OP-7.0-12.5-E10-B	√	-	7.0	6985	4039.9	7001.6	2.358	√	2.551	√	7.5	170.1	2.324	1.015
	ANT-OP-7.0-12.5-E10-C	√	-	7.0	6754.7	3900	6771.6	2.352	√	2.551	√	7.8	164.4	2.325	1.012
	ANT-OP-7.0-12.5-E10-D	√	-	7.0	6798	3931	6809.9	2.361	√	2.551	√	7.4	165.4	2.326	1.015
	ANT-OP-7.0-12.5-E10-E	√	-	7.0	6844.9	3956.5	6857.3	2.360	√	2.551	√	7.5	166.6	2.325	1.015
	ANT-OP-7.0-12.5-E10-F	√	-	7.0	6976.8	4038.8	6991.7	2.363	√	2.551	√	7.4	169.8	2.325	1.016
	ANT-OP-4.0-12.5-E10-A	√	-	4.0	7240.3	4217.8	7248.8	2.389	√	2.551	√	6.4	174.1	2.353	1.015
	ANT-OP-4.0-12.5-E10-B	√	-	4.0	7180.9	4212.2	7185.3	2.415	√	2.551	√	5.3	170.5	2.383	1.013
	ANT-OP-4.0-12.5-E10-C	√	-	4.0	6984.8	4091.6	6988.3	2.411	√	2.551	√	5.5	166.3	2.377	1.015
	ANT-OP-4.0-12.5-E10-D	√	-	4.0	7192.2	4208.8	7197.6	2.406	√	2.551	√	5.7	171.6	2.372	1.015
	ANT-OP-4.0-12.5-E10-E	√	-	4.0	7182.3	4207.7	7186.6	2.411	√	2.551	√	5.5	170.7	2.381	1.013
	ANT-OP-4.0-12.5-E10-F	√	-	4.0	7106.8	4165.7	7111.6	2.412	√	2.551	√	5.4	168.9	2.381	1.013
	ANT-OP-10.0-12.5-E10-A	√	-	10.0	6765.2	3860.5	6817.5	2.288	√	2.551	√	10.3	169.9	2.253	1.015
	ANT-OP-10.0-12.5-E10-B	√	-	10.0	6733	3846.8	6788.8	2.289	√	2.551	√	10.3	169.1	2.253	1.016
	ANT-OP-10.0-12.5-E10-C	√	-	10.0	6730	3841.8	6788.8	2.284	√	2.551	√	10.5	169.3	2.249	1.015
	ANT-OP-10.0-12.5-E10-D	√	-	10.0	6580.4	3753.8	6629.9	2.288	√	2.551	√	10.3	165.2	2.254	1.015
	ANT-OP-10.0-12.5-E10-E	√	-	10.0	6697.8	3832	6761.1	2.287	√	2.551	√	10.4	168.3	2.252	1.015
	ANT-OP-10.0-12.5-E10-F	√	-	10.0	6711.8	3841	6767	2.294	√	2.551	√	10.1	168.4	2.255	1.017
	ANT-BU-7.0-12.5-E10-A	√	+0.3	7.0	6809.7	3901.9	6823.9	2.330	√	2.492	√	6.5	168.1	2.292	1.017
	ANT-BU-7.0-12.5-E10-B	√	+0.3	7.0	6786	3880.2	6826	2.304	√	2.492	√	7.6	169.5	2.266	1.017
	ANT-BU-7.0-12.5-E10-C	√	+0.3	7.0	6851.1	3911.8	6882.6	2.306	√	2.492	√	7.5	170.6	2.273	1.015
	ANT-BU-7.0-12.5-E10-D	√	+0.3	7.0	6798.6	3890	6830.5	2.312	√	2.492	√	7.2	169.3	2.272	1.017
	ANT-BU-7.0-12.5-E10-E	√	+0.3	7.0	6774.6	3880.4	6797	2.323	√	2.492	√	6.8	167.8	2.285	1.017
	ANT-BU-7.0-12.5-E10-F	√	+0.3	7.0	6828.3	3898.5	6855.6	2.309	√	2.492	√	7.3	170.0	2.273	1.016

Project	Specimen ID	Compacted	AC%	Target AV%	Bulk Specific Gravity					MTSG		Air Voids	Gry. Ht.	Gmb Est.	Actual Corr. Fac.
					Dry Wt.	Submerged Wt.	SSD Wt.	BSG	Done		Done				
Sheboygan Cty Plymouth 12.5mm E-10	PLY-OP-7.0-12.5-E10-A	√	-	7.0	7079.4	4177.8	7124.4	2.403	√	2.588	√	7.2	169.5	2.363	1.017
	PLY-OP-7.0-B12.5-E10-	√	-	7.0	7076.2	4170.6	7121.6	2.398	√	2.588	√	7.4	169.6	2.361	1.016
	PLY-OP-7.0-12.5-E10-C	√	-	7.0	7074	4167.7	7110.5	2.404	√	2.588	√	7.1	169.3	2.364	1.017
	PLY-OP-7.0-12.5-E10-D	√	-	7.0	7075.7	4179.1	7117.2	2.408	√	2.588	√	7.0	169.2	2.366	1.018
	PLY-OP-7.0-12.5-E10-E	√	-	7.0	7079.7	4185.8	7128.7	2.406	√	2.588	√	7.1	169.3	2.366	1.017
	PLY-OP-7.0-12.5-E10-F	√	-	7.0	7079.8	4180.7	7126.9	2.403	√	2.588	√	7.2	169.7	2.361	1.018
	ANT-OP-4.0-12.5-E10-A	√	-	4.0	7314.2	4371.8	7324.4	2.477	√	2.588	√	4.3	169.7	2.439	1.016
	PLY-OP-4.0-12.5-E10-B	√	-	4.0	7316.9	4383.1	7329.6	2.483	√	2.588	√	4.1	169.8	2.438	1.018
	PLY-OP-4.0-12.5-E10-C	√	-	4.0	7310.3	4372.6	7320.4	2.480	√	2.588	√	4.2	169.6	2.439	1.017
	PLY-OP-4.0-12.5-E10-D	√	-	4.0	7307.8	4370.3	7318.4	2.479	√	2.588	√	4.2	169.5	2.440	1.016
	PLY-OP-4.0-12.5-E10-E	√	-	4.0	7309.6	4371.8	7326.1	2.474	√	2.588	√	4.4	169.8	2.436	1.016
	PLY-OP-4.0-12.5-E10-F	√	-	4.0	7317.7	4375.2	7327.2	2.479	√	2.588	√	4.2	169.8	2.439	1.016
	PLY-OP-10.0-12.5-E10-A	√	-	10.0	6857.6	4037.6	6975.2	2.334	√	2.588	√	9.8	169.1	2.295	1.017
	PLY-OP-10.0-12.5-E10-B	√	-	10.0	6861.5	4038.7	6976.8	2.335	√	2.588	√	9.8	169.4	2.292	1.019
	PLY-OP-10.0-12.5-E10-C	√	-	10.0	6856.5	4045.5	6974.7	2.341	√	2.588	√	9.6	169.1	2.294	1.020
	PLY-OP-10.0-12.5-E10-D	√	-	10.0	6856.1	4029.3	6970.8	2.331	√	2.588	√	9.9	169.1	2.294	1.016
	PLY-OP-10.0-12.5-E10-E	√	-	10.0	6853	4036.1	6964.8	2.340	√	2.588	√	9.6	168.9	2.296	1.019
	PLY-OP-10.0-12.5-E10-F	√	-	10.0	6860.2	4035.7	6970.5	2.338	√	2.588	√	9.7	169.4	2.292	1.020
	PLY-BU-7.0-12.5-E10-A	√	+0.3	7.0	7084.3	4156.6	7105.8	2.402	√	2.581	√	6.9	169.8	2.361	1.017
	PLY-BU-7.0-12.5-E10-B	√	+0.3	7.0	7082.1	4163.8	7114.7	2.400	√	2.581	√	7.0	169.9	2.359	1.017
	PLY-BU-7.0-12.5-E10-C	√	+0.3	7.0	7084.8	4166.8	7114.7	2.403	√	2.581	√	6.9	169.9	2.360	1.018
	PLY-BU-7.0-12.5-E10-D	√	+0.3	7.0	7082.8	4169.5	7114.8	2.405	√	2.581	√	6.8	169.8	2.360	1.019
	PLY-BU-7.0-12.5-E10-E	√	+0.3	7.0	7084.7	4169.2	7111.4	2.408	√	2.581	√	6.7	169.8	2.361	1.020
	PLY-BU-7.0-12.5-E10-F	√	+0.3	7.0	7103.7	4177.3	7133.9	2.403	√	2.581	√	6.9	170.3	2.360	1.018

Project	Specimen ID	Compacted	AC%	Target AV%	Bulk Specific Gravity					MTSG		Air Voids	Gry. Ht.	Gmb Est.	Actual Corr. Fac.
					Dry Wt.	Submerged Wt.	SSD Wt.	BSG	Done		Done				
Kenosha Cty Racine 12.5mm E-10	RAC-OP-7.0-12.5-E10-A	√	-	7.0	6865.6	3952.5	6903.8	2.326	√	2.510	√	7.3	168.9	2.300	1.011
	RAC-OP-7.0-12.5-E10-B	√	-	7.0	6860.8	3953.9	6901.2	2.328	√	2.510	√	7.2	169.8	2.286	1.018
	RAC-OP-7.0-12.5-E10-C	√	-	7.0	6873	3958.4	6913.5	2.326	√	2.510	√	7.3	169.2	2.299	1.012
	RAC-OP-7.0-12.5-E10-D	√	-	7.0	6869.6	3954.5	6905.5	2.328	√	2.510	√	7.2	169	2.300	1.012
	RAC-OP-7.0-12.5-E10-E	√	-	7.0	6855.6	3957.8	6893.4	2.335	√	2.510	√	6.9	168.9	2.297	1.017
	RAC-OP-7.0-12.5-E10-F	√	-	7.0	6877.1	3959.9	6903.6	2.336	√	2.510	√	6.9	169	2.303	1.015
	RAC-OP-4.0-12.5-E10-A	√	-	4.0	7071.6	4136.1	7085.7	2.397	√	2.510	√	4.5	168.8	2.371	1.011
	RAC-OP-4.0-12.5-E10-B	√	-	4.0	7082.3	4136	7093.4	2.395	√	2.510	√	4.6	169.1	2.370	1.010
	RAC-OP-4.0-12.5-E10-C	√	-	4.0	7078.8	4143.7	7092.5	2.401	√	2.510	√	4.3	168.9	2.372	1.012
	RAC-OP-4.0-12.5-E10-D	√	-	4.0	7093.7	4152.9	7104.6	2.403	√	2.510	√	4.2	169.1	2.374	1.012
	RAC-OP-4.0-12.5-E10-E	√	-	4.0	7064.2	4127.5	7076.1	2.396	√	2.510	√	4.5	168.8	2.368	1.012
	RAC-OP-4.0-12.5-E10-F	√	-	4.0	7096.4	4152.7	7110.3	2.399	√	2.510	√	4.4	169.4	2.371	1.012
	RAC-OP-10.0-12.5-E10-A	√	-	10.0	6626.1	3781.2	6739.4	2.240	√	2.510	√	10.7	169.3	2.215	1.011
	RAC-OP-10.0-12.5-E10-B	√	-	10.0	6651.8	3808.7	6768.5	2.247	√	2.510	√	10.5	170	2.214	1.015
	RAC-OP-10.0-12.5-E10-C	√	-	10.0	6640.5	3786.9	6755.8	2.237	√	2.510	√	10.9	169.8	2.213	1.011
	RAC-OP-10.0-12.5-E10-D	√	-	10.0	6623.1	3779.3	6736.7	2.240	√	2.510	√	10.8	169.4	2.212	1.012
	RAC-OP-10.0-12.5-E10-E	√	-	10.0	6642.2	3802.6	6771.1	2.238	√	2.510	√	10.8	170.1	2.210	1.013
	RAC-OP-10.0-12.5-E10-F	√	-	10.0	6655.2	3801.4	6762.2	2.248	√	2.510	√	10.4	170	2.215	1.015
	RAC-BU-7.0-12.5-E10-A	√	+0.3	7.0	6735.7	3872.4	6788.6	2.310	√	2.486	√	7.1	167.4	2.277	1.014
	RAC-BU-7.0-12.5-E10-B	√	+0.3	7.0	6781.9	3896.8	6826.5	2.315	√	2.486	√	6.9	168.3	2.280	1.015
	RAC-BU-7.0-12.5-E10-C	√	+0.3	7.0	6753.6	3880.2	6797.3	2.315	√	2.486	√	6.9	167.5	2.282	1.015
	RAC-BU-7.0-12.5-E10-D	√	+0.3	7.0	6752.8	3876	6797.9	2.311	√	2.486	√	7.0	167.6	2.280	1.014
	RAC-BU-7.0-12.5-E10-E	√	+0.3	7.0	6771.5	3883.5	6808.9	2.315	√	2.486	√	6.9	168	2.281	1.015
	RAC-BU-7.0-12.5-E10-F	√	+0.3	7.0	6786.7	3896.7	6827.5	2.316	√	2.486	√	6.9	168.2	2.283	1.014

Project	Specimen ID	Compacted	AC%	Target AV%	Bulk Specific Gravity					MTSG	Done	Air Voids	Gry. Ht.	Gmb Est.	Actual Corr. Fac.
					Dry Wt.	Submerged Wt.	SSD Wt.	BSG	Done						
Sheboygan Cty Cascade 19.0mm E-1	CAS-OP-7.0-19.0-E1-A	√	-	7.0	7062.2	4140.1	7096.6	2.389	√	2.578	√	7.4	169.3	2.361	1.012
	CAS-OP-7.0-19.0-E1-B	√	-	7.0	7058.1	4144.9	7102.9	2.386	√	2.578	√	7.5	169.2	2.361	1.011
	CAS-OP-7.0-19.0-E1-C	√	-	7.0	7059.7	4152.8	7095.9	2.399	√	2.578	√	7.0	169.2	2.361	1.016
	CAS-OP-7.0-19.0-E1-D	√	-	7.0	7065.4	4168.6	7109.9	2.402	√	2.578	√	6.8	169.5	2.359	1.018
	CAS-OP-7.0-19.0-E1-E	√	-	7.0	7062.3	4143.7	7094.3	2.394	√	2.578	√	7.2	169.5	2.358	1.015
	CAS-OP-7.0-19.0-E1-F	√	-	7.0	7060.3	4138.4	7094.8	2.388	√	2.578	√	7.4	169.3	2.360	1.012
	CAS-OP-4.0-19.0-E1-A	√	-	4.0	7290.1	4342.3	7300.5	2.464	√	2.578	√	4.4	169.8	2.430	1.014
	CAS-OP-4.0-19.0-E1-B	√	-	4.0	7286.6	4346.8	7296.6	2.470	√	2.578	√	4.2	169.8	2.428	1.017
	CAS-OP-4.0-19.0-E1-C	√	-	4.0	7291.1	4337.2	7298.5	2.462	√	2.578	√	4.5	169.9	2.428	1.014
	CAS-OP-4.0-19.0-E1-D	√	-	4.0	7293.1	4339.4	7302	2.462	√	2.578	√	4.5	169.9	2.429	1.013
	CAS-OP-4.0-19.0-E1-E	√	-	4.0	7290.7	4341.7	7302.2	2.463	√	2.578	√	4.5	169.9	2.428	1.014
	CAS-OP-4.0-19.0-E1-F	√	-	4.0	7293.5	4341.2	7302.1	2.463	√	2.578	√	4.5	169.8	2.431	1.013
	CAS-OP-10.0-19.0-E1-A	√	-	10.0	6828.1	3988.9	6917.5	2.332	√	2.578	√	9.6	169.1	2.285	1.020
	CAS-OP-10.0-19.0-E1-B	√	-	10.0	6826.2	3982.1	6912.2	2.330	√	2.578	√	9.6	169.4	2.280	1.022
	CAS-OP-10.0-19.0-E1-C	√	-	10.0	6830.6	3992.3	6933.7	2.322	√	2.578	√	9.9	169.9	2.275	1.021
	CAS-OP-10.0-19.0-E1-D	√	-	10.0	6832	3969.5	6936.1	2.303	√	2.578	√	10.7	170.1	2.273	1.013
	CAS-OP-10.0-19.0-E1-E	√	-	10.0	6830.4	3960	6919.6	2.308	√	2.578	√	10.5	169.8	2.276	1.014
	CAS-OP-10.0-19.0-E1-F	√	-	10.0	6831.8	3989.4	6924.7	2.327	√	2.578	√	9.7	169.8	2.277	1.022
	CAS-BU-7.0-19.0-E1-A	√	+0.3	7.0	6996.4	4086.3	7034	2.374	√	2.554	√	7.1	169.2	2.340	1.014
	CAS-BU-7.0-19.0-E1-B	√	+0.3	7.0	7006.6	4094.7	7044	2.376	√	2.554	√	7.0	169.4	2.341	1.015
	CAS-BU-7.0-19.0-E1-C	√	+0.3	7.0	7004.3	4105.8	7050.7	2.378	√	2.554	√	6.9	170.0	2.332	1.020
	CAS-BU-7.0-19.0-E1-D	√	+0.3	7.0	6997.9	4104.7	7048	2.378	√	2.554	√	6.9	169.7	2.334	1.019
	CAS-BU-7.0-19.0-E1-E	√	+0.3	7.0	7012.1	4096.3	7051.1	2.373	√	2.554	√	7.1	170.1	2.333	1.017
	CAS-BU-7.0-19.0-E1-F	√	+0.3	7.0	7005.3	4103.1	7043.1	2.383	√	2.554	√	6.7	169.6	2.337	1.019

Project	Specimen ID	Compacted	AC%	Target AV%	Bulk Specific Gravity					MTSG		Air Voids	Gry. Ht.	Gmb Est.	Actual Corr. Fac.
					Dry Wt.	Submerged Wt.	SSD Wt.	BSG	Done		Done				
Lincoln Cty Bloomville 19.0mm E-1	BLO-OP-7.0-19.0-E1-A	√	-	7.0	6904.9	3993	6946.9	2.338	√	2.521	√	7.3	169.4	2.307	1.013
	BLO-OP-7.0-19.0-E1-B	√	-	7.0	6910.2	3967.8	6932.2	2.331	√	2.521	√	7.5	169.5	2.307	1.010
	BLO-OP-7.0-19.0-E1-C	√	-	7.0	6902.6	3963.7	6945.1	2.315	√	2.521	√	8.2	171.9	2.272	1.019
	BLO-OP-7.0-19.0-E1-D	√	-	7.0	6911	3986.7	6945	2.336	√	2.521	√	7.3	169.5	2.307	1.013
	BLO-OP-7.0-19.0-E1-E	√	-	7.0	6908.8	3977.5	6936.3	2.335	√	2.521	√	7.4	169.4	2.308	1.012
	BLO-OP-7.0-19.0-E1-F	√	-	7.0	6908.9	3971.2	6933.6	2.332	√	2.521	√	7.5	169.4	2.308	1.011
	BLO-OP-4.0-19.0-E1-A	√	-	4.0	7130	4175.5	7138.4	2.406	√	2.521	√	4.5	169.7	2.378	1.012
	BLO-OP-4.0-19.0-E1-B	√	-	4.0	7129	4182.8	7144	2.407	√	2.521	√	4.5	169.8	2.376	1.013
	BLO-OP-4.0-19.0-E1-C	√	-	4.0	7124	4172	7133.4	2.406	√	2.521	√	4.6	169.6	2.377	1.012
	BLO-OP-4.0-19.0-E1-D	√	-	4.0	7121.4	4183.7	7135.9	2.412	√	2.521	√	4.3	169.6	2.376	1.015
	BLO-OP-4.0-19.0-E1-E	√	-	4.0	7120.7	4177.8	7134.2	2.409	√	2.521	√	4.5	169.8	2.373	1.015
	BLO-OP-4.0-19.0-E1-F	√	-	4.0	7136.4	4187.6	7149.5	2.409	√	2.521	√	4.4	169.9	2.377	1.014
	BLO-OP-10.0-19.0-E1-A	√	-	10.0	6686.9	3837	6771	2.279	√	2.521	√	9.6	168.6	2.244	1.015
	BLO-OP-10.0-19.0-E1-B	√	-	10.0	6687.9	3832	6767.6	2.278	√	2.521	√	9.6	168.6	2.245	1.015
	BLO-OP-10.0-19.0-E1-C	√	-	10.0	6682.8	3829.3	6766.4	2.275	√	2.521	√	9.7	168.9	2.239	1.016
	BLO-OP-10.0-19.0-E1-D	√	-	10.0	6691.4	3831.1	6773.1	2.274	√	2.521	√	9.8	169.0	2.241	1.015
	BLO-OP-10.0-19.0-E1-E	√	-	10.0	6686.3	3828.4	6770.6	2.273	√	2.521	√	9.9	168.8	2.242	1.014
	BLO-OP-10.0-19.0-E1-F	√	-	10.0	6682.9	3837.5	6762.1	2.285	√	2.521	√	9.4	168.4	2.246	1.018
	BLO-BU-7.0-19.0-E1-A	√	+0.3	7.0	6865.3	3960.1	6909.5	2.328	√	2.505	√	7.1	169.3	2.295	1.014
	BLO-BU-7.0-19.0-E1-B	√	+0.3	7.0	6864.6	3951.5	6890.9	2.335	√	2.505	√	6.8	169.2	2.296	1.017
	BLO-BU-7.0-19.0-E1-C	√	+0.3	7.0	6856.5	3956.2	6901.3	2.328	√	2.505	√	7.0	169.0	2.296	1.014
	BLO-BU-7.0-19.0-E1-D	√	+0.3	7.0	6854.6	3948	6892.4	2.328	√	2.505	√	7.1	169.0	2.295	1.014
	BLO-BU-7.0-19.0-E1-E	√	+0.3	7.0	6890.1	3967.2	6924.1	2.330	√	2.505	√	7.0	169.7	2.298	1.014
	BLO-BU-7.0-19.0-E1-F	√	+0.3	7.0	6875.3	3949.9	6903.9	2.327	√	2.505	√	7.1	169.5	2.295	1.014

Project	Specimen ID	Compacted	AC%	Target AV%	Bulk Specific Gravity					MTSG		Air Voids	Gry. Ht.	Gmb Est.	Actual Corr. Fac.
					Dry Wt.	Submerged Wt.	SSD Wt.	BSG	Done		Done				
Douglas Cty Brule 19.0mm E-0.3	BRU-OP-7.0-19.0-E0.3-A	√	-	7.0	7032.6	4136.9	7064.3	2.402	√	2.569	√	6.5	169.4	2.349	1.023
	BRU-OP-7.0-19.0-E0.3-B	√	-	7.0	7034	4144.2	7073.2	2.402	√	2.569	√	6.5	169.2	2.352	1.021
	BRU-OP-7.0-19.0-E0.3-C	√	-	7.0	7030.5	4137.5	7067.1	2.400	√	2.569	√	6.6	168.8	2.357	1.018
	BRU-OP-7.0-19.0-E0.3-D	√	-	7.0	7033.3	4138.3	7066.5	2.402	√	2.569	√	6.5	169.2	2.352	1.021
	BRU-OP-7.0-19.0-E0.3-E	√	-	7.0	7027.8	4113.5	7061.2	2.384	√	2.569	√	7.2	169.1	2.352	1.014
	BRU-OP-7.0-19.0-E0.3-F	√	-	7.0	7029.4	4128.8	7067.8	2.392	√	2.569	√	6.9	169.3	2.350	1.018
	BRU-OP-4.0-19.0-E0.3-A	√	-	4.0	7248.3	4304.2	7262.1	2.450	√	2.569	√	4.6	169.5	2.420	1.013
	BRU-OP-4.0-19.0-E0.3-B	√	-	4.0	7250.2	4308	7266	2.451	√	2.569	√	4.6	169.6	2.419	1.013
	BRU-OP-4.0-19.0-E0.3-C	√	-	4.0	7248.5	4305.5	7260.5	2.453	√	2.569	√	4.5	169.6	2.419	1.014
	BRU-OP-4.0-19.0-E0.3-D	√	-	4.0	7255.9	4324.2	7273.5	2.460	√	2.569	√	4.2	169.5	2.422	1.016
	BRU-OP-4.0-19.0-E0.3-E	√	-	4.0	7243.3	4300	7256	2.450	√	2.569	√	4.6	169.5	2.418	1.013
	BRU-OP-4.0-19.0-E0.3-F	√	-	4.0	7248.1	4302.4	7263.7	2.448	√	2.569	√	4.7	169.4	2.421	1.011
	BRU-OP-10.0-19.0-E0.3-A	√	-	10.0	6807.7	3927.7	6867.2	2.316	√	2.569	√	9.8	169.2	2.277	1.017
	BRU-OP-10.0-19.0-E0.3-B	√	-	10.0	6810.1	3925.5	6868.2	2.314	√	2.569	√	9.9	169.1	2.279	1.015
	BRU-OP-10.0-19.0-E0.3-C	√	-	10.0	6800.1	3923.1	6862.2	2.314	√	2.569	√	9.9	169.0	2.277	1.016
	BRU-OP-10.0-19.0-E0.3-D	√	-	10.0	6811	3945.5	6881.5	2.320	√	2.569	√	9.7	169.1	2.279	1.018
	BRU-OP-10.0-19.0-E0.3-E	√	-	10.0	6789.9	3914.6	6857.1	2.308	√	2.569	√	10.2	169.2	2.271	1.016
	BRU-OP-10.0-19.0-E0.3-F	√	-	10.0	6802.9	3932.9	6859.4	2.325	√	2.569	√	9.5	168.4	2.286	1.017
	BRU-BU-7.0-19.0-E0.3-A	√	+0.3	7.0	7019.6	4084	7042.6	2.373	√	2.553	√	7.1	169.9	2.338	1.015
	BRU-BU-7.0-19.0-E0.3-B	√	+0.3	7.0	7006.6	4105.8	7038.8	2.389	√	2.553	√	6.4	169.9	2.334	1.024
	BRU-BU-7.0-19.0-E0.3-C	√	+0.3	7.0	6994.2	4096.1	7031.2	2.383	√	2.553	√	6.7	170.2	2.325	1.025
	BRU-BU-7.0-19.0-E0.3-D	√	+0.3	7.0	7006	4089	7038.8	2.375	√	2.553	√	7.0	170.1	2.331	1.019
	BRU-BU-7.0-19.0-E0.3-E	√	+0.3	7.0	7010.3	4090.8	7049.4	2.369	√	2.553	√	7.2	170.2	2.331	1.017
	BRU-BU-7.0-19.0-E0.3-F	√	+0.3	7.0	7010.5	4086.1	7041.8	2.372	√	2.553	√	7.1	170.1	2.332	1.017

Project	Specimen ID	Compacted	AC%	Target AV%	Bulk Specific Gravity					MTSG		Air Voids	Gry. Ht.	Gmb Est.	Actual Corr. Fac.
					Dry Wt.	Submerged Wt.	SSD Wt.	BSG	Done		Done				
Dane Cty Waunakee 19.0mm E-3	KEE-OP-7.0-19.0-E3-A	√	-	7.0	6876.7	3965.7	6905.2	2.339	√	2.511	√	6.8	168.7	2.307	1.014
	KEE-OP-7.0-19.0-E3-B	√	-	7.0	6870.5	3973.9	6906.5	2.343	√	2.511	√	6.7	168.3	2.310	1.014
	KEE-OP-7.0-19.0-E3-C	√	-	7.0	6870.1	3964.1	6902.5	2.338	√	2.511	√	6.9	168.8	2.303	1.015
	KEE-OP-7.0-19.0-E3-D	√	-	7.0	6873.2	3983.5	6912.6	2.347	√	2.511	√	6.5	168.4	2.310	1.016
	KEE-OP-7.0-19.0-E3-E	√	-	7.0	6870	3983.5	6908.1	2.349	√	2.511	√	6.4	168.5	2.307	1.018
	KEE-OP-7.0-19.0-E3-F	√	-	7.0	6868.3	3971.6	6903.2	2.343	√	2.511	√	6.7	168.8	2.303	1.018
	KEE-OP-4.0-19.0-E3-A	√	-	4.0	7096.7	4163.6	7109.3	2.409	√	2.511	√	4.1	169.8	2.365	1.019
	KEE-OP-4.0-19.0-E3-B	√	-	4.0	7093.7	4168.4	7107.3	2.414	√	2.511	√	3.9	169.4	2.370	1.019
	KEE-OP-4.0-19.0-E3-C	√	-	4.0	7098.3	4160.2	7110.2	2.406	√	2.511	√	4.2	170.3	2.359	1.020
	KEE-OP-4.0-19.0-E3-D	√	-	4.0	7094	4165.2	7107.2	2.411	√	2.511	√	4.0	170.4	2.356	1.024
	KEE-OP-4.0-19.0-E3-E	√	-	4.0	7099.4	4163.2	7108.6	2.410	√	2.511	√	4.0	170.2	2.360	1.021
	KEE-OP-4.0-19.0-E3-F	√	-	4.0	7096	4160.5	7105.3	2.410	√	2.511	√	4.0	169.9	2.363	1.020
	KEE-OP-10.0-19.0-E3-A	√	-	10.0	6643.4	3794.1	6714.7	2.275	√	2.511	√	9.4	169.4	2.219	1.025
	KEE-OP-10.0-19.0-E3-B	√	-	10.0	6648.9	3809.4	6717.1	2.287	√	2.511	√	8.9	169.3	2.222	1.029
	KEE-OP-10.0-19.0-E3-C	√	-	10.0	6656.9	3809.8	6728.7	2.281	√	2.511	√	9.2	169.4	2.224	1.026
	KEE-OP-10.0-19.0-E3-D	√	-	10.0	6652.2	3809.9	6719.8	2.286	√	2.511	√	9.0	169.6	2.220	1.030
	KEE-OP-10.0-19.0-E3-E	√	-	10.0	6647.1	3822.4	6717.6	2.296	√	2.511	√	8.6	169.4	2.220	1.034
	KEE-OP-10.0-19.0-E3-F	√	-	10.0	6649.4	3809.9	6721.6	2.284	√	2.511	√	9.0	169.2	2.224	1.027
	KEE-BU-7.0-19.0-E3-A	√	+0.3	7.0	6852	3948.5	6886	2.333	√	2.495	√	6.5	169.9	2.282	1.022
	KEE-BU-7.0-19.0-E3-B	√	+0.3	7.0	6844.5	3951.4	6877.2	2.339	√	2.495	√	6.3	169.8	2.281	1.026
	KEE-BU-7.0-19.0-E3-C	√	+0.3	7.0	6883.4	3972.4	6918.5	2.336	√	2.495	√	6.4	169.8	2.294	1.019
	KEE-BU-7.0-19.0-E3-D	√	+0.3	7.0	6881.6	3969.3	6916.3	2.335	√	2.495	√	6.4	169.7	2.295	1.018
	KEE-BU-7.0-19.0-E3-E	√	+0.3	7.0	6882.4	3979.3	6921	2.340	√	2.495	√	6.2	169.8	2.294	1.020
	KEE-BU-7.0-19.0-E3-F	√	+0.3	7.0	6862.9	3968.6	6902.4	2.339	√	2.495	√	6.3	169.8	2.287	1.023

Project	Specimen ID	Compacted	AC%	Target AV%	Bulk Specific Gravity					MTSG		Air Voids	Gry. Ht.	Gmb Est.	Actual Corr. Fac.
					Dry Wt.	Submerged Wt.	SSD Wt.	BSG	Done		Done				
Marathon Cty Mosinee 19.0mm E-3	MOS-OP-7.0-19.0-E3-A	√	-	7.0	6686.5	3752.4	6712.4	2.259	√	2.445	√	7.6	169.4	2.234	1.011
	MOS-OP-7.0-19.0-E3-B	√	-	7.0	6697.9	3751.7	6716.7	2.259	√	2.445	√	7.6	169.6	2.235	1.011
	MOS-OP-7.0-19.0-E3-C	√	-	7.0	6703.2	3765.3	6734.1	2.258	√	2.445	√	7.7	169.8	2.234	1.011
	MOS-OP-7.0-19.0-E3-D	√	-	7.0	6699.3	3755.8	6723	2.258	√	2.445	√	7.7	169.8	2.233	1.011
	MOS-OP-7.0-19.0-E3-E	√	-	7.0	6691.6	3764.1	6723.2	2.261	√	2.445	√	7.5	169.5	2.234	1.012
	MOS-OP-7.0-19.0-E3-F	√	-	7.0	6695.3	3758.4	6722.8	2.259	√	2.445	√	7.6	169.5	2.235	1.010
	MOS-OP-4.0-19.0-E3-A	√	-	4.0	6921.2	3960.2	6927.6	2.332	√	2.445	√	4.6	170.1	2.303	1.013
	MOS-OP-4.0-19.0-E3-B	√	-	4.0	6922	3964.5	6928.3	2.336	√	2.445	√	4.5	170.2	2.301	1.015
	MOS-OP-4.0-19.0-E3-C	√	-	4.0	6919.6	3949.1	6925.2	2.325	√	2.445	√	4.9	170.3	2.299	1.011
	MOS-OP-4.0-19.0-E3-D	√	-	4.0	6925.2	3962.4	6930.8	2.333	√	2.445	√	4.6	170.3	2.301	1.014
	MOS-OP-4.0-19.0-E3-E	√	-	4.0	6915.7	3953.1	6921.6	2.330	√	2.445	√	4.7	170.0	2.302	1.012
	MOS-OP-4.0-19.0-E3-F	√	-	4.0	6916.7	3958	6922.5	2.333	√	2.445	√	4.6	170.0	2.302	1.013
	MOS-OP-10.0-19.0-E3-A	√	-	10.0	6474.2	3615.3	6559.3	2.199	√	2.445	√	10.1	168.5	2.174	1.011
	MOS-OP-10.0-19.0-E3-B	√	-	10.0	6468.6	3604.9	6561.8	2.188	√	2.445	√	10.5	169.4	2.161	1.012
	MOS-OP-10.0-19.0-E3-C	√	-	10.0	6465.6	3596.5	6566.7	2.177	√	2.445	√	11.0	169.7	2.156	1.010
	MOS-OP-10.0-19.0-E3-D	√	-	10.0	6466.9	3586.6	6572.6	2.166	√	2.445	√	11.4	170.2	2.150	1.007
	MOS-OP-10.0-19.0-E3-E	√	-	10.0	6445.5	3597.4	6555.7	2.179	√	2.445	√	10.9	169.5	2.152	1.013
	MOS-OP-10.0-19.0-E3-F	√	-	10.0	6468.2	3605.7	6571.1	2.181	√	2.445	√	10.8	169.8	2.156	1.012
	MOS-BU-7.0-19.0-E3-A	√	+0.3	7.0	6661.6	3740.1	6684.2	2.263	√	2.438	√	7.2	168.9	2.232	1.014
	MOS-BU-7.0-19.0-E3-B	√	+0.3	7.0	6659.2	3732.3	6682.4	2.257	√	2.438	√	7.4	169.0	2.230	1.012
	MOS-BU-7.0-19.0-E3-C	√	+0.3	7.0	6704	3750.3	6729.1	2.251	√	2.438	√	7.7	170.3	2.228	1.010
	MOS-BU-7.0-19.0-E3-D	√	+0.3	7.0	6707.2	3761.4	6737.1	2.254	√	2.438	√	7.5	170.2	2.230	1.011
	MOS-BU-7.0-19.0-E3-E	√	+0.3	7.0	6684	3742.1	6709.8	2.252	√	2.438	√	7.6	169.9	2.226	1.012
	MOS-BU-7.0-19.0-E3-F	√	+0.3	7.0	6682.1	3739.2	6702.9	2.255	√	2.438	√	7.5	169.7	2.228	1.012

Project	Specimen ID	Compacted	AC%	Target AV%	Bulk Specific Gravity					MTSG		Air Voids	Gry. Ht.	Gmb Est.	Actual Corr. Fac.
					Dry Wt.	Submerged Wt.	SSD Wt.	BSG	Done		Done				
Barron Cty Cumberland 19.0mm E-3	UMB-OP-7.0-19.0-E3-A	√	-	7.0	7068.5	4132.9	7086.4	2.393	√	2.586	√	7.5	169.3	2.363	1.013
	UMB-OP-7.0-19.0-E3-B	√	-	7.0	7082.5	4153.2	7106.6	2.398	√	2.586	√	7.3	169.5	2.365	1.014
	UMB-OP-7.0-19.0-E3-C	√	-	7.0	7075.1	4146.4	7100.4	2.395	√	2.586	√	7.4	169.5	2.362	1.014
	UMB-OP-7.0-19.0-E3-D	√	-	7.0	7068.6	4146.7	7095.4	2.397	√	2.586	√	7.3	169.3	2.363	1.015
	UMB-OP-7.0-19.0-E3-E	√	-	7.0	7073.3	4149.8	7094.9	2.402	√	2.586	√	7.1	169.4	2.363	1.016
	UMB-OP-7.0-19.0-E3-F	√	-	7.0	7075.5	4144.9	7096	2.398	√	2.586	√	7.3	169.5	2.362	1.015
	UMB-OP-4.0-19.0-E3-A	√	-	4.0	7310	4362.6	7319.1	2.473	√	2.586	√	4.4	169.8	2.436	1.015
	UMB-OP-4.0-19.0-E3-B	√	-	4.0	7316.7	4365.3	7325.3	2.472	√	2.586	√	4.4	170.0	2.436	1.015
	UMB-OP-4.0-19.0-E3-C	√	-	4.0	7309.6	4365.2	7319.1	2.475	√	2.586	√	4.3	169.7	2.437	1.015
	UMB-OP-4.0-19.0-E3-D	√	-	4.0	7309.1	4361.5	7316.8	2.473	√	2.586	√	4.4	169.8	2.436	1.015
	UMB-OP-4.0-19.0-E3-E	√	-	4.0	7312.9	4357.8	7319	2.470	√	2.586	√	4.5	169.8	2.437	1.013
	UMB-OP-4.0-19.0-E3-F	√	-	4.0	7312.6	4359.1	7319.6	2.470	√	2.586	√	4.5	169.8	2.437	1.014
	UMB-OP-10.0-19.0-E3-A	√	-	10.0	6851.6	3948.4	6921.1	2.305	√	2.586	√	10.9	170.4	2.275	1.013
	UMB-OP-10.0-19.0-E3-B	√	-	10.0	6853.5	3973.7	6927.3	2.320	√	2.586	√	10.3	169.9	2.283	1.017
	UMB-OP-10.0-19.0-E3-C	√	-	10.0	6851.5	3957.2	6923.2	2.310	√	2.586	√	10.7	170.1	2.279	1.013
	UMB-OP-10.0-19.0-E3-D	√	-	10.0	6845.1	3949.6	6915.7	2.308	√	2.586	√	10.8	170.2	2.276	1.014
	UMB-OP-10.0-19.0-E3-E	√	-	10.0	6856.1	3986.4	6941.1	2.320	√	2.586	√	10.3	169.9	2.284	1.016
	UMB-OP-10.0-19.0-E3-F	√	-	10.0	6846.9	3945.5	6917.3	2.304	√	2.586	√	10.9	169.8	2.282	1.010
	UMB-BU-7.0-19.0-E3-A	√	+0.3	7.0	7031.1	4114.6	7063.2	2.385	√	2.572	√	7.3	169.9	2.342	1.018
	UMB-BU-7.0-19.0-E3-B	√	+0.3	7.0	7053.3	4122.7	7076.6	2.388	√	2.572	√	7.2	170.0	2.348	1.017
	UMB-BU-7.0-19.0-E3-C	√	+0.3	7.0	7056.4	4131.9	7083.4	2.391	√	2.572	√	7.0	170.1	2.347	1.018
	UMB-BU-7.0-19.0-E3-D	√	+0.3	7.0	7049.2	4112.3	7073.9	2.380	√	2.572	√	7.5	170.2	2.344	1.016
	UMB-BU-7.0-19.0-E3-E	√	+0.3	7.0	7054	4124.3	7079.7	2.387	√	2.572	√	7.2	170.1	2.347	1.017
	UMB-BU-7.0-19.0-E3-F	√	+0.3	7.0	7054	4116.6	7076	2.384	√	2.572	√	7.3	170.0	2.348	1.015

Project	Specimen ID	Compacted	AC%	Target AV%	Bulk Specific Gravity					MTSG		Air Voids	Gry. Ht.	Gmb Est.	Actual Corr. Fac.
					Dry Wt.	Submerged Wt.	SSD Wt.	BSG	Done		Done				
Langlade Cty Antigo 19.0mm E-10	ANT-OP-7.0-19.0-E10-A	√	-	7.0	6934.4	4034.2	6969.9	2.362	√	2.535	√	6.8	170.0	2.308	1.023
	ANT-OP-7.0-19.0-E10-B	√	-	7.0	6940.8	4038.5	6973.6	2.365	√	2.535	√	6.7	170.0	2.310	1.024
	ANT-OP-7.0-19.0-E10-C	√	-	7.0	6946	4041.6	6979.3	2.364	√	2.535	√	6.7	169.9	2.313	1.022
	ANT-OP-7.0-19.0-E10-D	√	-	7.0	6946.7	4047.3	6979.2	2.369	√	2.535	√	6.5	170.0	2.312	1.025
	ANT-OP-7.0-19.0-E10-E	√	-	7.0	6937.1	4040.9	6973.7	2.365	√	2.535	√	6.7	169.8	2.312	1.023
	ANT-OP-7.0-19.0-E10-F	√	-	7.0	6947.5	4051.3	6988.1	2.366	√	2.535	√	6.7	170.0	2.313	1.023
	ANT-OP-4.0-19.0-E10-A	√	-	4.0	6991.9	4131.6	7003.3	2.435	√	2.535	√	4.0	165.9	2.385	1.021
	ANT-OP-4.0-19.0-E10-B	√	-	4.0	7170.6	4229.3	7183.4	2.427	√	2.535	√	4.2	170.2	2.384	1.018
	ANT-OP-4.0-19.0-E10-C	√	-	4.0	7166.8	4222.6	7174	2.428	√	2.535	√	4.2	169.9	2.387	1.017
	ANT-OP-4.0-19.0-E10-D	√	-	4.0	7176.6	4235.9	7189.7	2.430	√	2.535	√	4.2	170.3	2.385	1.019
	ANT-OP-4.0-19.0-E10-E	√	-	4.0	7169.4	4243.9	7186.3	2.437	√	2.535	√	3.9	170.2	2.384	1.022
	ANT-OP-4.0-19.0-E10-F	√	-	4.0	7173.5	4222.9	7182.9	2.423	√	2.535	√	4.4	170.3	2.384	1.017
	ANT-OP-10.0-19.0-E10-A	√	-	10.0	6712.5	3879.4	6807.6	2.292	√	2.535	√	9.6	169.4	2.242	1.022
	ANT-OP-10.0-19.0-E10-B	√	-	10.0	6720.9	3887.2	6802.1	2.306	√	2.535	√	9.0	169.7	2.241	1.029
	ANT-OP-10.0-19.0-E10-C	√	-	10.0	6722	3873.3	6801.8	2.295	√	2.535	√	9.5	169.7	2.242	1.024
	ANT-OP-10.0-19.0-E10-D	√	-	10.0	6722.3	3870.9	6791.8	2.301	√	2.535	√	9.2	169.2	2.248	1.024
	ANT-OP-10.0-19.0-E10-E	√	-	10.0	6719.2	3876.4	6798.3	2.300	√	2.535	√	9.3	168.8	2.253	1.021
	ANT-OP-10.0-19.0-E10-F	√	-	10.0	6713.9	3876.6	6794.1	2.301	√	2.535	√	9.2	169.4	2.243	1.026
	ANT-BU-7.0-19.0-E10-A	√	+0.3	7.0	6903.5	4005.1	6938.1	2.354	√	2.521	√	6.6	169.9	2.299	1.024
	ANT-BU-7.0-19.0-E10-B	√	+0.3	7.0	6913.1	4017.9	6953.7	2.355	√	2.521	√	6.6	170.0	2.301	1.023
	ANT-BU-7.0-19.0-E10-C	√	+0.3	7.0	6914.5	4016.7	6960.3	2.349	√	2.521	√	6.8	170.3	2.298	1.022
	ANT-BU-7.0-19.0-E10-D	√	+0.3	7.0	6911.6	4007.3	6954.2	2.345	√	2.521	√	7.0	169.8	2.303	1.018
	ANT-BU-7.0-19.0-E10-E	√	+0.3	7.0	6929.6	4031.9	6967.2	2.361	√	2.521	√	6.4	170.4	2.301	1.026
	ANT-BU-7.0-19.0-E10-F	√	+0.3	7.0	6974	4044.7	7014.5	2.348	√	2.521	√	6.9	171.5	2.301	1.020

Project	Specimen ID	Compacted	AC%	Target AV%	Bulk Specific Gravity					MTSG		Air Voids	Gry. Ht.	Gmb Est.	Actual Corr. Fac.
					Dry Wt.	Submerged Wt.	SSD Wt.	BSG	Done		Done				
Jackson Cty Northfield 19.0mm E-30	NOR-OP-7.0-19.0-E30-A	√	-	7.0	6857.1	4005.1	6884.5	2.381	√	2.505	√	4.9	169.8	2.285	1.042
	NOR-OP-7.0-19.0-E30-B	√	-	7.0	6853.5	3991.8	6881.1	2.372	√	2.505	√	5.3	169.8	2.284	1.039
	NOR-OP-7.0-19.0-E30-C	√	-	7.0	6847.9	4029.5	6881.5	2.401	√	2.505	√	4.2	170.1	2.278	1.054
	NOR-OP-7.0-19.0-E30-D	√	-	7.0	6853.2	4011.5	6881.3	2.388	√	2.505	√	4.7	170.1	2.280	1.047
	NOR-OP-7.0-19.0-E30-E	√	-	7.0	6850.9	3998.6	6876.3	2.381	√	2.505	√	5.0	169.7	2.285	1.042
	NOR-OP-7.0-19.0-E30-F	√	-	7.0	6852.6	4008.1	6883.1	2.384	√	2.505	√	4.9	169.7	2.285	1.043
	NOR-OP-4.0-19.0-E30-A	√	-	4.0	7074.9	4156.6	7106.9	2.398	√	2.505	√	4.3	174.7	2.292	1.046
	NOR-OP-4.0-19.0-E30-B	√	-	4.0	7072.4	4170.8	7098	2.416	√	2.505	√	3.6	173.3	2.309	1.046
	NOR-OP-4.0-19.0-E30-C	√	-	4.0	7063.8	4166.4	7081.3	2.423	√	2.505	√	3.3	171.7	2.328	1.041
	NOR-OP-4.0-19.0-E30-D	√	-	4.0	7066.2	4171.2	7079.4	2.430	√	2.505	√	3.0	171.1	2.337	1.040
	NOR-OP-4.0-19.0-E30-E	√	-	4.0	7060.4	4147	7083.3	2.405	√	2.505	√	4.0	173.3	2.305	1.043
	NOR-OP-4.0-19.0-E30-F	√	-	4.0	7066.5	4170	7079.8	2.429	√	2.505	√	3.1	170.1	2.351	1.033
	NOR-OP-10.0-19.0-E30-A	√	-	10.0	6618.9	3846.1	6676.1	2.339	√	2.505	√	6.6	169.9	2.205	1.061
	NOR-OP-10.0-19.0-E30-B	√	-	10.0	6621.9	3852.5	6688.4	2.335	√	2.505	√	6.8	170.0	2.204	1.059
	NOR-OP-10.0-19.0-E30-C	√	-	10.0	6623.8	3849.4	6684.8	2.336	√	2.505	√	6.7	169.6	2.210	1.057
	NOR-OP-10.0-19.0-E30-D	√	-	10.0	6611.1	3826.2	6687.6	2.310	√	2.505	√	7.8	170.2	2.198	1.051
	NOR-OP-10.0-19.0-E30-E	√	-	10.0	6613.8	3847.1	6664.8	2.347	√	2.505	√	6.3	169.1	2.213	1.061
	NOR-OP-10.0-19.0-E30-F	√	-	10.0	6633.8	3875.9	6689.9	2.357	√	2.505	√	5.9	170.0	2.208	1.068
	NOR-BU-7.0-19.0-E30-A	√	+0.3	7.0	6791.2	3984.6	6824.8	2.391	√	2.493	√	4.1	169.6	2.266	1.055
	NOR-BU-7.0-19.0-E30-B	√	+0.3	7.0	6828.8	3986.1	6857.6	2.378	√	2.493	√	4.6	170.2	2.270	1.047
	NOR-BU-7.0-19.0-E30-C	√	+0.3	7.0	6803.1	3984.9	6828.9	2.392	√	2.493	√	4.0	169.4	2.273	1.053
	NOR-BU-7.0-19.0-E30-D	√	+0.3	7.0	6803.6	3969.3	6830.3	2.378	√	2.493	√	4.6	169.7	2.269	1.048
	NOR-BU-7.0-19.0-E30-E	√	+0.3	7.0	6806.8	3973.5	6832.8	2.381	√	2.493	√	4.5	169.5	2.272	1.048
	NOR-BU-7.0-19.0-E30-F	√	+0.3	7.0	6816.6	3997.6	6843.8	2.395	√	2.493	√	3.9	169.7	2.273	1.054

Project	Specimen ID	Compacted	AC%	Target AV%	Bulk Specific Gravity					MTSG	Done	Air Voids	Gry. Ht.	Gmb Est.	Actual Corr. Fac.
					Dry Wt.	Submerged Wt.	SSD Wt.	BSG	Done						
Lincoln Cty Tomahawk 25.0mm E-3	TOM-OP-7.0-25.0-E3-OPEN-A	√	-	7.0	7000.2	4211.5	7048.4	2.468	√	2.560	√	3.6	169.7	2.334	1.057
	TOM-OP-7.0-25.0-E3-OPEN-B	√	-	7.0	7001.1	4212.5	7052	2.466	√	2.560	√	3.7	169.7	2.335	1.056
	TOM-OP-7.0-25.0-E3-OPEN-C	√	-	7.0	6996.2	4238.3	7058.2	2.481	√	2.560	√	3.1	171.2	2.313	1.073
	TOM-OP-7.0-25.0-E3-OPEN-D	√	-	7.0	6987.5	4207	7035.6	2.470	√	2.560	√	3.5	169.9	2.327	1.061
	TOM-OP-7.0-25.0-E3-OPEN-E	√	-	7.0	6994	4198.8	7039.3	2.462	√	2.560	√	3.8	169.7	2.332	1.056
	TOM-OP-7.0-25.0-E3-OPEN-F	√	-	7.0	6982.7	4212.3	7027.1	2.481	√	2.560	√	3.1	169.9	2.326	1.067
	TOM-OP-4.0-25.0-E3-OPEN-A	√	-	4.0	7226.5	4347.6	7252	2.488	√	2.560	√	2.8	169.8	2.408	1.033
	TOM-OP-4.0-25.0-E3-OPEN-B	√	-	4.0	7227.7	4342.2	7249.2	2.486	√	2.560	√	2.9	169.7	2.410	1.032
	TOM-OP-4.0-25.0-E3-OPEN-C	√	-	4.0	7229	4380.2	7263.9	2.507	√	2.560	√	2.1	171.8	2.381	1.053
	TOM-OP-4.0-25.0-E3-OPEN-D	√	-	4.0	7232.1	4381.2	7265.3	2.508	√	2.560	√	2.1	170.1	2.406	1.042
	TOM-OP-4.0-25.0-E3-OPEN-E	√	-	4.0	7234.4	4370	7264.4	2.499	√	2.560	√	2.4	169.9	2.410	1.037
	TOM-OP-4.0-25.0-E3-OPEN-F	√	-	4.0	7226.9	4380.8	7258	2.512	√	2.560	√	1.9	169.8	2.408	1.043
	TOM-OP-10.0-25.0-E3-OPEN-A	√	-	10.0	6766.4	4017.5	6829.1	2.407	√	2.560	√	6.0	169.1	2.264	1.063
	TOM-OP-10.0-25.0-E3-OPEN-B	√	-	10.0	6774.1	4014.2	6837.4	2.399	√	2.560	√	6.3	169.1	2.267	1.058
	TOM-OP-10.0-25.0-E3-OPEN-C	√	-	10.0	6765.8	4006.5	6827.4	2.398	√	2.560	√	6.3	168.8	2.268	1.057
	TOM-OP-10.0-25.0-E3-OPEN-D	√	-	10.0	6764.9	4029.8	6820.5	2.424	√	2.560	√	5.3	169.2	2.262	1.071
	TOM-OP-10.0-25.0-E3-OPEN-E	√	-	10.0	6773.8	4015.6	6834.2	2.403	√	2.560	√	6.1	168.9	2.269	1.059
	TOM-OP-10.0-25.0-E3-OPEN-F	√	-	10.0	6764.4	4072.1	6816.4	2.465	√	2.560	√	3.7	169.7	2.256	1.093
	TOM-BU-7.0-25.0-E3-OPEN-A	√	+0.3	7.0	6924.8	4080	6953.7	2.410	√	2.529	√	4.7	168.7	2.323	1.037
	TOM-BU-7.0-25.0-E3-OPEN-B	√	+0.3	7.0	6929.2	4097.9	6961.7	2.420	√	2.529	√	4.3	169.4	2.315	1.045
	TOM-BU-7.0-25.0-E3-OPEN-C	√	+0.3	7.0	6933.6	4099.8	6964.2	2.421	√	2.529	√	4.3	168.8	2.324	1.041
	TOM-BU-7.0-25.0-E3-OPEN-D	√	+0.3	7.0	6924.4	4183.6	6962.6	2.492	√	2.529	√	1.5	170.0	2.305	1.081
	TOM-BU-7.0-25.0-E3-OPEN-E	√	+0.3	7.0	6918	4168.3	6960.5	2.478	√	2.529	√	2.0	169.9	2.304	1.075
	TOM-BU-7.0-25.0-E3-OPEN-F	√	+0.3	7.0	6921.4	4107.3	6960.4	2.426	√	2.529	√	4.1	168.5	2.324	1.044

APPENDIX C. SPECIMEN VOLUMETRICS AFTER SAWING/CORING

Project	Specimen ID	Diameter Bottom 1	Diameter Bottom 2	Diameter Midpoint 1	Diameter Midpoint 2	Diameter Top 1	Diameter Top 2	Diameter Average	Diameter Std. Dev.	Height 1	Height 2	Height 3	Height 4	Height Average	Height Std. Dev.
Lincoln Cty Bloomville 19.0mm E-1	BLO-OP-7.0-19.0-E1-A	101.44	101.51	101.44	101.55	101.47	101.37	101.46	0.06	150.63	150.83	150.97	150.77	150.80	0.14
	BLO-OP-7.0-19.0-E1-D	101.67	101.45	100.97	101.25	101.33	101.01	101.28	0.27	150.73	150.83	150.62	150.70	150.72	0.09
	BLO-OP-7.0-19.0-E1-E	101.43	101.42	101.52	101.51	101.34	101.22	101.41	0.11	150.96	150.69	150.85	150.67	150.79	0.14
	BLO-OP-4.0-19.0-E1-D	101.42	101.49	101.51	101.49	101.49	101.37	101.46	0.05	151.36	150.59	150.68	150.77	150.85	0.35
	BLO-OP-4.0-19.0-E1-E	101.48	101.45	101.52	101.48	101.54	101.48	101.49	0.03	150.94	150.71	150.64	150.70	150.75	0.13
	BLO-OP-4.0-19.0-E1-F	101.43	101.31	101.41	101.44	101.38	101.37	101.39	0.05	150.84	150.73	150.76	150.64	150.74	0.08
	BLO-OP-10.0-19.0-E1-A	101.46	101.44	101.52	101.46	101.37	101.36	101.44	0.06	150.74	150.75	150.84	150.78	150.78	0.04
	BLO-OP-10.0-19.0-E1-C	101.50	101.55	101.54	101.21	101.23	101.20	101.37	0.17	150.67	150.83	150.88	150.94	150.83	0.12
	BLO-OP-10.0-19.0-E1-E	101.33	101.44	101.43	101.50	101.40	101.45	101.43	0.06	150.88	150.67	150.88	150.70	150.78	0.11
	BLO-BU-7.0-19.0-E1-C	101.25	101.46	101.42	101.45	101.43	101.44	101.41	0.08	150.77	150.84	150.64	150.74	150.75	0.08
	BLO-BU-7.0-19.0-E1-D	101.57	101.50	101.47	101.57	101.37	101.27	101.46	0.12	150.62	150.69	150.70	150.66	150.67	0.04
	BLO-BU-7.0-19.0-E1-F	101.60	101.47	101.53	101.38	101.47	101.39	101.47	0.08	150.77	150.95	150.88	150.93	150.88	0.08

Project	Specimen ID	Cut down	AC%	Target AV%	Bulk Specific Gravity					MTSG	Done	Air Voids	Ht.	Dia.	Gmb Est.	Actual Corr. Fac.
					Dry Wt.	Sub Wt.	SSD Wt.	BSG	Done							
Lincoln Cty Bloomville 19.0mm E-1	BLO-OP-7.0-19.0-E1-A	√	-	7.0	2855.2	1652	2861.8	2.360	√	2.521	√	6.4	150.8	101.5	2.342	1.008
	BLO-OP-7.0-19.0-E1-D	√	-	7.0	2849.8	1648.5	2856	2.360	√	2.521	√	6.4	150.7	101.3	2.347	1.006
	BLO-OP-7.0-19.0-E1-E	√	-	7.0	2854.3	1647	2859.3	2.354	√	2.521	√	6.6	150.8	101.4	2.344	1.005
	BLO-OP-4.0-19.0-E1-D	√	-	4.0	2972.3	1762.6	2975.6	2.450	√	2.521	√	2.8	150.9	101.5	2.437	1.005
	BLO-OP-4.0-19.0-E1-E	√	-	4.0	2963.7	1754.2	2967.3	2.443	√	2.521	√	3.1	150.7	101.5	2.430	1.005
	BLO-OP-4.0-19.0-E1-F	√	-	4.0	2954.3	1744.2	2957.6	2.435	√	2.521	√	3.4	150.7	101.4	2.427	1.003
	BLO-OP-10.0-19.0-E1-A	√	-	10.0	2793.9	1597.8	2810	2.305	√	2.521	√	8.6	150.8	101.4	2.293	1.005
	BLO-OP-10.0-19.0-E1-C	√	-	10.0	2740.3	1565.7	2753.8	2.306	√	2.521	√	8.5	150.8	101.4	2.251	1.025
	BLO-OP-10.0-19.0-E1-E	√	-	10.0	2793.4	1592.4	2803.5	2.306	√	2.521	√	8.5	150.8	101.4	2.293	1.006
	BLO-BU-7.0-19.0-E1-C	√	+0.3	7.0	2870.2	1660.3	2874.7	2.363	√	2.505	√	5.6	150.7	101.4	2.357	1.003
	BLO-BU-7.0-19.0-E1-D	√	+0.3	7.0	2860	1651.3	2863.7	2.359	√	2.505	√	5.8	150.7	101.5	2.348	1.005
	BLO-BU-7.0-19.0-E1-F	√	+0.3	7.0	2862.4	1653.1	2866.4	2.359	√	2.505	√	5.8	150.9	101.5	2.346	1.006

Project	Specimen ID	Diameter Bottom 1	Diameter Bottom 2	Diameter Midpoint 1	Diameter Midpoint 2	Diameter Top 1	Diameter Top 2	Diameter Average	Diameter Std. Dev.	Height 1	Height 2	Height 3	Height 4	Height Average	Height Std. Dev.
Marathon Cty Mosinee 19.0mm E-3	MOS-OP-7.0-19.0-E3-A	101.29	101.43	101.26	101.16	101.53	101.30	101.33	0.13	150.78	150.64	150.65	150.64	150.68	0.07
	MOS-OP-7.0-19.0-E3-B	101.46	101.51	101.47	101.62	101.46	101.56	101.51	0.07	150.69	150.67	150.50	150.31	150.54	0.18
	MOS-OP-7.0-19.0-E3-E	101.20	101.36	101.34	101.37	101.41	101.37	101.34	0.07	150.49	150.54	150.69	150.70	150.61	0.11
	MOS-OP-4.0-19.0-E3-A	101.30	101.26	101.29	101.34	101.40	101.42	101.34	0.06	150.68	150.74	150.57	150.69	150.67	0.07
	MOS-OP-4.0-19.0-E3-B	101.36	101.27	101.29	101.31	101.40	101.40	101.34	0.06	150.64	150.65	150.59	150.56	150.61	0.04
	MOS-OP-4.0-19.0-E3-D	101.30	101.39	101.37	101.36	101.40	101.40	101.37	0.04	150.71	150.65	150.47	150.41	150.56	0.14
	MOS-OP-10.0-19.0-E3-A	101.35	101.29	101.30	101.20	101.46	101.25	101.31	0.09	150.70	150.40	150.40	150.54	150.51	0.14
	MOS-OP-10.0-19.0-E3-B	101.25	101.24	101.18	101.26	101.40	101.29	101.27	0.07	150.58	150.48	150.72	150.67	150.61	0.11
	MOS-OP-10.0-19.0-E3-F	101.16	101.27	101.16	101.37	101.35	101.39	101.28	0.10	150.57	150.66	150.54	150.77	150.64	0.10
	MOS-BU-7.0-19.0-E3-A	101.22	101.20	101.16	101.25	101.25	101.32	101.23	0.05	150.64	150.52	150.73	150.83	150.68	0.13
	MOS-BU-7.0-19.0-E3-E	101.39	101.22	101.30	101.27	101.33	101.30	101.30	0.06	150.52	150.61	150.59	150.50	150.56	0.05
	MOS-BU-7.0-19.0-E3-F	101.31	101.32	101.27	101.29	101.35	101.28	101.30	0.03	150.58	150.43	150.48	150.55	150.51	0.07

Project	Specimen ID	Cut down	AC%	Target AV%	Bulk Specific Gravity					MTSG	Done	Air Voids	Ht.	Dia.	Gmb Est.	Actual Corr. Fac.
					Dry Wt.	Sub Wt.	SSD Wt.	BSG	Done							
Marathon Cty Mosinee 19.0mm E-3	MOS-OP-7.0-19.0-E3-A	√	-	7.0	2763.9	1558.2	2771.7	2.278	√	2.445	√	6.9	150.7	101.3	2.275	1.001
	MOS-OP-7.0-19.0-E3-B	√	-	7.0	2756.6	1547.3	2763	2.268	√	2.445	√	7.3	150.5	101.5	2.262	1.002
	MOS-OP-7.0-19.0-E3-E	√	-	7.0	2757.4	1552.2	2762.6	2.278	√	2.445	√	6.8	150.6	101.3	2.270	1.004
	MOS-OP-4.0-19.0-E3-A	√	-	4.0	2846.4	1637	2849	2.349	√	2.445	√	4.0	150.7	101.3	2.342	1.003
	MOS-OP-4.0-19.0-E3-B	√	-	4.0	2846.6	1638.2	2849.7	2.350	√	2.445	√	3.9	150.6	101.3	2.343	1.003
	MOS-OP-4.0-19.0-E3-D	√	-	4.0	2834.1	1626.2	2838	2.339	√	2.445	√	4.4	150.6	101.4	2.332	1.003
	MOS-OP-10.0-19.0-E3-A	√	-	10.0	2691	1495.5	2702.4	2.230	√	2.445	√	8.8	150.5	101.3	2.218	1.005
	MOS-OP-10.0-19.0-E3-B	√	-	10.0	2693.6	1502.6	2711.4	2.228	√	2.445	√	8.9	150.6	101.3	2.220	1.004
	MOS-OP-10.0-19.0-E3-F	√	-	10.0	2668.4	1479.1	2685.4	2.212	√	2.445	√	9.5	150.6	101.3	2.199	1.006
	MOS-BU-7.0-19.0-E3-A	√	+0.3	7.0	2746.5	1542.7	2752.1	2.271	√	2.438	√	6.9	150.7	101.2	2.265	1.003
	MOS-BU-7.0-19.0-E3-E	√	+0.3	7.0	2747.7	1544.1	2753.4	2.272	√	2.438	√	6.8	150.6	101.3	2.264	1.003
	MOS-BU-7.0-19.0-E3-F	√	+0.3	7.0	2737	1533.2	2743	2.262	√	2.438	√	7.2	150.5	101.3	2.256	1.003

Project	Specimen ID	Diameter Bottom 1	Diameter Bottom 2	Diameter Midpoint 1	Diameter Midpoint 2	Diameter Top 1	Diameter Top 2	Diameter Average	Diameter Std. Dev.	Height 1	Height 2	Height 3	Height 4	Height Average	Height Std. Dev.
Jackson Cty Northfield 19.0mm E-30	NOR-OP-7.0-19.0-E30-A	101.45	101.41	101.42	101.37	101.40	101.31	101.39	0.05	150.74	150.70	150.85	150.72	150.75	0.07
	NOR-OP-7.0-19.0-E30-E	101.46	101.37	101.43	101.32	101.36	101.30	101.37	0.06	150.59	150.75	150.67	150.92	150.73	0.14
	NOR-OP-7.0-19.0-E30-F	101.37	101.40	101.36	101.35	101.39	101.33	101.37	0.03	150.63	150.73	150.72	150.52	150.65	0.10
	NOR-OP-4.0-19.0-E30-A	101.37	101.55	101.36	101.58	101.33	101.48	101.45	0.11	150.71	150.68	150.73	150.58	150.68	0.07
	NOR-OP-4.0-19.0-E30-B	101.12	101.21	101.24	101.13	101.16	101.14	101.17	0.05	150.80	150.80	150.55	150.50	150.66	0.16
	NOR-OP-4.0-19.0-E30-E	101.20	101.15	101.29	101.30	101.33	101.23	101.25	0.07	150.83	150.76	150.91	150.72	150.81	0.08
	NOR-OP-10.0-19.0-E30-A	101.31	101.27	101.12	101.19	101.17	101.22	101.21	0.07	150.87	150.74	150.39	150.47	150.62	0.23
	NOR-OP-10.0-19.0-E30-B	101.30	101.51	101.50	101.30	101.15	101.24	101.33	0.14	150.70	150.84	150.41	150.39	150.59	0.22
	NOR-OP-10.0-19.0-E30-C	101.25	101.26	101.28	101.25	101.59	101.23	101.31	0.14	151.01	150.80	150.89	150.80	150.88	0.10
	NOR-BU-7.0-19.0-E30-B	101.41	101.53	101.37	101.49	101.39	101.43	101.44	0.06	150.72	150.73	150.78	150.94	150.79	0.10
	NOR-BU-7.0-19.0-E30-D	101.32	101.44	101.25	101.28	101.29	101.22	101.30	0.08	150.86	150.66	150.67	150.54	150.68	0.13
	NOR-BU-7.0-19.0-E30-E	101.26	101.27	101.22	101.47	101.26	101.43	101.32	0.10	150.62	150.73	150.64	150.72	150.68	0.06

Project	Specimen ID	Cut down	AC%	Target AV%	Bulk Specific Gravity					MTSG	Done	Air Voids	Ht.	Dia.	Gmb Est.	Actual Corr. Fac.
					Dry Wt.	Sub Wt.	SSD Wt.	BSG	Done							
Jackson Cty Northfield 19.0mm E-30	NOR-OP-7.0-19.0-E30-A	√	-	7.0	2917.9	1712.1	2920.2	2.415	√	2.505	√	3.6	150.8	101.4	2.397	1.008
	NOR-OP-7.0-19.0-E30-E	√	-	7.0	2907.9	1702.9	2910.7	2.408	√	2.505	√	3.9	150.7	101.4	2.390	1.007
	NOR-OP-7.0-19.0-E30-F	√	-	7.0	2916	1712	2918.8	2.416	√	2.505	√	3.5	150.7	101.4	2.398	1.007
	NOR-OP-4.0-19.0-E30-A	√	-	4.0	2937.6	1733.9	2940.5	2.435	√	2.505	√	2.8	150.7	101.4	2.412	1.009
	NOR-OP-4.0-19.0-E30-B	√	-	4.0	2963.1	1755.9	2965.2	2.450	√	2.505	√	2.2	150.7	101.2	2.447	1.001
	NOR-OP-4.0-19.0-E30-E	√	-	4.0	2947.5	1740	2951.1	2.434	√	2.505	√	2.9	150.8	101.3	2.427	1.003
	NOR-OP-10.0-19.0-E30-A	√	-	10.0	2825	1633.1	2832.9	2.355	√	2.505	√	6.0	150.6	101.2	2.331	1.010
	NOR-OP-10.0-19.0-E30-B	√	-	10.0	2818.8	1633.9	2831.1	2.354	√	2.505	√	6.0	150.6	101.3	2.321	1.014
	NOR-OP-10.0-19.0-E30-C	√	-	10.0	2813.2	1629.7	2823.6	2.356	√	2.505	√	5.9	150.9	101.3	2.313	1.019
	NOR-BU-7.0-19.0-E30-B	√	+0.3	7.0	2915.5	1717.5	2921.6	2.421	√	2.493	√	2.9	150.8	101.4	2.393	1.012
	NOR-BU-7.0-19.0-E30-D	√	+0.3	7.0	2896.9	1700	2902.2	2.410	√	2.493	√	3.3	150.7	101.3	2.385	1.010
	NOR-BU-7.0-19.0-E30-E	√	+0.3	7.0	2916.5	1711.1	2920.4	2.412	√	2.493	√	3.2	150.7	101.3	2.401	1.005